Department of Communications and Networking

# The Performance of Dense and Heterogeneous LTE Network Deployments within an Urban Environment

Kimmo Hiltunen

Aalto University

DOCTORAL DISSERTATIONS

Aalto University publication series
**DOCTORAL DISSERTATIONS** 51/2014

# The Performance of Dense and Heterogeneous LTE Network Deployments within an Urban Environment

**Kimmo Hiltunen**

A doctoral dissertation completed for the degree of Doctor of Science in Technology to be defended, with the permission of the Aalto University School of Electrical Engineering, at a public examination held at the lecture hall S3 of the school on 15 May 2014 at 12 noon.

**Aalto University**
**School of Electrical Engineering**
**Department of Communications and Networking**

**Supervising professor**
Prof. Riku Jäntti

**Thesis advisor**
Prof. Riku Jäntti

**Preliminary examiners**
Prof. Jukka Lempiäinen, Tampere University of Technology, Finland
Prof. Preben Mogensen, Aalborg University, Denmark

**Opponent**
Prof. Mikko Valkama, Tampere University of Technology, Finland

Aalto University publication series
**DOCTORAL DISSERTATIONS** 51/2014



ISBN 978-952-60-5650-0
ISBN 978-952-60-5651-7 (pdf)
ISSN-L 1799-4934
ISSN 1799-4934 (printed)
ISSN 1799-4942 (pdf)
http://urn.fi/URN:ISBN:978-952-60-5651-7

Unigrafia Oy
Helsinki 2014

Finland

441 697
Printed matter

Aalto University

# Abstract

Aalto University, P.O. Box 11000, FI-00076 Aalto www.aalto.fi

**Author**
Kimmo Hiltunen

**Name of the doctoral dissertation**
The Performance of Dense and Heterogeneous LTE Network Deployments within an Urban Environment

**Publisher** School of Electrical Engineering

**Unit** Department of Communications and Networking

**Series** Aalto University publication series DOCTORAL DISSERTATIONS 51/2014

**Field of research** Communications Engineering

**Manuscript submitted** 22 October 2013 **Date of the defence** 15 May 2014

**Permission to publish granted (date)** 6 March 2014 **Language** English

☒ **Monograph** ☐ **Article dissertation (summary + original articles)**

**Abstract**

Traffic in the mobile broadband networks is expected to grow very rapidly in the coming years. This traffic growth is caused both by the evolution of mobile terminals and by the increased use of more traffic-heavy services, such as video. In order to be able to meet the increased capacity needs, the existing mobile networks have to be densified, either by deploying new macro sites, or by deploying new low-power sites within traffic hotspots. This doctoral dissertation provides an overview of a few different network densification alternatives and compares their performance and energy-efficiency with the help of advanced radio network simulations. In addition, the impact of different network design choices is evaluated.

The results demonstrate that the heterogeneous network deployments are realistic alternatives to the traditional way of densifying mobile networks by deploying new macro sites. However, the price to pay is that a considerably larger number of new sites will be required to obtain the same network performance. Heterogeneous network deployments can be made more efficient by increasing the output power of the low-power eNodeBs or by carefully planning the locations of the low-power sites so that the obtained level of the traffic offloading can be maximized. The traffic offloading can be increased also with the help of biased cell selection, but in that case the quality of the downlink control signaling can become the limiting factor unless some form of enhanced inter-cell interference coordination mechanisms are applied at the same time.

The obtained results indicate that the densified macro deployment is in many cases the most energy-efficient network densification alternative. However, if some form of fast cell DTX is applied to idle cells, heterogeneous network deployments become much more competitive since the cost of fixed power consumption can be reduced. The energy-efficiency of densified network deployments can be enhanced also by switching off underutilized capacity cells, or by switching idle capacity cells to sleep mode. Finally, design choices aiming to reduce the required number of low-power cells are shown to be beneficial also from the network energy-efficiency point of view.

**Keywords** LTE, dense networks, heterogeneous networks, micro cells, pico cells, femto cells, performance, capacity, coverage, energy-efficiency, power consumption

**ISBN (printed)** 978-952-60-5650-0 **ISBN (pdf)** 978-952-60-5651-7

**ISSN-L** 1799-4934 **ISSN (printed)** 1799-4934 **ISSN (pdf)** 1799-4942

**Location of publisher** Helsinki **Location of printing** Helsinki **Year** 2014

**Pages** 281 **urn** http://urn.fi/URN:ISBN:978-952-60-5651-7

A! Aalto-yliopisto

**Tiivistelmä**

**Aalto-yliopisto, PL 11000, 00076 Aalto** www.aalto.fi

**Tekijä**
Kimmo Hiltunen

**Väitöskirjan nimi**
Tiheiden ja heterogeenisten LTE-verkkoratkaisujen suorituskyky kaupunkiympäristössä

**Julkaisija** Sähkötekniikan korkeakoulu

**Yksikkö** Tietoliikenne- ja tietoverkkotekniikan laitos

**Sarja** Aalto University publication series DOCTORAL DISSERTATIONS 51/2014

**Tutkimusala** Tietoliikennetekniikka

**Käsikirjoituksen pvm** 22.10.2013 **Väitöspäivä** 15.05.2014

**Julkaisuluvan myöntämispäivä** 06.03.2014 **Kieli** Englanti

☒ **Monografia** ☐ **Yhdistelmäväitöskirja (yhteenveto-osa + erillisartikkelit)**

**Tiivistelmä**

Matkaviestinverkkojen välittämän liikenteen arvioidaan kasvavan erittäin voimakkaasti tulevina vuosina. Tämä kasvu johtuu pääasiassa päätelaitteiden kehittymisestä ja entistä raskaampien palvelujen, erityisesti videon, yleistymisestä. Matkaviestinverkkojen kapasiteettia voidaan parantaa esimerkiksi pienentämällä solukokoa joko perinteisiä makrotukiasemia lisäämällä tai uusien, matalatehoisiin tukiasemiin perustuvien heterogeenisten verkkoratkaisujen avulla. Tämä väitöskirja tarjoaa hyvän yleiskuvan erilaisista tiheistä verkkoratkaisuista, sekä vertailee niiden suorituskykyä ja energiatehokkuutta radioverkkosimulointeja apuna käyttäen. Väitöskirja tutkii myös eri suunnitteluvaihtoehtojen vaikutusta verkkoratkaisujen suorituskykyyn.

Väitöskirjassa esitetyt tulokset osoittavat että heterogeenisten verkkoratkaisujen avulla voidaan saavuttaa sama suorituskyky kuin lisäämällä verkkoon uusia makrosoluja. Heterogeenisten verkkoratkaisujen pääasiallisena haittapuolena on halutun suorituskyvyn saavuttamiseksi tarvittavien solujen määrä kasvu tukiaseman lähetystehon pienentyessä. Tarvittavien tukiasemien määrää voidaan vähentää suunnittelemalla matalatehoisten tukiasemien sijannit siten, että niihin kytkeytyvän liikenteen määrä voidaan maksimoida. Matalatehoisten tukiasemien solukokoa ja siten myös tukiasemiin kytkeytyvän liikenteen määrää voidaan kasvattaa myös suosimalla solunvaihtojen yhteydessä matalatehoisia soluja voimakkaampien makrosolujen sijasta. Menetelmän haittana on kuitenkin laajennetun solun reunoilla olevien käyttäjien alalinkin laadun heikkeneminen, mistä johtuen menetelmän tehokas hyödyntäminen vaatiikin yleensä mekanismeja solujen välisten häiriöiden hallitsemiseksi.

Väitöskirjassa esitetyt tulokset osoittavat myös että tiheä makroverkko on yleensä kaikista energiatehokkain verkkoratkaisu. Heterogeenisten verkkoratkaisujen energiatehokkuutta voidaan parantaa huomattavasti sammuttamalla osa tukiasemasta aina kun tukiaseman ei tarvitse lähettää mitään signaaleja. Energiatehokkuutta voidaan parantaa entisestään huolellisen verkkosuunnittelun avulla, tai säätämällä verkon tarjoamaa kapasiteettia todellisen liikennetarpeen mukaan, huolehtien samalla kuitenkin riittävän peittoalueen turvaamisesta. Verkon kapasiteettia voidaan säätää sammuttamalla soluja joko kokonaan tai osittain aina, kun niitä ei tarvita riittävän suorituskyvyn tarjoamiseksi.

**Avainsanat** LTE, tiheät verkot, heterogeeniset verkot, mikrosolu, pikosolu, femtosolu, suorituskyky, kapasiteetti, peittoalue, energiatehokkuus, tehonkulutus

**ISBN (painettu)** 978-952-60-5650-0 **ISBN (pdf)** 978-952-60-5651-7

**ISSN-L** 1799-4934 **ISSN (painettu)** 1799-4934 **ISSN (pdf)** 1799-4942

**Julkaisupaikka** Helsinki **Painopaikka** Helsinki **Vuosi** 2014

**Sivumäärä** 281 **urn** http://urn.fi/URN:ISBN:978-952-60-5651-7

# Preface

The research work for this doctoral thesis has been carried out at the Wireless Access Networks group within Ericsson Research NomadicLab during 2010-2013. The work has been partially funded by the Academy of Finland (Doctoral studies of employed persons). Furthermore, parts of the research work have been done within the ECEWA (Energy and Cost Efficiency for Wireless Access) project and the Celtic-Plus project SHARING (Self-organized Heterogeneous Advanced RadIo Networks Generation), which have been partially funded by Tekes (the Finnish Funding Agency for Technology and Innovation).

Firstly, I wish to express my gratitude to my supervisor, Professor Riku Jäntti, for his guidance during the preparation of this thesis. I would also like to thank Professor (emeritus) Sven-Gustav Häggman for his guidance during my post-graduate studies at the Helsinki University of Technology during 1996-2005.

I would like to thank the thesis pre-examiners, Professor Jukka Lempiäinen from Tampere University of Technology and Professor Preben Mogensen from the Aalborg University, for their comments and suggestions.

I would like to express my sincere thanks to all the Ericsson colleagues around the globe that I have had the pleasure to work with during the years. You have really given me many valuable ideas on how to proceed with my research work, and lately, my thesis. In particular I would like to thank Bo Hagerman, Gunnar Bark, Anders Furuskär, Bogdan Timus, Sara Landström Arne Simonsson, Pål Frenger, Magnus Olsson, Henrik Asplund, Janne Peisa and Johan Torsner for all the discussions and comments.

Finally, I wish to express my warmest gratitude to my parents, Seppo and Eila, for all the support they have given me.

Kimmo Hiltunen
Espoo, 19 March 2014

# Contents

# Author's contributions

The main contribution of this thesis is two-fold: Firstly, to introduce both a system simulator platform and a deployment scenario enabling fair performance comparisons between different types of network densification alternatives. Secondly, to compare the performance and energy-efficiency of a few different network densification alternatives within an urban environment with the help of system simulations.

The author has been the main responsible for developing the deployment scenario, the simulation methodology and the simulator platform described in Chapter 4. A static version of the simulator was originally developed to enable Ericsson-internal studies during the years 2008-2009. The dynamic version of the simulator was developed during the first half of 2010.

Research work for this thesis has been conducted in the Wireless Access Networks research group within Ericsson Research NomadicLab during the years 2010-2013. Part of the research results have been documented in six published conference papers (references [146], [147], [150], [154], [155] and [156]). In addition to that, some research that has not been documented previously is shown here. This thesis gathers the obtained research results into a form of a monograph.

For all the publications as well as the other results presented in Chapters 4-9 the author has been responsible for the model development, all the numerical evaluations, result analysis and result documentation.

Some specific contributions in Chapter 4 worth highlighting include the uplink inter-cell interference control method based on the introduction of an interference margin, which the author has proposed and evaluated. Furthermore, the author has visualized the impact of CSG femto cell power adjustment on the overall system performance.

In case of Chapters 5-8, the author has among other things evaluated the performance of heterogeneous network deployments containing open access and hybrid mode femto eNodeBs, which have not been discussed in any large extent within the literature. Furthermore, the author has evaluated the impact of backhaul limitation and the impact of traffic-heavy users on the performance of heterogeneous femto deployments.

Finally, when it comes to the energy-efficiency evaluations in Chapter 9, the author has been responsible for developing the applied eNodeB power consumption model, the actual power consumption values and the three evaluated network adaptation methods (fixed, variable and sleep mode), based on the input and results from the EARTH project.

# List of abbreviations

| | |
|---|---|
| 3G | Third Generation Cellular System |
| 3GPP | Third Generation Partnership Project |
| 4G | Fourth Generation Cellular System |
| ACIR | Adjacent Channel Interference power Ratio |
| CAPEX | Capital Expenditure |
| CCH | Control Channel |
| CL | Coupling Loss |
| CoMP | Coordinated Multi-Point transmission and reception |
| CQI | Channel-Quality Indicator |
| CRS | Cell-specific Reference Signal |
| CSG | Closed Subscriber Group |
| CSI | Channel State Information |
| D2D | Device-to-Device |
| DAS | Distributed Antenna System |
| DFT | Discrete Fourier Transform |
| DFTS-OFDM | DFT-Spread OFDM |
| DL | Downlink, transmission from eNodeB to UE |
| DTX | Discontinuous Transmission |
| DwPTS | The downlink part of the special subframe (for TDD operation) |
| EARTH | Energy Aware Radio and Network Technologies |
| EGoS | Equal Grade of Service |
| eICIC | enhanced ICIC |
| eNodeB | E-UTRAN NodeB |
| EPC | Evolved Packet Core |
| E-UTRAN | Evolved UTRAN |
| EVM | Error Vector Magnitude |
| FDD | Frequency Division Duplex |
| FDMA | Frequency Division Multiple Access |
| FTP | File Transfer Protocol |
| GPRS | General Packet Radio System |
| GSM | Global System for Mobile communications |

| | |
|---|---|
| HARQ | Hybrid Automatic Repeat request |
| HCS | Hierarchical Cell Structure |
| HeNB | Home eNodeB |
| HII | High-Interference Indicator |
| HNB | Home NodeB |
| HSPA | High-Speed Packet Access |
| HW | Hardware |
| ICIC | Inter-Cell Interference Coordination |
| IoT | Interference over Thermal noise |
| IP | Internet Protocol |
| ISD | Inter-Site Distance |
| ITU | International Telecommunication Union |
| ITU-R | International Telecommunication Union - Radiocommunications Sector |
| LOS | Line-of-Sight |
| LPN | Low-Power Node |
| LTE | Long-Term Evolution |
| LTE-A | Long-Term Evolution-Advanced |
| MAC | Medium Access Control |
| MBSFN | Multicast-Broadcast Single Frequency Network |
| MIMO | Multiple-Input Multiple-Output |
| MME | Mobility Management Entity |
| MU-MIMO | Multi-User MIMO |
| N/A | Not Applicable |
| NLOS | Non-Line Of Sight |
| NodeB | A logical node handling transmission/reception in multiple cells. Often corresponding to a base station. |
| OFDM | Orthogonal Frequency Division Multiplexing |
| OFDMA | Orthogonal Frequency Division Multiple Access |
| OI | Overload Indicator |
| OPEX | Operational Expenditure |
| OSG | Open Subscriber Group |
| PBCH | Physical Broadcast Channel |
| PCFICH | Physical Control Format Indicator Channel |
| PCI | Physical Cell Identity |
| PDCCH | Physical Downlink Control Channel |
| PDSCH | Physical Downlink Shared Channel |
| PER | Packet Error Rate |
| PF | Proportionally Fair |
| PHICH | Physical Hybrid-ARQ Indicator Channel |
| PMI | Precoding Matrix Indicator |

| | |
|---|---|
| PRB | Physical Resource Block |
| PSS | Primary Synchronization Signal |
| PUCCH | Physical Uplink Control Channel |
| PUSCH | Physical Uplink Shared Channel |
| QAM | Quadrature Amplitude Modulation |
| RAN | Radio Access Network |
| RAT | Radio Access Technology |
| RF | Radio Frequency |
| RI | Rank Indicator |
| RLC | Radio Link Control |
| RNTP | Relative Narrowband Transmit Power |
| RR | Round Robin |
| RRM | Radio Resource Management |
| RRU | Remote Radio Unit |
| RSRP | Reference Signal Received Power |
| RSS | Received Signal Strength |
| RX | Receiver |
| S1 | The interface between eNodeB and Evolved Packet Core |
| S1-c | The control-plane part of S1 |
| S1-u | The user-plane part of S1 |
| SC-FDMA | Single-Carrier FDMA |
| SCH | Shared Channel |
| S-GW | Serving Gateway |
| SIMO | Single-Input Multiple-Output |
| SINR | Signal-to-Interference-and-Noise Ratio |
| SNR | Signal-to-Noise Ratio |
| SON | Self-Organizing Network |
| SSS | Secondary Synchronization Signal |
| SU-MIMO | Single-User MIMO |
| SW | Software |
| TC | Traffic Cluster |
| TCP | Transmission Control Protocol |
| TDD | Time Division Duplex |
| TTI | Transmission Time Interval |
| TX | Transmitter |
| UE | User Equipment |
| UL | Uplink, transmission from UE to eNodeB |
| UMi | Urban Micro channel model |
| UMTS | Universal Mobile Telecommunications System |
| UpPTS | The uplink part of the special subframe (for TDD operation) |

| | |
|---|---|
| UTRA(N) | UMTS Terrestial Radio Access (Network) |
| WCDMA | Wideband Code Division Multiple Access |
| WiFi | Wireless Fidelity, see also WLAN |
| WLAN | Wireless Local Area Network |
| X2 | The interface between eNodeBs |

# List of symbols

**Coverage and Capacity Evaluation**

| | |
|---|---|
| $\alpha_b$ | Path loss compensation factor for cell $b$ |
| $\beta$ | Overhead factor |
| $\gamma_{m,b}$ | SINR for UE $m$, served by eNodeB $b$ |
| $\gamma_{m,b,r}^{EVM}$ | EVM-limited SINR for UE $m$, served by eNodeB $b$ |
| $\Delta$ | UE-specific parameter for the uplink power control taking into account that the different modulation and coding schemes require different SINR |
| $\delta$ | UE-specific correction value used for uplink closed-loop power control |
| $\varepsilon$ | Error vector magnitude |
| $\eta$ | Bandwidth efficiency factor |
| $\mu$ | SNR efficiency factor |
| $\rho_{n,r}$ | Parameter indicating if neighbor $n$ is transmitting on PRB $r$ |
| $\phi_{m,p,b}$ | Ratio between the allowed uplink interference from UE $m$ served by eNodeB $p$ measured at the neighboring eNodeB $b$ and the applied $P_0$ within neighboring cell $b$ |
| $\phi_{p,b}$ | Ratio between the allowed uplink interference at eNodeB $b$ from the users served by eNodeB $p$, and the applied $P_0$ within cell $p$ |
| $\varphi_{m,b}$ | Fraction of time allocated for UE $m$ served by eNodeB $b$ |
| $\varphi_{n,r}$ | Fraction of time when neighbor $n$ is transmitting on PRB $r$ |
| $\chi_{n,r}$ | Adjacent channel interference power ratio for neighbor $n$ |
| | |
| $A_{macro}$ | Area of the evaluated macro cell |
| $A_{system}$ | Area of the evaluated macro cell layer |
| $B_{m,b}$ | Achievable bit rate for UE $m$, served by eNodeB $b$ |
| $B_{max}$ | Maximum achievable bit rate |
| $D$ | Inter-site distance |

| | |
|---|---|
| $h$ | Ratio between the total daily traffic and the busy hour traffic |
| $H_{baseline}$ | Site density of the baseline deployment |
| $H_{dense}$ | Site density of the densified macro deployment |
| $i_{LPN}$ | Interference margin for the uplink power control within the low-power cell |
| $I_{m,b,r}$ | Received interference power on PRB $r$ for a link between UE $m$ and eNodeB $b$ |
| $I_{m,b,r}^{EVM}$ | EVM-noise power on PRB $r$ for a link between UE $m$ and eNodeB $b$ |
| $I_{m,p,b}^{PRB}$ | Received uplink interference power per PRB from UE $m$ served by eNodeB $p$, measured at eNodeB $b$ |
| $k$ | Linear scalar allowing the slope of the femto eNodeB output power curve to be altered |
| $L_{m,b}^{DL}$ | Downlink coupling loss between UE $m$ and eNodeB $b$ |
| $L_{m,b}^{UL}$ | Uplink coupling loss between UE $m$ and eNodeB $b$ |
| $m$ | Number of days per month |
| $M_{m,b}$ | Number of occupied PRBs for UE $m$, served by eNodeB $b$ |
| $N_{m,b}$ | Thermal noise power for UE $m$, served by eNodeB $b$ |
| $N_b^{PRB}$ | Thermal noise power per PRB for receiver $b$ |
| $o$ | Operator market share |
| $O_{LPN}$ | Cell selection offset for the low-power cell |
| $p$ | Population density |
| $p_{m,b}$ | Scheduling priority for UE $m$ served by eNodeB $b$ |
| $P_{0,b}$ | Uplink received power target at eNodeB $b$ |
| $P_{0,m,b}$ | Uplink received power target for mobile $m$ served by eNodeB $b$ |
| $P_{CSG}$ | Maximum transmission power of the CSG femto cell |
| $P_{femto}$ | Maximum transmission power of the OSG femto cell |
| $P_{m,b}$ | Transmission power for a link between UE $m$ and eNodeB $b$ |
| $P_{m,b,r}$ | Transmission power of PRB $r$ for a link between UE $m$ and eNodeB $b$ |
| $P_{macro}$ | Maximum transmission power of the macro cell |
| $P_{max,CSG}$ | Maximum allowed total transmission power of the CSG cell |
| $P_{min,CSG}$ | Minimum allowed total transmission power of the CSG cell |
| $P_{n,r}$ | Transmission power of neighbor $n$ on PRB $r$ |
| $P_{LPN}$ | Maximum transmission power of the low-power cell |
| $P_{PUSCH}$ | Transmission power of the PUSCH |
| $P_{tx,CSG}$ | Adjusted, and unlimited, maximum transmission power of the CSG cell |

| | |
|---|---|
| $P_{UE}$ | Transmission power of the UE |
| $P_{UEmax}$ | Maximum allowed transmission power of the UE |
| $r$ | Portion of the downlink (or uplink) traffic |
| $R_{m,b}$ | Average throughput of UE $m$ served by eNodeB $b$ during the time step from $t_n$ to $t_{n+1}$ |
| $R_{m,b}^{EGoS}$ | Average throughput of UE $m$ served by eNodeB $b$ during the time step from $t_n$ to $t_{n+1}$, assuming an EGoS scheduler |
| $R_{m,b}^{PF}$ | Average throughput of UE $m$ served by eNodeB $b$ during the time step from $t_n$ to $t_{n+1}$, assuming a PF scheduler |
| $R_{m,b}^{RR}$ | Average throughput of UE $m$ served by eNodeB $b$ during the time step from $t_n$ to $t_{n+1}$, assuming a RR scheduler |
| $s$ | Service penetration |
| $S_{m,b}^{CRS}$ | Received CRS power (RSRP) for a link between UE $m$ and eNodeB $b$ |
| $S_{m,b}^{UL,PRB}$ | Received uplink power per PRB for a link between UE $m$ and eNodeB $b$ |
| $t_n$ | Time instant $n$ |
| $T_{area}$ | Area traffic during a busy hour |
| $T_{subs}$ | Monthly subscriber traffic |
| $U_b$ | Total number of active users served by eNodeB $b$ |
| $w$ | Desired range of the CSG femto cell |
| $W_{macro}$ | Received total power from the strongest macro cell |
| $Y$ | Offered macro cell traffic with respect to the baseline deployment |

**Wave Propagation**

| | |
|---|---|
| $\alpha$ | Log-linear distance-dependent wall penetration loss |
| $\theta$ | Grazing angle for the line-of-sight building penetration |
| $\theta_j$ | Change of direction for street segments $j$-1 and $j$ |
| $\lambda$ | Wavelength of the carrier frequency |
| $\nu$ | Exponent for the angle-dependency |
| $\rho$ | Correlation of fading values between a UE and the different eNodeBs |
| $\sigma$ | Standard deviation of the shadow fading |
| $\varphi$ | Street orientation angle |
| $\chi_{m,b}$ | Log-normally distributed shadow fading value |
| | |
| $b$ | Distance between buildings |
| $d$ | Distance between the transmitter and the receiver antennas |

| | |
|---|---|
| $D$ | Distance from the outdoor position to the reference point on the building wall |
| $d_{2D}$ | 2-dimensional distance within the building |
| $d_{3D}$ | 3-dimensional distance within the building |
| $d_a$ | Distance within apartments |
| $d_{cor}$ | Decorrelation distance for the shadow fading |
| $d_i$ | Distance within buildings |
| $d_s$ | Settled field distance |
| $f$ | Carrier frequency |
| $G_{eNB,m,b}$ | eNodeB antenna gain at the direction of UE $m$ |
| $G_{FH}$ | Floor height gain |
| $G_{UE,m,b}$ | UE antenna gain at the direction of eNodeB $b$ |
| $h_b$ | eNodeB antenna height |
| $h_m$ | UE antenna height |
| $h_{roof}$ | Height of the rooftops |
| $k$ | Number of floors traversed by the direct wave |
| $l$ | Distance between the transmitter and the receiver over which the buildings extend |
| $L_{m,b}$ | Coupling loss between UE $m$ and eNodeB $b$ |
| $L_{fsp,m,b}$ | Free-space loss between UE $m$ and eNodeB $b$ |
| $L_{msd}$ | Multiple screen diffraction loss |
| $L_{ori}$ | Street orientation factor |
| $L_{outdoor}$ | Distance-dependent path loss for an outdoor user |
| $L_p$ | Coupling loss for a link through outer building wall $p$ |
| $L_{penet}$ | Penetration loss |
| $L_{rts}$ | Diffraction loss from rooftop to street |
| $L_{scen,m,b}$ | Scenario-dependent path loss between UE $m$ and eNodeB $b$ |
| $p$ | Number of penetrated internal walls between apartments |
| $P_{Rx}$ | Received power |
| $P_{Tx}$ | Transmitted power |
| $q_j$ | Angle-dependency of the street-level propagation |
| $q_{90}$ | Angle-dependency constant for a 90-degree change of direction |
| $S$ | Perpendicular distance from the outdoor position towards the building wall |
| $s_j$ | Length of the $j$:th street segment |
| $w$ | Width of the street |
| $w_c$ | Width of the corridor |

| | |
|---|---|
| $W_e$ | Penetration loss through the external building wall at perpendicular penetration |
| $W_{ext}$ | Penetration loss through the external building wall for non-line-of-sight building penetration |
| $W_{Ge}$ | Additional penetration loss through the external building wall at small grazing angle |
| $W_{ge}$ | Additional wall penetration loss for the non-line-of-sight building penetration |
| $W_i$ | Penetration loss for the heavier walls between apartments |

**Energy Efficiency Evaluation**

| | |
|---|---|
| $\delta_b$ | Cell DTX parameter for cell $b$ |
| $\delta_{bln}$ | Cell DTX parameter for the baseline cells |
| $\delta_{cap}$ | Cell DTX parameter for the capacity cells |
| $\delta_{LPN}$ | Cell DTX parameter for the low-power cells |
| $\delta_{macro}$ | Cell DTX parameter for the macro cells |
| | |
| $C(t)$ | Density of the operational capacity cells as a function of time |
| $L$ | Density of the low-power cells |
| $M$ | Density of the macro cells |
| $P_{eNB}$ | Maximum eNodeB output power per cell |
| $P_{in}$ | Total eNodeB power consumption per cell |
| $P_{in,A}$ | Total eNodeB power consumption per cell during an active state |
| $P_{in,D}$ | Total eNodeB power consumption per cell during an idle state with cell DTX |
| $P_{in,I}$ | Total eNodeB power consumption per cell during an idle state without cell DTX |
| $P_{in}^{bln}(t)$ | Total power consumption of the baseline cells as a function of time |
| $P_{in}^{cap}(t)$ | Total power consumption of the capacity cells as a function of time |
| $P_{in}^{low-power}$ | Total power consumption of the low-power cell layer |
| $P_{in}^{macro}$ | Total power consumption of the macro cell layer |
| $P_{in,A}^{LPN}$ | Total low-power cell power consumption during an active state |
| $P_{in,I}^{LPN}$ | Total low-power cell power consumption during an idle state without cell DTX |
| $P_{in,A}^{cap}$ | Total capacity cell power consumption during an active state |

| | |
|---|---|
| $P_{in,I}^{cap}$ | Total capacity cell power consumption during an idle state without cell DTX |
| $P_{in,A}^{macro}$ | Total macro cell power consumption during an active state |
| $P_{in,I}^{macro}$ | Total macro cell power consumption during an idle state without cell DTX |
| $P_{in}^{OPEX}$ | Total OPEX-related power consumption |
| $P_{in}^{OPEX}(\delta)$ | Total OPEX-related power consumption as a function of the cell DTX parameter |
| $P_{in}^{OPEX}(t)$ | Total OPEX-related power consumption as a function of time |
| $P_{in}^{total}$ | Total network power consumption |
| $P_{in}^{total}(\delta)$ | Total network power consumption as a function of the cell DTX parameter |
| $P_{in}^{total}(t)$ | Total network power consumption as a function of time |
| $u_b$ | Average utilization of cell $b$ |
| $\bar{u}_{bln}(t)$ | Average utilization of the baseline cells as a function of time |
| $\bar{u}_{cap}(t)$ | Average utilization of the capacity cells as a function of time |
| $\bar{u}_{LPN}$ | Average cell utilization for the low-power cell layer |
| $\bar{u}_{macro}$ | Average cell utilization for the macro cell layer |

# 1. Introduction

## 1.1 High level problem definition and motivation

Traffic in the mobile networks is expected to grow very rapidly in the coming years [1]-[3]. For example, [1] estimates that the global mobile data traffic will be doubled every year. This traffic growth will be caused both by the evolution of mobile terminals (an increasing penetration of smart phones, tablets and mobile computers) and the increased use of more traffic-heavy services, especially video. It is also expected that the wider introduction of various cloud-based services and machine-to-machine communication will accelerate the traffic growth even further [1].

Another challenge for the mobile networks is the fact that the users expect to have cellular coverage everywhere, but at the same time the really high bit rates and traffic volumes are typically expected at specific locations, such as homes and offices. Hence, the mobile networks should be able to simultaneously provide both uniform coverage and non-uniform capacity.

As explained for example in [4]-[6], there are three possible ways to increase the capacity of a mobile network: increased spectrum, improved spectral efficiency and network densification. From the spectrum point of view, the capacity can be enhanced by deploying additional carriers, or by increasing the carrier bandwidth. The spectral efficiency can be improved both by improving the signal-to-interference-ratio for the link between the transmitter and the receiver and by introducing new techniques to enhance the utilization of the high signal-to-interference-ratio conditions. These techniques include for example advanced multi-antenna techniques (for example MIMO and beamforming), higher order modulation and advanced interference management (for example interference cancellation, inter-cell interference coordination and coordinated multipoint transmission and reception). However, although the achievable capacity gains via additional spectrum, and improvements in spectral efficiency are considerable, the substantial growth that is predicted for the mobile broadband revolution

will require also actions to densify the mobile networks, i.e. to increase the spatial reuse of the radio resources.

The traditional way to densify mobile networks has been to deploy new macro cells, either by adding new sectors to existing sites, or by deploying new macro sites. The benefit of a densified macro deployment is that the network performance can be improved with a fairly small amount of required new hardware, or new sites. However, as new macro sites are becoming increasingly difficult and often expensive to deploy, at least within urban environments, focus is put on the efforts to find more cost-efficient ways to densify the current networks. Examples of such include the recent evolution of *main-remote* -type of base stations and *site sharing* between operators, which both are reducing the cost of deploying new macro sites, and hence, are pushing the practical limits of macro cellular deployments farther than they are today.

An alternative to deploying new macro sites is to deploy low-power sites within traffic hotspots, i.e. the introduction of heterogeneous network deployments. In case of the heterogeneous network deployment, macro cells will provide uniform wide area coverage, while the small low-power cells deployed within traffic hotspots, small and medium enterprises and residential areas will take care of the majority of the traffic volume. The low-power cells can be either outdoor micro and pico cells deployed below the rooftops, or indoor pico and femto cells.

Given all these different alternatives to densify the current mobile networks, one of the most natural questions from the point of view of the operator is related to the total cost of the network deployment: Which of the alternatives is the most cost-efficient way to enhance the performance of the mobile network? Another motivation to find the most cost-efficient network deployment is that as a result of mobile subscriptions with flat-rate charging the revenues are not expected to grow in the same pace as the traffic grows within the mobile networks. Hence, the operators are forced to find out ways to reduce the cost per transferred bit in order to be profitable also in the future.

When it comes to the total cost of the network deployment, it consists of a large number of different components, related to both the capital expenditure (CAPEX) and the operational expenditure (OPEX), some of which are listed in Figure 1.1. In addition, the total cost of deploying and operating a radio network can include components such as radio network planning, core network and marketing, which should also be taken into account. Looking at the list it is quite easy to understand that many of the cost components will depend on both the number and the type of the sites to be deployed. Therefore, in order to be able to perform more detailed cost

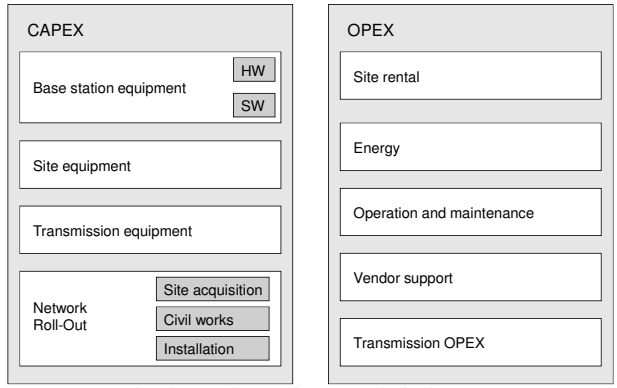


**Figure 1.1.** Components for the total cost of a network deployment.

comparisons, the performance of each of the deployment alternatives has to be evaluated first. In practice the aim of the performance evaluations is to find out the required number of new sites to be deployed in order to reach the desired coverage and capacity requirements.

One particular example of the OPEX-related cost is the total energy consumption of the network deployment. The total energy consumption can be divided into two parts: the energy consumed by the core network and the energy consumed by the radio access network, including the energy consumed by the mobile stations. It has been estimated that approximately 80% of the total energy is consumed by the radio access network [7]. Both parts, but in particular the energy consumption within the radio access network, will depend on the type and the number of the deployed base stations. On one hand, a macro site can be assumed to consume much more energy than for example a femto site. On the other hand, it could be expected that a much larger number of femto base stations than macro base stations has to be deployed in order to achieve the desired system performance.

## 1.2 Scope and contributions of the thesis

In order to be able to meet the rapidly increasing traffic needs, both in terms of user throughput and network capacity, the spatial reuse of radio resources has to be enhanced within the current mobile networks via network densification. Furthermore, considering the aim towards more cost-efficient network deployments, selection of the most appropriate network densification alternative for each of the scenarios becomes crucial for the operators. However, even a mobile network vendor, such as

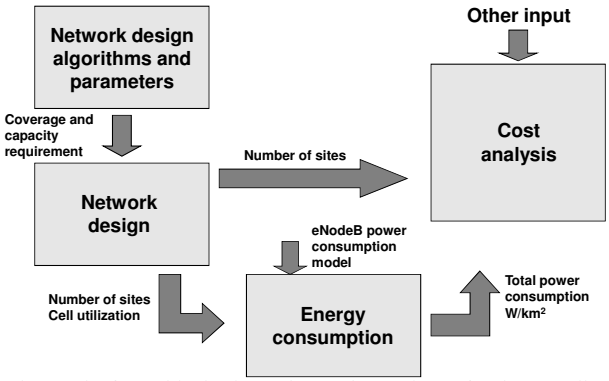


**Figure 1.2.** The results from this thesis can be used as an input for the overall cost analysis.

Ericsson, should be well informed of the characteristics and the efficiency of the different network densification alternatives. A network vendor should preferably be able to provide a solid message towards the operators, which deployment options are available to enhance the system performance, and when each of them should preferably be used. Furthermore, without good knowledge of the topic, it becomes hard for the vendor to stay on the edge of the development.

The scope of this thesis is to compare the performance and energy efficiency of a number of different network densification alternatives within an urban environment. As described in Figure 1.2 the two main outputs are: a) the required density of sites to be deployed, and b) the corresponding total network power consumption in order to fulfill the desired coverage and capacity requirements. These can then be used as an input for the more detailed cost estimations. The obtained results are expected to provide an answer to the fundamental question about what would be the most efficient alternative to enhance the mobile broadband coverage and capacity within an existing cellular network.

The thesis discusses also the impact of a number of design choices, for example with respect to the eNodeB transmission power, spectrum allocation, serving cell selection and access control. Furthermore, a few different ways to enhance the energy efficiency of densified network deployments are discussed and evaluated.

Compared to the previous work, the main contribution of this thesis is a performance comparison of the different network densification alternatives, considering both the downlink and the uplink characteristics. The performance of the different deployment alternatives is compared within the same urban environment, and assuming the same traffic distribution. Furthermore, the evaluation considers both the coverage and the capacity,

as well as the total power consumption, of the different network densification alternatives.

One of the main contributions is also the introduction of a system simulation scenario, which enables a fair comparison of the different network densification alternatives. The introduced scenario aims to model the user and site locations within traffic hotspots, as well as the average wave propagation between the nodes in an accurate and a comparable way. For example, a three-dimensional modeling of both the wave propagation and the traffic is assumed. Furthermore, the modeled indoor areas are divided into residential and non-residential areas, affecting in particular of the efficiency of the deployments with residential femto base stations. Unfortunately, the price of the more detailed models is that the general applicability of the obtained results becomes limited. Hence, the results shown in this thesis are mostly applicable only for the assumed scenario, and any general conclusions should be handled with care.

## 1.3 Previous contributions within the area

### 1.3.1 A brief look at the history

Heterogeneous network deployments as such have been studied already for a long time. For example, a deployment with small micro cells was proposed already in mid-1980s; see [8]-[11]. In the beginning of 1990s, a micro-cellular concept utilizing fiber optic transmission between the base station and the low-power micro units was introduced; see [12]-[14]. At the same time the integration of the macro cells with the micro cells started to become more interesting. The research topics were not that different from today: detection of hotspot areas, determination of the most appropriate micro cell size and position, resource management between the cell layers and admission control. A nice summary of the problems and proposed solutions is provided in [15]. Similar discussion is provided also in [16]-[22].

Initially, low-power nodes were seen as a lower cost alternative to satisfy local capacity needs, or to resolve coverage holes for example within indoor areas, instead of deploying new macro sites, or large in-building solutions. However, during the discussions about appropriate 3G mobile techniques, heterogeneous network deployments, or hierarchical cell structures, gained even more interest [23]. Again, the interference between the cell layers,

radio resource management and load balancing were hot topics, see for example the discussion in [24]-[29].

In the beginning of the new millennium, a somewhat more practical view on the WCDMA hierarchical cell structures was provided by Nokia Networks in [30]-[33]. Some other work, considering also the co-channel deployments of macro and low-power cells, can be found in [34]-[36]. Furthermore, the support for the new medium range (i.e. micro) and local area (i.e. pico) base station classes was introduced in 3GPP UTRA Release-6 [37][38].

There have been a few technical challenges that have contributed to the fact that heterogeneous WCDMA networks have not been widely deployed. These include for example link imbalance, mobility management and interference management. Although low-power WCDMA cells can co-exist with co-channel macro cells, a proper network planning is required to ensure a well-behaving network deployment. Therefore, heterogeneous networks have quite often been deployed as hierarchical cell structures (HCS), where the different cell layers are operating on different carrier frequencies. This reduces the near-far interference problems considerably.

During the recent years the interest in low-power base stations and heterogeneous network deployments has increased rapidly. This has been the result of the increasing availability and speeds of residential broadband connections, introduction of High-Speed Packet Access (HSPA), mobile broadband and flat-rate charging, as well as the activities within the area of self-organizing networks (SON). Traffic within the mobile networks has started to increase so quickly that the traditional ways to increase network capacity are not always sufficient, or cost-efficient. To meet those challenges, a concept called Home NodeB (HNB), or femto base station, was introduced. Some initial research results on the topic of 3G femto cells was published by Alcatel-Lucent Bell Laboratories in [39]-[43].

Perhaps the most visible actions during the recent years have been the start-up of the Femto Forum [44] in 2007, the Home (e)NodeB standardization activities within 3GPP for UTRA [45][46] and LTE Release-8 and beyond [47][48], as well as the activities to define an efficient support of different types of heterogeneous network deployments as part of 3GPP LTE Release-10 and Release-11 [49]. Initially, the main focus was on the introduction of Closed Subscriber Group (CSG) H(e)NBs. For example, many of the activities have been aiming to find and evaluate new ways to mitigate inter-cell interference within heterogeneous deployments containing CSG H(e)NBs [50][51]. Only recently, a wider focus on heterogeneous small cell deployments has been gaining ground, including topics such as deployment of open access [52] or enterprise femto cells [53]

and the integration of 3GPP femto cells with WLAN [54]. Furthermore, in addition to the traditional research areas, also some new ones such as energy-efficiency and the overall cost of deployment has been opened up. Related to the shifted focus of the industry activities, Femto Forum changed its name to Small Cell Forum in 2012 [55].

### 1.3.2 Previous contributions

This section provides some references to previous work performed on the topics that are the most relevant for this thesis: scenarios for heterogeneous network deployments, performance of heterogeneous network deployments, inter-layer interference management and energy-efficiency.

To support the various standardization-related performance evaluations, 3GPP has defined a number of reference scenarios for heterogeneous network deployments for example in [56] and [57]. Similarly, also the Femto Forum has defined scenarios to support the evaluation of the various heterogeneous femto deployments, see [50] and [58]. Furthermore, some additional small cell scenarios have been defined in [59]. These scenarios have been used as a starting point for the more evolved heterogeneous network scenarios introduced in this thesis.

The performance (coverage and capacity) of different types of heterogeneous network deployments has been widely discussed in the literature. However, since the performance of a network deployment is typically tightly coupled with the evaluation assumptions, the performance results cannot in most of the cases be reliably compared. An alternative would be to estimate the network performance for each of the deployment alternatives on a general level, assuming fairly simple models. By doing so, the comparisons become simple and they are not related to any specific scenario, but as a result the accuracy will be compromised. Examples of such general comparisons can be found for example in [62]-[65].

During the standardization of LTE Home eNodeBs within 3GPP, the topic of inter-cell interference management was discussed and investigated, as summarized in [47]. In addition, interference management methods related to UE transmission power adjustment are discussed for example in [66]-[72]. Furthermore, some discussion related to interference management via serving cell selection can be found in [73]-[77]. Finally, interference management via access control has been studied for example in [78] and [79], while the impact of spectrum allocation has been discussed in [80].

It is worth noting that a considerable amount of work has also been done related to fractional frequency reuse and different kinds of sub-carrier allocation schemes, see for example the results from the BeFemto project

[81]. The common denominator for all these schemes is that the neighboring cells aim to allocate non-overlapping sub-carriers to the users generating most of the inter-cell interference. Although these kind of schemes are effective to improve the quality of the data channels (Physical Downlink Shared Channel (PDSCH) and Physical Uplink Shared Channel (PUSCH)), they are not efficient in improving the quality of the 3GPP LTE Release-8 downlink control signaling, which is transmitted over the whole carrier bandwidth. Similarly, the schemes are not able to reduce the interference between the Physical Uplink Control Channels (PUCCH), which are always transmitted at the edges of the carrier bandwidth. Due to this, these kinds of schemes are ignored in this thesis.

When it comes to the energy-efficiency of heterogeneous network deployments, the level of interest and the availability of relevant publications have increased during the last few years. Some discussion on the topic can be found for example in [82]-[96]. Finally, a large amount of material related to the energy-efficiency can be found within the home page of the recently closed EARTH project [97]. In particular, the report summarizing the evaluation assumptions and models [98] and the report listing a number of potential methods to reduce the total energy consumption [99] can be highlighted.

## 1.4 Outline

The outline of this thesis is the following: In Chapter 2 a brief introduction of the 3GPP Long Term Evolution is given. In Chapter 3, the concept of heterogeneous network deployments is introduced and a number of technical challenges are discussed. In Chapter 4, the system simulator platform used for the performance evaluations and the most relevant simulator models are presented. Evaluation results for the homogeneous macro deployments, heterogeneous micro deployments and heterogeneous femto deployments are provided in Chapter 5, Chapter 6 and Chapter 7, respectively. Furthermore, the impact of various design choices is discussed and evaluated. The performance of the different network densification alternatives is compared in Chapter 8 from the user performance and the network capacity point of view. The total power consumption and energy-efficiency of the different network densification alternatives is evaluated in Chapter 9. Finally, some conclusions and proposals for future research are provided in Chapter 10.

# 2. Introduction to 3GPP Long Term Evolution

This chapter provides a very brief introduction to 3GPP Long Term Evolution (LTE) Release-8. Only the details that are the most relevant for this thesis are introduced. A much more comprehensive introduction can be found for example in [100]-[102] and in the 36-series of the 3GPP Technical Specifications [103]. Furthermore, some details are introduced also in Chapter 3, as well as in Chapter 4 together with the corresponding simulator modeling.

The text in this chapter is to a large extent based on the material in [100] and [104].

## 2.1 Radio interface architecture

LTE radio access network (RAN) architecture and interfaces are described in Figure 2.1. The evolved packet core (EPC) is responsible for functions not related to the radio interface, but needed for providing a complete mobile broadband network. This includes, for example, authentication, charging functionality and setup of end-to-end connections. EPC consists of several different types of nodes, two of which are described here. The Mobility Management Entity (MME) is the control-plane node of the EPC. Its responsibilities include connection and release of bearers to a UE, handling of IDLE to ACTIVE transitions and handling of security keys. The Serving Gateway (S-GW) is the user-plane node connecting the EPC to the LTE RAN. The S-GW acts as a mobility anchor when UEs move between eNodeBs, as well as a mobility anchor for other 3GPP technologies (GSM/GPRS and HSPA). Collection of information and statistics necessary for charging is also handled by the S-GW.

The LTE RAN is responsible for all radio-related functionality of the overall network including, for example, scheduling, radio resource management, retransmission protocols, coding and various multi-antenna schemes. In case of 3GPP LTE Release-8, RAN includes only one type of

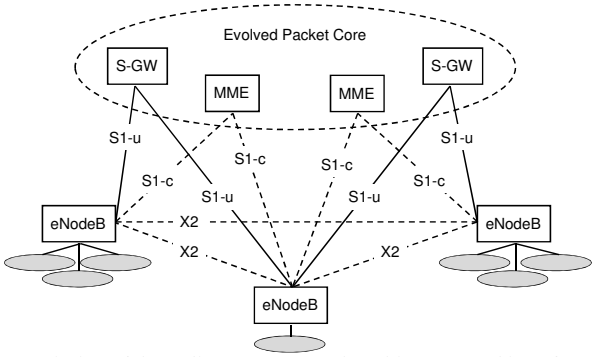


**Figure 2.1.** Description of the radio access network architecture and interfaces.

node, the eNodeB, which is responsible for all radio-related functions in one or several cells. The eNodeB is connected to the EPC by means of the *S1 interface*, more specifically to the S-GW by means of the *S1 user-plane part* (*S1-u*), and to the MME by means of the *S1 control-plane part* (*S1-c*). The *X2-interface*, connecting eNodeBs to each other, is mainly used to support active-mode mobility. The interface may also be used for multi-cell radio resource management functions such as Inter-Cell Interference Coordination (ICIC). The X2-interface is also used to support lossless mobility between neighboring cells by means of packet forwarding.

## 2.2 Basic principles

### 2.2.1 Transmission scheme

The basic transmission scheme for both the LTE downlink and uplink is OFDM. However, in order to improve the efficiency of the UE power amplifier, in uplink the DFT precoding is applied before OFDM modulation, leading to DFT-spread OFDM (DFTS-OFDM), also known as Single-Carrier FDMA (SC-FDMA).

In LTE OFDM the subcarrier spacing is equal to 15 kHz. In the time domain, LTE transmissions are organized into 10 ms *radio frames*, each of which is divided into ten equally sized 1 ms *subframes*. Each subframe consists of two equally sized *slots* of length 0.5 ms. Finally, each slot consists of either seven or six OFDM *symbols*, depending on whether a normal or an extended cyclic prefix is applied.

A *resource element*, consisting of one subcarrier during one OFDM symbol, is the smallest physical resource in LTE. Furthermore, as illustrated in Figure 2.2, resource elements are grouped into (physical)

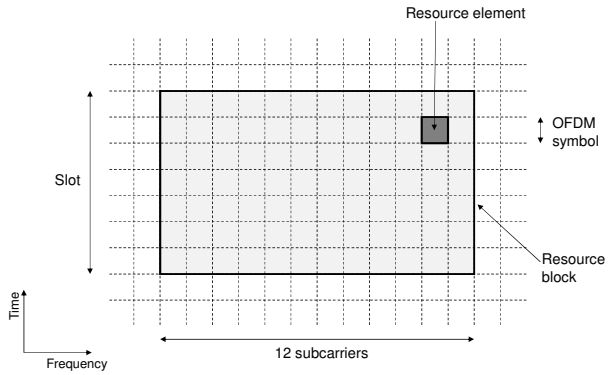


**Figure 2.2.** Description of the LTE time-frequency resource.

*resource blocks* (PRBs), where each resource block consists of 12 consecutive subcarriers in the frequency domain (i.e. a total of 180 kHz) and one 0.5 ms slot in the time domain. Although resource blocks are defined over one slot, the basic time domain unit for dynamic scheduling in LTE is one subframe, consisting of two consecutive slots.

### 2.2.2 Channel-dependent scheduling and rate adaptation

At the core of the LTE transmission scheme is the use of a *shared-channel* (SCH) transmission, where the overall time-frequency resource is dynamically shared between the users. In LTE, dynamic scheduling of resources is applied for both the downlink and the uplink transmissions independently.

The scheduler controls, for each subframe, to which users the different parts of the shared resource should be assigned. Another task for the scheduler is to perform *rate adaptation*, i.e. to determine the data rate (e.g. modulation and channel coding scheme) to be used for each transmission.

Scheduling should result in a balance between perceived end-user quality and overall system performance. *Channel-dependent scheduling* both in time and frequency domain is used to achieve high cell throughput. Transmissions can be carried out with higher data rates by transmitting on time-frequency resources with relatively good channel conditions. By doing so, fewer radio resources are consumed for any given information transferred, resulting in improved overall system efficiency.

To support the downlink scheduling, a UE may provide the network with channel state reports indicating the instantaneous downlink channel quality in both the time and frequency domains. The channel state is typically obtained by measuring on reference signals transmitted in the downlink. Based on the channel state reports, consisting of Channel-

Quality Indicators (CQI), Precoding Matrix Indicators (PMI) and Rank Indicators (RI), the downlink scheduler can assign resources for downlink transmission to different UEs, taking the channel quality into account in the scheduling decision.

The LTE uplink is based on orthogonal separation of different uplink transmissions and it is the task of the uplink scheduler to assign resources in both the time and frequency domains to different UEs. Scheduling decisions control which UEs are allowed to transmit within a cell during a given time interval. Furthermore, the scheduler decides for each UE, which frequency resources and transmission parameters, including data rate, shall be used.

### 2.2.3 Uplink power control

Since the LTE uplink is orthogonal, there is no interference between the users within the same cell. The amount of interference towards neighboring cells depends, among other things, on the position of the UE, i.e. the coupling loss from the UE to these victim cells and the transmission power of the UE. In general, UEs that are farther away from the neighboring cell may transmit with higher power than UEs that are near to the cell to create the same amount of interference.

The LTE *uplink power control* takes all these characteristics into consideration. Since the uplink is orthogonal, it is possible to multiplex signals from UEs with different received uplink powers in the same cell. In the short term, this means that instead of compensating for peaks in multipath fading by reducing power, one can exploit these peaks to increase the data rates by means of scheduling and rate adaptation. In the long term, one can set the received power target based on the coupling loss to the serving cell, giving the UEs that generate little interference a higher received power target.

Uplink power control for PUSCH transmission can be described by the following expression [105]:

$$P_{PUSCH} = \min(P_{UEmax},\ P_0 + 10\log_{10}(M) + \alpha L^{DL} + \Delta + \delta) \qquad (2.1)$$

In (2.1), $P_0$ is the desired received power per resource block and $M$ indicates the instantaneous PUSCH bandwidth measured in the number of resource blocks. Parameter $\alpha$ is the path loss compensation factor, and $L^{DL}$ is the downlink coupling loss between the UE and the serving eNodeB. Furthermore, parameter $\Delta$ can be used to take into account the fact that different signal-to-interference-and-noise ratios (SINR) are required for

different modulation schemes and coding rates used for the PUSCH transmission. Finally, the network can directly adjust the PUSCH transmission power by providing the UE with explicit power control commands that adjust the term $\delta$ in (2.1). These power control commands are accumulative, i.e. each received power control command increases or decreases the term $\delta$ by a certain amount.

As discussed for example in [106] and [107], a trade-off between uplink coverage and capacity is required when selecting a value for the $P_0$. If a larger $P_0$ is applied, the non-power-limited mobiles can achieve higher bit rates, which will in most of the cases lead to an increased maximum capacity of the system. However, as a result of the increased UE transmission powers, the level of inter-cell interference will increase as well, which will harm the performance of the power-limited cell-edge users.

The uplink power control can be further tuned by adjusting the value of the path loss compensation factor $\alpha$. If $\alpha$ is equal to 1, all users have the same target for the received power per PRB. If $\alpha$ is smaller than 1, then the target for the received power is reduced as a function of the coupling loss, which results in a combination of both a reduced inter-cell interference and a possibility to allow a higher received power for the users close to the serving eNodeB.

### 2.2.4 Inter-cell interference coordination

LTE is designed to be deployed with *full frequency reuse*, meaning that the same carrier frequency is reused in all cells. Although this kind of deployment is spectrally efficient, the downside is that the cell-edge users may suffer from a high level of inter-cell interference in downlink, and may at the same time generate a high level of inter-cell interference in uplink.

In order to be able to dynamically coordinate the scheduling in neighboring cells, and in that way to reduce the level and the impacts of inter-cell interference, 3GPP LTE Release-8 offers means for the neighboring eNodeBs to exchange information related to the scheduling strategy over the X2-interface. An eNodeB can then use this information provided by a neighboring eNodeB as input to its own scheduling process. The basic principle of such *inter-cell interference coordination* (ICIC) would be to avoid high power transmission on time-frequency resources on which the cell-edge users are scheduled in neighboring cells, i.e. users that would otherwise experience high interference and correspondingly low data rates. This kind of selective interference avoidance would benefit the quality of the cell-edge users and could also enhance the overall system performance.

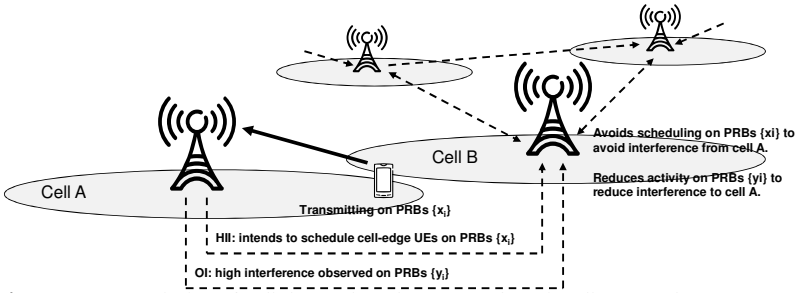


**Figure 2.3.** Description of uplink ICIC based on HII and OI signaling over the X2-interface.

To assist uplink interference coordination, 3GPP LTE Release-8 defines two messages: *High Interference Indicator* (HII) and *Overload Indicator* (OI), see Figure 2.3. For the downlink, the *Relative Narrowband Transmit Power Indicator* (RNTP) message is defined to support the ICIC (see Figure 2.4).

These messages can be characterized in the following way [100][108]:

- High Interference Indicator provides information, a bit per PRB, about the set of resource blocks within which the eNodeB is likely to schedule transmissions from cell-edge UEs, i.e. resource blocks on which a neighboring eNodeB can expect high interference. The receiving eNodeB can then take this information into account when scheduling its own cell-edge users.

- Overload Indicator is triggered when high uplink interference is detected by an eNodeB. It indicates at three levels (low/medium/high) the uplink interference experienced by a cell on its different resource blocks. A neighboring eNodeB receiving the OI message could then change its scheduling behavior to reduce the uplink interference towards the eNodeB issuing the OI.

- Relative Narrowband Transmit Power Indicator is similar to HII in the sense that it provides information, one bit per PRB, whether or not the transmit power of that resource block will be greater than a given threshold. The receiving eNodeB can take this information into account when scheduling its own users, especially the cell-edge users.

It should be noted that 3GPP LTE Release-8 provides only fairly simple means for ICIC and fails for instance to address mechanisms to manage the inter-cell interference on downlink control signaling, e.g. Physical Downlink Control Channel (PDCCH), Physical Hybrid-ARQ Indicator

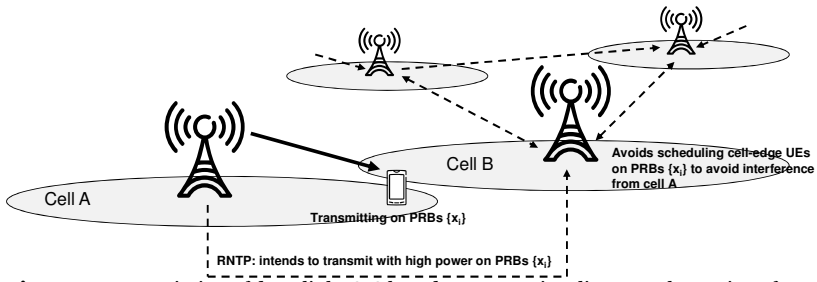


**Figure 2.4.** Description of downlink ICIC based on RNTP signaling over the X2-interface.

Channel (PHICH) and Physical Control Format Indicator Channel (PCFICH). 3GPP LTE Release-10 and Release-11 enhance among other things the X2-signaling in order to support more sophisticated ICIC algorithms, including enhanced ICIC in the time domain [100].

### 2.2.5 Hybrid-ARQ with soft combining

In LTE, *retransmissions* of missing or erroneously received data units are handled primarily by the Hybrid-ARQ (HARQ) mechanism in the MAC layer, complemented by the retransmission functionality of the RLC protocol. The reasons for having a two-level retransmission structure can be found in the trade-off between fast and reliable feedback of the status reports. The HARQ mechanism targets very fast retransmissions and, consequently, feedback on success or failure of the decoding attempt is provided to the transmitter after each received transport block. The downside is that the cost of highly reliable feedback can be very high in terms of required transmission power levels. Compared to the HARQ acknowledgements, the RLC status reports are transmitted relatively infrequently and therefore the cost of high reliability is relatively small. Hence, the combination of HARQ and RLC attains a good combination of small round-trip time and a modest feedback overhead where the two components complement each other – fast retransmissions due to the HARQ mechanism and reliable packet delivery due to RLC.

An important part of the HARQ mechanism is the use of *soft combining*, which implies that the receiver combines the received signal from multiple transmission attempts. In LTE, *incremental redundancy* is used as the soft combining strategy. With incremental redundancy, each retransmission does not have to be identical to the original transmission. Instead, multiple sets of coded bits are generated, each representing the same set of information bits. Whenever a retransmission is required, it typically uses a different set of coded bits than the previous transmission. The receiver

combines the retransmission with previous transmission attempts of the same packet. As the retransmission may contain additional parity bits not included in the previous transmission attempts, the resulting code rate is generally lowered by a retransmission. Furthermore, each retransmission does not necessarily have to consist of the same number of coded bits as the original and also the modulation scheme can be different for different retransmissions.

### 2.2.6 Multi-antenna transmission

LTE supports different *multi-antenna transmission techniques* as an integral part of the radio-interface specifications. Multi-antenna techniques can be utilized to achieve improved system performance, including improved system capacity and improved coverage, as well as improved service provisioning, e.g. higher per-user data rates. In general, multiple antennas can be used in different ways:

- Multiple receive antennas can be used for *receive diversity*, both for uplink and downlink. The simplest way of using multiple receive antennas is classical receive diversity to collect additional energy and suppress fading, but additional gains can be achieved in interference-limited scenarios if the antennas are also used to suppress interference.

- Multiple transmit antennas at the base station can be used for *transmit diversity* and different types of *beamforming* techniques. The main goal of beamforming is to improve the received SINR and eventually improve system capacity and coverage.

- *Spatial multiplexing*, or MIMO, utilizing multiple antennas at both the transmitter and the receiver is also supported. Spatial multiplexing referred to as single-user MIMO (SU-MIMO) results in an increased data rate, channel conditions permitting, in bandwidth-limited scenarios by providing several parallel data streams over the same radio link. For example, if both the transmitter and the receiver have four antennas, one can deliver up to four parallel data streams over the same radio link, effectively increasing the data rate by a factor of four. Alternatively, by combining the spatial properties with the appropriate interference-suppressing receiver processing, multiple UEs can transmit on the same time-frequency resource in order to improve the overall cell

**Table 2.1.** Channel bandwidths specified in LTE.

| Channel Bandwidth | Number of Resource Blocks |
|---|---|
| 1.4 MHz | 6 |
| 3 MHz | 15 |
| 5 MHz | 25 |
| 10 MHz | 50 |
| 15 MHz | 75 |
| 20 MHz | 100 |

capacity. This is sometimes referred to as multi-user MIMO (MU-MIMO).

In lightly loaded or small cell deployments, where the SINRs are often relatively high, spatial multiplexing can provide very high data rates and makes more efficient use of the radio resources. In other scenarios, for example in large cells or under a heavy network load, the observed channel quality does not allow for an extensive use of spatial multiplexing. In this case, the multiple transmit antennas are best used for single stream beamforming in order to enhance the quality of the signal. Since the multi-antenna scheme used is under control of the eNodeB, it can select the most appropriate scheme for each transmission.

Up to four parallel downlink data streams can be spatially multiplexed in 3GPP LTE Release-8. Furthermore, the supported beamforming is restricted to so-called codebook-based precoding. In later releases, the multi-antenna support is enhanced, both for beamforming (non-codebook-based precoding) and spatial multiplexing (up to eight parallel data streams in downlink and four parallel data streams in uplink).

### 2.2.7 Spectrum flexibility

LTE physical layer specification [109] allows the carrier to consist of any number of resource blocks in the frequency domain, ranging from a minimum of six resource blocks up to a maximum of 110 resource blocks. However, LTE radio frequency requirements in [110] and [111] are only specified for a limited set of transmission bandwidths, corresponding to a limited set of possible values for the number of resource blocks within a carrier, as listed in Table 2.1.

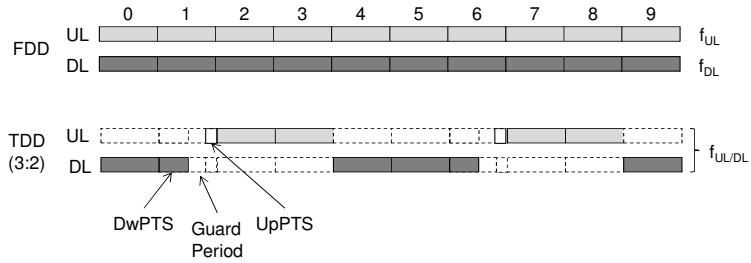


**Figure 2.5.** Uplink/downlink time-frequency structure for FDD and TDD.

In addition to the flexibility in transmission bandwidth, LTE supports also operation in both paired and unpaired spectrum by supporting both FDD and TDD-based duplex operation, see Figure 2.5. In case of FDD operation there are two carrier frequencies, one for uplink transmission and one for downlink transmission. During each frame there are thus ten uplink subframes and ten downlink subframes, and uplink and downlink transmissions can occur simultaneously within a cell. In case of TDD operation, there is only one carrier frequency and the uplink and downlink transmissions are separated in the time domain on a cell basis: as shown in Figure 2.5, some subframes are allocated for uplink transmissions and some subframes for downlink transmissions, with the switch between downlink and uplink occurring in the *special subframe* (subframe 1, and for some configurations, subframe 6). The special subframe is split into three parts: a downlink part (DwPTS), a guard period, and an uplink part (UpPTS). Different asymmetries in terms of the amount of resources allocated for uplink and downlink transmissions are provided through seven different downlink/uplink configurations (2:3, 3:2 (as shown in Figure 2.5), 4:1, 7:3, 8:2, 9:1 and 5:5).

# 3. Introduction to heterogeneous network deployments

This chapter provides a brief introduction to heterogeneous network deployments. In addition to the introduction of the different deployment alternatives, a number of technical challenges, such as link imbalance, serving cell selection, mobility management and inter-cell interference management, are also discussed.

## 3.1 Definitions and deployment alternatives

A heterogeneous network deployment can be defined as a mixture of cells with different characteristics. Often the main differences are related to the maximum base station output power, the location of the base station antennas and the type of the backhaul connection. A heterogeneous network deployment can also consist of cells with different radio access technologies, such as GSM, WCDMA, LTE, or WLAN.

A simple description of different kinds of heterogeneous network deployments is presented in Figure 3.1. The main principle is that a heterogeneous network deployment consists of a macro cell layer and a low-power cell layer. The macro cell layer is designed to provide wide area coverage, while the small low-power cells deployed within traffic hotspots are designed to take care of the majority of the local traffic volume, or to fill in some local coverage holes.

The different network components depicted in Figure 3.1 can be briefly characterized in the following way:

- Macro base stations have typically a high output power in the order of tens of Watts. The antennas are typically deployed above the rooftop level, and usually multiple macro cells (or sectors) are sharing the same macro site.

- Outdoor micro and pico base stations have a medium output power, in the order of a few Watts. Furthermore, their antennas have been

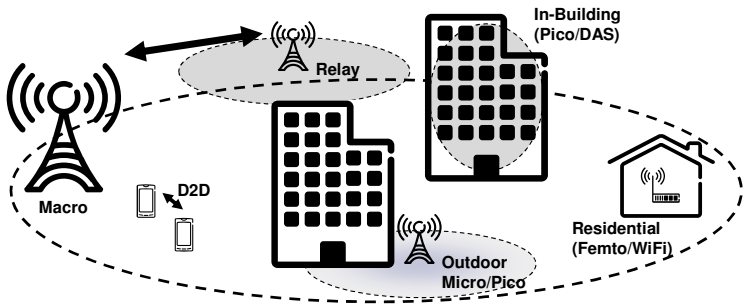


**Figure 3.1.** Description of heterogeneous network deployment.

deployed below the rooftops, e.g. on the building walls or on the street furniture.

- Some larger buildings, such as offices, hotels and shopping malls, can contain special in-building solutions to improve the coverage and capacity within that particular building. The (public) in-building solutions are typically based on some form of distributed antenna systems, or small pico base stations with a maximum output power less than one Watt. A distributed antenna system can be passive, utilizing coaxial cables or leaky cables to distribute the signal, or active, utilizing optical fibers. Hybrid solutions, utilizing both passive and active distribution techniques, are also common, in particular for larger in-building deployments.

- Residential in-building solutions include femto base stations and WLAN access points. Femto base stations are often defined as subscriber-deployed "home base stations", similar to WLAN access points [112], with a maximum output power equal to 100 mW or less [111]. What is typical for femto base stations is that they are designed to use a residential broadband connection as a backhaul towards the operator's core network. Furthermore, femto base stations are commonly designed to operate in a special *closed subscriber group* (CSG) mode, when only a pre-defined group of subscribers is allowed to be connected to the femto cell. In addition to the CSG mode, a so-called hybrid mode operation is also possible. In the hybrid mode, users outside the CSG are offered a limited access to the femto cell in order to reduce the interference problems, which are typical for co-channel CSG deployments.

- A relay node is defined here as a base station with a wireless backhaul realized over a cellular link. From the donor cell point of view, a relay node looks like a mobile station, while from the mobile

station point of view a relay node looks like an ordinary base station. Furthermore, depending on whether the backhaul and access links are operating on the same or different carrier frequencies, relays can be classified into inband and outband relays [113]. Finally, a relay can be either a single-RAT relay or a multi-RAT relay. In case of a single-RAT relay the donor and access links are utilizing the same radio access technology, whereas in case of a multi-RAT relay, different radio access technologies are utilized for the donor and access links. An example of a multi-RAT relay is the so-called fixed wireless terminal, or a wireless router, where the donor link is operating on a cellular radio access technology, e.g. WCDMA or LTE, while the access link is operating over WLAN.

- Device-to-device (D2D) communication is a concept, which is being discussed for 3GPP LTE Release-12 and beyond. In the concept, the UEs can setup direct communication links between each other, potentially reusing the spectrum of the overlying cellular network. D2D communication can be either network-assisted, or independent, i.e. operating without any network assistance or control. Further information on the D2D communication can be found for example in [114]-[118].

As mentioned, residential femto cells are commonly designed with a CSG mode. This avoids potential abuse by uninvited users in the area, who may use the full capacity of the femto cell and prevent access from the owner. Another reason for the CSG mode relates to the concerns that the femto cell owner would have to pay for extra wireline capacity that other, unknown users benefit from. More commonly, in enterprise and public indoor femto cell deployments, an open access (OSG) model is used enabling any subscriber from the host network to connect to the femto cells. In these scenarios the backhaul connection is provided and managed either by the network operator or the business enterprise. This removes the concerns about cost or quality of the broadband backhaul and provides service to all customers, prepaid, postpaid and roaming visitors [119].

The wireless system coverage can be extended also with different types of repeater nodes. A repeater receives the signal from the donor cell (downlink) or the UE (uplink), amplifies the received signal and re-transmits it either on the same or on a different frequency. Since a repeater does not create a new logical cell, it is not counted in this thesis as part of a heterogeneous network deployment.

This thesis considers only heterogeneous network deployments with a single radio access technology, namely LTE. Furthermore, this thesis does not consider the relay or repeater deployments, or device-to-device communication. Finally, in-building solutions utilizing various types of distributed antenna techniques are also excluded.

## 3.2 Technical challenges

There are a number of technical challenges related to the heterogeneous network deployments. This section will introduce a few of them in more detail: link imbalance, serving cell selection, mobility management and interference management.

Unless stated otherwise, all the equations in this section are expressed in the logarithmic scale.

### 3.2.1 Serving cell selection

In LTE, the serving cell is selected based on the received downlink signal strength (Reference Signal Received Power, RSRP), i.e. the strongest cell is normally selected as the serving cell. This is expressed also in (3.1), where $S_{m,b}^{CRS}$ denotes the RSRP from cell $b$, measured by mobile $m$. Furthermore, $M$ is the group of macro cells and $P$ is the group of low-power cells. The approach based on the downlink RSRP aims to connect the user to the cell that would be able to provide the best downlink SNR. In uplink, however, both the required UE transmission power and the received SNR are tightly related to the coupling losses between the UE and the candidate eNodeBs. In case of homogeneous network deployments, i.e. when the neighboring cells have similar characteristics, the strongest cell is typically also the closest cell from the coupling loss point of view. However, due to the different eNodeB transmission powers this is not necessarily the case for the heterogeneous network deployments. The *link imbalance* (see Figure 3.2) can result in scenarios, where a UE, served by a more powerful macro eNodeB, is generating quite high level of uplink interference towards a weaker, but closer, low-power eNodeB.

$$CellId_{serving,m} = \arg \max_{b \in M \cup P} S_{m,b}^{CRS} \tag{3.1}$$

Another problem with the RSRP-based serving cell selection is that the coverage area (or the *service area*) of a low-power cell can become quite

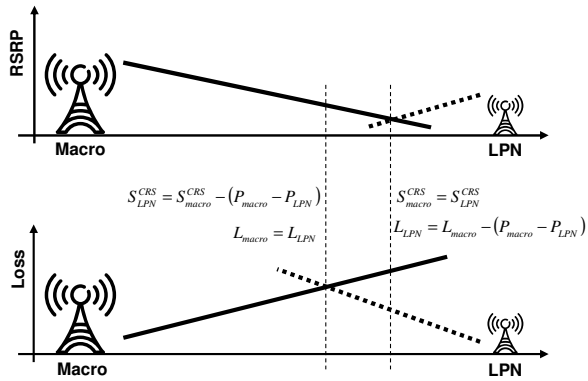


**Figure 3.2.** Description of the link imbalance.

limited, in particular when the low-power node has been deployed at a location with good macro cell coverage. In such scenarios the achieved traffic offloading may become limited, which means that it becomes highly important to find the most optimum location of the low-power node with respect to the hotspot traffic [120]. The above is demonstrated in Figure 3.3, where the service area of an outdoor micro cell is depicted for four different locations of the micro site. The impact of *biased cell selection* is further illustrated with cell selection offset of 0 dB (blue curve), 10 dB (red curve) and 16 dB (green curve). The evaluations follow the macro cell layer model which will be described in Chapter 4, assuming a macro eNodeB output power equal to 46 dBm. For the micro cell, the coupling loss is calculated based on the non-line-of-sight ITU-UMi propagation model described in [59], see (3.2). The micro eNodeB antenna is assumed to be omnidirectional, with maximum gain equal to 5 dBi. Furthermore, the micro eNodeB output power is assumed to be equal to 30 dBm. Finally, the impact of log-normal shadow fading is ignored for both the macro- and the micro-cellular propagation.

$$L_{micro} = 33.5 + 36.7 \log_{10}(d) \tag{3.2}$$

As can be seen, the size of the micro cell does indeed depend greatly on location of the micro site with respect to the macro site. Furthermore, with the help of biased cell selection, the service area of the micro cell can be considerably expanded.

The results shown in Figure 3.3 do not consider the impact of vertical eNodeB antenna patterns. This means that the macro cell signal strength increases when moving closer to the macro site. In practice, however, the antenna patterns are three-dimensional, with a decreasing vertical antenna gain when moving off the direction of the main lobe.

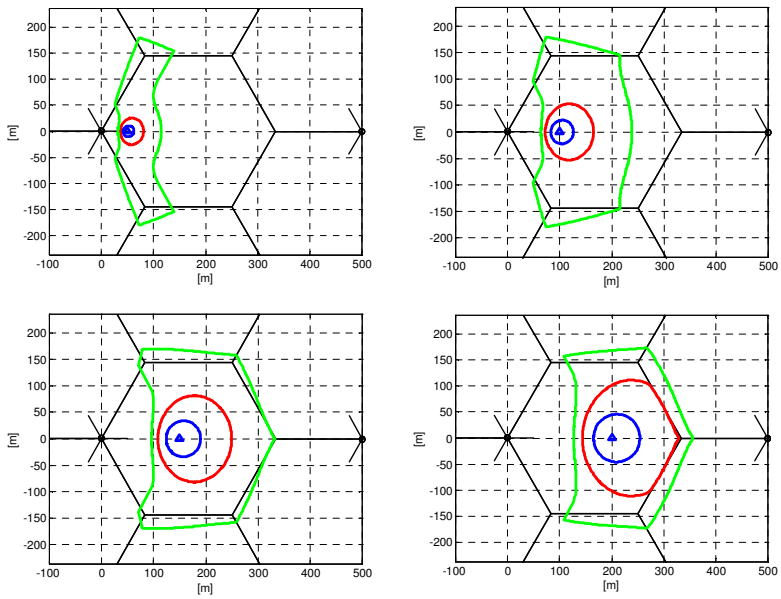


**Figure 3.3.** The size of the low-power cell service area depends on the location of the low-power site and the applied cell selection offset. 2-dimensional eNodeB antenna patterns are assumed.

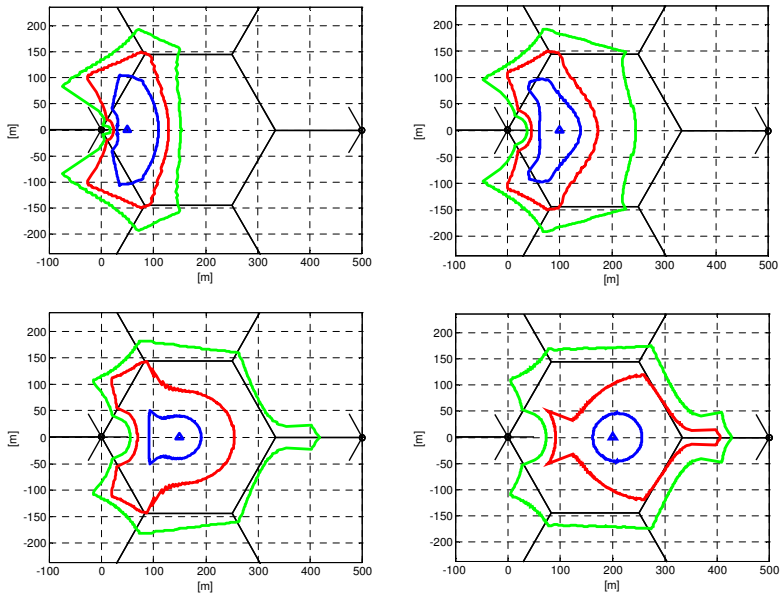


**Figure 3.4.** The size of the low-power cell service area depends on the location of the low-power site and the applied cell selection offset. 3-dimensional eNodeB antenna patterns are assumed.

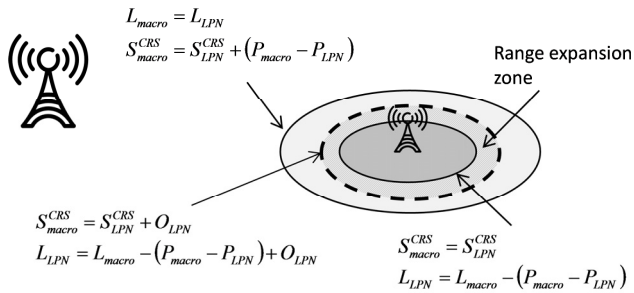


**Figure 3.5.** Description of the biased cell selection.

Taking also the vertical antenna gain into account, the corresponding micro cell service areas are depicted in Figure 3.4. The macro eNodeB antenna is assumed to have a vertical half-power beamwidth of 5 degrees, while the vertical half-power beamwidth of the omnidirectional micro eNodeB antenna is assumed to be equal to 148 degrees. As the macro cell signal strength is reduced for areas close to the macro site and close to the cell border, the micro cell coverage areas become considerably larger for those locations.

Next, two topics related to serving cell selection, i.e. biased cell selection, and link imbalance are discussed in more detail.

*Biased cell selection*

The footprint of a low-power cell can be expanded by adding a positive offset to the measured *RSRP* from the low-power node (LPN), see Figure 3.5. By doing so, the cell border moves closer to the border where the coupling losses are equal ("uplink cell border"). In case of *biased cell selection* (or *cell range expansion*), equation (3.1) can be rewritten as

$$CellId_{serving,m} = \arg \max_{b \in MUP} \{S_{m,b}^{CRS} + O_b\} \tag{3.3}$$

where $O_b$ is the cell selection offset applied for cell $b$. Assuming that $O_{macro}$ is equal to zero, UE can be defined to be located at the cell border between a macro and a low-power cell, if

$$S_{macro}^{CRS} = S_{LPN}^{CRS} + O_{LPN} \tag{3.4}$$

Assuming further that the cell-specific reference symbols (CRS) are allocated the same relative power in both cells, (3.4) can be rewritten as

$$P_{macro} - L_{macro}^{DL} = P_{LPN} - L_{LPN}^{DL} + O_{LPN} \tag{3.5}$$

where $P_{macro}$ and $P_{LPN}$ are the maximum output powers for the macro and the low-power eNodeBs, respectively. Furthermore, $L_{macro}^{DL}$ and $L_{LPN}^{DL}$ are the downlink coupling losses towards the macro and the low-power eNodeB, respectively. Looking at (3.5) it is quite straightforward to understand that if $O_{LPN} = P_{macro} - P_{LPN}$, the downlink cell border is co-located with the uplink cell border.

The advantages of biased cell selection include for example [121]:

- Enhanced uplink data rates. As a result of reduced uplink interference (see next section) and the fact that the uplink coupling loss is partially taken into account when associating users to the low-power node, uplink SINR is improved, which improves the achievable user bit rates.

- Increased capacity. As a result of the enhanced uplink data rates the uplink capacity will increase. However, even in downlink the gain of an increased traffic offloading from the macro to the low-power cell layer can outweigh the loss of not being able to receive transmissions from the strongest node.

- Relaxed low-power site deployment. By increasing the service area of a low-power node, the sensitivity to ideal placement within a traffic hotspot can be reduced.

The benefits gained from biased cell selection are highly dependent on the individual scenario, and in many cases, a modest cell range expansion is already sufficient. The downside of a biased cell selection is that if the applied cell selection offset is too large, the downlink performance will suffer. The reason for this is that a UE within the range expansion zone can experience very low downlink SINR. In particular, the low quality of the downlink control signaling will cause problems. Transmission of the downlink data symbols is less challenging as the ICIC methods supported by 3GPP LTE Release-8 can be utilized to ensure non-overlapping transmissions in the frequency domain.

*Link imbalance*

Let us assume the scenario depicted in Figure 3.6, where a cell border between a macro and a low-power eNodeB is shown. Furthermore, let us assume that UE1 is served by the low-power eNodeB, while UE2 is served by the macro eNodeB.

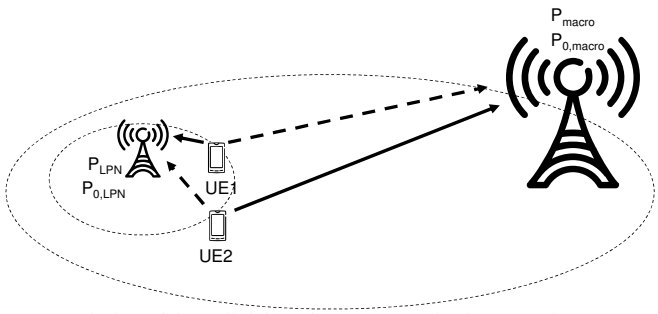


**Figure 3.6.** Description of the uplink interference scenarios between the macro and the low-power cell layer.

Assuming that the UE transmission powers are based on (2.1) with both Δ and $\delta$ equal to zero, the received uplink powers (per PRB) can be expressed as:

$$S_{1,LPN}^{UL,PRB} = P_{0,LPN} + \alpha_{LPN} L_{1,LPN}^{DL} - L_{1,LPN}^{UL} \tag{3.6}$$

$$S_{1,macro}^{UL,PRB} = P_{0,LPN} + \alpha_{LPN} L_{1,LPN}^{DL} - L_{1,macro}^{UL} \tag{3.7}$$

$$S_{2,macro}^{UL,PRB} = P_{0,macro} + \alpha_{macro} L_{2,macro}^{DL} - L_{2,macro}^{UL} \tag{3.8}$$

$$S_{2,LPN}^{UL,PRB} = P_{0,macro} + \alpha_{macro} L_{2,macro}^{DL} - L_{2,LPN}^{UL} \tag{3.9}$$

The problem with link imbalance can be demonstrated for example by comparing the level of interference generated by UE2 and the received signal power from UE1, measured at the low-power eNodeB and assuming that the downlink and uplink coupling losses are the same.

$$\begin{aligned} \gamma_{1,LPN} &= S_{1,LPN}^{UL,PRB} - S_{2,LPN}^{UL,PRB} \\ &= P_{0,LPN} - P_{0,macro} - (1 - \alpha_{LPN}) L_{1,LPN} \\ &\quad -\alpha_{macro} L_{2,macro} + L_{2,LPN} \end{aligned} \tag{3.10}$$

Based on (3.10), it is obvious that the signal-to-interference ratio $\gamma_{1,LPN}$ becomes worse together with an increased $L_{1,LPN}$ and $L_{2,macro}$, and/or reduced $L_{2,LPN}$. Therefore, to study the worst case scenario, let us assume that both UE1 and UE2 are located at, or very close to the cell border. Taking also the cell border definition in (3.5) into account,

$$L_{1,LPN} \approx L_{2,LPN} = P_{LPN} - P_{macro} + L_{macro} + O_{LPN} \tag{3.11}$$

Equation (3.10) can now be expressed as

$$\gamma_{1,LPN} = P_{0,LPN} - P_{0,macro} + \alpha_{LPN}(P_{LPN} - P_{macro} + O_{LPN}) + L_{macro}(\alpha_{LPN} - \alpha_{macro}) \quad (3.12)$$

As can be noticed, if $P_{0,LPN}$ would be equal to $P_{0,macro}$, the value of $\gamma_{1,LPN}$ would be reduced together with an increased difference between $P_{macro}$ and $P_{LPN}$. Applying a cell selection offset for the low-power cell would, however, improve the $\gamma_{1,LPN}$.

The impact of the low-power cell user on the uplink quality of the macro cell user can be evaluated by deriving the uplink signal-to-interference ratio for the macro cell user UE2:

$$\begin{aligned}\gamma_{2,macro} &= S_{2,macro}^{UL,PRB} - S_{1,macro}^{UL,PRB} \\ &= P_{0,macro} - P_{0,LPN} - (1 - \alpha_{macro})L_{2,macro} \\ &\quad -\alpha_{LPN}L_{1,LPN} + L_{1,macro}\end{aligned} \quad (3.13)$$

It is quite straightforward to see that $\gamma_{2,macro}$ increases if:

- $L_{2,macro}$ becomes smaller (UE2 moves closer to the serving macro eNodeB)
- $L_{1,LPN}$ becomes smaller (UE1 moves closer to the serving low-power eNodeB)
- $L_{1,macro}$ becomes larger (UE1 moves farther away from the cell border, i.e. closer to the serving low-power eNodeB)

As a worst case, let us again assume that both UE1 and UE2 are located at the cell border, and that $\alpha_{macro} = \alpha_{LPN} = 1$. Now, (3.13) can be expressed as

$$\gamma_{2,macro} = P_{0,macro} - P_{0,LPN} + P_{macro} - P_{LPN} - O_{LPN} \quad (3.14)$$

Hence, there will be a trade-off between the uplink quality of the low-power cell user and the macro cell user. As a summary, the uplink quality of the low-power cell user can be improved by:

- Increasing the output power of the low-power cell ($P_{LPN}$). As a result, the coverage area of the low-power cell will increase, leading to an increased traffic offloading from the macro to the low-power cell layer. Unfortunately, at the same time the uplink quality of the macro cell user will become worse.

- Increasing the uplink received power target for the low-power cell user ($P_{0,LPN}$). As a result, the transmission power of the low-power cell UE will increase, resulting in a worse uplink quality for the macro cell user.

- Applying a cell selection offset for the low-power cell ($O_{LPN}$). From the uplink point of view this will have the same impact as the increased $P_{LPN}$: increased low-power cell service area and increased traffic offloading, but at the same time a reduced uplink quality for the macro cell user.

### 3.2.2 Mobility management

Handovers are essential in order to provide a seamless service for users moving around within the system coverage area. Handovers can also be useful for load balancing purposes, i.e. when moving users at the border of adjacent or overlapping cells from the more congested cells to the less congested ones. In case of heterogeneous network deployments, there are at least three main challenges related to mobility management, as depicted in Figure 3.7:

- Handover from the macro cell to the low-power cell (scenario A).

- Handover from the low-power cell to the macro cell (scenario B).

- Users passing a low-power cell (scenario C).

As a result of the quite challenging propagation conditions, sometimes referred to as the *corner effects* (see Figure 3.8), the cell border between the macro and the low-power cell can be quite narrow, at least compared to the border area between two macro cells. This results in that the handover procedure becomes more sensitive to delays. In case of hand-in to the low-power cell, the risk is that before the handover procedure has been completed, the UE has moved too deep into the low-power cell area, causing excessive uplink interference towards the low-power cell users. Furthermore, in case of hand-out from the low-power cell, the risk is that the UE moves too far away from the serving low-power cell in order to receive the handover command in the downlink. A missed handover command can result in a radio link failure.

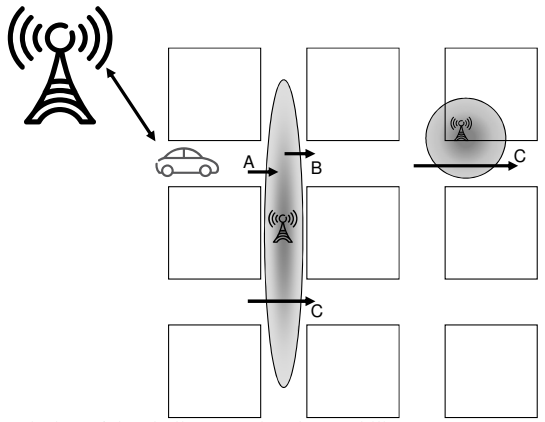


**Figure 3.7.** Description of the challenges related to mobility management within heterogeneous network deployments.

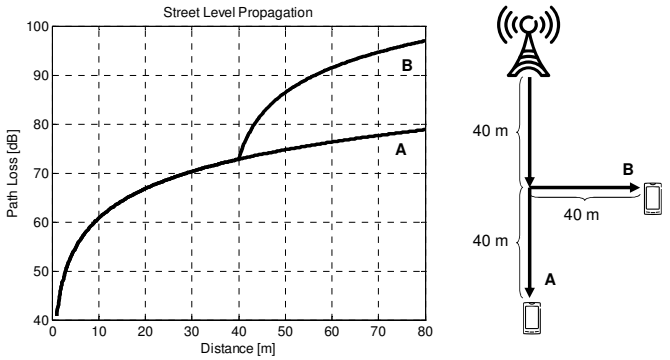


**Figure 3.8.** Street level propagation around a corner.

The third challenge is related to the fact that the coverage area of a low-power cell can in some cases be quite small compared to the speed of the user. This would then result in that the low-power cell would serve the user only for a short period of time. In order to save the signaling overhead, the system could in such scenarios consider the possibility to avoid handover from the macro to the low-power cell. However, the downside of the denied handover is that the inter-cell interference situation becomes worse. Both the downlink quality of the affected user, and the uplink quality of the low-power cell users will become worse, and most likely some interference management mechanisms are required to resolve the situation.

When it comes to the handover challenges within networks based on 3GPP LTE Release-8, many of the problems can be handled by carefully planning the network deployment, and adjusting the values of the various handover parameters. However, in case of the shared cell identity scheme [6][121], some new challenges arise. These are mostly related to the cell discovery in scenarios where all transmission points comprising a cell are

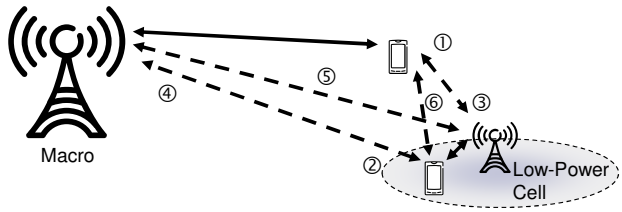


**Figure 3.9.** Inter-cell interference scenarios assuming both FDD and TDD mode of operation.

not transmitting CRS all the time. A more detailed discussion of this particular problem and the possible solutions is left out of this thesis.

The handover performance within a heterogeneous network deployment has been evaluated as part of the 3GPP LTE Release-11 standardization work. The obtained results can be found in [122].

### 3.2.3 Inter-cell interference management

The scope of the inter-cell interference management is to reduce the level of inter-cell interference, and by doing so, to improve mainly the cell-edge and average SINR and the corresponding user performance. The reduced inter-cell interference will of course benefit also the users close to the serving eNodeB, but since the quality of such users is typically very good, and often limited by the RF imperfections instead of the inter-cell interference, the achievable gains due to inter-cell interference management become quite limited.

There are six different inter-cell interference scenarios, see Figure 3.9, which are applicable to heterogeneous network deployments:

1. *Downlink interference from a low-power eNodeB to a macro cell UE*. This can be a problem if the low-power cell is operating in a CSG mode, and the macro cell UE is not allowed to connect to the low-power cell. Furthermore, there can be scenarios, where the macro cell UE is interfered by many close-by low-power eNodeBs.

2. *Downlink interference from a macro eNodeB to a low-power cell UE*. This can cause problems if biased cell selection is applied to the low-power cell. Furthermore, since the cell selection is based on the received downlink signal strength, a strong macro cell will limit the coverage area of the low-power cell.

3. *Uplink interference from a macro cell UE to a low-power eNodeB*. Due to the downlink transmission power difference, this will be a

problem as soon as the macro cell UE is close enough to the low-power eNodeB. The interference situation can become even worse if the low-power eNodeB is operating in a CSG mode.

4. *Uplink interference from a low-power cell UE to a macro eNodeB.* The impact of one low-power cell UE is quite small, unless a large cell selection offset is applied to the low-power eNodeB, or the low-power eNodeB is aggressively desensitized (high $P_{0,LPN}$ compared to $P_{0,macro}$). However, this kind of interference can become a problem if the macro cell contains a large number of low-power cells, since then there can potentially be several simultaneously scheduled low-power cell users generating interference under the same macro cell.

5. *Interference between a macro eNodeB and a low-power eNodeB.* In case of an unsynchronized TDD deployment, downlink transmission within cell 1 may overlap with uplink transmission within cell 2. Hence, downlink transmission from eNodeB 1 will interfere the uplink reception at eNodeB 2.

6. *Interference between a macro cell UE and a low-power cell UE.* In a scenario, where downlink transmission within cell 1 overlaps with uplink transmission within cell 2, uplink transmission of UE 2 will interfere the downlink reception of (potentially close-by) UE 1.

The scenarios 1-4 are common for both FDD and synchronized[1] TDD deployments, while scenarios 5 and 6 are applicable only for unsynchronized[2] TDD deployments. As discussed for example in [123]-[125] the performance of an unsynchronized TDD deployment will in many cases suffer from inter-cell interference, in particular for the uplink direction (i.e. interference scenario 5). Based on the findings in [125], unsynchronized TDD can be applicable for isolated pico cells, or for light-loaded scenarios, where the probability of neighboring cells containing simultaneously active users is low.

[1] Synchronized TDD deployment refers to a network deployment, where neighboring cells have the same UL:DL ratio and where the uplink slots in one cell are always aligned with the uplink slots in neighboring cells. Hence, if the impact of propagation delay differences is ignored, there will never be time instants when uplink slots are interfered by downlink slots from neighboring cells.

[2] In case of an unsynchronized TDD deployment, there are time instants when uplink slots in one cell are interfered by downlink slots from neighboring cells, or vice versa. This unsynchronization can be caused for example by different UL:DL ratios applied for the neighboring cells.

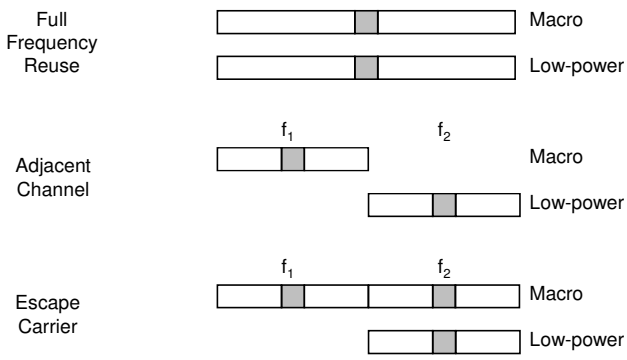


**Figure 3.10.** Description of the static spectrum allocation alternatives.

Next, some of the above interference scenarios are discussed in more detail, and some possible inter-cell interference management methods, available within 3GPP LTE Release-8, are introduced.

*Inter-cell interference management in frequency domain*

In case of the inter-cell interference management in frequency domain, the simultaneous transmissions from neighboring cells are allocated separate frequency resources. From the static spectrum allocation point of view, three different deployment alternatives can be defined, as described in Figure 3.10:

- *Full Frequency Reuse*. The low-power cell layer is operating on the same carrier frequency as the macro cell layer.
- *Adjacent Channel Deployment*. Macro and the low-power cell layer are operating on separate and non-overlapping carrier frequencies, either on the same or different frequency band.
- *Escape Carrier,* or *Partial Overlap*. Multiple carrier frequencies have been allocated to the macro cell layer. Low-power cell layer is reusing some of the macro carriers, leaving at least one macro carrier free from inter-layer interference.

*Full frequency reuse* (also known as *reuse-one* or *co-channel deployment*) is a spectrally efficient deployment, but the downside is that the cell-edge users may suffer from a high level of inter-cell interference in downlink, and may at the same time generate a high level of inter-cell interference in uplink. Deployment with *separate carriers* is quite efficient from the inter-cell interference point of view, but the spectral efficiency can be clearly worse than in case of a full frequency reuse. The *escape carrier deployment*

is a kind of a *fractional frequency reuse* scheme, where the cell-edge macro UEs are served on frequency $f_1$, while the other macro UEs can be served on frequency $f_2$. Users within the low-power cells are served only on frequency $f_2$. A normal inter-frequency handover is applied to move macro UEs between $f_1$ and $f_2$, depending for example on the level of experienced interference.

As already introduced in Section 2.2.4, 3GPP LTE Release-8 offers means to dynamically coordinate the frequency domain scheduling in neighboring cells. However, the downside of the Release-8 ICIC is that the transmissions of the downlink control signaling cannot be dynamically coordinated. A solution to this problem, carrier aggregation with cross carrier scheduling, is introduced in 3GPP LTE Release-10 [121].

*Inter-cell interference management in time domain*

In case of inter-cell interference management in time domain, neighboring cells are sharing the same frequency resources, but the cells are coordinated to avoid simultaneous transmissions. 3GPP LTE Release-8 does not offer any efficient means to dynamically coordinate transmissions in the time domain between different eNodeBs, i.e. over the X2-interface. However, coordination within an eNodeB is possible, for example with the help of a centralized scheduler.

Support for time domain ICIC (known as enhanced ICIC, eICIC) over the X2-interface is introduced in 3GPP LTE Release-10 [100]. The mechanism is enhanced further in 3GPP LTE Release-11 [121][126].

*Inter-cell interference management in power domain*

In case of inter-cell interference management in power domain, neighboring cells are sharing the same frequency resources, and are allowed to transmit at the same time, but their transmission powers are adjusted to reduce the level of inter-cell interference. This kind of method can be used to a) adjust the coverage area of a low-power cell, b) reduce the downlink interference from a CSG cell towards close-by non-CSG users, and c) reduce the uplink interference between a low-power cell and a macro cell. Next, cases b) and c) will be discussed in more detail.

During the standardization of home eNodeB, the need to have appropriate interference mitigation mechanisms was widely discussed [47][48]. However, no such mechanisms were standardized. Furthermore, the implementation of such methods was not mandated. Yet another fact limiting the possibilities of implementing highly dynamic ICIC, is that the

X2-interface between a macro eNodeB and a home eNodeB has not been defined before 3GPP LTE Release-11.

The need for downlink interference mitigation within the femto deployments is closely related to the introduction of CSG. When a user is located close to a CSG eNodeB, but is not allowed to connect to it, the non-CSG user will experience the CSG eNodeB as a source of downlink interference, resulting in an area, *dead zone*, around the CSG eNodeB where the downlink quality is poor. The most straightforward way to avoid this kind of inter-cell interference would be to allocate a separate carrier frequency, or separate carrier frequencies, for the CSG cells. The adjacent carrier attenuation would in most of the cases result in a sufficiently low level of inter-cell interference for an acceptable network operation. However, for scenarios where a co-channel deployment of CSG and non-CSG cells is desired, some power or time domain ICIC mechanisms are required.

Downlink interference problems can for example be mitigated by adjusting the maximum output power of the CSG femto eNodeB ($P_{CSG}$): a lower output power will result in a smaller dead zone for the non-CSG users and vice versa. Unfortunately, as the output power is lowered, the coverage area and the downlink performance of the CSG cell will become worse.

$$P_{CSG} = \max\left(P_{min,CSG},\ \min\left(P_{max,CSG}, P_{tx,CSG}\right)\right) \tag{3.15}$$

As indicated by (3.15), $P_{CSG}$ will typically be limited by a certain minimum and a maximum value. In order to protect the downlink reception of the close-by adjacent channel mobiles, in particular the ones being served by another operator, the LTE standard includes a requirement for the maximum allowed total transmission power for the different base station classes. For example, in case of a home base station class, the maximum allowed total transmission power is equal to 20 dBm (100 mW), while in case of the local area base station class it is specified to be equal to 24 dBm (250 mW) [111]. Furthermore, in case of the home base station class, the LTE standard includes also an additional limitation for the maximum allowed total transmission power as a function of the RSRP measured on an adjacent channel that belongs to another operator [111]. The main purpose of the second limitation is to enhance the protection of the UEs belonging to other operators for scenarios, where the adjacent channel RSRP is fairly weak, but still measurable. It is also worth noting that 3GPP LTE Release-10 introduces yet another limitation for the maximum allowed total transmission power of home base station class, namely as a function of the measured co-channel RSRP and uplink interference power [127]. In this

thesis, the femto eNodeBs are assumed to belong to the home base station class, and since no neighboring operators are modeled, $P_{max,CSG}$ is assumed to be equal to 20 dBm.

The value of $P_{min,CSG}$ is implementation-specific, i.e. the standard does not require that a home eNodeB should be able to lower its maximum output power to a certain level. In case of scenarios with a low macro cell interference, the value of $P_{min,CSG}$ is a trade-off between the inter-cell interference towards the close-by macro users and the minimum achieved femto cell coverage area: A higher $P_{min,CSG}$ will increase the femto cell coverage area and improve the performance of the femto users, but at the same time it will increase the interference towards the close-by macro users.

A number of different methods to control the CSG femto eNodeB output power have been discussed within 3GPP [128][129]:

- Power setting based on the strongest received macro eNodeB power at the femto eNodeB.
- Power setting based on the path loss between a femto eNodeB and a macro UE.
- Power setting based on objective SINR of the femto UE.
- Power setting based on objective SINR of the macro UE.

Since the methods listed above do not require any new UE measurements or air-interface signaling, they are applicable also for 3GPP LTE Release-8 UEs. Some of the methods do, however, require a possibility to exchange information between the cell layers. Furthermore, all of the methods assume that at least some of the algorithm parameters can be adjusted by the operator. Finally, it is assumed that the femto eNodeB is able to perform a number of downlink measurements on the neighboring macro cells, and potentially also on the neighboring femto eNodeBs [47]. Next, the first method is discussed in more detail.

The scope of the first method is to aim for a roughly constant CSG femto cell area independent on the location of the CSG femto cell with respect to the macro cell. Assuming that the received signal strength from the strongest macro eNodeB, measured at the femto eNodeB, is equal to $W_{macro}$, the femto eNodeB transmission power becomes equal to

$$P_{CSG} = \max\left(P_{min,CSG},\ \min\left(P_{max,CSG}, kW_{macro} + w\right)\right) \tag{3.16}$$

where $k$ is a linear scalar that allows the slope of the power mapping curve to be altered. Furthermore, the dynamic range of the power control can be adjusted via parameter $w$, which can be interpreted as the desired range of the CSG femto cell. In practice, the femto eNodeB will not be able to measure the $W_{macro}$. Therefore, a more practical approach for the femto eNodeB would be to perform RSRP measurements on the neighboring macro cells, define the appropriate CRS transmission power based on (3.16), and map that into the corresponding $P_{CSG}$.

The problem with this approach is that it is based on downlink measurements performed by the femto eNodeB, which do not necessarily reflect the interference situation at the border between the macro and the femto cell. Therefore, a simple two-step approach could be taken instead. During the first step, i.e. when the CSG femto eNodeB is initialized, $P_{CSG}$ is set based on the $W_{macro}$ estimated by the femto eNodeB. Later on, i.e. during the femto cell operation, the initial femto eNodeB measurements can be refined with the support of the corresponding femto UE measurements.

Another possible way to enhance the performance of the CSG power adjustment algorithm is to take the existence of any close-by victim UEs into account. If no victim UEs are detected, considerably less stringent limitations for the CSG femto eNodeB transmission power can be applied. The detection of the victim UEs could be done by the femto eNodeB [47], or based on the information provided by the neighboring eNodeBs (serving the victim UEs). In the latter case it is assumed that the cell layers are able to exchange information with each other.

Uplink interference between the low-power cell and the macro cell is caused by the link imbalance, as discussed in Section 3.2.1. Hence, as a result of the downlink transmit power difference, a macro user located close to the border between the macro and the low-power cell can cause a high level of uplink interference at the low-power eNodeB. In case of CSG, the non-CSG user can potentially come even closer to the low-power eNodeB resulting in worse uplink problems than with OSG.

The impact of this kind of uplink interference can be mitigated in the power domain by desensitizing the low-power cells. Desensitization can be achieved for example by introducing an *interference margin* for the uplink power control within the low-power cell so that

$$P_{0,LPN} = P_{0,macro} + i_{LPN} \tag{3.17}$$

Taking this into account, the signal-to-interference ratio in (3.12) can be re-written as

$$\gamma_{1,LPN} = i_{LPN} + \alpha_{LPN}(P_{LPN} - P_{macro} + O_{LPN}) + L_{macro}(\alpha_{LPN} - \alpha_{macro}) \quad (3.18)$$

Assuming that $\alpha_{macro} = \alpha_{LPN} = 1$, (3.18) becomes equal to

$$\gamma_{1,LPN} = i_{LPN} + P_{LPN} - P_{macro} + O_{LPN} \quad (3.19)$$

The main purpose of the interference margin is to reduce the impact of uplink interference from close-by macro UEs towards the low-power eNodeBs. Applying a higher $i_{LPN}$ will improve the uplink quality and further, the performance of the users within the low-power cells. The downside of the interference margin is that the uplink interference from the low-power cells towards the macro eNodeBs increases, reducing the performance of the macro users. This can be verified by expressing the uplink signal-to-interference ratio of the macro cell user, given in (3.14), as a function of the interference margin:

$$\gamma_{2,macro} = P_{0,macro} - P_{0,LPN} + P_{macro} - P_{LPN} - O_{LPN} = P_{macro} - P_{LPN} - O_{LPN} - i_{LPN} \quad (3.20)$$

Hence, the value of $\gamma_{2,macro}$ depends on the size of the interference margin $i_{LPN}$ with respect to the transmit power difference between the macro and the low-power nodes. A larger $i_{LPN}$ results in a lower $\gamma_{2,macro}$ and vice versa. Furthermore, if a cell selection offset is applied to extend the range of the low-power cell, the uplink interference towards the macro eNodeB is increased. A higher $P_{0,macro}$ could compensate for the additional uplink interference, but that would not help the situation for the power-limited cell-edge users served by the macro eNodeBs. A somewhat similar situation arises, when the number of users served by the low-power eNodeBs increases, e.g. as a result of an increased density of the low-power cells. As the number of simultaneously scheduled users under one macro cell increases, the total uplink interference could increase as well. Hence, a trade-off is required to balance the uplink interference between the different cell layers.

If the main goal is to enhance the performance of the worst users in the system, instead of aiming to maximize the overall system capacity, two key objectives can be highlighted:

1. Increasing the $P_{0,macro}$, whenever made possible by the traffic offloading from macro to low-power cells. Traffic offloading can motivate the use of a larger $P_{0,macro}$ for example when the low-

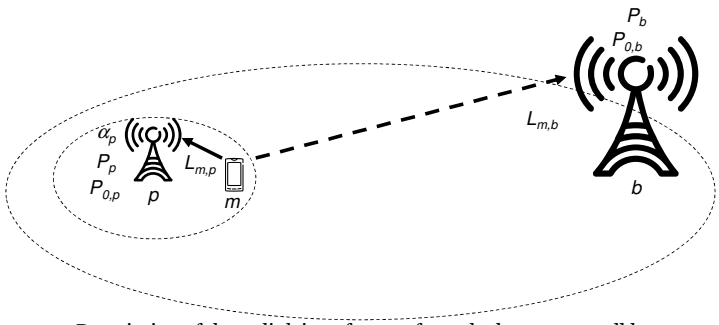


**Figure 3.11.** Description of the uplink interference from the low-power cell layer towards the macro cell layer.

power cells are offloading the most power-limited users from the macro cell. One possible way to realize this objective would be to monitor the level of power-limited macro mobiles in the system (or in a macro cell), and to adjust $P_{0,macro}$ accordingly.

2. Keeping the uplink interference from low-power cells under control, e.g. by limiting the value of the $P_{0,LPN}$. Other possible options to limit the interference towards the macro cells include the use of a lower $\alpha_{LPN}$ and the limitation of the maximum allowed UE transmission power ($P_{UEmax}$) within the low-power cells.

In order to discuss the second objective in more detail, let us start by looking at the level of uplink interference at macro eNodeB $b$, generated by a user $m$, which is served by a low-power eNodeB $p$ (see Figure 3.11):

$$I_{m,p,b}^{PRB} = P_{0,p} - (1 - \alpha_p)L_{m,p} - (L_{m,b} - L_{m,p}) \tag{3.21}$$

Based on the cell border definition:

$$L_{m,b} - L_{m,p} \geq P_b - P_p - O_p \tag{3.22}$$

where $P_b$ and $P_p$ are the maximum output powers of the macro and the low-power cell, respectively. Furthermore, $O_p$ is the applied cell selection offset for the low-power cell. As can be seen in (3.21), the uplink interference depends on:

- Coupling loss difference between the link from the low-power cell user towards the macro eNodeB and the link towards the serving low-power eNodeB ($L_{m,b} - L_{m,p}$). If the user moves away from the cell border, towards the serving eNodeB, the coupling loss

difference increases and the level of uplink interference is reduced. Hence, the users that are located close to the cell border are the most harmful.

- Assumed $P_0$ at the low-power cell: a higher $P_{0,p}$ will result in higher uplink interference and vice versa. In order to limit the level of interference, the applied $P_{0,p}$ can be limited either on the cell, or on the user level. The latter means that the $P_{0,p}$ is reduced only for the users that are located sufficiently close to the cell border, i.e. the ones that would otherwise generate too high level of uplink interference towards the macro cell.

- Assumed $\alpha$ at the low-power cell: a higher $\alpha_p$ will result in higher uplink interference and vice versa. If the uplink interference is adjusted by adjusting the value of $\alpha_p$ it should most likely be coupled with the adjustment of the $P_{0,p}$ in order not to harm the overall uplink performance within the low-power cell too much.

What is not directly visible in (3.21) is the impact of the maximum UE transmission power limitation. As can be noticed in (2.1), the UE transmission power increases together with the increased path loss towards the serving eNodeB. By adjusting the $P_{UEmax}$ within the low-power cell, the interference towards the macro cell can be limited.

Finally, in order to derive an expression for the applied $P_0$ within the low-power cell ($P_{0,p}$), let us first focus on the maximum allowable $P_0$ for an individual user ($P_{0,m,p}$). From (3.21)

$$P_{0,m,p} = I_{m,p,b}^{PRB} - \alpha_p L_{m,p} + L_{m,b} \tag{3.23}$$

The received interference power $I_{m,p,b}^{PRB}$ can be expressed also as a relation to the $P_0$ value applied at the macro eNodeB ($P_{0,b}$):

$$P_{0,m,p} = P_{0,b} + \phi_{m,p,b} - \alpha_p L_{m,p} + L_{m,b} \tag{3.24}$$

Hence, assuming the same (maximum allowed) $P_{0,b} + \phi_{m,p,b}$ for all users within a low-power cell, the closer to the serving eNodeB $p$ user $m$ is, the higher $P_{0,m,p}$ can be allowed.

Instead of applying user-specific $P_0$ values, it may be more practical to apply the same $P_0$ for all users within the low-power cell. In order to derive an expression for the cell-specific $P_0$ ($P_{0,p}$), let us assume that UE $m$ is

located at the border between the low-power and the macro cell. Hence, (3.24) becomes equal to

$$P_{0,p} = P_{0,b} + \phi_{p,b} + (1 - \alpha_p)L_{m,p} + P_b - P_p - O_p \quad (3.25)$$

or alternatively

$$P_{0,p} = P_{0,b} + \phi_{p,b} + (1 - \alpha_p)L_{m,b} + \alpha_p(P_b - P_p - O_p) \quad (3.26)$$

In practice, the system can include multiple simultaneously active low-power cell users that are generating interference towards the same macro cell. This means that the maximum tolerable $\phi_{p,b}$ will depend both on the density of the low-power cells and the network load, i.e. how likely it will be that a low-power cell has an active user. However, as a result of the increased density of the low-power cells, also the traffic offloading will increase. The traffic offloading could enable the use of a higher $P_{0,b}$, which would make the remaining macro users more tolerable against an increased $I_{m,p,b}^{PRB}$. Yet another thing to take into account when defining the target value for $\phi_{p,b}$ is the fact that the interfering low-power cell users are typically located within the low-power cell area, and not on the worst case positions on the cell border as assumed in (3.25) and (3.26).

As a summary, the appropriate $P_0$ for the low-power cell depends on the following:

- The density of the low-power cells. On one hand, a higher density of low-power cells can increase the average uplink interference towards the macro cells, implying a lower $\phi_{p,b}$. On the other hand, the increased traffic offloading could allow the use of a higher $P_{0,b}$.

- The network load. As a result of the increased network load, average uplink interference towards the macro cell layer increases, which leads to a lower $\phi_{p,b}$ and hence, a lower $P_{0,p}$.

- The transmit power difference between the cell layers. An increased transmission power for the low-power cell increases the coverage area, as well as the traffic offloading, which both lead to a lower $P_{0,p}$ (lower $\phi_{p,b}$).

- The applied cell selection offset. The use of a larger cell selection offset will increase the size of the low-power cell, as well as the traffic offloading, leading to a lower $P_{0,p}$ (lower $\phi_{p,b}$).

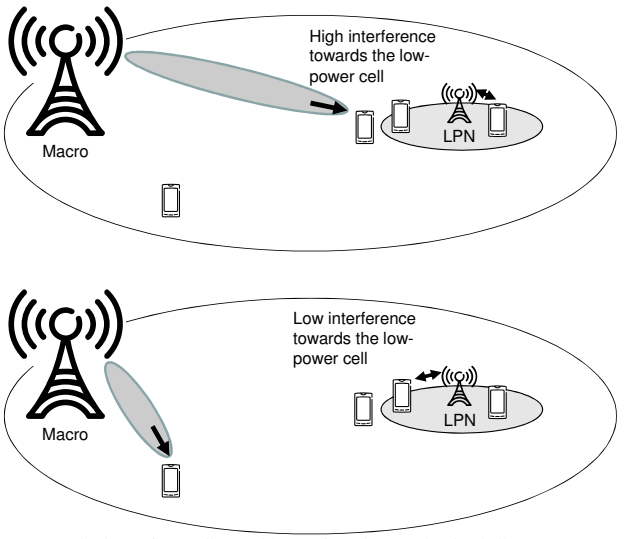


**Figure 3.12.** Description of coordinated beamforming and scheduling.

Very recently, the topic of coordinated $P_0$ values between the macro and co-channel low-power cells has been discussed and evaluated in [130] and [131]. The obtained conclusions are similar to the ones listed above.

*Inter-cell interference management in spatial domain*

In case of inter-cell interference management in spatial domain, inter-cell interference is reduced with the help of beamforming, or other multi-antenna techniques. 3GPP LTE Release-8 does not offer any efficient means to perform coordinated interference management in spatial domain, at least not over the X2-interface. 3GPP LTE Release-10 and Release-11, however, introduce a concept called the coordinated multipoint transmission and reception (CoMP), which includes features to coordinate the transmissions from multiple transmission points in the spatial domain [132][133]. One such feature is the coordinated beamforming and scheduling, see Figure 3.12, which means that the beamforming weights of the interfering transmission points are selected so that the inter-cell interference is minimized.

# 4. Introduction to the system simulator platform

This chapter provides an introduction to the system simulator platform used in this thesis. Detailed descriptions of both the assumed network deployments and simulator models are given. Furthermore, the main simulation parameters are listed and discussed.

Unless stated otherwise, the equations presented in this chapter are expressed in the linear domain.

## 4.1 Modeling of system simulators

In practice it is computationally impossible to perform large-scale system simulations with a single simulator approach. This is due to the fact that such simulator would require modeling of a) a single radio link with modulation waveforms, coding/decoding and other transmitter/receiver algorithms, b) radio network with a possibly large number of base stations and a high number of mobile stations generating traffic and interference and transmitting signals, and c) different kinds of radio protocols. In addition, an accurate evaluation of the radio link performance requires simulations on the symbol level, while the evaluation of traffic and mobility models require long simulations with a large number of base stations and mobiles. Simulations with high resolution and long duration would lead to extremely long simulation times. Therefore, the system simulator has to be divided into smaller parts each specified to their specific tasks. An example of such division is a link level simulator, a radio network level simulator and a protocol level simulator.

System simulation involves several fundamental parts that are modeled and implemented to the simulator: traffic models, mobility models, wave propagation models (antennas, multipath environment, distance-dependent propagation, shadow fading), network layout, multiple access dependent modeling and modeling of radio resource management (RRM)

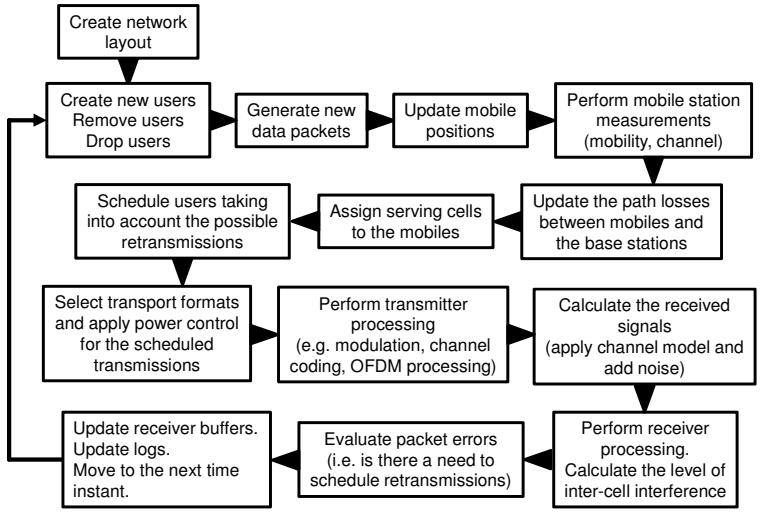


**Figure 4.1.** Description of a dynamic system simulator.

algorithms. A simulator may employ all of the models or only a sub-set of them.

A radio network simulator can be static or dynamic. A static simulator refers to a simple system simulator with no user mobility or traffic models, while a dynamic simulator is a system simulator with a detailed modeling of the dynamic behavior of the radio network, as shown in Figure 4.1. Generally speaking, a static system simulation can be seen as a snapshot of a time-dynamic system. Both methods have their pros and cons, and one cannot replace the other. Static simulations are typically used to obtain rough and fast estimates of the performance of both the individual users and the system as a whole. Dynamic simulations are required in particular when developing and evaluating the performance of various radio resource management algorithms, or when evaluating the impact of different traffic models.

One traditional and efficient way to simplify and speed up system simulations is to run separate link and system level simulations. Link level simulations and simulators are needed to build models, which predict the receiver performance, e.g. in terms of packet error rate (PER), taking into account various link level aspects such as channel estimation, interleaving and decoding. The system level simulations are needed to model a system with a large number of mobile terminals and base stations, and algorithms operating in such a system.

Due to the fact that the overall simulation is divided into two parts, a method to interconnect the two simulators has to be defined. This method is often called as the *link-to-system interface*. Traditionally, a so-called

*average value interface* has been assumed, where the (average) reception error probability is given as a function of the average SINR of the received signal. Alternatively, the interface can provide a mapping between the average SINR and the corresponding average (achievable) bit rate, see for example the model defined in [134]. The average value interface is not accurate if there are fast changes in the channel conditions or interference, which means that it is suitable for static simulations. Dynamic simulations including fast resource scheduling and fast link adaptation require a more accurate link performance model accounting for the instantaneous channel and interference conditions. Examples of such link performance models can be found for example in [135].

What is also very typical for system simulations, is that the obtained simulation results are tightly coupled with the simulation scenario, models and assumptions. Taking this aspect into account, system simulations can be categorized in the following way:

- *Technology benchmarking*. This category contains fair technology comparisons, focusing primarily on the relative results. The evaluations are usually based on agreed and harmonized models and assumptions. For example, most of the technology comparisons performed within the 3GPP belong to this group.

- *Case studies*. The level of realism is increased compared to the technology benchmarking, and scenario-specific models and parameters are assumed. Some of the applied models are still ideal, while the others are a bit more realistic, taking for example the RF imperfections and measurement errors into account. The simulations performed for this thesis are good examples of typical case studies.

- *Deployment studies*. The aim is to visualize the expected system performance in a practical deployment scenario. The simulations are based on real network data (obtained directly from the operator and/or via measurements), three-dimensional maps, building database, and traffic measurements collected from the live network. Furthermore, the link performance of both the base stations and the mobile stations is modeled as accurately as possible.

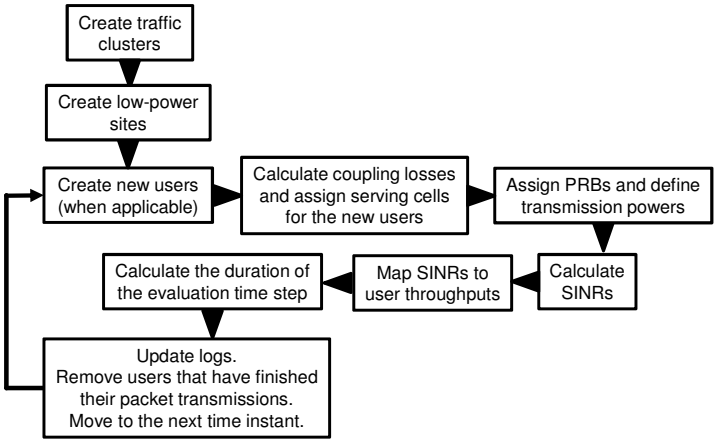


**Figure 4.2.** An overview of the simulation flow during a semi-static snapshot.

## 4.2 Description of the assumed system simulator platform

The system simulator platform assumed in this thesis is a mixture of a static and a dynamic system simulator. This kind of a semi-static (or semi-dynamic) system simulator models the arrival and removal of users, as well as packet transmissions, but not the mobility of the users. Furthermore, fast radio resource management, such as the user scheduling, is not modeled in detail. In all, the assumed simulator platform is mainly targeted for comparing the performance of the various network deployment alternatives from the coverage and capacity point of view.

For each of the simulated scenarios, results are collected from a desired number of snapshots. Nearly all of the simulations in this thesis assume semi-static snapshots, which means that during a snapshot the system is simulated for at least 30 seconds. An overview of a semi-static snapshot is given in Figure 4.2. In the beginning of each snapshot, the desired number traffic clusters are generated within the system area defined by the size of the macro cell layer. Furthermore, the desired number of low-power sites are created within the traffic clusters. The semi-static snapshot is divided into a number of evaluation time steps, which are assumed to be considerably longer than the TTI of 1 ms. During these evaluation time steps, user traffic (i.e. packet transmissions) is modeled, new users are created and old users are removed in order to model the impacts of dynamically variable levels of inter-cell interference and serving cell load on the observed user performance. However, the users are assumed to be static (i.e. not moving) and only an average impact of the fast radio resource management is taken into account. Finally, the performance of each active

user is estimated and the contents of the transmission and reception buffers are updated accordingly.

For some special cases, mostly related to estimating preferred values for some simulation parameters, the system performance is evaluated with static snapshots, i.e. by ignoring the time-domain modeling of both the user traffic and the inter-cell interference.

The various simulation steps are described in more detail in the following sub-sections.

### 4.2.1 Deployment scenario

Reference [56] defines a number of scenarios and models for heterogeneous network simulations, which have been widely used both within and outside the 3GPP. However, since each of the scenarios considers only one specific type of heterogeneous network deployment, their applicability for fair comparisons between the different deployment alternatives can be questioned. Therefore, a slightly different type of modeling is assumed in this thesis.

The assumed model can be seen as a combined and an enhanced version of [56] and the dual-strip model presented in [61]. The main difference compared to [56] is related to the modeling of the traffic hotspot, both when it comes to the user and the eNodeB locations within the traffic hotspot, and the wave propagation between the nodes. Furthermore, a three-dimensional model of both the user locations and the wave propagation is introduced. The purpose of the changes is to enable more reliable performance comparisons for deployment scenarios, where the environment and traffic distribution is assumed to be fixed, but the types and the locations of the eNodeBs are varied. Further benefits of the advanced model include for example a variable number of traffic hotpots per macro cell, variable locations of the traffic hotspots with respect to the macro site, building-to-building wave propagation within a traffic hotspot and a correlation between the locations of the residential users and the femto eNodeBs. The assumed model is simplified in the sense that all traffic hotspots look alike, both when it comes to the total number of floors, sizes of the floors and the distribution of the public and the residential floors.

In an urban environment large part of the mobile broadband traffic will typically be clustered within buildings. In order to model that, the simulated system area has been divided into 100 m × 100 m bins, where each bin can either be a *traffic cluster* (i.e. a traffic hotspot) or an *outdoor bin*. A traffic cluster bin contains two identical, five-floor buildings, as described in Figure 4.3 and Figure 4.4. Each floor is assumed to contain a

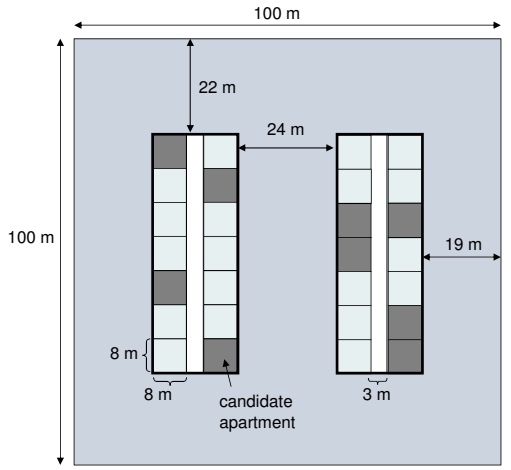


**Figure 4.3.** Horizontal layout of a traffic cluster bin. The residential indoor traffic is assumed to be originated only from a sub-set of apartments, the so-called candidate apartments, which are highlighted with a darker color.

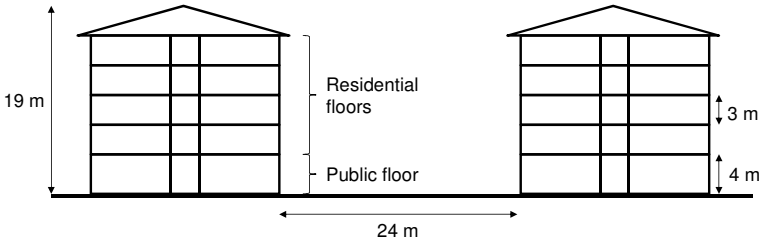


**Figure 4.4.** Vertical layout of a traffic cluster bin. Both buildings are assumed to have five identical floors. The ground floor is assumed to contain public indoor areas, while the other four floors are assumed to contain residential apartments.

total of 14 apartments of 64 m$^2$ in size. Furthermore, the ground floor is always assumed to be "public", i.e. it is assumed to contain shops, offices, restaurants, cafes and similar indoor areas. Hence, each traffic cluster contains a total of 112 residential apartments[3]. The height of the ground floor is assumed to be equal to 4 meters, while the height of the residential floors is assumed to be equal to 3 meters. In all, the height of each building is assumed to be equal to 19 meters.

The population density within the simulated area is assumed to be equal to 10000 persons per square kilometer, which is assumed to correspond to an urban environment, roughly equal to downtown Stockholm [136] or areas just outside the center of London (e.g. Camden [137]). Assuming an average of two persons per household, the assumed population density corresponds to 5000 households (residential apartments) per square kilometer, which results in an average of 45 traffic clusters per square

[3] Two buildings, four residential floors per building, 14 apartments per floor.

kilometer[4]. It should also be noted that the density of traffic clusters is kept constant during the simulation runs but their locations are selected randomly for each snapshot, assuming a uniform distribution over the system area.

As a default, the service penetration is assumed to be equal to 90% and the operator market share is assumed to be equal to 30%. Based on these values, it is assumed that 27% of the residential apartments, the so-called *candidate apartments*, can contain residential users. In Figure 4.3, the candidate apartments are highlighted with a darker color. Keeping in mind the assumption of 5000 residential apartments per square kilometer, the density of candidate apartments becomes approximately equal to 1350 apartments/km$^2$.

Although not specifically modeled, an outdoor bin can also be assumed to contain non-residential buildings. Furthermore, they can also contain indoor users that are served by specific in-building solutions operating on a different band or even on a different radio access technology compared to the evaluated system. In all, the main assumption is that during a snapshot an outdoor bin does not contain any indoor users that could potentially be served by the macro cells or by the close-by low-power cells.

The simulated urban macro cell layer consists of seven three-sector sites in a homogeneous hexagonal pattern. A wrap-around technique is applied to remove border effects that may otherwise arise due to the limited size of the simulated system [138]. As a default, an inter-site distance (ISD) equal to 500 meters is assumed (the so-called *baseline deployment*), which means that each macro cell includes an average of 3.2 traffic clusters. Furthermore, the antennas are assumed to be deployed at a height of 24 meters, i.e. 5 meters above the rooftops.

Outdoor micro sites are assumed to be located only within the traffic clusters. Furthermore, the micro sites are always located in between the two buildings, at a distance of 4 meters from the closest building wall, as illustrated in Figure 4.5. In the simulator, the micro site density is defined as the average number of micro sites per traffic cluster. If the assumed average density of micro sites is less or equal to one site per traffic cluster, a traffic cluster can have a maximum of one micro site, and the affected traffic clusters are selected randomly. If the assumed density of micro sites is larger than one, then each traffic cluster contains at least one micro site. Furthermore, the clusters that contain also a second micro site are selected randomly.

[4] This results in a scenario, where an average of 45% of the bins are traffic clusters and the remaining 55% are outdoor bins.

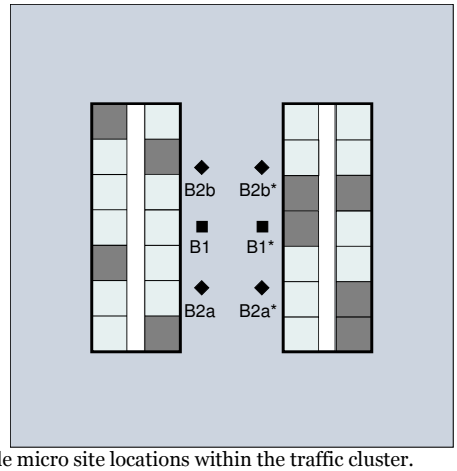


**Figure 4.5.** Possible micro site locations within the traffic cluster.

If a traffic cluster has one micro site, it is located in the center of the traffic cluster, on either side of the street area between the buildings (locations B1 and B1* in Figure 4.5). If a traffic cluster has two micro sites, they are located off the center of the traffic cluster in order to improve the micro cell coverage at both ends of the buildings. Again, the side of the street is randomly selected for each micro site (locations B2a and B2a* for the first micro site, B2b and B2b* for the second micro site, see Figure 4.5).

Residential femto sites are assumed to be located within the candidate apartments, as illustrated by the stars in Figure 4.6. Location of the femto eNodeB within the candidate apartment is selected randomly. Furthermore, the height of the femto eNodeB antenna is assumed to be 1.5 meters above the floor level. The density of femto eNodeBs is expressed as *femto penetration*, which is defined as the percentage of the candidate apartments including a femto eNodeB. For example, if the femto penetration is equal to 50%, then half of the candidate apartments include a femto eNodeB. Since the evaluated system area is assumed to have 1350 candidate apartments per square kilometer, femto penetration equal to 50% corresponds to a density of 675 femto eNodeBs per square kilometer.

### 4.2.2 User distribution and traffic model

In case of data services, for example file transfer (FTP), much larger portion of the users can be assumed to be located indoors compared to for example the voice service. Therefore, the simulations in this thesis assume that 80% of the users are located inside buildings, and 20% of the users are located inside vehicles. Indoor users can be located only within the traffic clusters, assuming a uniform distribution between the buildings and all floors,

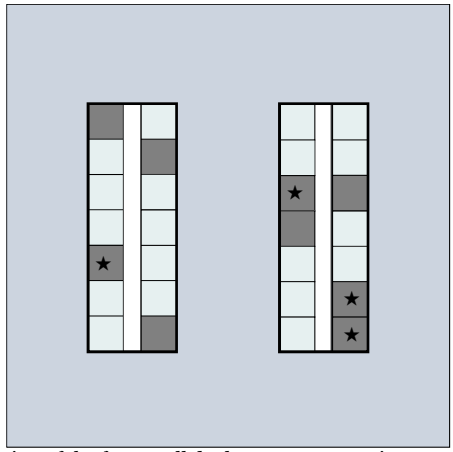

**Figure 4.6.** Description of the femto cell deployment. Femto sites are assumed to be deployed always within the candidate apartments.

including also the public areas on the ground floors. In practice this means that 64% of the users are located inside the residential candidate apartments, 16% within the non-residential ground floor areas and 20% inside vehicles. The in-vehicle users are uniformly distributed over all bins. Keeping in mind the 45/55 distribution between the traffic clusters and the outdoor bins, it can be estimated that 89% of the total traffic is generated within the traffic hotspots.

New users are created at random locations within the system area, following the desired indoor/in-vehicle user ratio. User mobility is not modeled, meaning that during the life-time of a user, the location of the user stays the same. A simple packet transmission model is assumed for the semi-static snapshots, whereas a full buffer traffic model is assumed for the static snapshots. The assumed packet transmission model is similar to the FTP traffic model 1 in [56], i.e. each user is assumed to download or upload a packet with a fixed size of 500 kilobytes, after which the user leaves the system. Since each user is assumed to generate an equal amount of traffic, the overall traffic distribution will follow the locations of the users. Keeping also in mind that the simulator does not model any visiting residential users, the overall traffic distribution could be interpreted also so that a certain subscriber consumes 64% of the traffic at home, 16% within non-residential indoor locations and 20% inside vehicles.

The assumption of a uniform traffic distribution between subscribers may be sufficient for network dimensioning purposes, but it does not necessarily reflect the reality, where the amount of monthly traffic can have large variations between the subscribers. Therefore, in Section 7.4 the impact of non-uniform user traffic is briefly evaluated. For that evaluation, the simulator is enhanced with a model for *traffic-heavy subscribers*. The

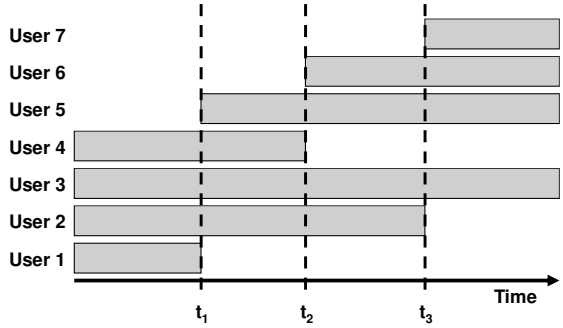


**Figure 4.7.** Description of the default user generation process, where the number of new users is equal to the number of removed users.

implemented model is based on two fundamental assumptions: a) 20% of the subscribers generate approximately 80% of the total traffic, and b) the distribution of the total traffic between the residential indoor, non-residential indoor and in-vehicle locations is kept intact. By doing so, only the distribution of the residential traffic needs to be modified compared to the simulations with uniform subscriber traffic. For the residential part, the assumption that 20% of the subscribers generate approximately 80% of the traffic means that 20% of the candidate apartments (the so-called *traffic-heavy apartments*) generate approximately 50% of the total traffic, while the remaining 80% of the candidate apartments generate 14% of the total traffic. In all, the total traffic distribution becomes now: 50% in traffic-heavy apartments, 14% in the other candidate apartments, 16% in non-residential indoor areas and 20% inside vehicles. In the simulator, the traffic-heavy apartments are selected randomly for each snapshot.

The assumed user distribution will affect two things: a) distribution of the coupling losses between the users and the eNodeBs, and b) the ability of the low-power cells to offload users from the macro cells. The first one is a result of the fact that if a large portion of the users are located indoors, also the coupling losses towards outdoor eNodeBs are typically larger compared to a scenario where most of the users are located outdoors. The latter can be motivated by the fact that if the users are clustered into traffic hotspots, it becomes easier to offload traffic from the macro cells by deploying low-power cells.

During the semi-static snapshot, new users are as a default created following the number of removed users as described in Figure 4.7. In the figure, user 1 finishes its packet transmission at time instant $t_1$, while users 2, 3 and 4 have still data left to transmit. User 1 is removed and a new user, user 5, is created at a random position within the system area (independently of the location of the removed user 1). Based on the evaluated user throughputs (for users 2, 3, 4 and 5) and the amount of data

left in the transmission buffers, user 4 is estimated to be the next one to finish its transmission at time instant $t_2$. After user 4 has been removed, user 6 is created. Finally, at time instant $t_3$, user 2 is removed and user 7 is created. The benefit of this kind of approach is that the number of simultaneously active users (within the system area) is kept constant, and the system stability maintained also at high levels of network load. The drawback is that the level of offered area traffic will depend on the observed user performance. Furthermore, even though the total number of active users stays constant within the system area, there can be large variations when it comes to the number of users simultaneously served by individual cells.

In some special cases, where a fixed level of offered area traffic is desired, independently of the system performance, new users are created according to a Poisson process as described in [138]. Hence, in this case the input to the system simulation is not the total number of simultaneously active users as in the previous case, but the offered area traffic expressed as GB/h/km$^2$. In the simulator, the desired offered area traffic is then mapped to the corresponding user arrival rate, keeping in mind that each user is assumed to transmit a packet with a fixed size of 500 kilobytes. It should be noted that with the Poisson process method, the number of simultaneously active users is varying during the snapshot. Therefore, a simple user dropping model has been implemented in order to maintain the system stability also at high levels of offered area traffic, and to avoid excessive queue build-up. In the model, a user is dropped if the average user throughput is found to be below a pre-defined threshold.

The two different methods to create new users, fixed number of simultaneously active users and the Poisson process, are compared in Figure 4.8 and Figure 4.9. The evaluation is performed for the baseline deployment, and either the same average number of simultaneously active users (an average of 0.6 simultaneously active users per cell, i.e. a total of 13 simultaneously active users within the system area) or the same level of served area traffic (50 GB/h/km$^2$) has been assumed for both methods. Assuming the same average number of simultaneously active users, the Poisson process method results in a better average user performance (30.4 Mbps versus 28.4 Mbps), but in a worse performance of the worst 5$^{th}$ percentile of the users (3.3 Mbps versus 4.1 Mbps). In addition, the Poisson process method results in a lower level of the served area traffic (46 GB/h/km$^2$ versus 50 GB/h/km$^2$) compared to the method based on a fixed number of simultaneously active users. This is due to the fact that most of the time the Poisson process results in a lower than average number of simultaneously active users, leading to lower level of cell utilization, and

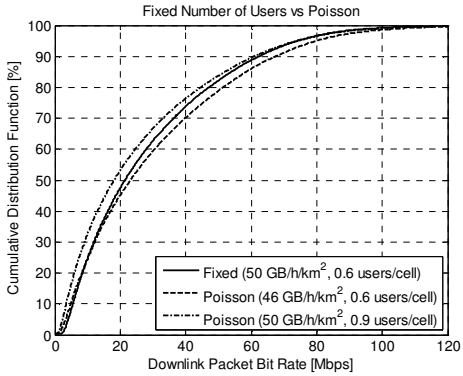


**Figure 4.8.** Comparison of the different user generation processes from the downlink user performance point of view.

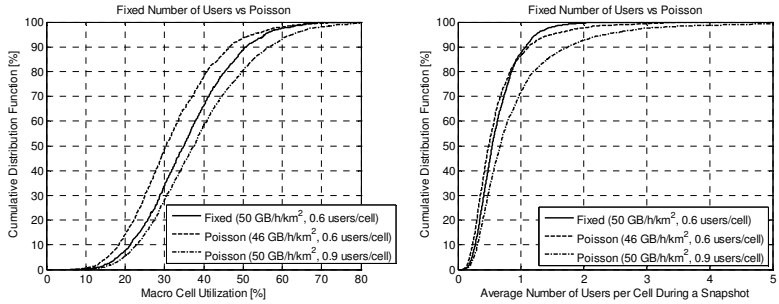


**Figure 4.9.** Comparison of the different user generation processes from the network load point of view.

further to a lower level of inter-cell interference. However, during some periods of time the number of simultaneously active users is clearly higher than the average, which hurts the statistics for the worst 5$^{th}$ percentile of users.

When the same level of served area traffic is assumed for both methods, the approach with a fixed number of simultaneously active users results in a slightly better average user performance (28.4 Mbps versus 25.9 Mbps). For the worst 5$^{th}$ percentile of users the difference becomes larger (4.1 Mbps versus 2.3 Mbps). As demonstrated by the results in Figure 4.9, the reason for this performance difference is that for the same level of served area traffic, the network load, both in terms of average cell utilization and the average number of simultaneously active users per cell, becomes higher with the Poisson process method.

### 4.2.3 Propagation models

Path loss between a macro eNodeB and an outdoor UE position is calculated using the model defined in [139]. A deployment with remote radio units (RRUs) is assumed, which means that the feeder loss between the eNodeB and the antenna can in practice be neglected. A three-dimensional macro eNodeB antenna model [140] is assumed, with a maximum antenna gain equal to 18 dBi. Furthermore, the macro eNodeB antennas are assumed to be downtilted to improve the system performance. The downtilt angle is adjusted together with the assumed inter-site distance.

The building penetration loss is based on the non-line-of-sight penetration model defined in [141]. The model assumes an average loss of 12 dB for the penetrated outer wall. Furthermore, the inner wall and furniture losses are taken into account with a simple model resulting in an additional loss equal to $0.8d_i + 10w_i$ dB, where $d_i$ is the indoor distance and $w_i$ is the number of penetrated thick walls, as drawn in Figure 4.3. This same wall loss model is applied also for all the other propagation models, when applicable. Finally, the macro propagation includes also a model for the floor height gain [141], equal to 0.7 dB/m, with respect to the ground floor level.

Micro and femto eNodeB antennas are assumed to be omnidirectional with maximum antenna gains equal to 5 dBi and 2 dBi, respectively. The applied micro propagation within a traffic cluster follows the recursive model in [142], while the propagation between the bins is calculated using the model defined in [139]. The micro-cellular building penetration is calculated as a combination of the non-line-of-sight penetration model, and the line-of-sight penetration model described in [141] and [143]. For the line-of-sight model, the outer wall penetration loss is assumed to be in the range of 7-27 dB [141], depending on the angle of penetration.

The applied indoor propagation model is based on the multi-wall model defined in [141]. In addition to the already described model for the wall and furniture losses, the floor penetration loss follows the model in [141], assuming that the loss for the first penetrated floor is equal to 18.3 dB [56].

Finally, a log-normal shadow fading component is also added for all links. However, fast fading is not modeled. Therefore, the results can be viewed as the performance averaged over a sufficiently long time period. The standard deviation of the shadow fading component is assumed to be equal to 8 dB for macro propagation, and equal to 10 dB for micro and indoor propagation.

A more detailed description of the applied propagation models is provided in Annex B.

### 4.2.4 Radio resource management models

In case of macro, micro and open access (OSG) femto cells, the serving cell selection is based on the received downlink signal strength (RSRP). The user is assumed to be served by the strongest cell, taking a 3 dB handover margin into account. The handover margin is modeled so that the serving cell is randomly selected from the group of candidate cells consisting of the strongest cell as defined by (3.3), and all the other cells that are not more than 3 dB weaker than the strongest cell. The cell selection offset is assumed to be equal to zero as a default for all cells.

In case of CSG femto cells, only the users that are located within the same apartment as the femto eNodeB are allowed to connect to it. Furthermore, the normal RSRP-based cell selection criterion has to be fulfilled. A simplification is that the simulator does not model any visiting users, i.e. users that are located within a femto apartment, but are not included in the CSG. Similarly, the model does not consider scenarios, where some of the CSG users are located just outside the femto apartment. Hence, it is assumed that the CSG femto cells are not able to offload any in-vehicle users, users located within the non-residential indoor areas, or users located within residential non-femto apartments.

The simulator does not model the TTI structure in detail. Instead, the performance of each active user is evaluated only at time instants, when new users are entering, or old users are leaving the system (e.g. time instants $t_1$, $t_2$ and $t_3$ in Figure 4.7). In between those time instants, the system is assumed to be static. Therefore, the simulator considers only the average impact of the time domain scheduling; both for the uplink inter-cell interference (as discussed in Section 4.2.5) and for the mapping between the achievable bit rate and the user throughput (see Section 4.2.6).

For simplicity, no frequency domain multiplexing of users is assumed in the downlink. Thus, only time domain scheduling of users is assumed, and each scheduled user is assigned all resource blocks and all eNodeB transmission power.

In case of uplink, the simulator models both open loop power control and frequency domain multiplexing of users. Based on (2.1), the transmission power for UE $m$ served by eNodeB $b$ is calculated as:

$$P_{m,b} = \min\{P_{UEmax}, P_{0,b} + 10\log_{10}(M_{m,b}) + \alpha_b L_{m,b}^{DL}\} \quad \text{[dBm]} \quad (4.1)$$

The number of assigned uplink PRBs ($M_{m,b}$) depends on the number of simultaneously scheduled users and the assumed uplink frequency domain scheduling method. An equal grade of service (EGoS) scheduling is assumed in this thesis, which means that the available PRBs are divided so that the achievable user bit rates become roughly equal. In the assumed EGoS scheme, each simultaneously scheduled user, up to six simultaneously active users per cell, is initially assigned one PRB. If the user does not have sufficient amount of transmit power to reach SNR larger than -10 dB, the user is dropped, and the assigned PRB is released, resulting in a zero user throughput. The remaining PRBs are divided between the scheduled users so that the estimated average rates become roughly equal. In practice this means that a user in a poor position is assigned more PRBs than a user in a good position. However, frequency domain information about the channel quality or uplink interference is not taken into account, when assigning specific PRBs to the UEs. Finally, if a cell has more than six simultaneously active users, time domain scheduling of users is assumed as well.

### 4.2.5 SINR calculation

*SINR for user data (PDSCH and PUSCH)*

Next step in the simulation flow is the calculation of the signal-to-interference-plus-noise ratio (SINR) for each of the active users. In the simulator, the SINR for a certain user is calculated as a logarithmic average over the SINRs of the assigned PRBs [135]. Hence, the logarithmic SINR for UE $m$, served by eNodeB $b$ is calculated as

$$\gamma_{m,b} = \frac{10}{M_{m,b}} \sum_{r=1}^{M_{m,b}} \log_{10}\left(\frac{P_{m,b,r}}{L_{m,b} I_{m,b,r}}\right) \quad \text{[dB]} \qquad (4.2)$$

where $P_{m,b,r}$ is the transmission power per (assigned) PRB. Furthermore, the received interference power per PRB is calculated as

$$I_{m,b,r} = N_m^{PRB} + \sum_{\substack{n=1 \\ n \neq b}}^{B} \frac{\rho_{n,r} P_{n,r}}{\chi_{n,r} L_{m,n}} \qquad (4.3)$$

for the downlink, and as

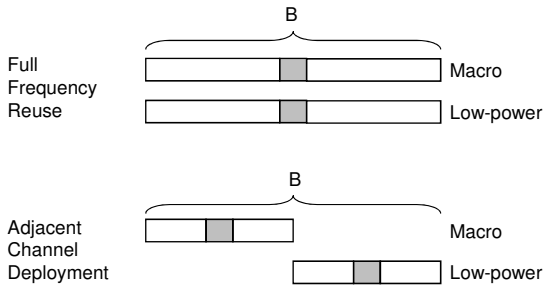


**Figure 4.10.** Description of the assumed spectrum allocation schemes. For all scenarios, the system bandwidth is assumed to be equal to B.

$$I_{m,b,r} = N_b^{PRB} + \sum_{\substack{n=1 \\ n \neq m}}^{U} \frac{\rho_{n,r} \varphi_{n,r} P_{n,r}}{\chi_{n,r} L_{n,b}} \tag{4.4}$$

for the uplink. In (4.3) and (4.4), $B$ and $U$ correspond to the total number of eNodeBs and simultaneously active UEs within the system, respectively. Furthermore, $N_m^{PRB}$ and $N_b^{PRB}$ are the thermal noise powers per PRB for UE $m$ and eNodeB $b$, respectively. Parameter $\rho_{n,r}$ models the activity of the neighboring transmitters: If transmitter $n$ (eNodeB for downlink or UE for uplink) is occupying PRB $r$, $\rho_{n,r}$ is equal to one, otherwise $\rho_{n,r}$ is assumed to be equal to zero (synchronized deployment) or equal to 0.1 (unsynchronized deployment, see the discussion in Section 7.5.3). Parameter $\varphi_{n,r}$ indicates the fraction of time allocated for user $n$, modeling the impact of uplink time domain scheduling on the average inter-cell interference. Finally, parameter $\chi_{n,r}$ models the adjacent channel interference power ratio (ACIR) between the receiver and the transmitter.

Nearly all scenarios in this thesis assume full frequency reuse between the cells, i.e. all cells are operating on the same carrier frequency, see Figure 4.10. For such scenarios, parameter $\chi_{n,r}$ is equal to 1. For some specific scenarios it is assumed that the macro and the low-power cell layers have been allocated separate carrier frequencies. However, for all scenarios and deployments the total system bandwidth is kept the same. For example, in case of a 20 MHz system bandwidth there are four different spectrum allocation alternatives: full frequency reuse (20 MHz macro, 20 MHz low-power), 15 MHz macro + 5 MHz low-power, 10 MHz macro + 10 MHz low-power and 5 MHz macro + 15 MHz low-power. In order to derive the $\chi_{n,r}$ values for the three adjacent channel alternatives, a worst case approach is assumed, where the adjacent channel attenuation is assumed to be equal to 33 dB [110][111] over the whole neighboring carrier. Since the interference $I_{m,b,r}$ in (4.3) and (4.4) is calculated for a PRB and not for the whole carrier

bandwidth, the value of $\chi_{n,r}$ becomes equal to 2000 (33 dB) for all the assumed adjacent channel alternatives.

*SINR for the downlink control signaling*

In some particular deployment scenarios, also the quality of the downlink control signaling, in particular the quality of the CRS, PBCH and PSS/SSS is taken into account. The quality, or SINR, of the downlink control signaling is calculated as

$$\gamma_{m,b,s} = \frac{P_{m,b,s}}{L_{m,b}\left(N_{m,s} + \sum_{\substack{n=1 \\ n \neq b}}^{B} \frac{\rho_{n,s} P_{n,s}}{\chi_{n,s} L_{m,n}}\right)} \tag{4.5}$$

where $P_{m,b,s}$ is the transmission power allocated for the control symbol in question. If a synchronized deployment of cells is assumed, CRS, PBCH and PSS/SSS will collide with the corresponding symbols in other cells even when no users are scheduled (i.e. $\rho_{n,s} = 1$), otherwise the value of $\rho_{n,s}$ will depend on the activity of the neighboring cell. The value of $\chi_{n,s}$ will depend on the assumed spectrum allocation between the cell layers, as discussed in the previous section.

### 4.2.6 SINR-to-throughput mapping

Once the SINR has been calculated, it is mapped to an average bit rate using a model based on a modified Shannon capacity formula, see for example [134]. The *achievable bit rate*, i.e. the average bit rate the user is expected to receive when scheduled, for a certain user $m$ served by eNodeB $b$ is calculated (in Mbps) as

$$B_{m,b} = \begin{cases} 0.18 M_{m,b} \beta \cdot \min\left\{B_{max}, \eta \log_2\left(1 + \frac{\gamma_{m,b,lin}}{\mu}\right)\right\} & , \gamma_{m,b,lin} \geq 0.1 \\ 0 & , \gamma_{m,b,lin} < 0.1 \end{cases} \tag{4.6}$$

Values of the maximum spectral efficiency $B_{max}$, bandwidth efficiency factor $\eta$ and the SNR efficiency factor $\mu$ in (4.6) are set based on the assumed multi-antenna and modulation and coding scheme. Furthermore, value of the overhead factor $\beta$ is determined by the assumed HARQ retransmission overhead, control information overhead, as well as the overhead caused by the CRS, PBCH and PSS/SSS.

In reality, the link performance, and hence, the achievable bit rate, is degraded gracefully when the quality of the downlink control signaling is getting worse. For example, when it comes to the impact of CRS-interference, a brief discussion on the topic can be found in [144]. In the simulator, however, the applied model taking the quality of the CRS into account is very simple: If the SINR of the downlink control signaling is less than the given threshold, the user is dropped and the bit rate is set to zero. Otherwise the achievable bit rate is calculated as defined in (4.6).

Finally, in order to calculate the throughput for a certain user $m$, the impact of time domain scheduling has to be taken into account. Since the simulator does not model the TTI structure in detail, a simplified model is implemented instead. The model is based on a fundamental assumption that the system is static in between time instants $t_n$ and $t_{n+1}$, see Figure 4.7. Furthermore, in order to simplify the analysis of the average user throughput, it is assumed that the time step $t_{n+1} - t_n$ is long enough so that the system has converged into a scenario where the user-specific scheduling weights within a certain cell have become approximately equal.

In order to define the mapping between the achievable bit rate $B_{m,b}$ and the average user throughput, let us first define an expression for a generic scheduling weight, or priority, for a user $m$ being served by cell $b$ as:

$$p_{m,b} = \frac{B_{m,b}^{\alpha}}{R_{m,b}^{\beta}} \tag{4.7}$$

where $R_{m,b}$ is the historical average data rate, or average throughput, for user $m$ during time step $t_{n+1} - t_n$. Furthermore, parameters $\alpha$ and $\beta$ adjust the fairness of the scheduling algorithm. The average rate can be expressed also as a product of the achievable bit rate ($B_{m,b}$) and the fraction of time allocated for user $m$ ($\varphi_{m,b}$). Hence,

$$p_{m,b} = \frac{B_{m,b}^{\alpha}}{R_{m,b}^{\beta}} = \frac{B_{m,b}^{\alpha}}{\varphi_{m,b}^{\beta} B_{m,b}^{\beta}} = \frac{B_{m,b}^{\alpha-\beta}}{\varphi_{m,b}^{\beta}} \tag{4.8}$$

In general, the scheduling algorithm operating on the TTI level selects always the user that has the highest $p_{m,b}$. In a static scenario the $B_{m,b}$ values stay constant, but the $\varphi_{m,b}$ values are changed after each TTI: assuming that user $m$ is scheduled, $\varphi_{m,b}$ increases, while $\varphi_{n,b}$ ($n \neq m$) becomes smaller.

It should be noted that if $\alpha = 0$ and $\beta = 1$, the scheduler aims to balance the average rates, i.e. an *equal grade of service* (EGoS, also known as *max-*

*min*) scheduling is assumed, which in practice means that a user in a worse position is scheduled more often compared to a user in a good position. The opposite ($\alpha = 1,\ \beta = 0$) leads to a *max-rate* scheduler, which schedules always the user with the best $B_{m,b}$. If $\alpha = \beta$, then the scheduler aims to give each user an equal share of the time, resulting in a *round-robin* (RR) scheduler. Finally, if $\alpha = 1$ and $\beta < 1$, a *proportionally fair* (PF) scheduler is assumed.

As already mentioned, it is assumed that the time step $t_{n+1} - t_n$ is long enough so that the system has converged into a scenario, where

$$p_{1,b} \approx p_{2,b} \approx \cdots \approx p_{U_b,b} \tag{4.9}$$

and

$$\sum_{n=1}^{U_b} \varphi_{n,b} = 1 \tag{4.10}$$

where $U_b$ is the number of simultaneously active users in cell $b$. It should be noted that the requirement of balanced scheduling priorities excludes the use of max-rate scheduler. Solving (4.9) and (4.10) for $\varphi_{m,b}$ and multiplying that with the achievable bit rate $B_{m,b}$ results in an average throughput $R_{m,b}$ equal to

$$R_{m,b} = \varphi_{m,b} B_{m,b} = \frac{B_{m,b}^{\alpha/\beta}}{\sum_{n=1}^{U_b} B_{n,b}^{(\alpha/\beta)-1}} \tag{4.11}$$

Taking the values of $\alpha$ and $\beta$ into account, the average throughputs for the three different scheduler algorithms can be expressed as

$$R_{m,b}^{EGoS} = \frac{1}{\sum_{n=1}^{U_b} B_{n,b}^{-1}} \tag{4.12}$$

$$R_{m,b}^{RR} = \frac{B_{m,b}}{U_b} \tag{4.13}$$

$$R_{m,b}^{PF} = \frac{B_{m,b}^{1/\beta}}{\sum_{n=1}^{U_b} B_{n,b}^{(1/\beta)-1}} \tag{4.14}$$

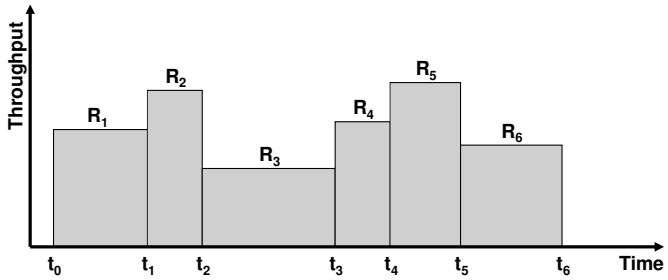


**Figure 4.11.** Calculation of the packet bit rate.

Finally, it should be noted that the simulator includes also a simple model for hybrid ARQ (HARQ) retransmission overhead, included in the overhead parameter $\beta$ in (4.6), without modeling the actual retransmissions. Another thing to note is that the simulator does not model the impact of RLC and TCP/IP protocols on the user performance. As discussed in [145], the achievable user performance is often limited by the TCP and not by the air-interface when applications consisting of transmissions of small packets are assumed. However, the TCP slow-start mechanism has little or no impact on the time it takes to transmit a large file. Since the impact of TCP is ignored in this thesis, the obtained results can be interpreted to correspond to results for real-life scenarios where the users are transmitting large files, much larger than the 500 kB assumed during the simulations.

### 4.2.7 Calculation of the user performance and the system capacity

During the simulations the user performance is modeled in terms of a *packet bit rate*, which is defined as the size of the transmitted packet divided by the packet delay, i.e. the time required to transmit the packet. Even though the evaluations do not consider user mobility, the throughput of each user can still vary during the packet transmission as a result of users leaving and entering the system. This is visualized in Figure 4.11, where a user is assumed to start the packet transmission at time instant $t_0$, and the transmission is assumed to continue until time instant $t_6$. The throughput $R_n$ is assumed to vary during the packet transmission. However, during a certain evaluation time step, the throughput is assumed to be constant.

The system performance (system capacity) is expressed as a *served area traffic* ($T_{area}$), which is defined as the total amount of data successfully transmitted in all cells divided by the system area. Since the macro cell layer is assumed to contain a total of 21 hexagonal cells, the system area can be calculated as

**Table 4.1**. Parameters for traffic calculations.

| Parameter | Value |
|---|---|
| Population density ($p$) | 10000 persons/km² |
| Operator market share ($o$) | 30% |
| Service penetration ($s$) | 90% |
| Days per month ($m$) | 30 |
| Daily traffic/busy hour traffic ($h$) | 12 |

$$A_{system} = 21A_{macro} = 21\left(1.5\sqrt{3}\left(\frac{D}{3}\right)^2\right) \tag{4.15}$$

where $D$ is the assumed inter-site distance. The relationship between the area traffic and the *monthly subscriber traffic* ($T_{subs}$) can be expressed as

$$T_{area} = T_{subs} \cdot \frac{r \cdot p \cdot o \cdot s}{m \cdot h} = T_{subs} \cdot \frac{15r}{2} \tag{4.16}$$

where the parameter values listed in Table 4.1 have been taken into account. Furthermore, parameter $r$ indicates the portion of the downlink (or uplink) traffic.

From the network dimensioning point of view, two requirements can be set: *coverage requirement* and *capacity requirement*. In this thesis the coverage requirement is defined as the average busy hour packet bit rate for the worst 5th percentile of the users, also referred to as the *cell-edge packet bit rate* (or the *cell-edge user throughput*). The capacity requirement is defined in this thesis as the served area traffic during a busy hour. For an acceptable network deployment, both requirements have to be fulfilled at the same time, as demonstrated in Figure 4.12.

The above means in practice that the system capacity is in thesis defined as the maximum achievable served area traffic, while still fulfilling the desired cell-edge user throughput. This will in many cases be considerably lower than the served area traffic of a fully-loaded system. The offered area traffic and the served area traffic are in this thesis expressed as GB/h/km². An alternative way would be to express them as Mbps/km² (10 GB/h/km² is approximately equal to 22 Mbps/km²). Furthermore, in case of homogeneous macro deployments, the average area traffic can be expressed also as Mbps/cell. For example, in case of the baseline deployment with ISD equal to 500 meters, 10 GB/h/km² becomes approximately equal to 1.6 Mbps/cell.

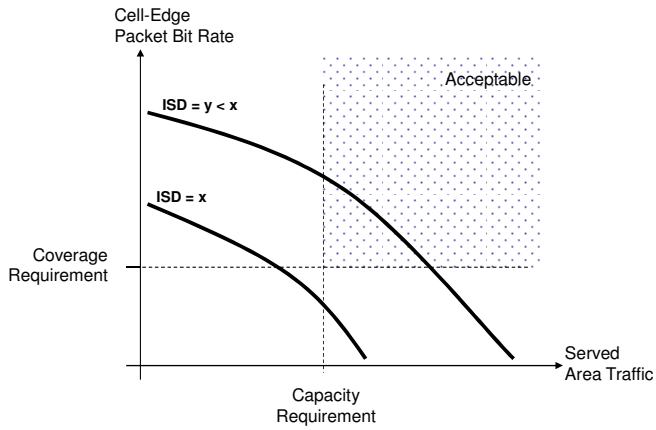


**Figure 4.12.** An acceptable network deployment has to fulfill both the coverage and the capacity requirement at the same time.

## 4.3 Discussion on the assumed simulation parameters

### 4.3.1 General parameters

A number of general simulation parameters, applicable for both the downlink and the uplink, are listed in Table 4.2. Some of them are discussed in more detail in this section.

Both the number of snapshots and the duration of a snapshot are trade-offs between the simulation speed and the accuracy of the results. If a larger number of independent snapshots is assumed, a wider span of scenarios can be covered, which improves the accuracy of the end-results, but increases the required simulation time. Similarly, if the system is evaluated for a longer time during a snapshot, the number of users contributing to the final results becomes larger. Since the expected user throughputs are so high in downlink, it is assumed that snapshot duration of 30 seconds is able to provide sufficient accuracy even for the lowest network load. As the network load is increased, a larger number of users is logged, which improves the accuracy of the results. In uplink, the user throughputs are considerably lower, and as a consequence, the length of the snapshot is increased for the lowest network loads. A more detailed analysis of the impact of these two parameters on the statistical accuracy of the results is provided in Annex A.

The evaluated LTE system is assumed to be operating on the FDD mode, and it is assumed to be based on 3GPP LTE Release-8. A detailed

**Table 4.2.** General simulation parameters.

| Parameter | Value |
|---|---|
| Number of snapshots | 100 |
| Duration of a snapshot | 30 s (downlink)<br>30 s ... 400 s (uplink) |
| Network operating mode | LTE FDD (Release-8) |
| Carrier frequency | 2.6 GHz |
| Carrier bandwidth | 20 MHz |
| Frequency planning | Full Frequency Reuse |
| Maximum eNodeB output power | 46 dBm (macro)<br>30 dBm (micro)<br>20 dBm (femto) |
| Scheduler (time domain) | Equal Grade of Service |
| Scheduler (frequency domain, UL only) | Equal Grade of Service |
| Error Vector Magnitude | 0% |
| Minimum allowed SINR for CRS, PBCH, PSS/SSS | -∞ dB (macro, micro)<br>-7 dB (femto) |
| Traffic model | Packet (500 kB) transmission |

evaluation of the advanced interference management methods introduced in 3GPP LTE Release-10 and Release-11 is left out of this thesis.

As a default, all cells are assumed to be operating on the same 20 MHz carrier, which means that the low-power cells are assumed to reuse the whole macro cell carrier. In addition to the full frequency reuse, also the performance of an adjacent channel deployment is evaluated for some specific heterogeneous deployment scenarios.

The assumed maximum output powers for the different eNodeB types are similar to the ones typically assumed for example within the 3GPP evaluations: 46 dBm (40 W), 30 dBm (1 W) and 20 dBm (100 mW) for the macro, outdoor micro and indoor femto cell, respectively. It should be noted that the eNodeB output power is defined as the total power over all transmit antenna branches. Hence, since each of the eNodeBs has two transmit antennas, the maximum output power per antenna is assumed to be equal to 43 dBm, 27 dBm and 17 dBm.

An equal grade of service scheduler has been assumed for all the simulations, which means that during a simulation time step the active users within a certain cell are assumed to have the same average throughput. Generally speaking, the differences between the different

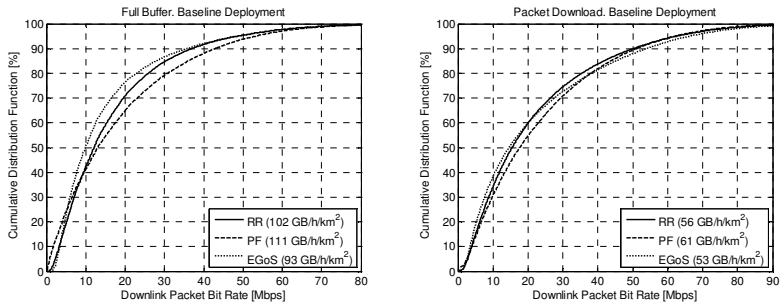


**Figure 4.13.** Downlink user performance with different scheduling algorithms.

scheduling algorithms are fairly small at low system loads, i.e. when a cell has only a few simultaneously active users. Due to the fairly high coverage requirements, this kind of situation will quite often be the case in this thesis. However, in addition to the traffic load, also the traffic behavior affects the overall scheduling performance. This is demonstrated in Figure 4.13, where the downlink performance of the three different scheduling algorithms, round robin (RR), proportional fair (PF) with $\beta = 0.5$ and equal grade of service (EGoS), is compared. Furthermore, an average of one active user per cell, i.e. a total of 21 simultaneously active users within the system area, is assumed.

As expected, the differences between the scheduler algorithms are small. In case of the full buffer traffic model, the proportional fair algorithm results in the highest capacity, but performs the worst at the cell-edge. Equal grade of service offers the best cell-edge throughput, but the worst system capacity. The performance of the round robin scheduler is in between PF and EGoS. The reason for these results is that the assumed PF scheduler assigns a fairly strong weight on the achievable bit rate, punishing the users in poor radio conditions. While this kind of strategy is good from the overall system throughput point of view, it may result in a poor cell-edge performance. The situation is the opposite with EGoS, which focuses on the performance of the worst users, but with the cost of a lower system throughput.

For the scenario with packet download, the differences become even smaller. From the system throughput point of view the order is the same: PF provides the best capacity, followed by RR and EGoS. However, when it comes to the cell-edge performance, all three algorithms result in roughly the same performance. The reason for this is that since the users have finite transmission buffers, assigning higher weights for users with good radio conditions does not harm the performance of the poor users as much as it does with the full buffer traffic model.

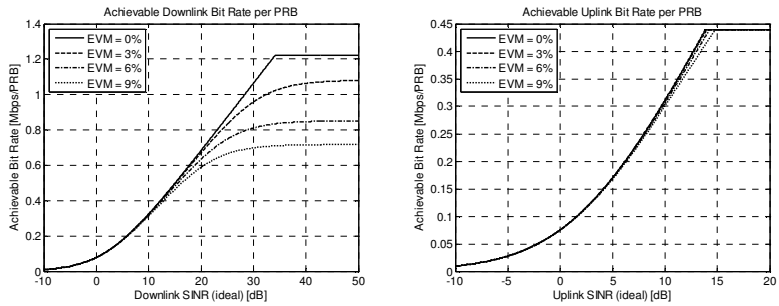


**Figure 4.14.** EVM-limited achievable downlink and uplink bit rate as a function of the ideal SINR.

The impact of various RF imperfections can be taken into account with the help of the error vector magnitude (EVM). In simple terms, EVM quantifies how far the actual received constellation symbols are from their ideal locations as if they had been sent by an ideal transmitter. EVM can be modeled as an additional noise, proportional to the amount of transmitted carrier signal. With EVM defined as a percentage ($\varepsilon$ %), the *EVM noise* can be calculated as

$$I_{m,b,r}^{EVM} = \frac{P_{m,b,r}(0.01\varepsilon)^2}{L_{m,b}} \tag{4.17}$$

Taking (4.17) into account, the *EVM-limited SINR* per PRB can be written as

$$\gamma_{m,b,r}^{EVM} = \frac{P_{m,b,r}}{L_{m,b}I_{m,b,r} + L_{m,b}I_{m,b,r}^{EVM}} \tag{4.18}$$

and further

$$\gamma_{m,b,r}^{EVM} = \left(\frac{1}{\gamma_{m,b,r}} + \left(\frac{\varepsilon}{100}\right)^2\right)^{-1} \tag{4.19}$$

The simulations discussed in this thesis ignore the impact of EVM, which overestimates the achievable bit rates at higher levels of ideal SINR, as shown in Figure 4.14. Therefore, also the gain of network densification will be overestimated. However, the error is estimated to become smaller for relative comparisons between the different network densification alternatives. The situation is different in uplink, where the users will very seldom experience high SINR levels due to the applied power control. Furthermore, as demonstrated by the curves in Figure 4.14, the maximum allowed modulation and coding scheme (i.e. maximum allowed achievable

bit rate per PRB) is reached before the EVM has any greater impact on the link performance. Therefore, only a very limited estimation error is expected.

In case of the baseline deployment, the densified macro deployment and the heterogeneous micro deployment the quality of the downlink control signaling (CRS, PBCH and PSS/SSS) is not taken into account. This can overestimate the downlink quality of the users located at the cell-edge. However, the quality of the downlink control signaling is taken into account when evaluating the impact of the biased cell selection or the performance of the heterogeneous femto deployments. It should be noted that the applied SINR threshold (i.e. -7 dB) is at a similar level compared to the minimum requirement for the detection of the PBCH given in [110].

### 4.3.2 Additional parameters for downlink

Parameters for the downlink SINR-to-throughput mapping are listed in Table 4.3. Looking at the assumed parameter values, the following comments can be made:

- Downlink control channel overhead is assumed to be equal to 28.9% for the macro cells, which is based on the assumption that three out of 14 symbols have been reserved to carry the downlink control information (PDCCH, PCFICH and PHICH) [100]. The remaining downlink overhead is caused by the CRS, PBCH and PSS/SSS. Since two transmit antenna ports are assumed, the CRS overhead becomes equal to 9.5%[5] [100]. Furthermore, as described in [100], the combined overhead caused by PBCH and PSS/SSS is equal to 0.33%, assuming a carrier bandwidth of 20 MHz.

- The low-power cells are assumed to be less loaded than the macro cells, and hence, the required downlink control information overhead is reduced to two out of 14 symbols [100]. Since the number of transmit antennas is assumed to be the same for both the macro and the low-power cells, also the downlink overhead caused by the CRS is the same. Thus, total downlink control channel overhead within the low-power cells becomes equal to 21.8%.

- HARQ retransmission overhead is assumed to be equal to 10%. Taking both the control channel overhead and the HARQ retransmission overhead into account, the value of $\beta$ in (4.6)

[5] It should be noted that the combined overhead for PDCCH, PCFICH, PHICH and CRS is equal to 28.6%

**Table 4.3.** Additional parameters for the downlink.

| Parameter | Value |
|---|---|
| Number of symbols reserved for PDCCH, PHICH and PCFICH | 3 (macro)<br>2 (micro, femto) |
| HARQ retransmission overhead | 10% |
| Implementation margin | 2 dB |
| Multi-antenna scheme and the highest modulation scheme | 2x2 SU-MIMO<br>64 QAM |
| Parameters for the SINR-to-bit rate mapping for macro cells | $B_{max} = 10.6$<br>$\beta = 0.64$<br>$\eta = 1$<br>$\mu = 1.67$ |
| Parameters for the SINR-to-bit rate mapping for low-power cells | $B_{max} = 10.6$<br>$\beta = 0.70$<br>$\eta = 1$<br>$\mu = 1.67$ |
| UE noise figure | 8 dB |

becomes equal to $(1 - 0.1)(1 - 0.289) \approx 0.64$ for the macro cells, and equal to $(1 - 0.1)(1 - 0.218) \approx 0.70$ for the low-power cells.

- A 2 dB implementation margin is assumed, i.e. $\mu = 1.67$. Furthermore, based on a comparison against more detailed link simulations, the value of $\eta$ is assumed to be equal to 1.

- A 2x2 SU-MIMO scheme is assumed for downlink, with 64 QAM as the highest modulation scheme. Dual-stream transmission has been enabled. Assuming a peak code rate equal to 0.95, the peak spectral efficiency ($B_{max}$) becomes approximately equal to[6] 10.6 bits/Hz.

### 4.3.3 Additional parameters for uplink

Parameters related to uplink SINR-to-throughput mapping, control channel overhead and power control are listed in Table 4.4. Looking at the parameter values, the following comments can be made:

- Uplink control channel overhead is assumed to be caused by the demodulation reference signals (one out of seven symbols) [100],

[6] Two data streams, 12 subcarriers per PRB (180 kHz), 14 symbols per 1 ms, 6 bits per symbol.

**Table 4.4.** Additional parameters for the uplink.

| Parameter | Value |
|---|---|
| Uplink control channel overhead | 14.3% |
| Number of PRBs reserved for PUCCH | 4 |
| HARQ retransmission overhead | 10% |
| Implementation margin | 2 dB |
| Multi-antenna scheme and the highest modulation scheme | 1x2 SIMO<br>16 QAM |
| Parameters for the SINR-to-bit rate mapping | $B_{max} = 3.17$<br>$\beta = 0.77$<br>$\eta = 0.8$<br>$\mu = 1.67$ |
| Maximum UE output power | 23 dBm |
| eNodeB noise figure | 3 dB (macro, micro)<br>8 dB (femto) |
| Path loss compensation factor | 1 |
| Parameter $P_0$ | See Section 4.3.4 and Annex C |

while the impact of the sounding reference signals has not been taken into account.

- A total of 4 resource blocks have been reserved for PUCCH [100], which means that a maximum of 96 resource blocks can be used for data transmission (PUSCH).

- HARQ retransmission overhead is assumed to be equal to 10%. Hence, the value of $\beta$ becomes equal to $(1 - 0.1)(1 - 0.143) \approx 0.77$ for the uplink.

- A 2 dB implementation margin is assumed, i.e. $\mu = 1.67$. Furthermore, the value of $\eta$ is assumed to be equal to 0.8.

- A 1x2 SIMO scheme with 16 QAM as the highest modulation scheme is assumed for uplink. Assuming a peak code rate equal to 0.85, the peak spectral efficiency becomes approximately equal to[7] 3.17 bits/Hz.

- In order to reduce the impact of the interference from the close-by adjacent channel UEs, as well as for cost and implementation

[7] One data stream, 12 subcarriers per PRB, 14 symbols per 1 ms, 4 bits per symbol.

reasons, the receiver sensitivity of a femto eNodeB is allowed to be worse than the receiver sensitivity of a macro eNodeB [111]. In the simulator, a 5 dB higher noise figure is assumed for the femto eNodeBs compared to the macro and micro eNodeBs.

- In order to cope with the co-channel uplink interference between the cell layers, different $P_0$ values are assumed for the macro and the low-power cells. A more detailed discussion on this *uplink interference margin* is provided in the next section.

### 4.3.4 Discussion on the uplink received signal power target

As a result of network densification the availability of resources increases in the time, frequency and the power domain. The increased availability of resources in the time domain means that the users can be scheduled more often. Furthermore, the increased availability of resources in the frequency domain is related to the fact that the users are allowed to occupy a larger number of PRBs. Finally, the increased availability of resources in the power domain means that a higher received signal power target ($P_0$) can be allowed for the uplink power control.

There are a few reasons why a densified network deployment allows the use of a higher $P_0$. Firstly, since the coupling loss between a UE and the serving eNodeB is reduced, a higher received power target can be applied while still maintaining the same UE transmission power. Secondly, the reduced coupling loss towards the serving eNodeB and further, the higher received carrier power will improve the SINR, even though the interfering UEs would maintain their transmission power. Finally, as a result of the improved SINR, the users will experience higher achievable bit rates, resulting in shorter packet transmission times, and hence, less average interference towards the neighboring eNodeBs.

Performing a sufficiently accurate analytical analysis to find the most appropriate combination of $P_{0,macro}$, $\alpha_{macro}$, $\alpha_{LPN}$ and $P_{0,LPN}$ for each of the assumed network deployments could be quite complex. Therefore, an approach based on system simulations has been selected instead. Some simplifications have been assumed: Firstly, full path loss compensation is assumed for all cells ($\alpha_{macro} = \alpha_{LPN} = 1$). Secondly, no additional limitations of the maximum allowed UE transmit power are applied. Finally, it is assumed that the $P_0$ adjustments are applied on the cell, and not on the individual user level.

The applied $P_0$ values have been selected mainly from the maximized cell-edge user throughput point of view for each of the network deployment

**Table 4.5.** Assumed $P_0$ values for the densified macro deployment.

| Inter-Site Distance | Macro $P_0$ |
|---|---|
| 500 m | -119 dBm |
| 400 m | -116 dBm |
| 300 m | -112 dBm |
| 250 m | -110 dBm |
| 200 m | -106 dBm |

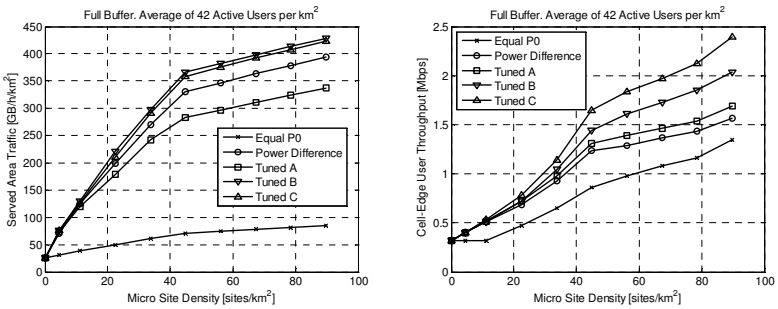


**Figure 4.15.** Observed served area traffic (left) and cell-edge user throughput (right) as a function of the micro site density for the evaluated $P_0$ adjustment methods.

alternatives. For simplicity, the evaluations have been performed with the static simulation mode, i.e. assuming a full buffer traffic model. Furthermore, the evaluations have been performed only for one network load level, equal to 63 simultaneously active users within the system area. Hence, the assumption in this thesis is that the applied $P_0$ values will not be varied as a function of the network load. The other simulation parameters have been the same as in Table 4.2 and Table 4.4.

To start with, a list of the assumed $P_0$ values for the densified macro deployment is provided in Table 4.5. When it comes to the heterogeneous network deployments, the link imbalance between the macro and the low-power cell layer could result in uplink interference problems at the low-power eNodeB. As discussed in Section 3.2.3, the solution proposed in this thesis is to introduce an interference margin for the uplink power control within the low-power cell so that $P_{0,LPN} = P_{0,macro} + i_{LPN}$.

The results presented in Figure 4.15 compare four different $P_0$ adjustment methods within the heterogeneous micro deployment: *Equal* $P_0$ ($P_{0,macro} = P_{0,micro} = -119$ dBm), *Power difference* ($P_{0,macro} = -119$ dBm, $P_{0,micro} = -103$ dBm), *Tuned A* ($P_{0,macro} = -119$ dBm, see Table 4.6 for $P_{0,micro}$),

**Table 4.6.** Uplink power control parameters for heterogeneous micro deployment.

| Micro Site Density [sites /traffic cluster] | Micro Site Density [sites /km²] | Traffic Offloading [%] | *Tuned A* | *Tuned B* | *Tuned C* | |
|---|---|---|---|---|---|---|
| | | | Micro $P_0$ [dBm] | Macro $P_0$ [dBm] | Macro $P_0$ [dBm] | Micro $P_0$ [dBm] |
| 0 | 0 | 0 | N/A | -119 | -119 | N/A |
| 0.1 | 4.49 | 13.2 | -102 | -118 | -118 | -102 |
| 0.25 | 11.22 | 27.5 | -104 | -118 | -118 | -103 |
| 0.5 | 22.43 | 43.2 | -105 | -115 | -115 | -102 |
| 0.75 | 33.65 | 55.4 | -105 | -114 | -113 | -101 |
| 1 | 44.87 | 64.3 | -106 | -112 | -111 | -100 |
| 1.25 | 56.09 | 66.1 | -106 | -112 | -111 | -100 |
| 1.5 | 67.30 | 68.0 | -106 | -112 | -111 | -100 |
| 1.75 | 78.52 | 70.0 | -106 | -112 | -111 | -100 |
| 2.0 | 89.74 | 71.7 | -106 | -112 | -111 | -100 |

*Tuned B* (see Table 4.6 for $P_{0,macro}$, $P_{0,micro} = P_{0,macro} + 16$ dB) and *Tuned C* (see Table 4.6 for both $P_{0,macro}$ and $P_{0,micro}$).

As demonstrated by the simulation results, the simple and straightforward solution based on the eNodeB transmission *power difference* improves both the capacity and the coverage of the system compared to the scheme where the same $P_0$ is applied in all cells. However, it becomes quite clear, that the system performance can be enhanced by tuning the $P_0$ values a bit further.

In case of the *Tuned A* method, $P_{0,macro}$ is kept fixed at -119 dBm, while the value of $P_{0,micro}$ is tuned to maximize the performance of the cell-edge users. As can be noticed, the difference between $P_{0,macro}$ and the adjusted $P_{0,micro}$ decreases as the density of micro sites increases. The reason for this is that the size of the interference margin has to be reduced to limit the uplink interference towards the macro cells. Compared to the *Power Difference* method, *Tuned A* results in a worse system performance, but in an improved cell-edge performance. The observed performance difference is caused by the reduced $P_{0,micro}$, which reduces the performance of the micro users but improves the performance of the worst macro users due to the reduced level of uplink interference.

Looking at the $P_{0,macro}$ values for the *Tuned B* and *Tuned C* methods, it becomes clear that the $P_{0,macro}$ can be increased as the density of micro

**Table 4.7.** Values of $\phi_{micro}$ for the *Tuned C* method.

| Micro Site Density [sites/traffic cluster] | Traffic Offloading [%] | $\phi_{micro}$ [dB] |
|---|---|---|
| 0 | 0 | N/A |
| 0.1 | 13.2 | 0 |
| 0.25 | 27.5 | -1 |
| 0.5 | 43.2 | -3 |
| 0.75 | 55.4 | -4 |
| 1 | 64.3 | -5 |
| 1.25 | 66.1 | -5 |
| 1.5 | 68.0 | -5 |
| 1.75 | 70.0 | -5 |
| 2.0 | 71.7 | -5 |

cells and the traffic offloading increases. Furthermore, in case of the *Tuned C* method also the value of $P_{0,micro}$ is slightly increased together with an increased traffic offloading. Since the $P_{0,macro}$ is increased considerably more, the interference margin is reduced together with an increased traffic offloading. The reason why the $P_{0,macro}$ can be increased with an increasing micro site density is that the remaining macro users are less power-limited and can afford a higher received power target. An increased $P_{0,macro}$ improves also the protection against the interference from micro users. Hence, also the value of $P_{0,micro}$ can be slightly increased, while still maintaining an acceptable quality for the cell-edge users. Looking at the results in Figure 4.15, both *Tuned B* and *Tuned C* result in a similar system performance. However, when it comes to the performance of the cell-edge users, *Tuned C* is clearly better. Therefore, the *Tuned C* method has been applied in this thesis.

According to the analysis presented in Section 3.2.3, and assuming further that $P_{max,b} - P_{max,p} = 16$ dB, $\alpha_p = 1$ and $O_p = 0$ dB, $P_{0,micro}$ can be expressed as

$$P_{0,micro} = P_{0,macro} + \phi_{micro} + 16 \quad \text{[dBm]} \quad (4.20)$$

The values of $\phi_{micro}$ for the *Tuned C* method are listed in Table 4.7. The applied $P_0$ values for the other heterogeneous network deployments are listed in Annex C. In general, changes in the applied cell selection offset or

micro eNodeB output power would indicate a need to modify also the $P_0$ values for both cell layers. The main principle is that if the cell selection offset or the micro eNodeB output power is increased, the value of $P_{0,micro}$ should most likely be decreased to limit the uplink interference towards the macro cell. At the same time, the possibilities to increase the value of $P_{0,macro}$ should be re-evaluated, as the level of traffic offloading from the macro to the micro cell layer increases. Adjacent channel deployments will typically allow the use of a higher $P_{0,micro}$ since the inter-layer interference is attenuated. Furthermore, a narrower carrier bandwidth allows the use of a higher $P_{0,macro}$ and $P_{0,micro}$ while still keeping the same total UE transmission power.

### 4.3.5 Interference management models and parameters for the CSG femto deployments

*Downlink inter-layer interference mitigation*

The assumed CSG femto eNodeB transmission power adjustment method is based on the total received power from the strongest macro cell ($W_{macro} = P_{macro} - L_{macro}$), measured by the CSG femto eNodeB. Furthermore, it is assumed that the value of $w$ in (3.16) is assumed to be the same for all CSG femto eNodeBs. Finally, the parameter $k$ in (3.16) is assumed to be equal to one. Hence,

$$P_{CSG} = \max\left(P_{min,CSG}, \min\left(P_{max,CSG}, W_{macro} + w\right)\right) \quad \text{[dBm]} \quad (4.21)$$

In (4.21), $P_{max,CSG}$ is assumed to be equal to 20 dBm [111]. In order to find the largest possible value of parameter $w$, given the value of $P_{min,CSG}$, so that the downlink performance of the remaining macro users is not significantly degraded, a number of system simulations are run. The simulations assume a synchronized deployment of macro and femto eNodeBs, and offered area traffic equal to 50 GB/h/km$^2$. The results are shown for two different values of femto penetration, 30% and 50%, and for two different values of $P_{min,CSG}$: 0 dBm and -10 dBm.

Figure 4.16 presents the $P_{CSG}$ distributions for $P_{min,CSG}$ equal to -10 dBm. As can be seen, very few femto eNodeBs are limited by the $P_{max,CSG}$ at least up to $w = 65$ dB, but a large part of the femto eNodeBs are limited by the assumed minimum transmission power, even with $P_{min,CSG} = -10$ dBm. Assuming a higher $P_{min,CSG}$, the probability that $P_{CSG}$ is limited by $P_{min,CSG}$ increases. For example, with $P_{min,CSG} = 0$ dBm and $w = 60$ dB, only 20% of the femto eNodeBs are able to adjust their power to a desired value.

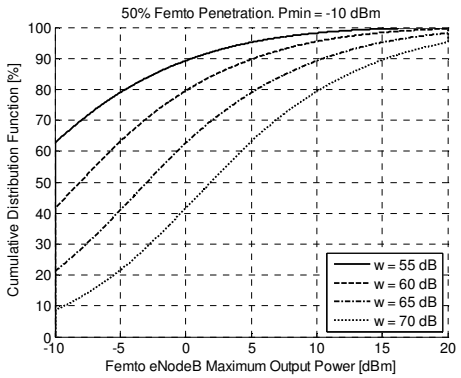


**Figure 4.16.** Distribution of the maximum femto eNodeB output power for different values of the power adjustment constant *w*.

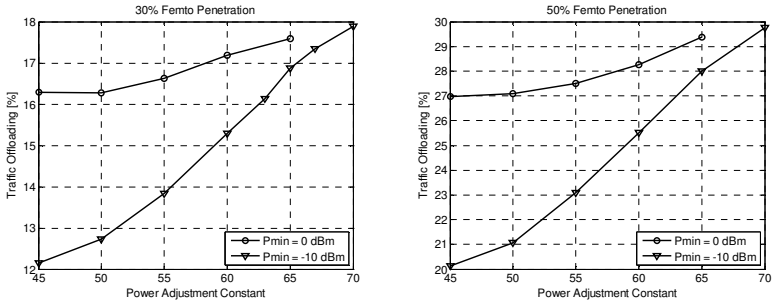


**Figure 4.17.** Observed traffic offloading as a function of the power adjustment constant *w*.

Overall traffic offloading and the femto cell coverage probability within the femto apartment are studied in Figure 4.17 and Figure 4.18, respectively. The results demonstrate how the increased power adjustment constant *w* improves both the femto cell coverage and the overall traffic offloading. Due to the assumption that only the users located within the femto apartment are allowed to connect to the CSG femto eNodeB, the overall traffic offloading cannot be better than 19.2% with the femto penetration equal to 30%. In case of the 50% femto penetration the maximum achievable level of traffic offloading increases to 32%. The results indicate also that a lower $P_{min,CSG}$ reduces the observed femto cell coverage and the traffic offloading. This is quite easy to understand by looking at the curves in Figure 4.16. For example, if *w* is assumed to be equal to 60 dB, the reduced $P_{min,CSG}$ (from 0 dBm to -10 dBm) will result in a reduced output power for 80% of the femto eNodeBs.

Results for the user dropping probability as a function of the power adjustment constant *w* are shown in Figure 4.19. Here, a user is assumed to be dropped if the SINR of the downlink control signaling is less than -7

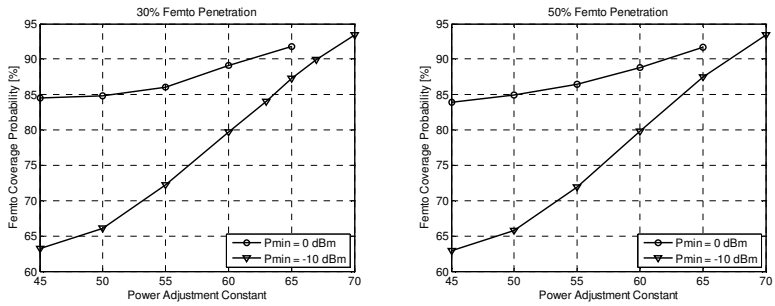


**Figure 4.18.** Observed femto cell coverage probability within a femto apartment as a function of the power adjustment constant $w$.

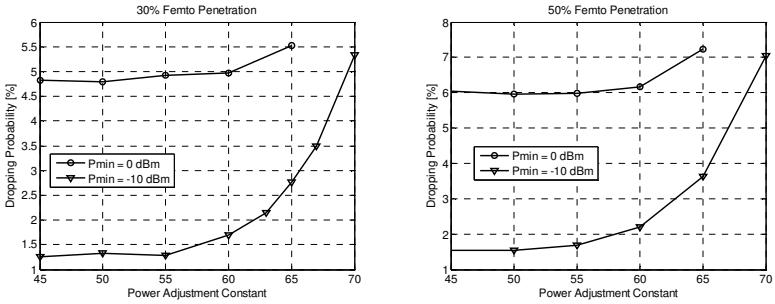


**Figure 4.19.** User dropping probability as a function of the power adjustment constant $w$. Femto penetration equal to 30% or 50% is assumed.

dBm or if the downlink throughput is less than 150 kbps. A closer look at the results reveals that the reason behind all the dropped connections is the poor quality of the downlink control signaling. Furthermore, approximately 98% of the dropped users are served by the macro eNodeBs, and half of them are located either on the ground floor or on the 1st floor. Looking at the results in Figure 4.19, the impact of both $P_{min,CSG}$ and $w$ becomes clear. To start with, a lower $P_{min,CSG}$ will reduce the $P_{CSG}$ for lower values of $w$, and hence, the inter-cell interference towards the neighboring users. Similarly, an increased $w$ will increase the $P_{CSG}$ and further, the level of the inter-cell interference.

Performance of the worst users is shown in Figure 4.20 (all users), Figure 4.21 (macro users) and Figure 4.22 (femto users). The first thing to notice is that by lowering the $P_{min,CSG}$ from 0 dBm to -10 dBm seems to clearly improve the performance of the worst macro users. In fact, with $P_{min,CSG}$ equal to 0 dBm, more than 5% of the macro users experience a poor quality of the downlink control signaling, resulting in a dropped connection. With $P_{min,CSG}$ equal to -10 dBm the quality of the downlink control signaling is improved, which reduces the dropping probability and improves the quality of the worst users.

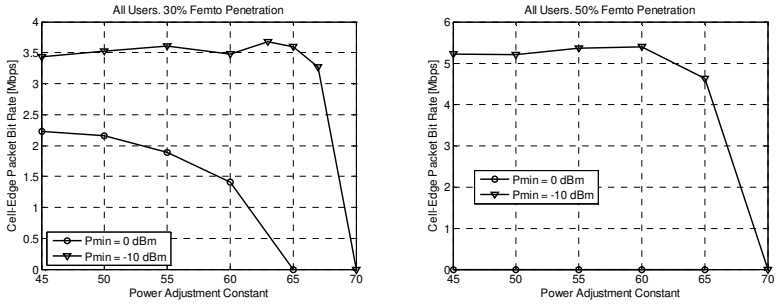


**Figure 4.20.** Performance of the worst 5th percentile of users as a function of the power adjustment constant *w*.

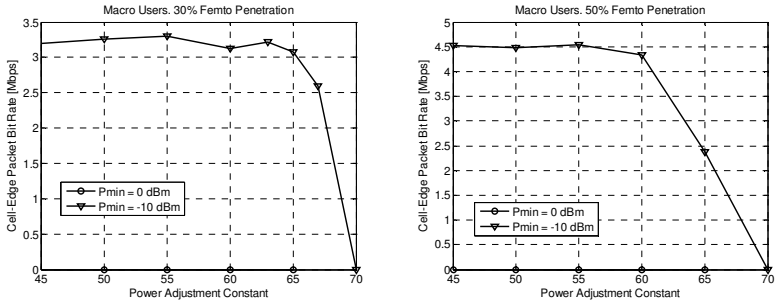


**Figure 4.21.** Performance of the worst 5th percentile of the macro users as a function of the power adjustment constant *w*.

It becomes also clear that an increased *w* will lead to a higher $P_{CSG}$, and further, to a higher level of inter-cell interference towards the users in neighboring apartments or inside vehicles, i.e. users that are not allowed to connect to the CSG femto eNodeB. Looking at the results with $P_{min,CSG}$ equal to -10 dBm, performance of the worst macro users seems to be quite stable for *w* smaller than 60-65 dB. Deployment with a higher density of femto cells seems to be more sensitive to the value of *w*, despite the increased traffic offloading.

When it comes to the performance of the worst femto users, shown in Figure 4.22, the impact of both $P_{min,CSG}$ and *w* is the opposite compared to the impact towards the macro users. This is due to the fact that an increased $P_{CSG}$ will increase the downlink SINR, and hence, the downlink throughput of the femto users.

Based on the results shown above, the value of the minimum CSG femto eNodeB output power $P_{min,CSG}$ is in this thesis assumed to be equal to -10 dBm and the power adjustment constant *w* is assumed to be equal to 60 dB for all CSG femto cells operating on the same carrier frequency as the macro cell layer. In case of adjacent channel CSG femto deployments, the adjacent channel attenuation would allow the use of a considerably larger

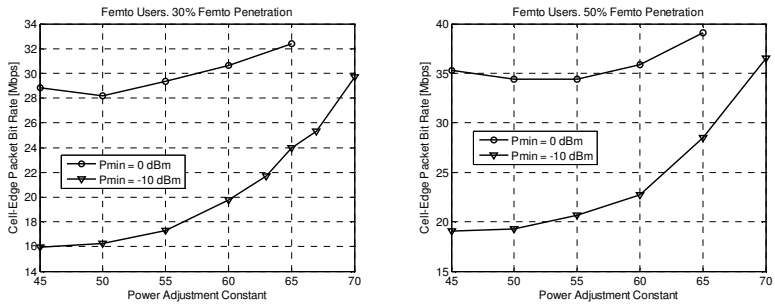


**Figure 4.22.** Performance of the worst 5th percentile of the femto users as a function of the power adjustment constant $w$.

value of parameter $w$. However, the benefit of having a variable $P_{CSG}$ based on an adjacent channel $W_{macro}$ is found to be quite small. Therefore, a fixed $P_{CSG}$ is assumed in this thesis for any adjacent channel CSG femto deployments.

It should be highlighted that the selection of both $P_{min,CSG}$ and $w$ is highly scenario-dependent. For example, $P_{min,CSG}$ equal to 0 dBm and $w$ equal to 60 dB are assumed in [70]. The overall scenario differs, however, considerably from the scenario assumed in this thesis. In [70], the CSG femto eNodeBs are deployed inside detached houses, which means that the probability of having many close-by non-CSG mobiles becomes considerably smaller than in case of a femto deployment inside a block of apartments. Since the number of potentially interfered macro users is low, a higher $P_{CSG}$ can be allowed.

*Uplink inter-layer interference mitigation*

Uplink inter-layer interference mitigation is based on a method where the $P_0$ value is adjusted at the CSG femto eNodeBs. Based on the discussion in Section 3.2.3, an approach is taken where all the CSG femto eNodeBs are adjusting their $P_{0,CSG}$ so that the estimated uplink interference at the closest macro eNodeB does not exceed a certain level, i.e. based on equation (3.25). For simplicity, the same $\phi_{CSG}$ is assumed for all CSG femto cells. Furthermore, $\alpha_{CSG}$ is assumed to be equal to one. Hence, (3.25) becomes equal to

$$P_{0,CSG} = P_{0,macro} + \phi_{CSG} + P_{macro} - P_{CSG} - O_{CSG} \qquad \text{[dBm]} \quad (4.22)$$

In order to find out the most appropriate $\phi_{CSG}$ values for the different femto densities, system simulations have been run, following the same kind of methodology as in Section 4.3.4. The scope of the simulations has been

**Table 4.8.** Uplink power control parameters for a few different heterogeneous CSG femto deployments.

| Femto Penetration [%] | Cell Selection Offset [dB] | Macro $P_0$ [dBm] | $\phi_{CSG}$ [dB] |
|---|---|---|---|
| 30 | 0 | -119 | -14 |
| 30 | 3 | -119 | -15 |
| 30 | 6 | -119 | -16 |
| 50 | 0 | -118 | -16 |
| 50 | 3 | -118 | -17 |
| 50 | 6 | -118 | -18 |

to find the most appropriate combinations of $P_{0,macro}$ and $\phi_{CSG}$ so that the cell-edge performance is maximized. Furthermore, the $P_{CSG}$ values are obtained from (4.20), assuming that $P_{min,CSG}$ is equal to -10 dBm and $w$ is equal to 60 dB for all the CSG femto eNodeBs. The results are shown in Table 4.8.

# 5. Performance of the macro cellular network

In this chapter the performance of both the baseline macro deployment and the densified macro deployment are evaluated. The baseline deployment is assumed to consist of a homogeneous macro cellular network with inter-site distance (ISD) equal to 500 meters. Performance of the densified macro deployment is investigated by evaluating the performance of a number of homogeneous macro cellular deployments with different inter-site distances. During the evaluations, the density of the traffic clusters is kept constant, which means that the average number of traffic clusters per macro cell is reduced with a smaller inter-site distance.

The evaluations consider both the downlink and the uplink performance. Furthermore, the user performance within various three-dimensional locations is visualized.

Some of the results presented in this chapter have already been published as part of papers [146] and [147].

## 5.1 Performance of the baseline deployment

### 5.1.1 Downlink performance

Results for the downlink packet bit rate and the average cell utilization as a function of the served area traffic are shown in Figure 5.1. Three different packet bit rate curves are shown: average of all users, cell-edge (i.e. the worst 5$^{th}$ percentile of users) and the best 5$^{th}$ percentile of users. Looking at the results, the connection between the user performance and the system performance becomes clear: When the network load (i.e. the served area traffic) increases, performance of the individual users decreases. There are two main reasons behind the degraded user performance: Firstly, the average level of inter-cell interference is increased as a result of the increased cell utilization, which results in a worse SINR, and hence, in a

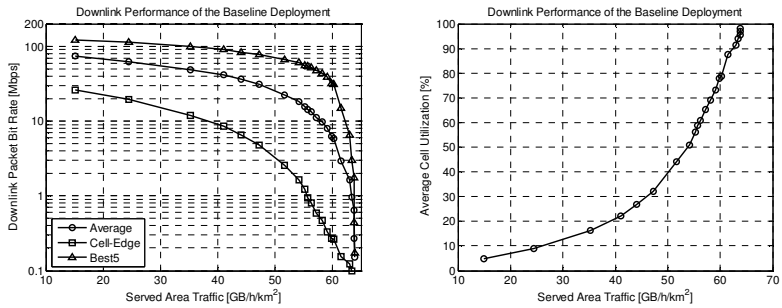


**Figure 5.1.** Downlink packet bit rate and the average cell utilization as a function of the served area traffic for the baseline deployment.

**Table 5.1.** Downlink performance of the baseline deployment.

| Coverage Req [Mbps] | Maximum served area traffic | | | Average cell utilization [%] |
|---|---|---|---|---|
| | GB/h/km² | Mbps/km² | Mbps/cell | |
| 1 | 55.6 | 123.7 | 8.9 | 58.3 |
| 2 | 53.1 | 118.1 | 8.5 | 48.3 |
| 4 | 48.7 | 108.3 | 7.8 | 36.3 |
| 10 | 38.5 | 85.6 | 6.2 | 19.7 |
| 20 | 23.6 | 52.5 | 3.8 | 8.7 |
| 30 | - | - | - | - |

reduced achievable bit rate. Secondly, together with the increasing cell utilization, the probability of having multiple simultaneously active users per cell increases, which reduces the average user throughput.

The results in Figure 5.1 can be utilized to define the maximum served area traffic for a number of desired busy hour cell-edge packet bit rates (*coverage requirements*, as defined in Section 4.2.7), see Table 5.1. As can be seen, the highest coverage requirement that the baseline deployment can fulfill is approximately equal to 26 Mbps. The maximum area capacity of the fully-loaded baseline deployment is approximately equal to 64 GB/h/km² (i.e. equal to 142 Mbps/km² or 10.3 Mbps/cell). Since the approach in this thesis is to guarantee the desired cell-edge performance, the network cannot be operated at full load. Therefore, the maximum system capacity will become lower than 64 GB/h/km². For example, if the desired coverage requirement is equal to 1 Mbps, the corresponding maximum served area traffic becomes equal to 55.6 GB/h/km² and the

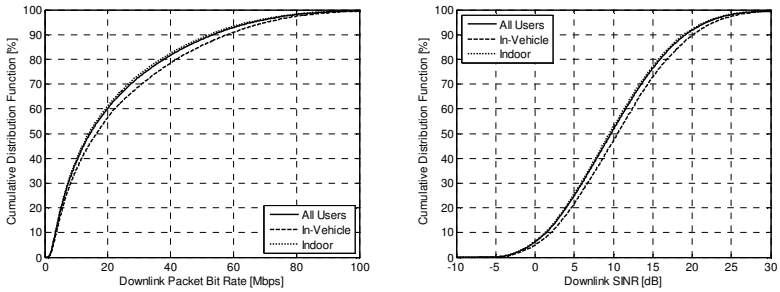


**Figure 5.2.** Distributions of the observed downlink packet bit rates and the SINR values, assuming a served area traffic equal to 51.7 GB/h/km².

maximum allowed average cell utilization[8] equal to 58.3%, meaning that the cells are idle in 41.7% of the time. If the coverage requirement is increased, both the maximum served area traffic and the maximum allowed average cell utilization are reduced.

Performance of the individual users can be visualized by evaluating the baseline deployment for an operating point with served area traffic equal to 51.7 GB/h/km². For that particular network load level, the observed average and cell-edge packet bit rates are equal to 22.2 and 2.5 Mbps, respectively. Furthermore, the average cell utilization is equal to 44.1%. Distributions of the downlink packet bit rates and SINRs are presented in Figure 5.2 for all users, for all in-vehicle users and for all indoor users. As can be noticed, performance of the in-vehicle users is slightly better than the performance of the indoor users. However, the difference in terms of both the user throughput and the SINR is clearly smaller than what the coupling loss differences would suggest, see Figure 5.3. This means that within the investigated scenario the inter-cell interference is in many of the cases dominating over the receiver noise level, i.e. the system is not power-limited. However, since the user performance is still showing a slight dependency on the coupling loss, the system is not entirely interference-limited either.

An even more detailed view of the user performance is provided in Figure 5.4, where the users are divided into six different groups based on their location: in-vehicle (InV), ground floor (GF), 1st floor (1F), 2nd floor (2F), 3rd floor (3F), and 4th floor (4F). The average and the worst 5th percentile of the downlink packet bit rates for each of the user locations are presented, together with the locations of the worst and the best performing decile of users. As can be noticed, the observed average user performance becomes

[8] Cell utilization indicates the fraction of time a cell is in active state, i.e. serving at least one user, during a snapshot. The average cell utilization is then calculated over all cells and snapshots.

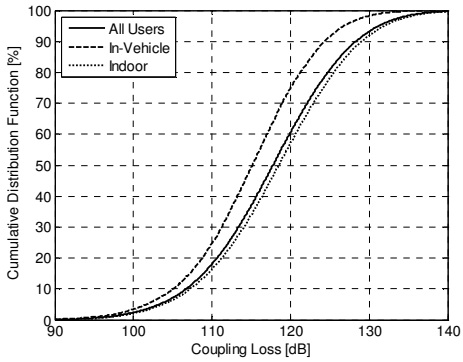


**Figure 5.3.** Distribution of the observed coupling loss values for the baseline deployment.

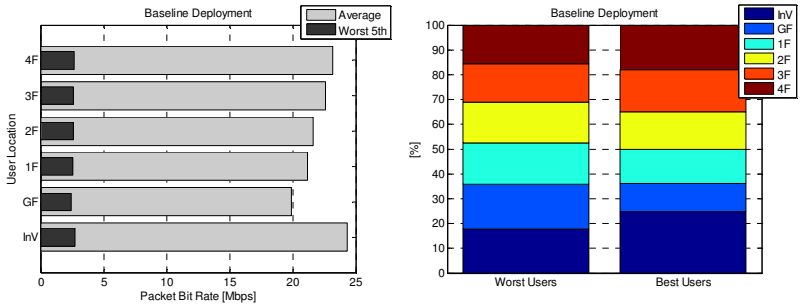


**Figure 5.4.** Observed downlink user performance for the different user locations, and the locations of the worst and the best performing decile of users for the baseline deployment.

better when moving upwards inside the building, i.e. when the coupling loss towards the serving eNodeB becomes smaller as a result of the floor height gain. When it comes to the locations of the worst performing users, they seem to be fairly uniformly distributed over the different locations. However, it should be kept in mind that in average each floor level carries 16% of the total traffic, while 20% of the traffic is generated outside the buildings. This means that the indoor areas include a slightly larger group of the worst users than would be suggested by the overall traffic distribution. At the same time, the in-vehicle users are slightly underrepresented within the group of the worst performing users. However, the differences are not remarkable. The fact that the floor height gain has a much larger impact on the average user performance compared to the performance of the worst users suggests that the main reason for the poor downlink performance is the number of simultaneously active users within the serving cell, instead of for example the large coupling loss towards the serving eNodeB.

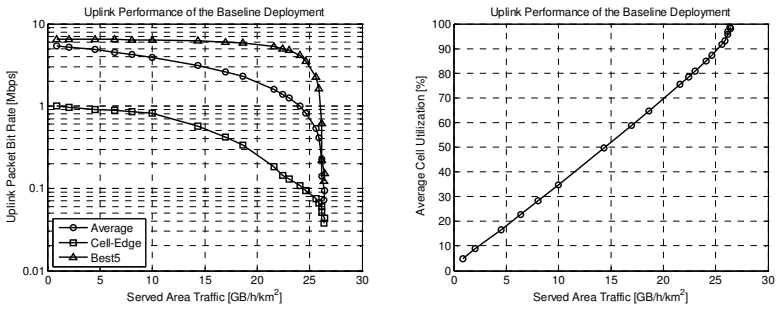


**Figure 5.5.** Uplink packet bit rate and the average cell utilization as a function of the served area traffic for the baseline deployment.

The observed performance of the best performing users depends clearly on the user location or in general on the coupling loss towards the serving macro eNodeB. The reason for this is that the best user performance is typically observed in the scenarios where the users are alone in the serving cell, and at the same time the level of inter-cell interference is low. For such power-limited (or noise-limited) scenarios, the achieved SINR and user throughput depend mostly on the coupling loss between the UE and the serving eNodeB.

### 5.1.2 Uplink performance

Results for the uplink packet bit rate and the average cell utilization as a function of the served area traffic are shown in Figure 5.5. The overall trends are the same for both downlink and uplink, but the absolute uplink performance is clearly lower. As can be seen, the highest uplink coverage requirement that the baseline deployment can fulfill is approximately equal to 1 Mbps. Furthermore, the maximum uplink served area traffic of a fully-loaded baseline deployment is approximately equal to 26.4 GB/h/km², i.e. 58.7 Mbps/km² or 4.2 Mbps/cell.

Similar to the downlink, the results in Figure 5.5 can be utilized to define the maximum uplink served area traffic for a number of desired uplink coverage requirements, see Table 5.2. The situation is the same as in downlink: In order to guarantee the desired cell-edge user throughput, the network cannot be operating at full load. Furthermore, when the coverage requirement is increased, the corresponding maximum served area traffic and the maximum average cell utilization become lower.

A more detailed investigation of the user performance is performed for a network operating point with served area traffic equal to 14.3 GB/h/km². The corresponding average and cell-edge packet bit rates are equal to 3.1 and 0.6 Mbps, respectively. Furthermore, the average cell utilization is

**Table 5.2.** Uplink performance of the baseline deployment.

| Coverage Req [Mbps] | Maximum served area traffic | | | Average cell utilization [%] |
|---|---|---|---|---|
| | GB/h/km² | Mbps/km² | Mbps/cell | |
| 0.1 | 24.4 | 54.2 | 3.9 | 86.2 |
| 0.25 | 20.3 | 45.1 | 3.3 | 70.7 |
| 0.5 | 15.6 | 34.7 | 2.5 | 54.1 |
| 1 | 0.88 | 2.0 | 0.14 | 4.8 |
| 2 | - | - | - | - |
| 4 | - | - | - | - |

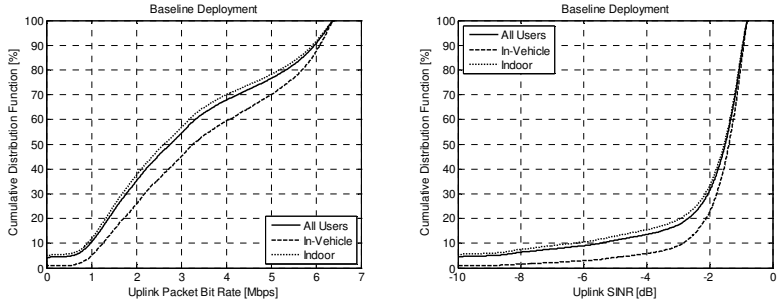


**Figure 5.6.** Distribution of the observed uplink packet bit rates and the SINR values, assuming a served area traffic equal to 14.3 GB/h/km².

equal to 49.6%. The observed distributions of the uplink packet bit rates and the uplink SINR values are shown in Figure 5.6. For uplink, performance of the in-vehicle users is clearly better than the performance of the indoor users. One can also notice that approximately 5% of the indoor users have a zero uplink throughput, i.e. their coupling loss towards the serving eNodeB is too high to enable a SINR of at least -10 dB, as explained in Chapter 4. At the same time, only 1% of the in-vehicle users do not have any uplink coverage. The fact that the coupling loss has a clear impact on the user performance suggests that the investigated uplink scenario is in general much more power-limited than the downlink.

The above can be verified also by taking a closer look at the user performance for the different locations, see Figure 5.7. As can be noticed, the impact of the coupling loss towards the serving eNodeB on the observed user performance is considerable. When it comes to the locations of the worst performing decile of users, more than half of them are located either on the ground floor or on the 1st floor. In fact, on those floor levels, more than 5% of the users do not have sufficient uplink coverage. It is also clearly

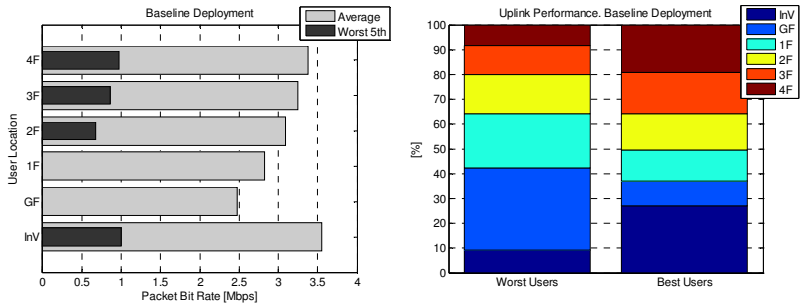


**Figure 5.7.** Observed uplink user performance for the different user locations, and the locations of the worst and the best performing decile of users for the baseline deployment.

visible that the observed user performance improves as a function of the floor level. The best uplink performance is observed for the in-vehicle users. This is verified also by the locations of the best performing decile of users, which can be typically found either on the upper floor levels, or inside the vehicles, i.e. in locations with the lowest coupling losses towards the serving eNodeBs.

## 5.2 Performance of the densified macro network

### 5.2.1 Downlink performance

As indicated by (4.12), user throughput ($R_{m,b}^{EGoS}$) is proportional to the achieved bit rate ($B_{m,b}$), and inversely proportional to the number of simultaneously active users ($U_b$). Furthermore, as indicated by (4.6), the achieved bit rate depends among other things on the SINR ($\gamma_{m,b}$) and the amount of frequency domain resources ($M_{m,b}$).

In general, when the number of cells is increased within a certain geographical area, the size of a cell becomes smaller. Assuming that the area density of the offered traffic stays the same, the offered traffic per cell is reduced, proportionally to the area of the cell, as demonstrated by Figure 5.8. The curve in Figure 5.8 is calculated as

$$Y = \frac{100 H_{baseline}}{H_{dense}} = \frac{100}{4.5\sqrt{3}\left(\frac{0.5}{3}\right)^2 H_{dense}} \approx \frac{461.9}{H_{dense}} \quad [\%] \qquad (5.1)$$

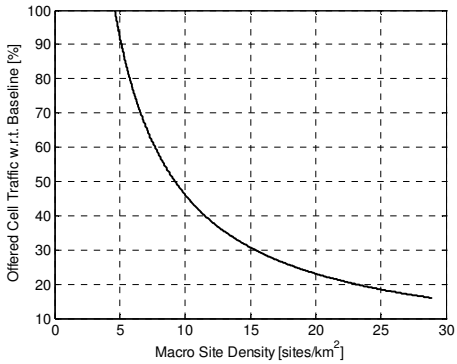


**Figure 5.8.** Offered traffic per cell decreases together with an increasing density of cells.

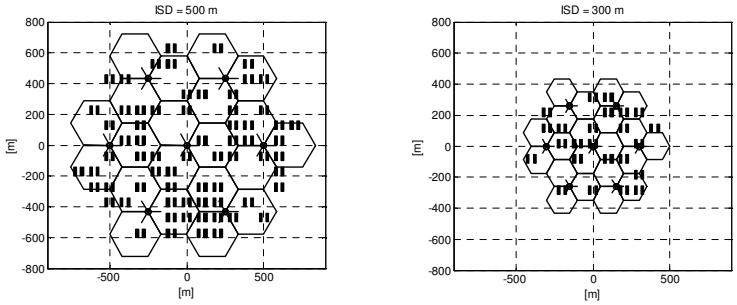


**Figure 5.9.** Average number of traffic clusters per macro cell is decreased together with a reduced inter-site distance.

where $H_{baseline}$ and $H_{dense}$ are the site densities of the baseline deployment and the densified macro deployment, respectively.

In the simulator, the reduced offered traffic (per cell) is modeled via the assumption of a fixed area density of traffic clusters. In practice it means that when the inter-site distance is reduced, the average number of traffic clusters per macro cell and therefore also the level of offered traffic is reduced as well, as demonstrated in Figure 5.9.

Traffic offloading as a result of the reduced inter-site distance is verified by the simulation results in Figure 5.10. The simulations are performed for a number of homogeneous macro deployments with different inter-site distances, assuming a fixed level of offered area traffic equal to 55 GB/h/km². According to the results, the reduced offered traffic (per cell) leads to a reduced average number of simultaneously active users (per cell), and further, to a lower level of average cell utilization. Lower average cell utilization results in a lower level of inter-cell interference, and further, in an improved SINR, as demonstrated by the curves in Figure 5.11. Another

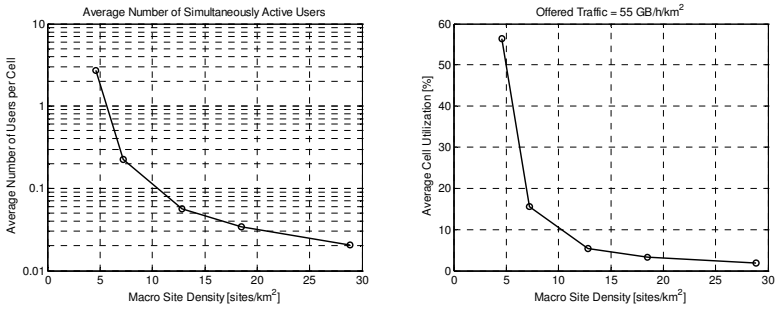


**Figure 5.10.** Average number of simultaneously active users per cell and average macro cell utilization as a function of the macro site density. Offered area traffic equal to 55 GB/h/km² is assumed.

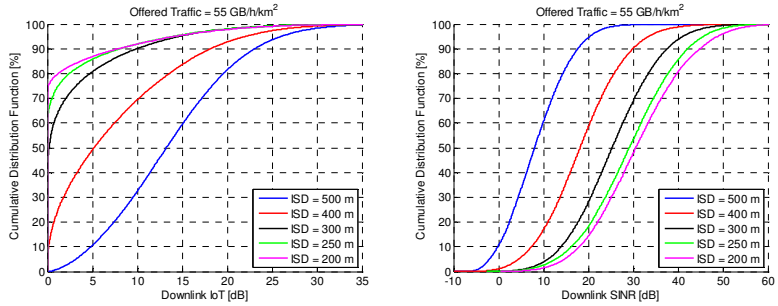


**Figure 5.11.** Distribution of the downlink IoT and the SINR with different inter-site distances, assuming a fixed offered area traffic equal to 55 GB/h/km².

factor contributing to the improved SINR is the reduced coupling loss towards the serving eNodeB.

As a result of the reduced number of simultaneously active users per cell, the served users are allowed to consume more resources, both in time, frequency and power domain. The improved SINRs, and the increased amount of resources in frequency and power domain, when applicable, result in higher achievable bit rates for the scheduled users. In addition, the increased availability of time domain resources leads to improved user throughputs, as demonstrated in Figure 5.12. Finally, as a result of the increased user throughputs, the users can complete their packet transmissions quicker, which reduces the average cell utilization even more than the straightforward resource addition via cell splitting would suggest.

There are a few details worth highlighting in the results presented in Figure 5.10 – Figure 5.12. According to the results for higher levels of macro site density in Figure 5.10, both the average number of simultaneously active users and the average cell utilization become smaller than 0.05, which means that there are periods of time when the whole system is idle, i.e. the system does not contain any active users. Furthermore, the results in Figure 5.11 indicate that for ISDs smaller than 400 meters, there is an

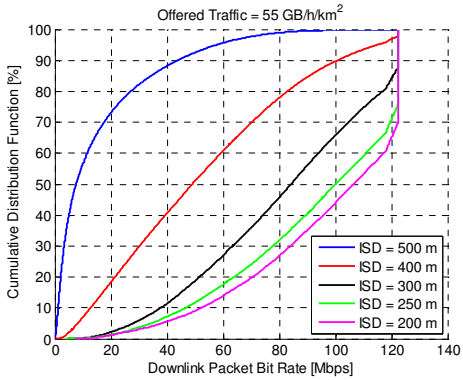


**Figure 5.12.** Distribution of the downlink packet bit rates with different values of the inter-site distance, assuming an offered area traffic equal to 55 GB/h/km².

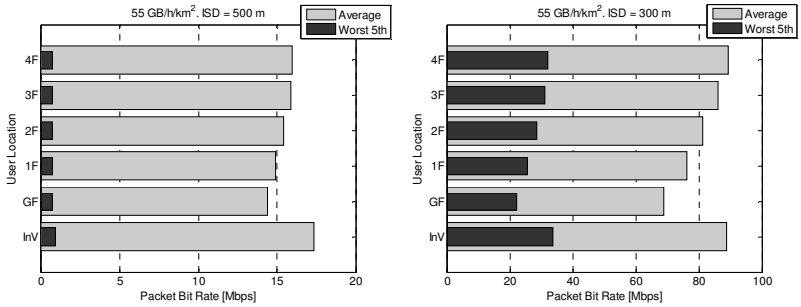


**Figure 5.13.** Average and the worst 5th percentile of the downlink packet bit rates for the different user locations. Inter-site distance equal to 500 m or 300 m is assumed.

increasing probability that a user is alone in the system, i.e. the downlink IoT is equal to 0 dB. Finally, the results in Figure 5.12 demonstrate that for ISD smaller than 400 meters, the downlink performance for some of the users is limited by the maximum allowed link-level performance (multi-antenna, and modulation and coding scheme), and not by the interference.

Next, the average user performance and the performance of the worst 5th percentile of the users is studied a bit closer for two different ISDs, 500 m and 300 m, assuming a fixed offered area traffic equal to 55 GB/h/km² for both deployments. Looking at the results in Figure 5.13, the first thing to notice is the considerably improved user performance as a result of the network densification[9]. When the ISD is reduced from 500 m to 300 m, the average packet bit rate is increased from 15.7 Mbps to 82.0 Mbps. At the

[9] The results in Figure 5.13 (Poisson process) and in Figure 5.1 (fixed number of simultaneously active users) confirm the analysis in Section 4.2.2 identifying the differences between the two user generation methods. Assuming the same level of served area traffic (55 GB/h/km²), the method based on Poisson process results in a worse average packet bit rate (15.7 Mbps vs. 16.5 Mbps), as well as in a worse cell-edge packet bit rate (0.74 Mbps vs. 1.39 Mbps).

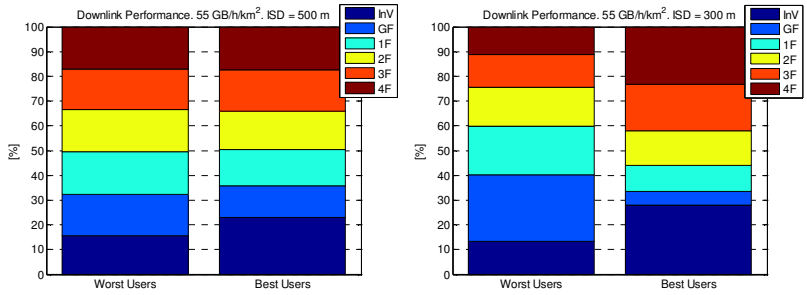


**Figure 5.14.** Locations of the worst and the best performing users, assuming an inter-site distance of 500 m or 300 m.

same time, the cell-edge user performance is dramatically improved from 0.74 Mbps to 27.9 Mbps. In addition, the average user performance depends clearly on the coupling loss, while the performance of the worst 5$^{th}$ percentile of the users is much more uniform, at least for ISD equal to 500 m. This is due to the fact that the poor user performance is caused mainly by the inter-cell interference, or by the long scheduling queues within the serving cell. The higher percentiles of the user performance are reached within the scenarios, where the level of inter-cell interference is low, and/or when the load in the serving cell is low. In case of a smaller ISD, the system becomes less interference-limited due to the reduced average cell utilization (56.4% → 5.3%), and the dependency on the coupling loss becomes more visible even for the worst 5$^{th}$ percentile of the users. At the same time, the difference between the average user performance and the worst 5$^{th}$ percentile is considerably reduced.

Similar conclusions can be drawn when looking at the locations of the worst and the best performing decile of users, shown in Figure 5.14. In case of ISD equal to 500 m, the worst users are fairly uniformly distributed between the different user locations. The in-vehicle users are underrepresented within the group of the worst users, while the different indoor areas are slightly overrepresented. When the ISD is reduced to 300 m, the dependency on the coupling loss becomes very clear. Now, the ground floor and the 1$^{st}$ floor are clearly overrepresented, while the 3$^{rd}$ floor, 4$^{th}$ floor and in particular the in-vehicle users are underrepresented.

When it comes to the locations of the best performing decile of users, the situation becomes the opposite. Now, the users that have the lowest coupling losses towards the serving macro eNodeBs will experience the best performance. In practice this means users located inside vehicles, or on the upper floor levels. This kind of behavior becomes even more visible when the network has become less interference-limited as a result of the network densification.

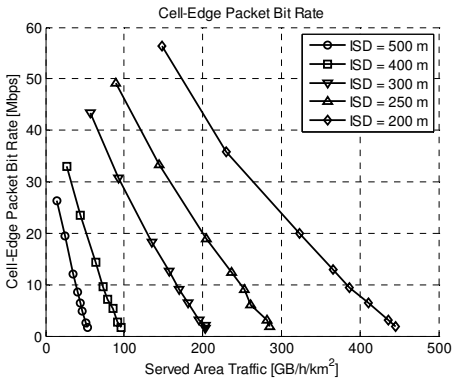


**Figure 5.15.** Downlink cell-edge packet bit rate as a function of the served area traffic for homogeneous macro deployments with different inter-site distances.

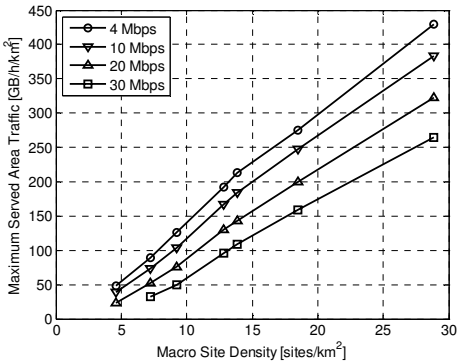


**Figure 5.16.** Maximum downlink served area traffic as a function of the macro site density for a few different coverage requirements.

The maximum downlink capacity of the densified macro deployment is obtained by evaluating the cell-edge packet bit rate as a function of the served area traffic for a number of different homogeneous macro deployments with different ISDs, see Figure 5.15. The obtained curves are then utilized to define the maximum downlink served area traffic values, which are still able to fulfill the desired coverage requirements equal to 4-30 Mbps, see Figure 5.16. The coverage requirements have been set so that the assumed network deployment would be able to provide an "ADSL-like" user experience also for the cell-edge.

The results indicate that the system coverage and capacity can be considerably improved by densifying the macro deployment, which is line with the results shown for example in [88] and [148]. The difference is, however, that the system capacity is increased almost linearly as a function of the macro site density (indicating that the *densification efficiency* stays constant), while both [88] and [148] indicate that the densification efficiency will be reduced as a function of the macro site density due to the

fact that the (relative) level of inter-cell interference will increase, and hence, the achievable SINRs will become worse as a result of network densification. Since the overall evaluation methodology and the evaluation assumptions differ considerably between the studies, it will be difficult to pinpoint any single reason for the different results. Most likely it will be a combined impact of at least the following factors:

- The evaluation in both [88] and [148] assume fully-loaded networks, meaning that all the eNodeBs are constantly transmitting with full power. This is a major difference compared to the evaluation in this thesis, where the performance evaluation is performed for a network, which is not fully-loaded (the actual level of network load will depend on the desired coverage requirement). For example, for a coverage requirement equal to 4 Mbps, the average cell utilization is approximately equal to 36%. If a higher coverage requirement is assumed, the average cell utilization will become lower and vice versa.

- The evaluation in both [88] and [148] is based on the observed SINR values, which is not the case in this thesis. Here, the evaluation is based on observed user throughputs, taking into account the impact of the scheduler on both the user and the system performance.

- When the macro cells are made smaller, while still keeping the same density and sizes of the traffic hotspots, the traffic distribution becomes more clustered (see Figure 5.9). This will then make the offered load more non-uniform between the cells; some cells can be very heavy-loaded, while some other cells can be very light-loaded.

- As already mentioned, the maximum system capacity is in this thesis defined as a combination of both a cell-edge user throughput and the served area capacity. For a medium- to high-loaded network, the results have indicated that the cell-edge performance is quite often limited by the long scheduling queues. When the cells become smaller and the traffic becomes more clustered, some cells can become very high-loaded, limiting the overall cell-edge performance. In practice this means that in order to fulfill the desired coverage requirement, the average cell utilization has to be reduced together with an increasing macro cell density. As a result, the level of inter-cell interference will be reduced and the SINR improved for the users, which are not limited by the scheduler.

**Table 5.3.** Required density of new macro sites (sites/km²) to fulfill the desired downlink coverage and capacity requirements.

| Coverage Req | Capacity Requirement | | | |
|---|---|---|---|---|
| | 50 GB/h/km² | 100 GB/h/km² | 150 GB/h/km² | 200 GB/h/km² |
| 4 Mbps | 0.1 | 3.2 | 5.9 | 8.8 |
| 10 Mbps | 0.9 | 4.2 | 7.2 | 10.5 |
| 20 Mbps | 2.5 | 6.1 | 9.8 | 13.9 |
| 30 Mbps | 4.2 | 8.6 | 13.1 | 17.9 |

- Both [88] and [148] assume macro cellular propagation models, which include a LOS-component. Furthermore, [148] is assuming a three-dimensional ray-tracing model. Compared to the semi-statistical model without LOS or street-canyon propagation applied in this thesis, the analysis in both [88] and [148] will most likely be based on more accurate coupling loss estimates, in particular for the very dense macro cell deployments.

For light-loaded scenarios, i.e. with a high coverage requirement, and in particular for the low levels of network densification, the impact of inter-cell interference is low, and the uncertainties related to the propagation modeling have a smaller impact. However, once the network load is increased, the impact of propagation, scheduler and traffic clustering cannot be ignored. In all, it is likely that the results presented in this thesis for the densified macro deployments are somewhat too optimistic, but in order to be able to quantify the difference, more work would be needed.

When the capacity of the different deployment alternatives is compared, the main principle is to find the lowest density of new sites to be deployed on top of the baseline deployment (with a site density equal to 4.6 sites/km²), so that both the desired coverage requirement and the desired capacity requirement can be fulfilled at the same time. The required site densities for the densified macro deployment are listed in Table 5.3. Furthermore, the levels of the traffic offloading and the average cell utilization are listed in Table 5.4 and in Table 5.5, respectively. As can be noticed, the system coverage is increased, i.e. the coverage requirement increased under the same capacity requirement, as a result of both a densified network deployment (resulting in a reduced level of offered traffic per cell) and a reduced maximum utilization of the cell resources. Similarly, the system capacity is improved, i.e. the capacity requirement is increased

**Table 5.4.** Observed level of traffic offloading for the desired network operating points.

| Coverage Req | Capacity Requirement | | | |
|---|---|---|---|---|
| | 50 GB/h/km² | 100 GB/h/km² | 150 GB/h/km² | 200 GB/h/km² |
| 4 Mbps | 1.7% | 40.8% | 56.2% | 65.5% |
| 10 Mbps | 15.9% | 47.8% | 61.0% | 69.5% |
| 20 Mbps | 34.7% | 56.8% | 68.1% | 75.0% |
| 30 Mbps | 47.5% | 65.1% | 73.9% | 79.5% |

**Table 5.5.** Average macro cell utilization for the desired network operating points.

| Coverage Req | Capacity Requirement | | | |
|---|---|---|---|---|
| | 50 GB/h/km² | 100 GB/h/km² | 150 GB/h/km² | 200 GB/h/km² |
| 4 Mbps | 36.3% | 37.2% | 37.5% | 37.5% |
| 10 Mbps | 20.2% | 22.4% | 24.2% | 24.7% |
| 20 Mbps | 11.6% | 13.9% | 15.3% | 15.6% |
| 30 Mbps | 7.0% | 9.6% | 10.5% | 11.1% |

under the same coverage requirement, as a result of both the network densification and the increased maximum utilization of the cell resources.

### 5.2.2 Uplink performance

Since a flat power spectrum and no user multiplexing in the frequency domain is assumed for the downlink transmissions, network densification will increase the availability of resources only in the time domain. The situation is, however, different for the uplink, where the availability of resources is increased also in the frequency and the power domain. In practice this means that a) the users are allowed to occupy a larger number of PRBs, and b) higher $P_0$ values can be allowed for the uplink power control. All of these facts will contribute to increased user throughputs, as demonstrated by the results in Figure 5.17.

The impact of network densification on the uplink user performance is studied further in Figure 5.18 and in Figure 5.19, assuming offered area traffic equal to 20 GB/h/km². The results in Figure 5.18 indicate that when the ISD is reduced from 500 m and 300 m, the average packet bit rate is increased from 2.1 to 12.9 Mbps, and the cell-edge packet bit rate is

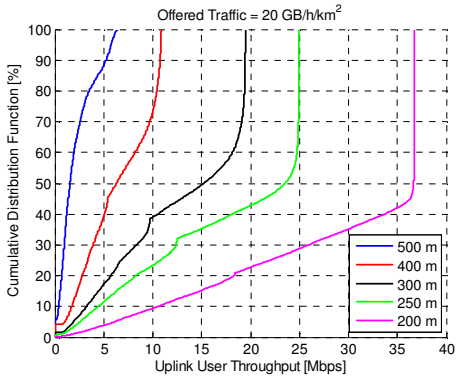


**Figure 5.17.** Distribution of the observed uplink packet bit rates, assuming a fixed offered area traffic equal to 20 GB/h/km².

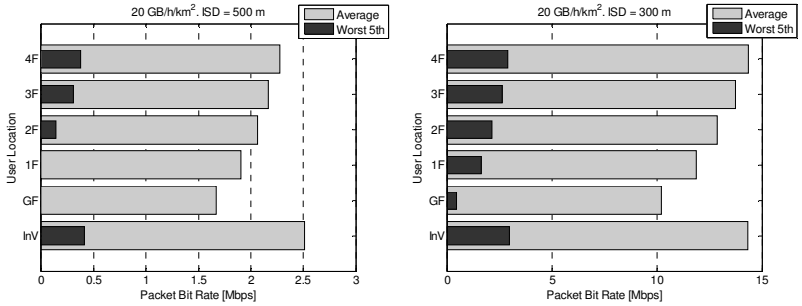


**Figure 5.18.** Average and the worst 5th percentile of the uplink packet bit rates for the different user locations. An inter-site distance equal to 500 m or 300 m is assumed.

increased from 0 to 1.9 Mbps. At the same time the average cell utilization is reduced from 67.2% to 11.1%. The obtained results indicate that both the average user performance and the performance of the worst 5th percentile of the users have a clear dependency on the coupling loss. Hence, the poor user performance is caused mainly by the lack of sufficient UE transmission power to compensate for the coupling loss towards the serving eNodeB. This is also the case for the densified network deployment; Even though the coupling losses are reduced (see Figure B.6 in Annex B), the UE transmission powers are not reduced, since the users occupy a larger number of PRBs and aim for a higher received power (i.e. the values of $M_{m,b}$ and $P_{0,b}$ in (4.1) will be increased).

Locations of the worst and the best performing decile of users are shown in Figure 5.19. As can be seen, there is a clear dependency on the coupling loss. Almost half of the worst performing users are located either on the ground floor or on the 1st floor. Similarly, more than 60% of the best performing users are located either inside vehicles, or on the upper floor levels. When the ISD is reduced, the distribution of the worst and the best

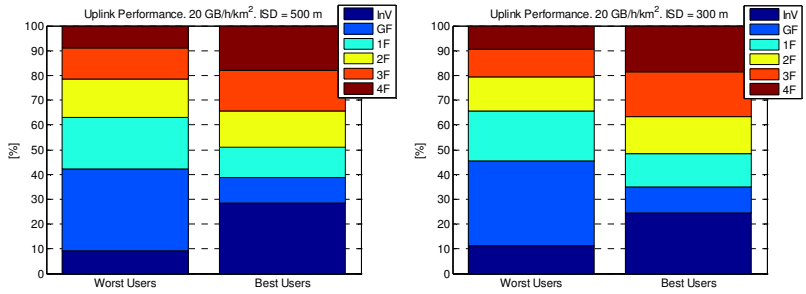


**Figure 5.19.** Locations of the worst and the best performing users, assuming an inter-site distance of 500 m or 300 m.

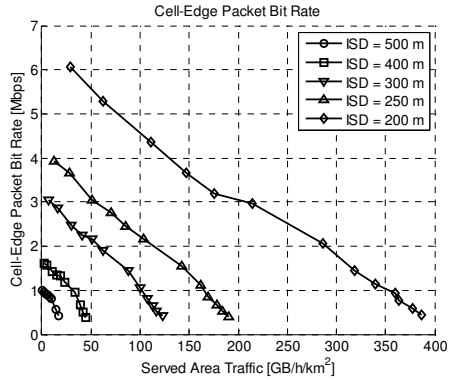


**Figure 5.20.** Uplink cell-edge packet bit rate as a function of the served area traffic for homogeneous macro deployments with different inter-site distances.

users becomes slightly more uniform, but indicates still a clear dependency on the coupling loss. This is well in line with the conclusion that the uplink is mainly power-limited.

Results for the uplink capacity evaluation are shown in Figure 5.20. According to the results, uplink seems to experience larger relative network densification gains compared to the downlink. A similar conclusion can be drawn by looking at the curves in Figure 5.21 and the values in Table 5.6, which indicate the required macro site density and the required density of new macro sites, respectively, to fulfill the desired uplink coverage and capacity requirements. In fact, while the densification efficiency stays roughly constant for the downlink, in uplink it seems to increase as a function of the macro site density. The uncertainties listed for the downlink can be expected to be valid for the uplink as well. However, there is one specific difference making the network densification even more efficient for the uplink, namely the increased $P_0$ as a function of the macro site density, see Table 4.5 and the discussion within Section 4.3.4.

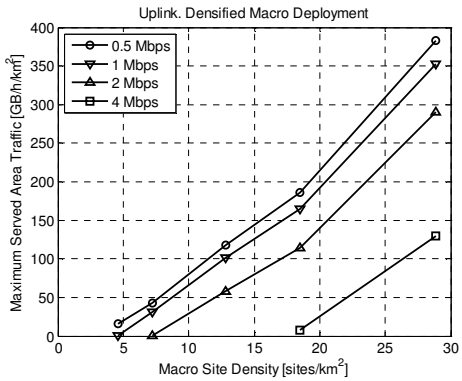


**Figure 5.21.** Maximum uplink served area traffic as a function of the macro site density for a few different coverage requirements.

**Table 5.6.** Required density of new macro sites (sites/km²) to fulfill the desired uplink coverage and capacity requirements.

| Coverage Req | Capacity Requirement | | | |
|---|---|---|---|---|
| | 30 GB/h/km² | 60 GB/h/km² | 90 GB/h/km² | 120 GB/h/km² |
| 0.5 Mbps | 1.4 | 3.9 | 6.1 | 8.4 |
| 1 Mbps | 2.5 | 4.9 | 7.3 | 9.8 |
| 2 Mbps | 5.5 | 8.4 | 11.4 | 14.2 |
| 4 Mbps | 16.3 | 18.7 | 21.1 | 23.5 |

Finally, results for the observed levels of traffic offloading and the average cell utilizations are listed in Table 5.7 and in Table 5.8, respectively. Similar to the downlink, the improved system coverage is obtained by densifying the network deployment and by reducing the maximum utilization of the cell resources. Furthermore, the improved system capacity is obtained by densifying the network, as well as by increasing the maximum utilization of the cell resources (in particular for the higher coverage requirements).

## 5.3 Summary of the evaluation results

Results for the baseline deployment indicate that the downlink performance is quite often interference-limited, in particular when it comes to the performance of the cell-edge users, while the uplink performance is clearly power-limited. In other words, in downlink the poor user performance is caused by the high load within the serving cell, while in

**Table 5.7.** Observed levels of traffic offloading for the desired network operating points.

| Coverage Req | Capacity Requirement | | | |
|---|---|---|---|---|
| | 30 GB/h/km² | 60 GB/h/km² | 90 GB/h/km² | 120 GB/h/km² |
| 0.5 Mbps | 23.2% | 45.8% | 57.1% | 64.5% |
| 1 Mbps | 35.2% | 51.5% | 61.2% | 68.0% |
| 2 Mbps | 54.4% | 64.6% | 71.2% | 75.5% |
| 4 Mbps | 77.9% | 80.2% | 82.0% | 83.5% |

**Table 5.8.** Average cell utilization for the desired network operating points.

| Coverage Req | Capacity Requirement | | | |
|---|---|---|---|---|
| | 30 GB/h/km² | 60 GB/h/km² | 90 GB/h/km² | 120 GB/h/km² |
| 0.5 Mbps | 57.7% | 60.8% | 60.5% | 60.2% |
| 1 Mbps | 43.2% | 47.6% | 50.8% | 51.5% |
| 2 Mbps | 17.7% | 30.0% | 32.5% | 34.7% |
| 4 Mbps | 7.8% | 10.8% | 13.8% | 16.8% |

uplink the main reason for the poor user performance is the large coupling loss between the user and the serving eNodeB. As a result, the worst performing downlink users are fairly uniformly distributed over the different user locations, while the worst performing uplink users can typically be found on the ground floor and on the 1st floor, which also have the largest coupling losses towards the closest macro eNodeBs. What is also visible in the uplink results is the impact of floor height gain, meaning that the user performance is improved as a function of the floor level.

As a result of the densified macro network, the offered load per cell is reduced, reducing both the average cell utilization and the level of inter-cell interference, and improving the SINR. Furthermore, since the average number of simultaneously active users is reduced, the scheduled users are able to consume more resources both in time, frequency and power domain. The improved SINRs and the increased amount of resources in the frequency and power domain result in higher achievable bit rates for the scheduled users. In addition, the increased availability of the time domain resources results in improved user throughputs. Finally, as a result of the increased user throughputs, the users can complete their packet

transmissions quicker, which reduces the average cell utilization even more than what the straightforward resource addition would suggest.

The obtained results indicate that the most site-efficient way[10] to achieve the desired coverage improvement is to densify the network deployment and at the same time to reduce the maximum utilization of the cell resources. Furthermore, the most site-efficient way to improve the system capacity is to densify the network deployment and at the same time to increase the maximum utilization of the cell resources, while still making sure that the desired coverage requirement is fulfilled.

The results indicate also that the relative densification gains are larger for the uplink than they are for the downlink. One explanation for this is that while in downlink the network densification increases the availability of resources only in time domain, in uplink the availability of resources is increased also in frequency and power domain.

[10] The most site-efficient deployment is the one that can achieve the desired system performance with the lowest number of new sites to be deployed.

# 6. Performance of the heterogeneous micro deployment

This chapter discusses the performance of various types of heterogeneous micro deployments. The assumed network layout consists of a homogeneous macro cell layer with an inter-site distance of 500 meters (baseline deployment), and a micro cell layer with micro sites deployed within the traffic clusters. As a default, the micro eNodeB output power is assumed to be equal to 1 W, and the antennas are assumed to be deployed at a height of 5 m above the street level (i.e. 14 m below the rooftops).

First, the system performance as a function of the micro site density is evaluated. Then, the impact of micro eNodeB output power on the observed traffic offloading and the overall system performance is studied. Finally, the achievable gains with the help of biased cell selection and the adjacent channel deployment of the cell layers are evaluated as well.

Some of the results presented in this chapter have already been published as part of papers [146] and [147].

## 6.1 Downlink performance

As an alternative to deploying new macro sites the system performance can be improved also by deploying new low-power sites into the traffic clusters. The motivations for the improved system performance are the same as for the densified macro deployment: Firstly, the SINR and the achievable bit rate will be improved both as a result of a lower level of inter-cell interference and as a result of lower coupling losses towards the serving eNodeBs. Secondly, as a result of the reduced number of simultaneously active users per cell, the scheduled users are allowed to consume more resources, which results in improved achievable bit rates and user throughputs.

The improved system performance can be verified by evaluating the performance of a heterogeneous micro deployment as a function of the

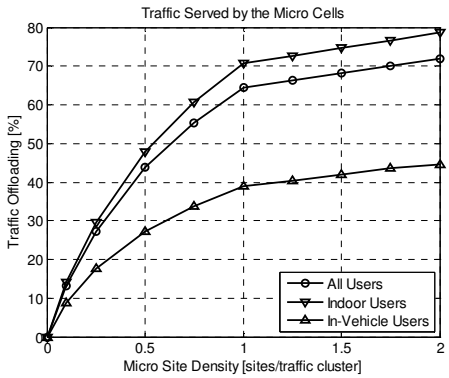


**Figure 6.1.** Observed traffic offloading as a function of the macro site density.

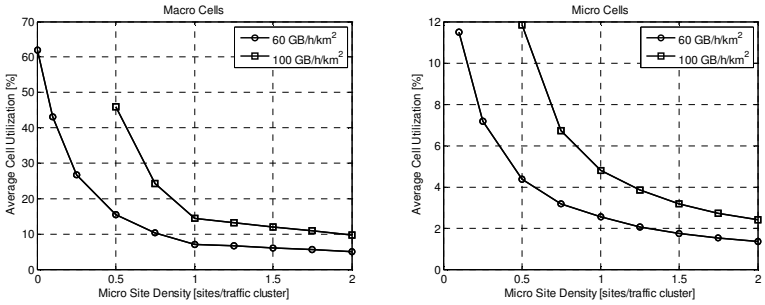


**Figure 6.2.** Average macro and micro cell utilization as a function of the micro site density.

micro site density. During the evaluations the level of offered area traffic is fixed either to 60 GB/h/km² or to 100 GB/h/km². To start with, results for the observed traffic offloading are shown in Figure 6.1 and the results for the average macro and micro cell utilization are shown in Figure 6.2. As expected, the traffic offloading increases as a function of the micro site density. However, the increase rate is found to decrease as a function of the micro site density, which suggests that the new micro cells offload traffic not only from the macro cells, but also from the neighboring micro cells. This becomes even more evident for micro site densities larger than one site per traffic cluster. When it comes to the results for the average cell utilization, the observed gains are larger than what would be suggested by the traffic offloading. This is a result of the fact that due to the improved SINRs and the increased amount of resources in the time domain, the users can finish their packet transmissions quicker, which reduces the average macro cell utilization more than the spatial resource addition would suggest. This is also the reason, why the average micro cell utilization is reduced more than what would be suggested by the traffic offloading towards the new micro cells.

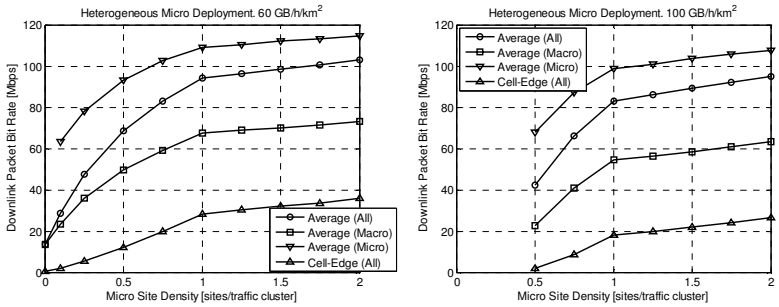


**Figure 6.3.** Downlink user performance as a function of the micro site density.

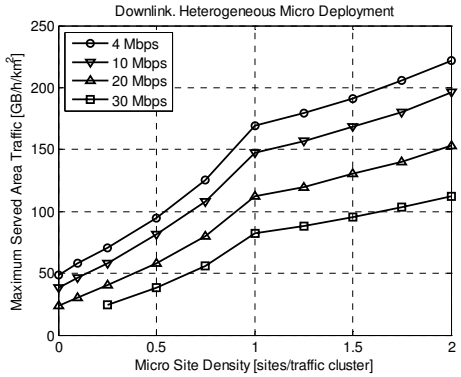


**Figure 6.4.** Maximum downlink served area traffic as a function of the micro site density for a few different coverage requirements.

Results for the downlink user performance are shown in Figure 6.3. As can be seen, introduction of micro cells under the macro cell layer is clearly beneficial for the downlink user performance. One can also see that most of the gains are achieved when each traffic cluster has received one micro cell; deploying also a second micro cell brings only minor gains. Finally, the performance of the users served by the micro eNodeBs is clearly better than the performance of the users served by the macro eNodeBs.

A wider view on the system performance can be obtained by looking at the results for the maximum downlink served area traffic as a function of the micro site density, see Figure 6.4. As can be noticed, heterogeneous micro deployments improve both the coverage and the capacity compared to the baseline deployment. This is demonstrated also by the results in Table 6.1, indicating the required density of micro sites to be deployed in order to fulfill the desired coverage and capacity requirements.

Results for the corresponding levels of traffic offloading are shown in Table 6.2. Furthermore, results for the average macro cell utilization and the average micro cell utilization are shown in Table 6.3 and Table 6.4, respectively. As can be seen, the situation is similar to the densified macro

**Table 6.1.** Required micro site density (sites/km²) to fulfill the desired downlink coverage and capacity requirements.

| Coverage Req | Capacity Requirement | | | |
|---|---|---|---|---|
| | 50 GB/h/km² | 100 GB/h/km² | 150 GB/h/km² | 200 GB/h/km² |
| 4 Mbps | 0.6 | 24.5 | 40.0 | 74.0 |
| 10 Mbps | 6.6 | 30.3 | 48.3 | - |
| 20 Mbps | 17.3 | 40.5 | 87.1 | - |
| 30 Mbps | 29.7 | 73.4 | - | - |

**Table 6.2.** Observed levels of traffic offloading for the desired network operating points.

| Coverage Req | Capacity Requirement | | | |
|---|---|---|---|---|
| | 50 GB/h/km² | 100 GB/h/km² | 150 GB/h/km² | 200 GB/h/km² |
| 4 Mbps | 1.7% | 45.6% | 60.3% | 69.2% |
| 10 Mbps | 17.3% | 51.8% | 64.8% | - |
| 20 Mbps | 36.1% | 60.7% | 71.4% | - |
| 30 Mbps | 51.2% | 69.3% | - | - |

deployment: The most site-efficient way to improve the system coverage is to densify the network deployment and to reduce the maximum cell resource utilization at the same time. Furthermore, the most site-efficient way to enhance the system capacity is to densify the network deployment and to increase the maximum cell resource utilization. The difference compared to the densified macro deployment is that when it comes to the network operating points with the highest capacity requirements (150 and 200 GB/h/km²), the gain of network densification is too low, which means that also the average micro cell resource utilization has to be lowered in order to fulfill the desired coverage and capacity requirements. Hence, from the system capacity point of view the micro cell layer has to be overdimensioned in order to be able to fulfill also the coverage requirement.

The potential for further capacity and coverage enhancements is evaluated for a deployment with two micro sites within each of the traffic clusters, and for an operating point with served area traffic equal to 197 GB/h/km². The observed average and cell-edge packet bit rates are equal to 71 and 9.7 Mbps, respectively. Furthermore, 28% of the traffic is served by the macro cells, while 72% of the traffic is served by the micro cells. Finally,

**Table 6.3.** Average macro cell utilization for the desired network operating points.

| Coverage Req | Capacity Requirement | | | |
|---|---|---|---|---|
| | 50 GB/h/km² | 100 GB/h/km² | 150 GB/h/km² | 200 GB/h/km² |
| 4 Mbps | 36.5% | 40.0% | 45.1% | 49.0% |
| 10 Mbps | 21.0% | 25.8% | 30.5% | - |
| 20 Mbps | 12.1% | 15.5% | 17.8% | - |
| 30 Mbps | 7.9% | 10.3% | - | - |

**Table 6.4.** Average micro cell utilization for the desired network operating points.

| Coverage Req | Capacity Requirement | | | |
|---|---|---|---|---|
| | 50 GB/h/km² | 100 GB/h/km² | 150 GB/h/km² | 200 GB/h/km² |
| 4 Mbps | 1.3% | 10.3% | 12.3% | 10.3% |
| 10 Mbps | 5.7% | 7.2% | 8.7% | - |
| 20 Mbps | 3.5% | 4.9% | 4.1% | - |
| 30 Mbps | 2.5% | 2.8% | - | - |

the average macro cell utilization is equal to 32%, while the average micro cell utilization is equal to 7%.

Figure 6.5 presents both the level of the observed traffic offloading and the average packet bit rates (in Mbps) for the different user locations. The level of traffic offloading within each of the areas is indicated by the length of the dark grey bars. As can be noticed, 45% of the in-vehicle users are served by the micro cells. Furthermore, as a result of the increasing signal strength of the macro cells, the level of traffic offloading is reduced from 86% to 70% when moving upwards inside the building.

Results for the average downlink packet bit rate, as indicated by the numbers on the bars, demonstrate the benefit of being served by the micro eNodeBs. The average downlink packet bit rate is around 35 Mbps for the macro users, while at the same time the micro users achieve an average downlink packet bit rate of 85 Mbps. The average macro user performance is almost the same for all of the investigated areas, but the average micro user performance is affected by the inter-layer interference. The best micro user performance is observed on the ground floor, where also the interference from the macro cells is the weakest. The observed average floor-level performance, indicated by the numbers inside the brackets, is

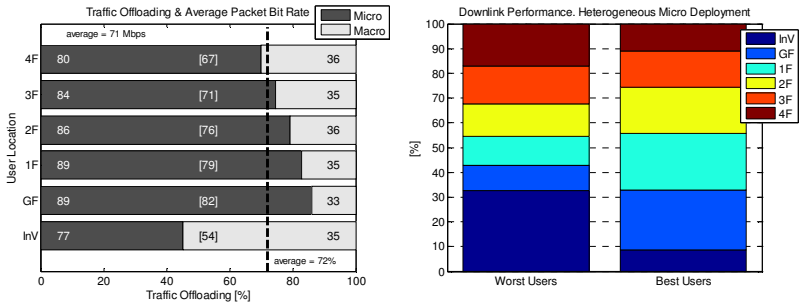


**Figure 6.5.** Observed traffic offloading and the average downlink packet bit rate for the different user locations (left), and the locations of the worst and the best performing decile of the users (right). Heterogeneous micro deployment with two micro sites per traffic cluster and served area traffic equal to 197 GB/h/km² are assumed.

affected by the traffic offloading. In practice it means that the users on the 4th floor have in average worse performance compared to the users on the ground floor, which is a clear difference compared to the densified macro deployment.

Locations of the worst and the best performing decile of users are studied in Figure 6.5. As can be seen, the locations of the best performing users, which are all served by the micro eNodeBs, follow the observed traffic offloading statistics quite nicely. When it comes to the worst performing users, roughly 74% of them are served by the macro eNodeBs. Approximately one third of the worst performing users are located inside vehicles, while the rest are distributed over the different floor levels following roughly the distribution of the macro users. Hence, in order to further enhance the downlink performance of the heterogeneous micro deployment, enhancing the traffic offloading, and further, the performance of the in-vehicle users and the users located on the upper floor levels should be in focus. Two possible methods to achieve this, adjusting the output power of the micro eNodeBs and the biased cell selection, are discussed in Section 6.3 and Section 6.4, respectively. Yet another way to improve the performance of the worst users would be to densify the macro cell layer together with the introduction of micro cells within the traffic clusters.

## 6.2 Uplink performance

The gain of network densification on the uplink is demonstrated by evaluating the performance of a heterogeneous micro deployment as a function of the micro site density. As discussed in Section 4.3.4, and listed in Table 4.6, micro cells offload many of the most power-limited indoor

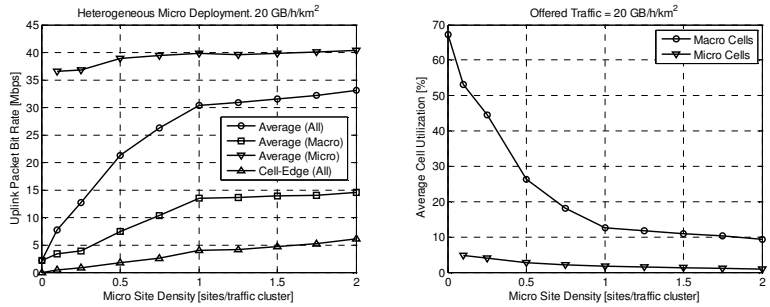


**Figure 6.6.** Uplink user performance and the average cell utilizations as a function of the micro site density.

users, which means that the value of $P_{0,macro}$ can be increased from -119 dBm to -111 dBm for the remaining macro users, when the micro site density is increased from zero to two micro sites per traffic cluster. As a result, the performance of the macro users is considerably improved. Another motivation for the improved macro user performance is the increased amount of resources both in time and frequency domain as a result the traffic offloading.

The results in Figure 6.6 demonstrate the benefit of being served by the micro eNodeB. The main reason for the considerably higher micro user performance is the difference between the applied $P_{0,micro}$ and $P_{0,macro}$. In fact, the user performance within the micro cells seems to quite often be limited by the maximum allowed modulation and coding scheme, and not by the received power target, inter-cell interference or UE transmission power. It would therefore be quite safe to claim that the assumed $P_{0,micro}$ is too high, resulting in an unnecessary high interference towards the macro cell layer. However, one should keep in mind that the assumed network load, 20 GB/h/km², is very low in this example. At higher network loads the level of inter-cell interference increases, and the interference margin included in the $P_{0,micro}$ becomes more useful.

Figure 6.7 shows the results for the maximum uplink served area traffic as a function of the micro site density. Furthermore, Table 6.5 lists the required micro site densities to fulfill the desired coverage and capacity requirements. Similar to the downlink, also in uplink most of the gains can be achieved by deploying one micro site within each of the traffic clusters. However, uplink seems to benefit much more from the heterogeneous micro deployment compared to the downlink. One reason for this is that the uplink in the baseline deployment is considerably more power-limited than the downlink, which means that the worst uplink users can typically be found within areas that have the highest coupling loss towards the serving eNodeB, e.g. on the ground floors. Due to the EGoS scheduling, poor

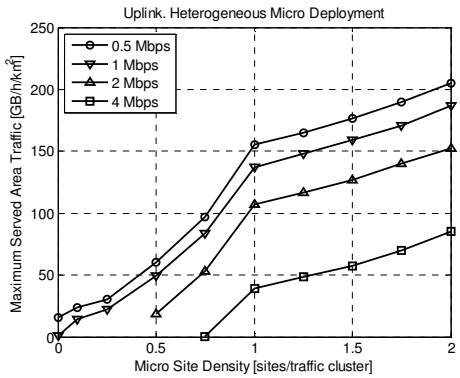


**Figure 6.7.** Maximum uplink served area traffic as a function of the micro site density for a few different coverage requirements.

**Table 6.5.** Required micro site density (sites/km²) to fulfill the desired uplink coverage and capacity requirements.

| Coverage Req | Capacity Requirement | | | |
|---|---|---|---|---|
| | 30 GB/h/km² | 60 GB/h/km² | 90 GB/h/km² | 120 GB/h/km² |
| 0.5 Mbps | 11.2 | 22.3 | 31.5 | 38.1 |
| 1 Mbps | 14.4 | 25.9 | 35.0 | 41.3 |
| 2 Mbps | 26.1 | 35.1 | 41.3 | 59.9 |
| 4 Mbps | 42.2 | 69.5 | - | - |

performance of the worst users will hurt the overall performance of the cell. When micro sites are deployed within the traffic clusters, indoor users experiencing the highest coupling losses towards the macro eNodeBs are likely to be served by the micro eNodeBs instead. The macro cell can therefore experience a large offloading gain both as a result of a lower number of simultaneously served users, and also as a result of improved achievable rates for the worst users.

Finally, results for the observed levels of traffic offloading for the desired network operating points are presented in Table 6.6, and the results for the average macro and micro cell utilizations are collected in Table 6.7 and in Table 6.8.

Next, the uplink performance of a heterogeneous micro deployment with two micro sites per traffic closer is studied a bit closer. At the selected network operating point the served uplink area traffic is equal to 178 GB/h/km² and the average and the cell-edge packet bit rates are equal to 27 Mbps and 1.3 Mbps, respectively. Furthermore, the average macro cell

**Table 6.6.** Observed levels of traffic offloading for the desired network operating points.

| Coverage Req | Capacity Requirement | | | |
|---|---|---|---|---|
| | 30 GB/h/km² | 60 GB/h/km² | 90 GB/h/km² | 120 GB/h/km² |
| 0.5 Mbps | 27.1% | 43.1% | 52.8% | 58.8% |
| 1 Mbps | 31.9% | 47.3% | 56.3% | 61.3% |
| 2 Mbps | 47.4% | 56.4% | 61.5% | 67.1% |
| 4 Mbps | 62.1% | 68.3% | - | - |

**Table 6.7.** Average macro cell utilizations for the desired network operating points.

| Coverage Req | Capacity Requirement | | | |
|---|---|---|---|---|
| | 30 GB/h/km² | 60 GB/h/km² | 90 GB/h/km² | 120 GB/h/km² |
| 0.5 Mbps | 64.3% | 72.0% | 76.4% | 80.7% |
| 1 Mbps | 51.0% | 61.2% | 67.6% | 73.1% |
| 2 Mbps | 29.6% | 44.7% | 53.7% | 60.6% |
| 4 Mbps | 17.7% | 28.8% | - | - |

**Table 6.8.** Average micro cell utilizations for the desired network operating points.

| Coverage Req | Capacity Requirement | | | |
|---|---|---|---|---|
| | 30 GB/h/km² | 60 GB/h/km² | 90 GB/h/km² | 120 GB/h/km² |
| 0.5 Mbps | 5.7% | 9.0% | 11.4% | 13.8% |
| 1 Mbps | 4.8% | 7.8% | 10.2% | 12.4% |
| 2 Mbps | 3.4% | 6.2% | 8.7% | 8.9% |
| 4 Mbps | 2.6% | 3.6% | - | - |

utilization is equal to 77% and the average micro cell utilization is equal to 10%.

Results for the average packet bit rate are shown in Figure 6.8. What is different compared to the downlink results in Figure 6.5 is the large difference between the average macro user and the average micro user performance. While in downlink the average micro user throughput is roughly twice the average macro user throughput, in uplink the corresponding ratio is approximately equal to 8. Another thing worth

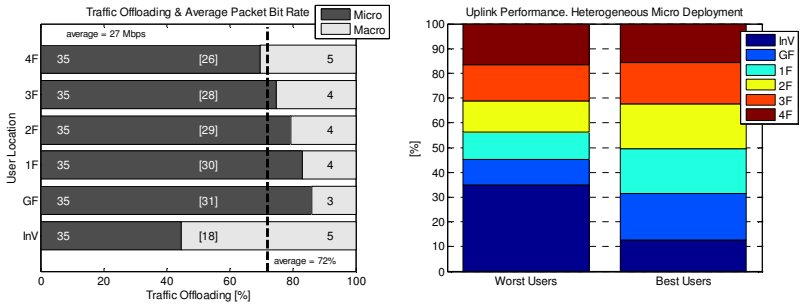


**Figure 6.8.** Observed traffic offloading and the average uplink packet bit rate for the different user locations (left), and the locations of the worst and the best performing decile of the users (right). Heterogeneous micro deployment with two micro sites per traffic cluster and served area traffic equal to 178 GB/h/km² are assumed.

highlighting is that the average micro user performance is almost the same for all the indoor areas. This is related to the fact that the performance of a great majority of the micro users is limited by the modulation and coding scheme, and not by the UE transmission power or the inter-cell interference.

The best performing users are all served by the micro eNodeBs. Furthermore, their performance is in fact equal to the maximum throughput allowed by the modulation and coding scheme. When it comes to the locations of the worst performing decile of users, the only major difference compared to the downlink is that in practice all users belonging to the worst decile are served by the macro eNodeBs. Hence, in order to further enhance the uplink performance of the heterogeneous micro deployment, enhancing the performance of the in-vehicle users and the users on the upper floors should be in focus. Similar to the downlink, it can be achieved for example by adjusting the output power of the micro eNodeBs, by applying biased cell selection, or by densifying the macro cell layer together with the introduction of new micro cells.

## 6.3 Impact of eNodeB output power on system performance

The obtained simulation results for the heterogeneous micro deployment suggest that the traffic offloading, i.e. the ability of the micro cells to cover the whole hotspot area, is playing a major role. As already demonstrated, adding a second micro site into the traffic cluster increases the level of traffic offloading, but the achievable gains are quite moderate. In this section an alternative approach is discussed, that is the adjustment of the micro eNodeB output power.

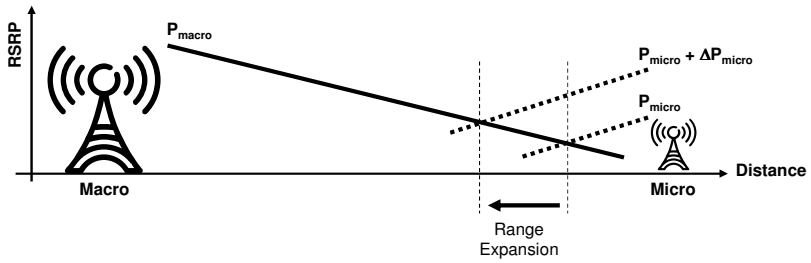


**Figure 6.9.** An increased output power will increase the coverage area of the low-power cell.

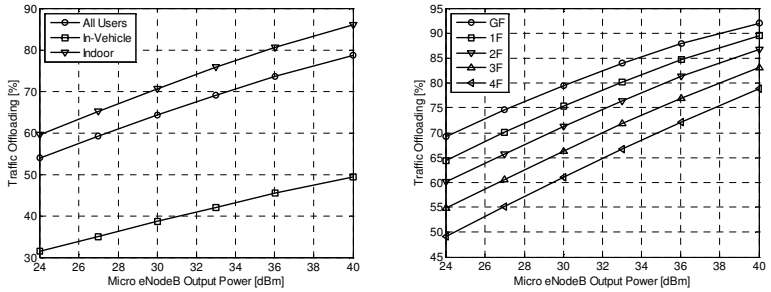


**Figure 6.10.** Observed traffic offloading as a function of the micro eNodeB output power for a heterogeneous micro deployment with one micro site per traffic cluster.

In general, assuming that the serving cell selection is based on the downlink signal strength (RSRP), the size of the micro cell depends on the micro eNodeB output power ($P_{micro}$), see Figure 6.9: A higher $P_{micro}$ will result in a larger micro cell area and vice versa. As a result of the increased cell area, the micro cell is able to offload a larger number of users from the macro cell, improving the performance of the remaining macro users. However, the gains achieved by increasing the $P_{micro}$ even further become limited once the micro cell is able to cover the whole traffic hotspot. As demonstrated in Figure 3.3, the size of the micro cell depends also on the location of the micro site with respect to the micro site. Ideally speaking, in order to cover equally-sized traffic hotspots, a higher $P_{micro}$ would be required for traffic hotspots located close to the micro site, compared to the traffic hotspots located farther away. In this thesis, however, the applied value of $P_{micro}$ is not assumed to depend on the location of the micro site.

The impact of adjusted $P_{micro}$ on the system performance is evaluated with system simulations. In the first phase, a deployment with one micro site per traffic cluster is simulated with different values of $P_{micro}$. During the simulations, the offered area traffic is assumed to be equal to 100 GB/h/km².

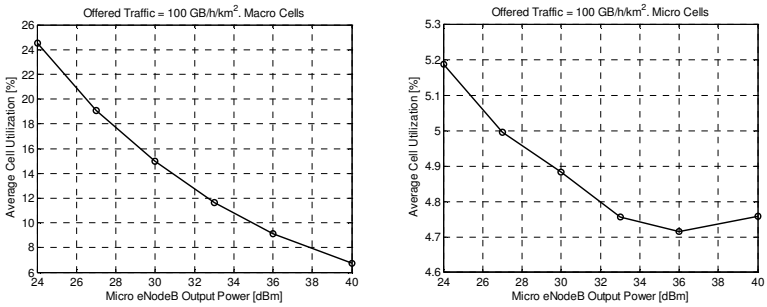


**Figure 6.11.** Average macro and micro cell utilization as a function of the micro eNodeB output power for a heterogeneous micro deployment with one micro site per traffic cluster.

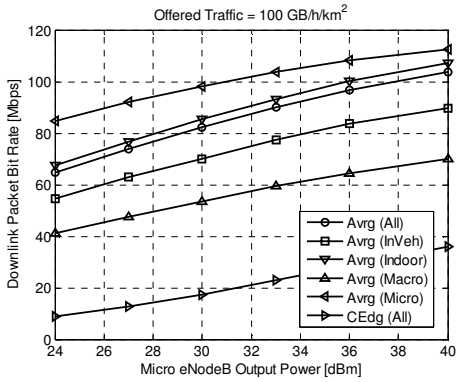


**Figure 6.12.** Downlink user performance as a function of the micro eNodeB output power for a heterogeneous micro deployment with one micro site per traffic cluster.

Results for the observed traffic offloading and the average cell utilizations are presented in Figure 6.10 and Figure 6.11, respectively. Furthermore, results for the downlink (average (*Avrg*) and cell-edge (*CEdg*)) user performance as a function of the $P_{micro}$ are presented in Figure 6.12. As a result of the increased $P_{micro}$, a) traffic offloading is increased, b) performance of the remaining macro users is improved, and c) average macro cell utilization becomes lower. The increased traffic offloading will improve the performance of the remaining macro users due to: a) lower level of inter-cell interference and improved SINRs, and b) lower number of simultaneously active users per macro cell. When it comes to the average utilization of the micro cells, it is negatively affected by the increased offered traffic as a result of the cell range expansion. However, as a result of the reduced average macro cell utilization, as well as the increased $P_{micro}$, the micro users will experience improved SINRs, as demonstrated by the results in Figure 6.13. Since the gains due to the improved SINRs are larger than the losses related to an increased level of offered micro cell traffic, the

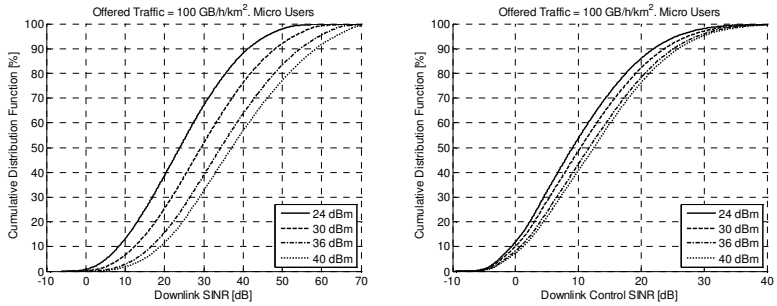


**Figure 6.13.** Distribution of the downlink SINR values for the micro users, assuming different values of the micro eNodeB output power.

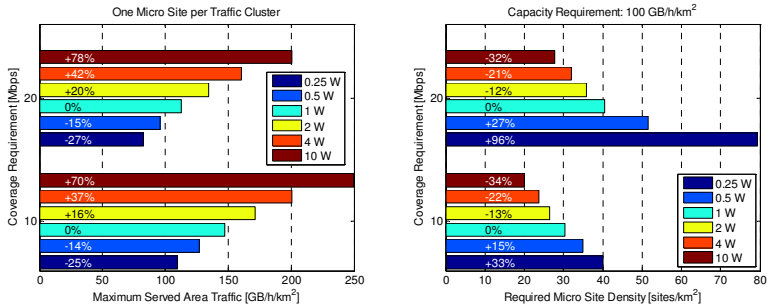


**Figure 6.14.** Required micro site density as a function of the micro eNodeB output power to fulfill the desired coverage and capacity requirements.

average utilization of the micro cells is reduced, and the average throughput of the micro users is improved together with an increasing $P_{micro}$.

The curves in Figure 6.12 indicate that the indoor users benefit a bit more from the increased $P_{micro}$ compared to the in-vehicle users. This is due to the fact that micro cell range expansion is beneficial mostly for the users inside the traffic clusters. At the same time, in-vehicle users located outside the traffic clusters can only benefit from the traffic offloading, but can also suffer from the increased level of inter-layer interference.

The results shown in this section suggest that as a result of the increased $P_{micro}$ and the improved user performance, the network is able to serve a higher traffic volume while still fulfilling the desired coverage requirement. Alternatively, the network is able to fulfill the desired coverage and capacity requirements with a lower density of micro sites. Both of these are demonstrated in Figure 6.14, where the different bars indicate a) the maximum served area traffic when the coverage requirement is equal to either 10 Mbps or 20 Mbps, and b) the required density of micro sites to fulfill both a capacity requirement of 100 GB/h/km² and a coverage requirement of either 10 Mbps or 20 Mbps. The numbers on the bars indicate the relative difference compared to a deployment with $P_{micro}$ equal

to 1 W. For example, a deployment with $P_{micro}$ equal to 2 W requires 12-13% less micro sites than a deployment with 1 W output power. Similarly, a deployment with 4 W or 10 W output power requires 21-22% or 32-34% less micro sites, respectively, than a deployment with $P_{micro}$ equal to 1 W. One can also see that if $P_{micro}$ is lowered from 1 W to 500 mW, the required number of sites becomes 15-27% larger, depending on the coverage requirement. Furthermore, if $P_{micro}$ is as low as 250 mW, the required number of micro sites increases considerably compared to a deployment with 1 W output power.

## 6.4 Impact of biased cell selection and spectrum allocation

Applying a cell selection offset equal to $O_{micro}$ to the micro cell is from the cell selection point of view equal to increasing the output power of the micro eNodeB with the same amount. As discussed in Section 3.2.1, the problem with the *biased cell selection* is that if the cell layers are operating on the same carrier frequency, users located within the extended area, and served by the weaker micro cell, can suffer from a very poor downlink quality due to the interference received from the stronger macro cell. Quality of the data symbols can be improved by utilizing the normal 3GPP LTE Release-8 ICIC mechanisms. However, those mechanisms will not be able to improve the quality of the downlink control signaling. In order to resolve also that problem, a number of enhanced ICIC (eICIC) methods have been introduced as part of 3GPP LTE Release-10 and Release-11.

Performance of the biased cell selection is evaluated in this section. The evaluation does not assume any dynamic ICIC methods, but the impact of a static interference management via adjacent channel deployment of the cell layers is considered. Furthermore, the evaluations are performed for two different heterogeneous micro deployments: a deployment with one micro site per traffic cluster and a deployment with an average of one micro site per macro cell. The latter corresponds to a deployment where 31% of the traffic clusters have a micro site.

For both deployments, three different scenarios are evaluated:

- Co-channel deployment of macro and micro cells, ignoring the quality of the downlink control signaling (*R1/without CCH*).
- Co-channel deployment of macro and micro cells, taking the quality of the downlink control signaling into account with SINR threshold equal to -7 dB (*R1/with CCH*).

- Adjacent channel deployment of macro and micro cells, taking the quality of the downlink control signaling into account with SINR threshold equal to -7 dB (*AC/with CCH*).

When the cell layers are operating on separate carrier frequencies, the problem with the quality of the downlink control signaling becomes considerably smaller. Hence, considerably larger cell selection offsets can be applied before the negative impact on the downlink quality becomes visible. However, the obvious cost with the adjacent channel deployment is that the peak data rates are reduced for all users as a result of the splitted carrier bandwidth. The carrier bandwidths allocated for the macro and the micro cell layer depend on the assumed micro site density. For the deployment with one micro site per traffic cluster, the best system performance is achieved, when the system bandwidth of 20 MHz is divided equally between the macro and the micro cell layer. However, when the micro site density is reduced to one micro site per macro cell, the best performance is obtained by allocating 15 MHz for the macro cell layer and 5 MHz for the micro cell layer. This is due to the relatively low level of traffic offloading, which puts quite high requirements on the capacity of the macro cell layer.

### 6.4.1 One micro site per traffic cluster

Results for the observed traffic offloading and the average cell utilizations are shown in Figure 6.15 and Figure 6.16, respectively. Furthermore, results for the downlink user performance as a function of the applied micro cell offset ($O_{micro}$) are presented in Figure 6.17. The offered area traffic is assumed to be equal to 100 GB/h/km$^2$.

As expected, from the traffic offloading point of view there is no difference between the method where the $P_{micro}$ is increased from 30 dBm to 40 dBm, and the method where the $O_{micro}$ is increased from 0 dB to 10 dB. Moreover, in case of the co-channel deployment, the results for the average macro cell utilization look approximately the same for both cell range expansion methods (Figure 6.16 vs. Figure 6.11), i.e. when the level of cell range expansion is increased from 0 dB to 10 dB the average macro cell utilization is reduced from 15% to 7%. However, when it comes to the results for the average micro cell utilization, there is a clear difference. If the cell range expansion is based on an increased $P_{micro}$, the average micro cell utilization is marginally reduced from 4.9% to 4.7%, while in case of the biased cell selection the average micro cell utilization increases from 4.9%

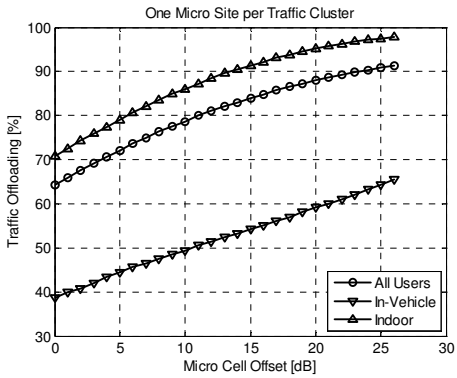


**Figure 6.15.** Observed traffic offloading as a function of the applied micro cell offset. A deployment with one micro site per traffic cluster is assumed.

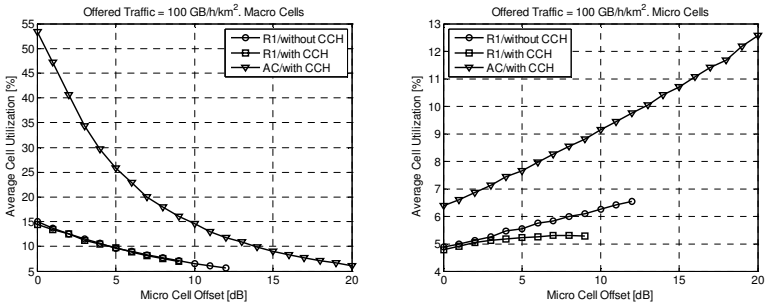


**Figure 6.16.** Average macro and micro cell utilization as a function of the micro cell offset for a heterogeneous micro deployment with one micro site per traffic cluster.

to 6.2% (*R1/without CCH*). The reason for this is the reduced performance of the micro users, as demonstrated by the results in Figure 6.17.

The obtained results show very similar trends as the ones presented in [77] and [149]: Firstly, the traffic offloading can be increased by applying a larger $O_{micro}$. Secondly, the cell-edge user performance is improved as a result of the increased $O_{micro}$. However, after a certain point, an increased $O_{micro}$ results in a worse cell-edge user performance. In [149], the optimum value of $O_{micro}$ is found to be equal to 6 dB when no ICIC mechanisms are applied, while in this section the best cell-edge performance is achieved with $O_{micro}$ equal to 9 dB (*R1/without CCH*), 4 dB (*R1/with CCH*) or 12 dB (*AC/with CCH*). As demonstrated by the results in [149], the cell-edge performance can be further improved by applying a time domain eICIC mechanism, allowing the use of higher values of $O_{micro}$.

The reduced micro user performance compared to the approach with an increased $P_{micro}$ is a result of the fact that the downlink quality of the micro users is considerably worse, as shown by the curves in Figure 6.18 (compared to the corresponding results in Figure 6.13). In case of the

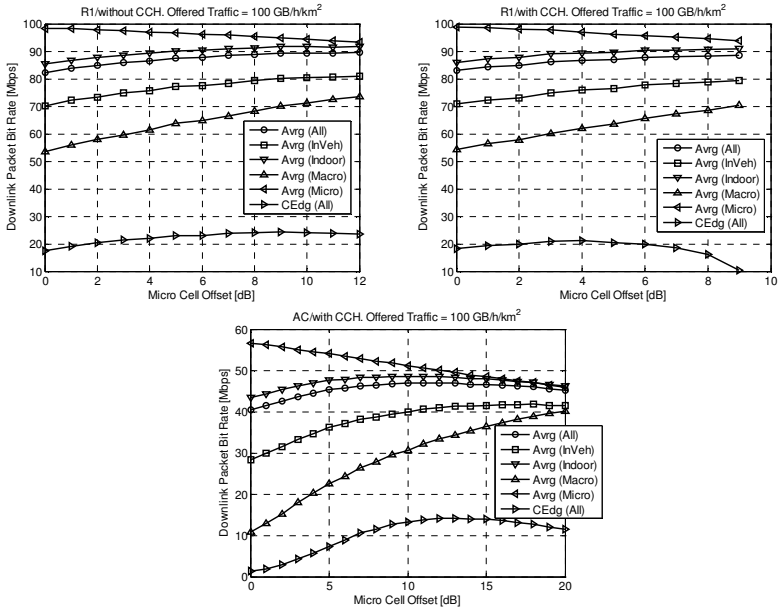


**Figure 6.17.** Downlink user performance as a function of the micro cell offset for a heterogeneous micro deployment with one micro site per traffic cluster.

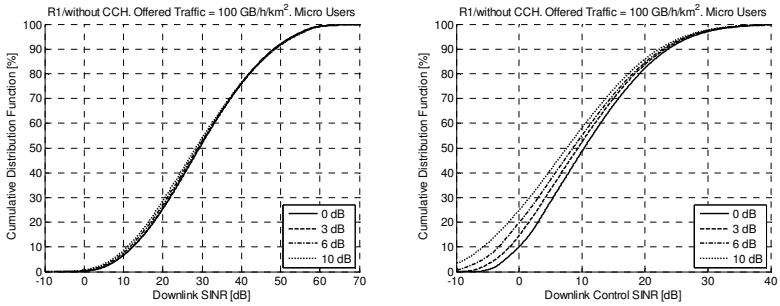


**Figure 6.18.** Distribution of the downlink SINR values for the micro users, assuming different values of the micro cell offset.

increased $P_{micro}$ the downlink SINR, and further the average micro user throughput is improved together with the increasing $P_{micro}$. However, in case of biased cell selection, the downlink SINR is marginally reduced together with the increasing $O_{micro}$. Since the changes in the downlink quality are not able to compensate for the increased offered load, the average micro user throughput is reduced. Finally, in case of the adjacent channel deployment, the desired amount of traffic has to be served with half the bandwidth, which results in a greatly increased average cell utilization for both the macro and the micro cell layer. At the same time, the observed user performance is considerably reduced.

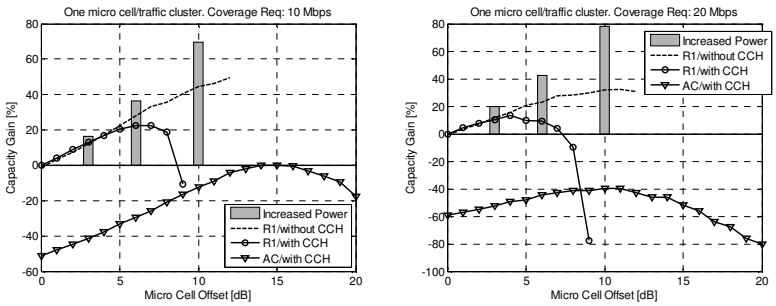


**Figure 6.19.** Downlink capacity gain as a function of the micro cell offset, assuming a deployment with one micro site per traffic cluster.

The curves in Figure 6.18 demonstrate that the biased cell selection has a clear negative impact on the quality of the downlink control signaling within the micro cells. When the quality of the downlink control signaling is taken into account, users with the worst downlink quality are dropped, which results in a reduced micro user performance (dropped users get a zero throughput), but also in a reduced micro cell utilization (micro cells do not need to serve the users with the worst downlink quality).

Results for the downlink capacity gain as a function of the applied $O_{micro}$ are shown in Figure 6.19 for two different coverage requirements: 10 Mbps and 20 Mbps. The gain is calculated with respect to the co-channel deployment with $O_{micro}$ equal to zero. As a comparison, the corresponding capacity gains for the approach with an increased $P_{micro}$ are also included, assuming $P_{micro}$ equal to 2 W (3 dBW), 4 W (6 dBW) and 10 W (10 dBW).

It becomes obvious that the capacity gains obtained with the biased cell selection are lower than the corresponding gains achieved by increasing the $P_{micro}$. Another thing worth highlighting is that when the biased cell selection is applied, the lower coverage requirements seem to experience higher gains. This can be explained by the fact that the lower coverage requirements have also less stringent SINR requirements. If the quality of the downlink control signaling is taken into account, the maximum capacity gain is reached with $O_{micro}$ equal to 4-7 dB, depending on the desired coverage requirement.

As a result of the reduced carrier bandwidths, adjacent channel deployment with $O_{micro}$ equal to zero suffers from a 40-60% capacity loss compared to the reference deployment. The capacity can be increased by increasing the $O_{micro}$, i.e. by offloading more users from the macro cell layer to the micro cell layer, but the performance of the co-channel deployment is not reached.

As discussed in Section 6.2, uplink (cell-edge) performance is limited by the macro users, in particular by the macro users located inside vehicles.

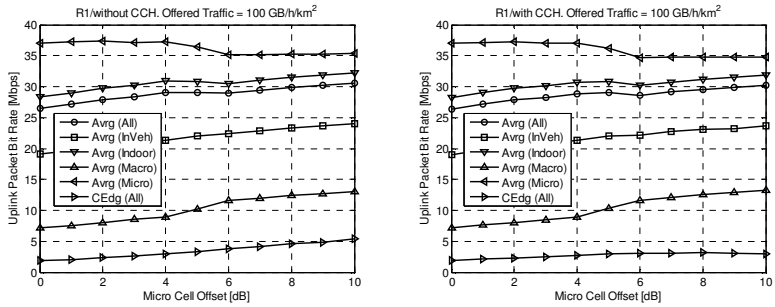


**Figure 6.20.** Uplink user performance as a function of the micro cell offset for a heterogeneous micro deployment with one micro site per traffic cluster.

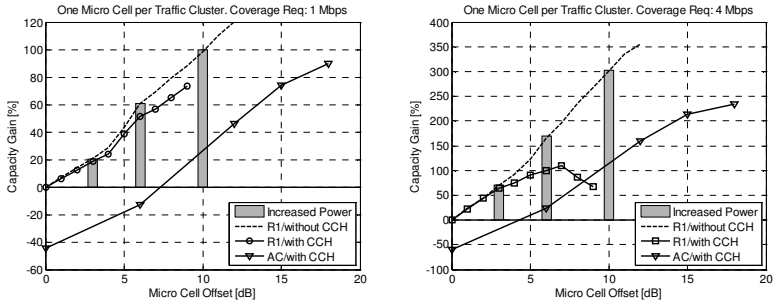


**Figure 6.21.** Uplink capacity gain as a function of the micro cell offset, assuming a deployment with one micro cell per traffic cluster.

When biased cell selection is applied, the level of traffic offloading is increased, increasing the amount of users that can enjoy the considerably better uplink throughputs offered by the micro cells. Furthermore, as a result of the increased traffic offloading, the remaining macro users can benefit from the reduced level of inter-cell interference, as well as the increased amount of resources in the time, frequency and power domain. As a result, the average macro user performance is considerably improved, as shown in Figure 6.20. However, the average micro user throughput is reduced as a function of $O_{micro}$. This is due to the facts that the offered load per micro cell is increased, and the $P_{0,micro}$ lowered as a function of $O_{micro}$.

Despite the fact that the average micro user performance suffers as a result of the biased cell selection, the overall uplink system capacity is improved, as demonstrated by the results in Figure 6.21. The results indicate partly similar trends as the downlink results, but there are also some differences. The first difference is that the uplink benefits more from the biased cell selection compared to the downlink. This is caused by the large difference between the average macro and the average micro user performance. Hence, the gain of being served by the micro eNodeB is considerable. The second difference is that when the quality of the

downlink control signaling is ignored, the approach with the increased $P_{micro}$ gives the same capacity gains as the approach based on the biased cell selection. The reason for this is quite simple: Since the impact of biased cell selection on the downlink quality is ignored, the results reflect solely the impact of the increased micro cell service area on the uplink performance. However, when the quality of the downlink control signaling is taken into account, it has a clear negative impact on the observed capacity gains.

The third difference is related to the performance of the adjacent channel deployment. As already discussed, downlink does not benefit from the splitted carrier bandwidth. The situation is somewhat different for uplink, mainly due to the fact that in uplink it is possible to adjust the received SNR (per PRB) by adjusting the number of PRBs allocated to the UE. For the power-limited UEs the received SNR per PRB can be increased by dividing the total transmission power over a smaller number of PRBs. For the UEs that are not power-limited, a smaller number of occupied PRBs allows the use of a higher received power target, while still keeping the same total UE power. For many UEs this can mean that even though the UE is occupying less PRBs, the achievable bit rate becomes higher, both as a result of the improved SNR, and as a result of a lower average level of inter-cell interference. However, since the observed gains are small, co-channel deployment results in a better performance than the adjacent channel deployment when the same value of $O_{micro}$ is assumed. But since the adjacent channel deployment allows the use of much larger values of $O_{micro}$, it can therefore result in a higher maximum uplink capacity. This is in particular the case for the higher coverage requirements, where both high SINRs and sufficiently low number of simultaneously active users are required.

### 6.4.2 One micro site per macro cell

As shown in the previous section, biased cell selection is beneficial for a deployment where each traffic cluster includes a micro site. This section evaluates the achievable capacity gains in a scenario, where each macro cell contains in average one micro site, or in other words, 31% of the traffic clusters contain a micro site. The main difference is that the cell range expansion is not able to increase the overall traffic offloading as much as in the previous scenario. This is illustrated in Figure 6.22.

Results for the downlink capacity gain are shown in Figure 6.23. As can be noticed, the obtained capacity gains are only marginal. For example, if the quality of the downlink control signaling is taken into account, the

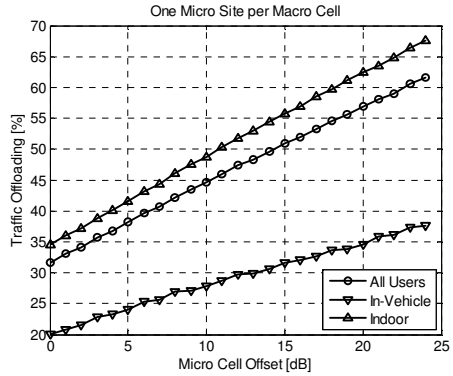


**Figure 6.22.** Observed traffic offloading as a function of the micro cell offset. A deployment with an average of one micro site per macro cell is assumed.

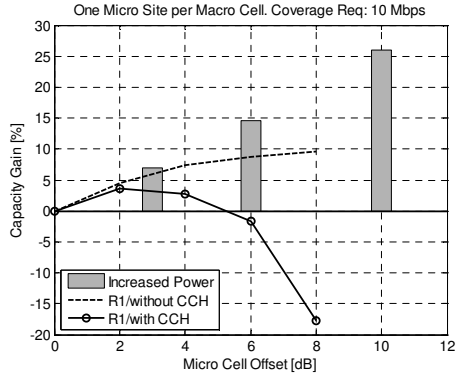


**Figure 6.23.** Downlink capacity gain as a function of the micro cell offset, assuming a deployment with an average of one micro site per macro cell.

maximum achievable capacity gain is less than 5%. Furthermore, the downlink capacity is reduced for $O_{micro}$ larger than 6 dB. Similar to the previous scenario, cell range expansion based on the increased $P_{micro}$ outperforms the biased cell selection. However, the obtained gains are considerably smaller than for the scenario with a higher density of micro sites.

Even for this scenario, the average macro user performance is improved as a function of $O_{micro}$. However, the observed gains are clearly smaller than the ones observed in Figure 6.17. At the same time, the cell-edge user performance experiences only very marginal gains. When the results are studied a bit closer, it becomes evident that the reduced gains are to a large extent caused by the considerably reduced average micro user performance as a function of $O_{micro}$. With large values of $O_{micro}$ the micro cells are offloading an increasing amount of users from bins that do not contain any micro sites. These users are often located on the ground floor, and

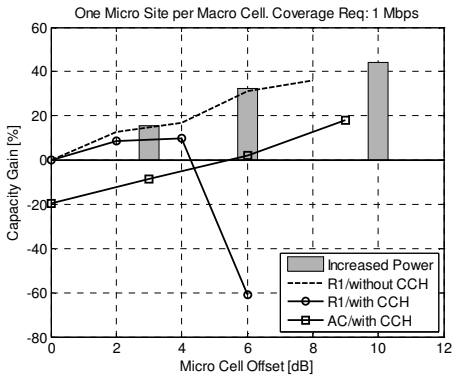


**Figure 6.24.** Uplink capacity gain as a function of the micro cell offset, assuming a deployment with an average of one micro site per macro cell.

experience a fairly large coupling loss towards the closest macro site. Since these users are also quite far away from the serving micro eNodeB, their performance will remain at a low level even after the change of the serving cell layer.

Results for the uplink capacity gain are shown in Figure 6.24. Similar to the scenario with a higher density of micro sites, the performance of the approach with an increased $P_{micro}$ is roughly the same as the performance of the biased cell selection when the quality of the downlink control signaling is ignored. However, the obtained capacity gains are considerably smaller than for the scenario with one micro site per traffic cluster. For example, if the quality of the downlink control signaling is taken into account, the maximum achievable capacity gain is approximately equal to 10%. The obtained results can be motivated by the fact that the micro users located within the extension area are too far away from the serving micro eNodeB to really gain from the change of the serving cell layer.

The uplink performance of the adjacent channel deployment suffers initially from the splitted carrier bandwidth, but becomes in the end slightly better than the performance of the co-channel deployment. However, it does not reach the performance of the cell range expansion based on the increased $P_{micro}$.

As a summary, cell range expansion based on the biased cell selection does not provide as large capacity gains as the approach based on an increased $P_{micro}$. However, the benefit of biased cell selection is that it is simple and inexpensive to introduce into the network. The results indicate also that the performance of the biased cell selection is limited by the quality of the downlink control signaling. However, even though the impact of downlink control signaling would be ignored, biased cell selection would lead to considerable gains on the system-level performance only in

scenarios, where it would result in a sufficiently large increase in traffic offloading from the macro to the micro cell layer.

## 6.5 Summary of the evaluation results

The results presented in this chapter indicate that the heterogeneous micro deployment is a realistic alternative to the densified macro deployment. However, the price to pay is that the required number of new sites becomes considerably larger. As demonstrated by the evaluation results, heterogeneous micro deployment requires approximately 7-9 times as many new sites as the densified macro deployment to fulfill the same downlink coverage and capacity requirements. For uplink, the heterogeneous deployment is found to be slightly more efficient, but the heterogeneous micro deployment requires still approximately 3-8 times as many sites as the densified macro deployment. One reason why the uplink benefits more from the heterogeneous deployment is that the uplink in the baseline deployment is considerably more power-limited than the downlink. When micro sites are deployed within the traffic clusters, indoor users experiencing the highest coupling losses towards the macro eNodeBs, which often are the most expensive users from the radio resources' point of view, are likely to be served by the micro cells instead. The macro cells can therefore experience large offloading gains both as a result of a lower number of simultaneously served users, and also as a result of improved achievable bit rates for the worst performing users.

Furthermore, the results indicate that the most site-efficient way to improve the system coverage (i.e. to increase the desired coverage requirement under the same capacity requirement) within a heterogeneous micro deployment is to deploy new micro sites within the traffic clusters, and at the same time to reduce the maximum utilization of the cell resources. Similarly, the most site-efficient way to enhance the system capacity (while keeping the same coverage requirement) is to densify the micro layer, and to increase the maximum utilization of the cell resources. The difference compared to the densified macro deployment is that when it comes to the network operating points with the highest downlink capacities, the gain of network densification is too low, which means that in order to enhance also the system capacity, the maximum utilization of the cell resources has to be lowered and not increased.

In case of the heterogeneous micro deployment, the worst performing users are located either inside the vehicles, or on the floors high up in the buildings. Furthermore, a great majority of the worst performing users are

served by the macro eNodeBs. The reason for this is that a micro eNodeB can offer its users much better throughput, in particular in the uplink, than a macro eNodeB. Therefore, the average user performance will follow the observed levels of traffic offloading.

The micro cell service areas can be extended either by increasing the transmission power of the micro eNodeB, or with the help of biased cell selection. As a result of this kind of cell range expansion, the required number of micro sites to reach the desired coverage and capacity requirements can be reduced. In addition to that, uplink interference from the close-by macro UEs towards the micro eNodeB is reduced. From the traffic offloading point of view both methods look the same. Hence, increasing the transmission power of the micro eNodeB with $\xi$ dB is equal to the scenario where a cell selection offset equal to $\xi$ dB is applied instead. However, when it comes to the downlink SINR experienced by the micro cell users within the range expansion area, the method based on increased transmission power has a clear advantage due to the fact that the received signal power is $\xi$ dB higher, while the inter-layer interference and noise powers are the same as in case of biased cell selection.

An effective way to reduce the inter-layer interference is to allocate separate carrier frequencies for the cell layers. By doing so the inter-layer interference is suppressed by the adjacent channel attenuation offered by both the transmitter and the receiver. However, assuming that the system bandwidth is not increased, there will be a trade-off between the improved SINR and the reduced carrier bandwidths. Therefore, the achievable gains compared to the co-channel deployment of macro and micro cells become highly scenario-dependent. Downlink, which is quite often capacity-limited, does not benefit from spectrum splitting since the loss due to the reduced carrier bandwidth is greater than the gain of an improved SINR. In case of uplink, the performance is quite often limited by the UE transmission power or by the quality of the downlink control signaling. For both cases, the spectrum splitting can in fact be beneficial.

# 7. Performance of the heterogeneous femto deployment

Heterogeneous network deployments based on residential femto base stations have been very widely discussed and studied during the recent years. Studies have been performed within the 3GPP, Small Cell Forum, as well as in the academia. The main focus has been on the performance and evolution of CSG femto base stations, while deployment scenarios based on open access (OSG) femto base stations, or femto base stations operating in the hybrid access mode, have received much less attention. One reason could be that the challenging inter-cell interference problems related to the CSG have opened up possibilities to develop new and innovative schemes for the inter-cell interference management. Another reason, related to the overall business case, can be that base stations utilizing the residential broadband connection as a backhaul, have commonly been assumed to be based on CSG and not on OSG.

This chapter focuses mainly on the performance of the heterogeneous OSG femto deployments. First, the technology potential of deployments utilizing small residential eNodeBs is evaluated. The term *technology potential* is related to the fact that as a default the evaluation assumes OSG cells, unlimited backhaul capacity and a fairly high femto eNodeB output power. The impacts of CSG, limited backhaul capacity and a lower eNodeB output power are studied separately in the following sections. In addition, the impact of a targeted introduction of femto cells into an existing LTE macro network is also evaluated.

Some of the results presented in this chapter have already been published as part of papers [146], [147] and [150].

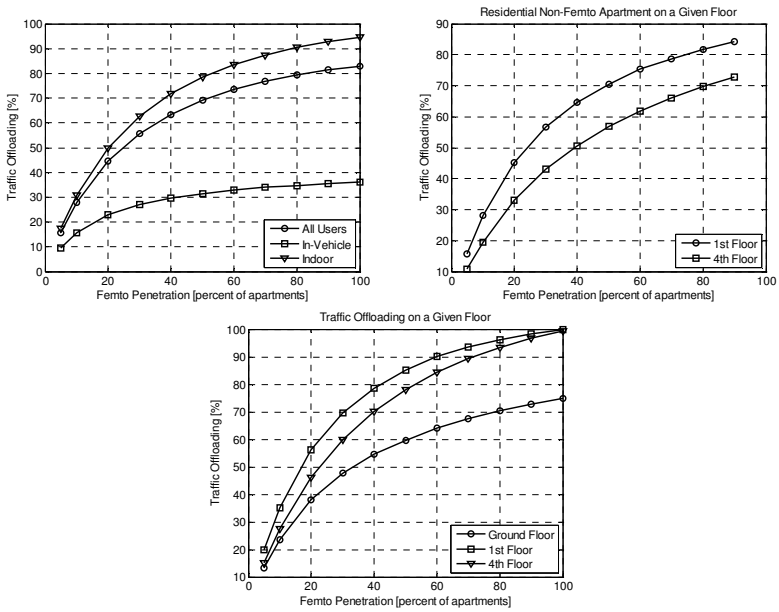


**Figure 7.1.** Observed traffic offloading as a function of the femto penetration, assuming OSG femto eNodeBs with an output power equal to 100 mW.

## 7.1 Technology potential of small residential eNodeBs

Traffic offloading as a function of the femto penetration is evaluated in Figure 7.1. As can be seen, OSG femto cells with maximum output power equal to 100 mW are able to offload up to 82% of the traffic when all candidate apartments include a femto eNodeB. At that point, 95% of the indoor users and 36% of the in-vehicle users are served by the femto eNodeBs. The highest level of traffic offloading is experienced on the 1st floor and the traffic offloading is observed to decrease for the upper floor levels as a result of the increased macro cell signal strength. Even though the non-residential ground floor does not include any femto cells, up to 75% of the ground floor users can be offloaded as a result of the floor-to-floor leakage of the femto eNodeB signal. The impact of this floor-to-floor leakage is visualized also by the results for the traffic offloading within the residential non-femto apartments.

As a result of the increased traffic offloading, average macro cell utilization becomes lower (Figure 7.2), which reduces the level of inter-cell interference, improves the SINR, and in the end, improves the achievable bit rates. As a result of the increased achievable bit rates, as well as the reduced number of simultaneously active users sharing the resources in

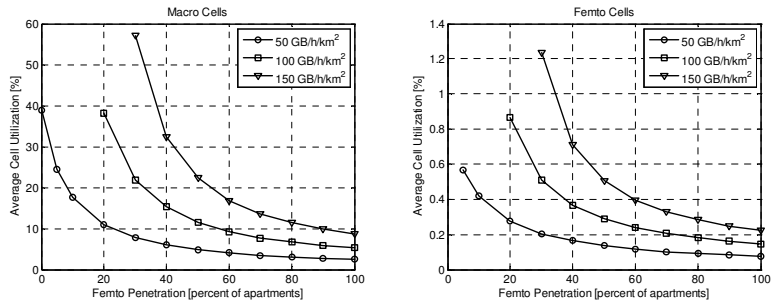


**Figure 7.2.** Average macro and femto cell utilization as a function of the femto penetration. The different curves correspond to different levels of offered area traffic.

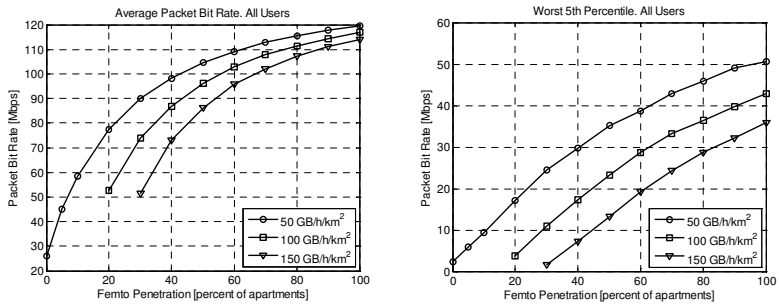


**Figure 7.3.** Average downlink user performance and the performance of the worst 5th percentile of the users as a function of the femto penetration. The different curves correspond to different levels of offered area traffic.

time domain, packet bit rates are improved as demonstrated by the results in Figure 7.3.

Downlink performance is investigated in more detail for a scenario with 50% femto penetration and offered area traffic equal to 150 GB/h/km². Figure 7.4 presents the observed average user performance for the different locations, as well as the locations of the worst and the best performing decile of users. Results for the average user performance indicate a few things worth highlighting. To start with, the performance of the femto users is considerably better than the performance of the macro users. For example, the average downlink packet bit rate for the macro users is equal to 45 Mbps, while the average downlink packet bit rate for the femto users is equal to 105 Mbps. Secondly, femto users located on the femto floors experience much better performance compared to femto users located on the ground floor or inside vehicles. This is caused mainly by the lower coupling losses towards the serving femto eNodeB, which improves the SINR. Thirdly, the average macro user performance is improved as a function of the floor level, i.e. as a result of the floor height gain. Finally, the average user performance for each of the areas depends mostly on the

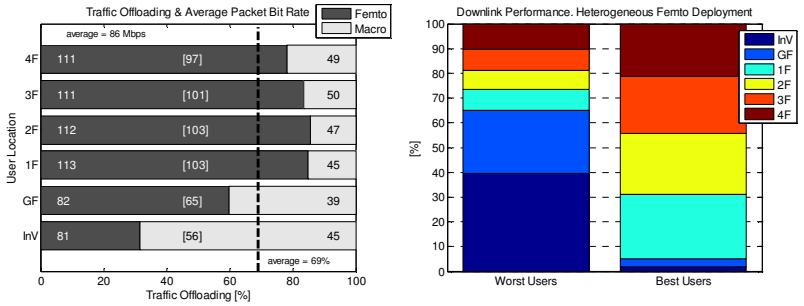


**Figure 7.4.** Traffic offloading and the average user performance for the different user locations (left), and locations of the worst and the best performing downlink users. A heterogeneous femto deployment with 50% femto penetration and offered area traffic equal to 150 GB/h/km² are assumed.

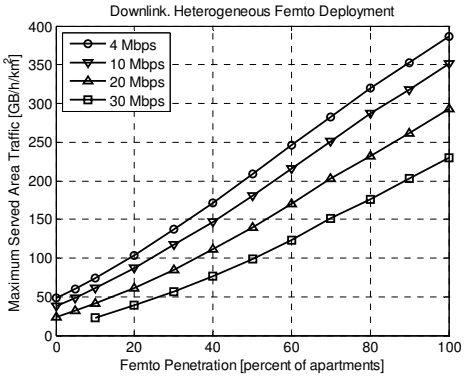


**Figure 7.5.** Maximum downlink served area traffic as a function of the femto penetration for the different coverage requirements.

observed traffic offloading: Higher level of traffic offloading results in better average user performance and vice versa.

The best performing users are concentrated on the residential femto floors, while the users experiencing the worst downlink performance are to a large extent located inside vehicles or on the ground floor, i.e. within locations that experience the lowest level of traffic offloading. That is also the reason behind the fact that a very large majority of the worst performing users are served by the macro eNodeBs.

Results for the maximum downlink served area traffic as a function of the femto site density are shown in Figure 7.5 and in Table 7.1. Compared to the corresponding results for the heterogeneous micro deployment, heterogeneous femto deployment requires approximately 8.3-11.9 times as many new sites to be deployed. The reason for this is that while an outdoor micro eNodeB can potentially provide coverage inside multiple buildings and on multiple floors, the coverage area of an indoor femto eNodeB is

**Table 7.1.** Required femto site density (sites/km²) to fulfill the desired downlink coverage and capacity requirements.

| Coverage Req | Capacity Requirement | | | |
|---|---|---|---|---|
| | 50 GB/h/km² | 100 GB/h/km² | 150 GB/h/km² | 200 GB/h/km² |
| 4 Mbps | 7.1 | 255.0 | 458.4 | 646.5 |
| 10 Mbps | 75.2 | 329.6 | 554.5 | 752.0 |
| 20 Mbps | 192.7 | 481.8 | 723.1 | 938.8 |
| 30 Mbps | 351.9 | 682.6 | 943.7 | 1205.4 |

**Table 7.2.** Observed levels of traffic offloading for the desired network operating points.

| Coverage Req | Capacity Requirement | | | |
|---|---|---|---|---|
| | 50 GB/h/km² | 100 GB/h/km² | 150 GB/h/km² | 200 GB/h/km² |
| 4 Mbps | 1.6% | 42.5% | 58.6% | 67.8% |
| 10 Mbps | 17.0% | 49.3% | 63.9% | 71.4% |
| 20 Mbps | 34.9% | 59.9% | 70.5% | 76.4% |
| 30 Mbps | 51.1% | 69.2% | 76.6% | 81.1% |

**Table 7.3.** Average macro cell utilization for the desired network operating points.

| Coverage Req | Capacity Requirement | | | |
|---|---|---|---|---|
| | 50 GB/h/km² | 100 GB/h/km² | 150 GB/h/km² | 200 GB/h/km² |
| 4 Mbps | 36.4% | 42.3% | 47.5% | 51.2% |
| 10 Mbps | 21.2% | 27.1% | 31.6% | 34.1% |
| 20 Mbps | 12.4% | 16.0% | 18.9% | 22.2% |
| 30 Mbps | 7.9% | 10.8% | 12.9% | 15.0% |

much more limited. That is why a much larger number of femto sites is required to offer the same level of coverage and traffic offloading.

Results for the observed traffic offloading are collected in Table 7.2, and the results for the average macro and femto cell utilizations are listed in Table 7.3 and Table 7.4, respectively. Compared to the densified macro deployment, a higher level of traffic offloading is required to reach the same network performance. This is due to the fact that the femto cells have only

**Table 7.4.** Average femto cell utilization for the desired network operating points.

| Coverage Req | Capacity Requirement | | | |
|---|---|---|---|---|
| | 50 GB/h/km² | 100 GB/h/km² | 150 GB/h/km² | 200 GB/h/km² |
| 4 Mbps | 0.09% | 0.95% | 1.01% | 1.02% |
| 10 Mbps | 0.49% | 0.63% | 0.69% | 0.71% |
| 20 Mbps | 0.31% | 0.39% | 0.45% | 0.49% |
| 30 Mbps | 0.21% | 0.28% | 0.33% | 0.35% |

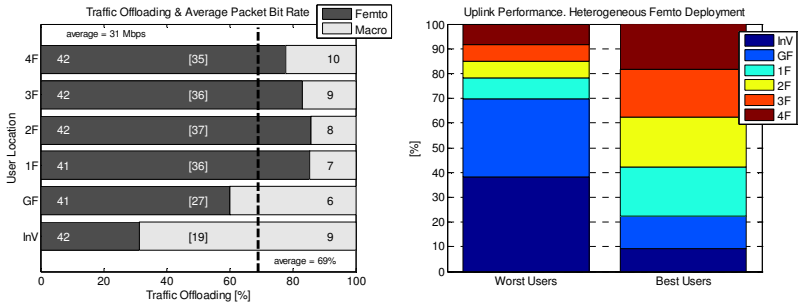


**Figure 7.6.** Traffic offloading and the average user performance for the different user locations (left), and locations of the worst and the best performing uplink users (right).

limited possibilities to offload in-vehicle users and users located on the ground floor. Despite the higher level of traffic offloading, the macro cell utilization is higher than in the densified macro deployment. The reason for it is the worse average performance of the macro users, mainly as a result of the larger coupling losses towards the serving macro eNodeBs.

Uplink user performance is studied for a heterogeneous femto deployment with 50% femto penetration, assuming an offered area traffic equal to 100 GB/h/km². For the evaluated scenario, the average macro cell utilization is equal to 52% and the average femto cell utilization is equal to 0.6%. Results for the average uplink user performance and the locations of the worst and the best performing users are shown in Figure 7.6. Considering all the users in the system, the average packet bit rate is equal to 31 Mbps, and the cell-edge packet bit rate is equal to 2.1 Mbps. Furthermore, the performance of the femto users is much better than the performance of the macro users. For example, the average packet bit rate is equal 8.1 Mbps for the macro users, while it is equal to 41.5 Mbps for the femto users. The only major difference compared to the corresponding downlink results in Figure 7.4 is that the average femto performance is roughly equal for the different user locations. This is a result of the fact that

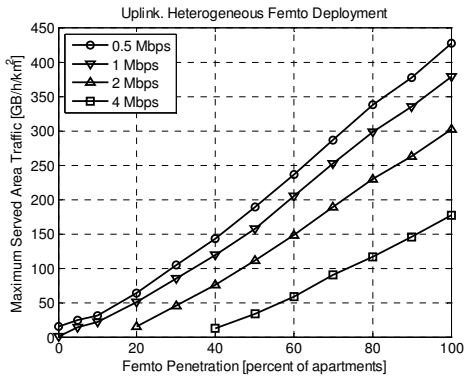


**Figure 7.7.** Maximum uplink served area traffic as a function of the femto penetration for a number of different coverage requirements.

**Table 7.5.** Required femto site density (sites/km²) to fulfill the desired uplink coverage and capacity requirements.

| Coverage Req | Capacity Requirement | | | |
|---|---|---|---|---|
| | 30 GB/h/km² | 60 GB/h/km² | 90 GB/h/km² | 120 GB/h/km² |
| 0.5 Mbps | 122.3 | 254.3 | 358.9 | 462.9 |
| 1 Mbps | 175.6 | 308.8 | 428.8 | 546.7 |
| 2 Mbps | 338.0 | 472.9 | 596.4 | 708.8 |
| 4 Mbps | 651.9 | 823.2 | 951.9 | 1103.2 |

the uplink performance of the femto users is limited by the maximum allowed modulation and coding scheme and not by the UE transmission power or the inter-cell interference. The locations of the best performing users are following the observed levels of traffic offloading. When it comes to the worst performing decile of users, in practice all of them are served by the macro eNodeBs, and in addition to that, more than 70% of them are located either inside the vehicles or on the ground floor. This is a result of the low level of traffic offloading experienced within those areas.

Results for the maximum uplink served area traffic as a function of the femto site density are collected in Figure 7.7 and in Table 7.5. As an example, assuming a coverage requirement of 1 Mbps, and capacity requirements of {30, 60, 90, 120} GB/h/km², femto penetrations equal to {13%, 23%, 32%, 40%} are required. Compared to the corresponding results for the heterogeneous micro deployment, heterogeneous femto deployment requires approximately 10.9-15.5 times as many new sites. Hence, compared to the heterogeneous micro deployment, heterogeneous femto deployment is less efficient to provide uplink than downlink coverage and

**Table 7.6.** Observed levels of traffic offloading for the desired network operating points.

| Coverage Req | Capacity Requirement | | | |
|---|---|---|---|---|
| | 30 GB/h/km² | 60 GB/h/km² | 90 GB/h/km² | 120 GB/h/km² |
| 0.5 Mbps | 25.5% | 42.5% | 51.8% | 58.9% |
| 1 Mbps | 32.8% | 47.8% | 57.1% | 63.6% |
| 2 Mbps | 50.0% | 59.3% | 65.6% | 70.1% |
| 4 Mbps | 67.9% | 73.6% | 76.7% | 79.6% |

**Table 7.7.** Average macro cell utilization for the desired network operating points.

| Coverage Req | Capacity Requirement | | | |
|---|---|---|---|---|
| | 30 GB/h/km² | 60 GB/h/km² | 90 GB/h/km² | 120 GB/h/km² |
| 0.5 Mbps | 67.6% | 76.2% | 81.6% | 85.5% |
| 1 Mbps | 52.0% | 64.7% | 71.6% | 76.1% |
| 2 Mbps | 30.0% | 45.1% | 54.1% | 60.4% |
| 4 Mbps | 17.4% | 27.2% | 34.8% | 40.0% |

**Table 7.8.** Average femto cell utilization for the desired network operating points.

| Coverage Req | Capacity Requirement | | | |
|---|---|---|---|---|
| | 30 GB/h/km² | 60 GB/h/km² | 90 GB/h/km² | 120 GB/h/km² |
| 0.5 Mbps | 0.44% | 0.72% | 0.96% | 1.15% |
| 1 Mbps | 0.36% | 0.62% | 0.81% | 0.95% |
| 2 Mbps | 0.26% | 0.46% | 0.61% | 0.72% |
| 4 Mbps | 0.18% | 0.31% | 0.42% | 0.50% |

capacity. The reason for this is that while in downlink the overall traffic offloading is having a large impact on the results, in uplink the ability to offload the most power-limited ground floor users is playing a bigger role.

Results for the observed levels of traffic offloading and the average macro and femto cell utilizations are collected in Table 7.6 - Table 7.8. What is different compared to the downlink is that the required level of traffic offloading to reach a certain network performance is lower than in case of the densified macro deployment. The reason for this is that even though the

ground floor areas do not contain any femto cells, the cells on the upper floors are still able to offload users with the worst macro coverage. These users are also the most expensive ones, when it comes to the utilization of the macro cell resources.

## 7.2 Impact of backhaul limitation

Femto eNodeBs are designed to use a residential broadband connection as a backhaul. Hence, it can very well happen that the maximum throughput offered by the backhaul connection is lower than the throughput achievable over the air-interface. The impact of this kind of backhaul limitation on the overall system performance is discussed in this section.

This section evaluates only the impact of the backhaul limitation on the downlink performance. However, also in uplink there can be a large gap in between the user throughputs achieved over the air-interface, and the typical uplink bit rates of the residential broadband connections. Therefore, the impact of backhaul limitation on the uplink performance should also be studied before any firm conclusions could be drawn on this topic.

The implemented backhaul limitation model is very simple and will most likely result in slightly too pessimistic results. In the assumed model, the downlink SINR is calculated in the same way as without any backhaul limitations, i.e. using equation (4.2). The maximum backhaul throughput is then taken into account as an additional limitation when the SINR is mapped to the corresponding achievable bit rate using equation (4.6). The model does not, however, take into account the fact that that the downlink scheduler may change its behavior either in time or power domain to adapt to the backhaul limitations. In practice this would mean that the femto user would be scheduled less often, or with a reduced downlink transmission power. In both cases, the average femto eNodeB transmission power and the average level of inter-cell interference between the femto cells would become lower than in the model implemented in the simulator. It should also be noted that in reality the momentary air-interface bit rate can exceed the backhaul throughput, for example when the femto eNodeB is transmitting data, which it has been buffering. However, the average throughput over the air-interface will not exceed the maximum throughput of the backhaul connection.

The impact of backhaul limitation is demonstrated in Figure 7.8, where a heterogeneous femto deployment with 50% femto penetration is evaluated under a fixed offered traffic of 150 GB/h/km$^2$. The evaluations compare the system performance with four different maximum throughputs of the femto

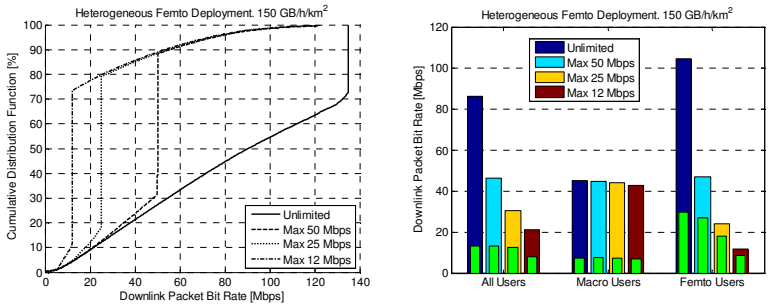


**Figure 7.8.** Distribution of the downlink packet bit rates and the average user performance for four different maximum throughputs of the femto backhaul. A deployment with 50% femto penetration and an offered area traffic equal to 150 GB/h/km² are assumed.

backhaul: unlimited, maximum of 50 Mbps, maximum of 25 Mbps and maximum of 12 Mbps. The figure on the left shows the distributions of the downlink packet bit rates, while the figure on the right shows the average packet bit rates (multi-colored bars) as well as the packet bit rates for the worst 5th percentile of the users (green bars). In general, the performance of the femto users is dramatically reduced as a result of the limited backhaul. However, the impact on the performance of the macro users is quite small despite the fact that the average femto eNodeB utilization increases at the same time from 0.5% to 2.9%. An interesting thing to note is that even though the performance of the femto users is greatly reduced, the impact on the overall system performance is still fairly small, i.e. the overall system performance is still limited by the performance of the macro users. The system performance is affected only when the maximum throughput of the femto backhaul is close to the performance of the worst macro users.

Finally, the impact of the femto backhaul limitation on the network dimensioning is studied in Figure 7.9. The curves present the maximum downlink served area traffic as a function of the femto penetration with different levels of the femto backhaul limitation. Two coverage requirements, 10 Mbps and 20 Mbps, are assumed. As can be seen, the required femto penetration is not affected until the backhaul limitation has come close to the coverage requirement. Furthermore, if the coverage requirement is larger than the maximum throughput of the femto backhaul, no acceptable heterogeneous femto deployment can be found. As an example, let us assume a coverage requirement of 10 Mbps and a capacity requirement of 150 GB/h/km². Now, if the maximum throughput of the femto backhaul is equal to 50, 25, or 12 Mbps, the required number of femto eNodeBs increases with 0.8%, 3.8% or 54.2% compared to the scenario with an unlimited femto backhaul.

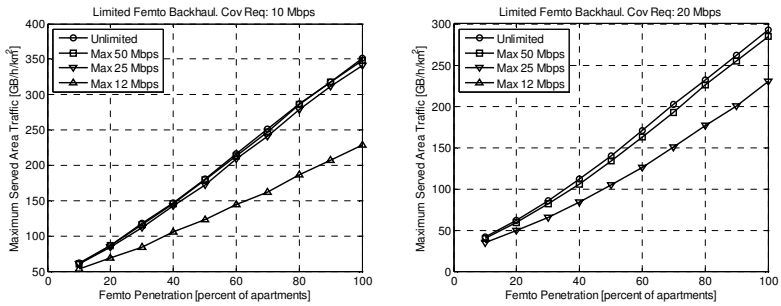


**Figure 7.9.** Maximum downlink served area traffic as a function of the femto penetration with different levels of the femto backhaul limitation.

## 7.3 Impact of OSG femto eNodeB output power

When the femto cell is accessible for all users, there is much less need to implement any special interference mitigation mechanisms, which would adjust the output power of the femto eNodeB based for example on the received signal strength of the surrounding cells. One could, however, think of implementing such methods to control the coverage area of the OSG cell, for example to limit the leakage towards the outdoor users in order to reduce the problems related to mobility management, or to limit the amount of offloaded traffic in scenarios with a limited backhaul capacity. This section does not propose, or evaluate the performance of any dynamic OSG femto eNodeB output power adjustment algorithms. Instead, the system performance is evaluated with different fixed values of the OSG femto eNodeB output power ($P_{femto}$).

One obvious consequence of an increased $P_{femto}$ is that the femto cell coverage area is expanded. As a result, the femto cell coverage within the femto apartment is improved and the overall traffic offloading from the macro to the femto cell layer is increased, as demonstrated in Figure 7.10. The dashed line in Figure 7.10 (graph on the right) indicates the maximum achievable traffic offloading for a reference scenario, where only the users located within the femto apartments can be offloaded. As can be seen, the applied $P_{femto}$ has a great impact on the observed traffic offloading outside the femto apartments. Another result of the femto cell leakage outside the femto apartment is the observed non-linear traffic offloading as a function of the femto penetration. When $P_{femto}$ is low (1 mW), only a very small overlap between the femto cells is observed and the traffic offloading increases almost linearly. However, as $P_{femto}$ increases, so does also the level of the femto cell overlap, which results in a non-linear increase of the traffic offloading.

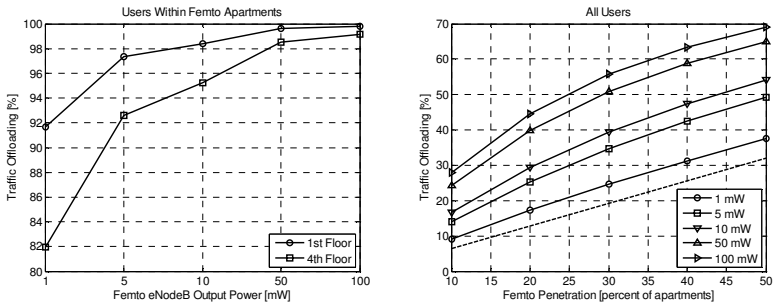


**Figure 7.10.** Femto cell coverage probability within a femto apartment on the 1st floor and on the 4th floor (left), and the overall traffic offloading as a function of the femto penetration (right), assuming different values of the femto eNodeB output power.

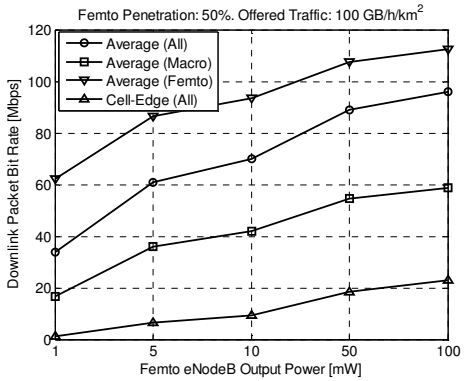


**Figure 7.11.** The impact of the femto eNodeB output power on the average and the cell-edge packet bit rates.

Next, the downlink performance is evaluated for a scenario with 50% femto penetration and offered area traffic equal to 100 GB/h/km². The results in Figure 7.11 demonstrate how the increased $P_{femto}$ (1 mW → 5 mW → 10 mW → 50 mW → 100 mW) improves the downlink user performance. More specifically, the performance of the macro users is improved as a result of the increased traffic offloading (37% → 49% → 54% → 65% → 69%), and the reduced level of inter-cell interference caused by the reduced average macro cell utilization (57% → 30% → 24% → 14% → 12%). The main reason for the improved femto user performance is the increased downlink SINR due to the increased carrier power and the reduced inter-cell interference from the macro cells. One of the consequences of the improved femto user performance is that the average femto cell utilization becomes lower (0.42% → 0.33% → 0.32% → 0.30% → 0.29%) despite the fact that the offered traffic per femto cell increases.

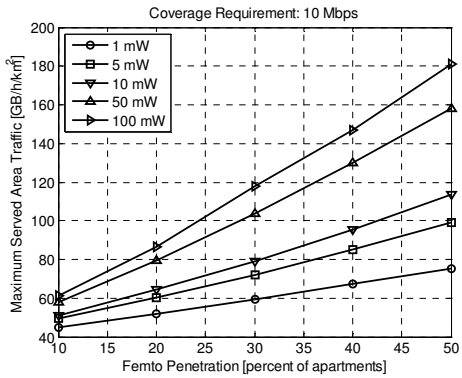


**Figure 7.12.** Maximum downlink served area traffic as a function of the femto penetration for different values of the femto eNodeB output power. Coverage requirement equal to 10 Mbps is assumed.

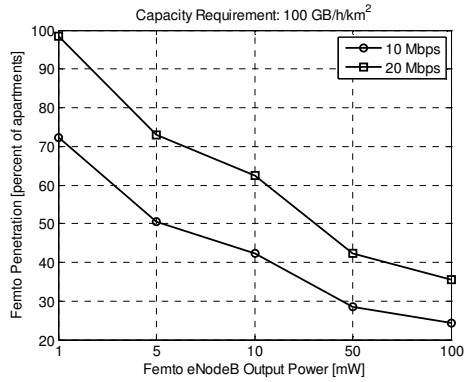


**Figure 7.13.** Required femto penetration to fulfill a capacity requirement equal to 100 GB/h/km² and a coverage requirement equal to 10 Mbps or 20 Mbps.

As a result of the increased traffic offloading the overall system capacity increases. This is demonstrated in Figure 7.12, where the maximum downlink served area traffic is shown as a function of the femto penetration, assuming a coverage requirement of 10 Mbps. As can be noticed, the capacity gain due to an increased $P_{femto}$ becomes larger as a function of the femto penetration. One of the main reasons for this is that as a result of the increased traffic offloading, and the improved user performance, higher levels of average cell utilization can be allowed before the desired coverage limits are reached.

As a result of the increased system capacity, a smaller number of femto eNodeBs is required to fulfill the desired coverage and capacity requirement. This is demonstrated in Figure 7.13, where the required femto penetration to fulfill a capacity requirement of 100 GB/h/km² is presented for two different coverage requirements: 10 Mbps and 20 Mbps. Compared to a deployment with $P_{femto}$ equal to 100 mW, deployment with $P_{femto}$

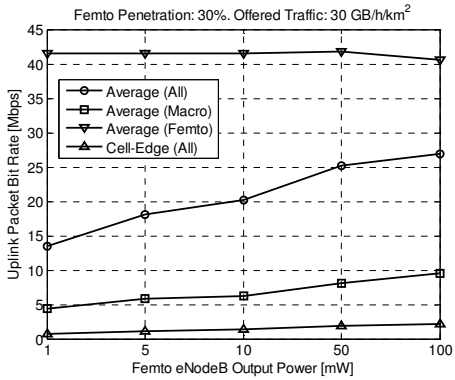


**Figure 7.14.** Impact of the femto eNodeB output power on the average and the cell-edge uplink packet bit rates.

equal to 1 mW requires roughly 2.7-3.0 times as many femto eNodeBs. If $P_{femto}$ is equal to 5 mW, roughly twice as many femto eNodeBs is required than with $P_{femto}$ equal to 100 mW. Finally, with $P_{femto}$ equal to 10 mW and 50 mW, the required number of femto eNodeBs becomes 75% and 18% larger, respectively, compared to the deployment with $P_{femto}$ equal to 100 mW.

Referring to the discussion in Section 4.3.4, an adjusted $P_{femto}$ would indicate the need to modify the $P_{0,macro}$ and $P_{0,femto}$ accordingly. An increased $P_{femto}$ would suggest that the value of $P_{0,macro}$ could be increased, while the value of $P_{0,femto}$ should most likely to be reduced to limit the uplink interference towards the macro eNodeBs. This is indeed the case, as indicated by the tuned $P_0$ values listed in Table C.6 (Annex C). One can also notice that the absolute value of the backoff parameter $\phi_{femto}$ is reduced together with an increasing $P_{femto}$.

Results for the impact of $P_{femto}$ on the uplink user performance are shown in Figure 7.14. The performance evaluation is performed for a deployment with 30% femto penetration and assuming offered area traffic equal to 30 GB/h/km$^2$. The results indicate how the average uplink performance of the macro users is improved as $P_{femto}$ is increased. At the same time, the average uplink performance of the femto users stays almost the same due to the fact that for a great majority of the femto users the uplink performance is limited by the maximum allowed modulation and coding scheme. The overall system performance is improved mostly as a result of the increased traffic offloading (25% → 34% → 39% → 51% → 56%) but also partially as a result of the improved performance of the macro users. Performance of the macro users is improved as a result of the increased traffic offloading, reduced macro cell utilization (55% → 45% → 41% → 31% → 26%), reduced

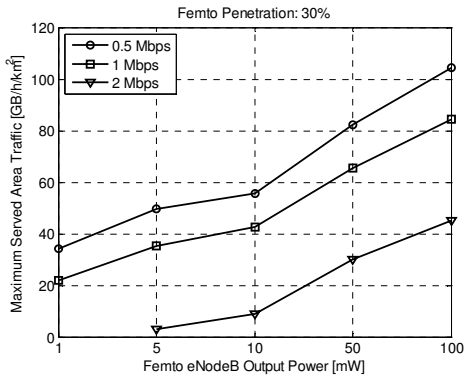


**Figure 7.15.** Impact of the femto eNodeB output power on the maximum uplink served area traffic, assuming three different coverage requirements.

inter-cell interference and increased $P_{0,macro}$. The reason why the average performance of the femto users is reduced for $P_{femto}$ equal to 100 mW is the fact that the assumed value of $P_{0,femto}$ (-99 dBm) is low enough to become the limiting factor for the femto user performance.

Results for the impact of $P_{femto}$ on the maximum uplink served area traffic are shown in Figure 7.15. The evaluation is performed for a deployment with 30% femto penetration and three different coverage requirements (0.5, 1 and 2 Mbps) are assumed. As can be seen, the uplink capacity is considerably increased when $P_{femto}$ becomes higher. Similar to the downlink, one key contributor to the improved system capacity is the fact that due to the traffic offloading and the improved performance of the macro users, the network can be allowed to operate at a higher load level before the desired coverage limit is reached. For the results in Figure 7.15, the average macro cell utilization increases from 65% to 84% (coverage requirement equal to 0.5 Mbps), from 43% to 71% (1 Mbps) and from 6% to 40% (2 Mbps). At the same time also the average femto cell utilization increases from 0.13% to 1.07% (0.5 Mbps), from 0.08% to 0.78% (1 Mbps) and from 0.01% to 0.38% (2 Mbps).

## 7.4 Impact of non-uniform user traffic and targeted deployment of femto eNodeBs

This section evaluates the impact of both a non-uniform subscriber traffic, as described in Section 4.2.2, and a targeted deployment of femto eNodeBs. Instead of the random femto deployment assumed so far, one could think of a somewhat more intelligent approach where the femto eNodeBs are deployed to improve the coverage, or to offload as much of the traffic as

possible. Therefore, this section evaluates the performance of the following femto deployment alternatives:

- Random selection of femto apartments (RND)
- Deployment based on the macro cell signal strength, starting from the apartments with the worst macro coverage (COV)
- Deployment focusing on the traffic-heavy apartments (20% of all candidate apartments), assuming a random selection of apartments (HVYR)
- Deployment focusing on the traffic-heavy apartments, starting from the ones with the worst macro coverage (HVYC)

The approach taking the macro cell coverage into account has two advantages. Firstly, the traffic offloading is targeted towards the users that have the worst macro coverage, which can quite often be also the most expensive users from the overall macro cell performance point of view. Secondly, the femto eNodeBs are deployed within areas with a weak macro cell, which leads to increased femto cell coverage areas. As a result of the floor height gain, apartments with the worst macro cell coverage are to a large extent found on the lower floor levels. Hence, the downside of the coverage-based femto deployment is that at low levels of femto penetration the floor-level distribution of the femto sites is quite non-uniform, meaning that most of the femto sites are concentrated on the lower residential floor levels. At the same time, the femto site density becomes lower on the upper floor-levels, which can be expected to result in reduced traffic offloading and worse user performance.

In case of the traffic-based deployments, femto eNodeBs are deployed first within the traffic-heavy apartments, and only after that within the other candidate apartments. This kind of approach maximizes the amount of traffic offloaded from the macro layer with the minimum amount of femto eNodeBs. In case of HVYR, a random selection of femto apartments, first from the group of the traffic-heavy apartments and then from the remaining candidate apartments, is assumed. In case of HVYC, the selection of the femto apartments is based on both the user traffic and the macro cell coverage.

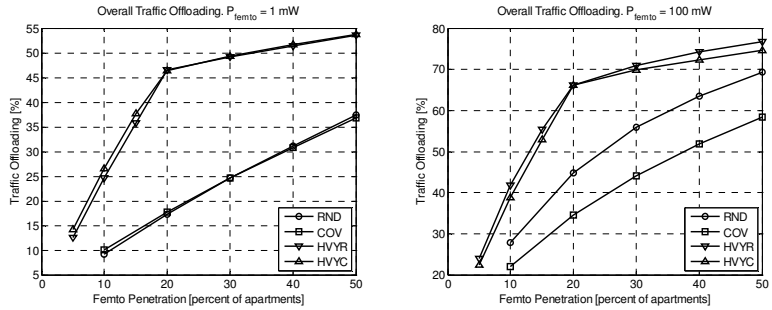


**Figure 7.16.** Observed traffic offloading as a function of the femto penetration, assuming femto eNodeB output power equal to 1 mW or 100 mW.

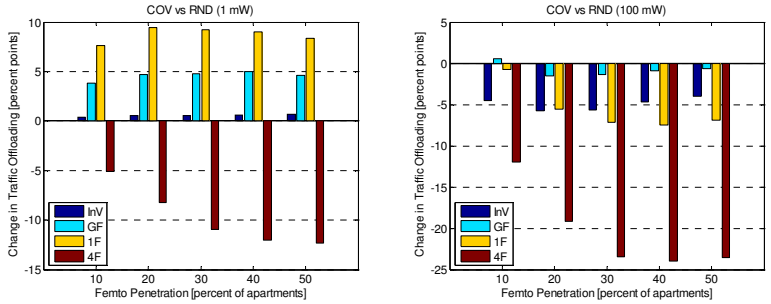


**Figure 7.17.** Comparison between the coverage-based and the random selection of femto apartments from the traffic offloading point of view, considering different user locations. Femto eNodeB output power equal to 1 mW or 100 mW is assumed.

### 7.4.1 Impact on traffic offloading

Performance evaluation is initiated by investigating the impact of the different femto deployment alternatives on the overall traffic offloading. As indicated by the curves in Figure 7.16, the coverage-based deployment results in a reduced traffic offloading for almost all of the studied scenarios. Only the scenarios with a low femto penetration and a low $P_{femto}$ benefit marginally from the coverage-based deployment of femto eNodeBs. The main reason for this is the fact that the OSG femto cells are able to offload users also outside the actual femto apartment. Therefore, an approach which spreads the femto cells more uniformly between the floors and buildings can provide a better overall traffic offloading compared to a more clustered deployment of femto cells.

The above can be verified by studying the traffic offloading a bit closer for the different user locations. As demonstrated in Figure 7.17, the coverage-based femto deployment with a low $P_{femto}$ improves the traffic offloading on the non-residential ground floor and on the 1st floor, which is a result of

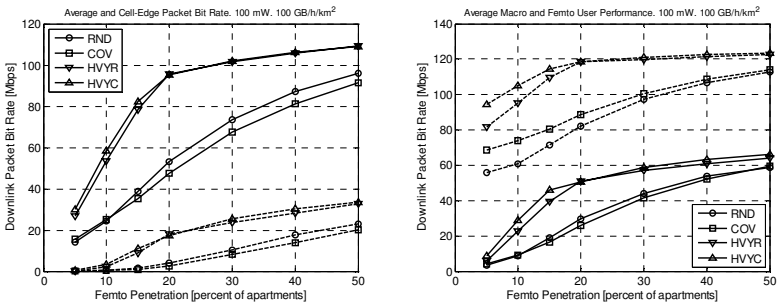


**Figure 7.18.** Observed user performance as a function of the femto penetration for the evaluated femto deployment alternatives.

the fact that the density of the femto eNodeBs is in general increased on the lower residential floors. Unfortunately, this leads to a considerably reduced traffic offloading on the upper floor levels. In case of a high $P_{femto}$, traffic offloading is in practice reduced for all user locations.

The traffic-based deployment alternatives result in a considerably increased traffic offloading compared to the random deployment. The evaluations assume that approximately 50% of the total traffic is generated in 20% of the candidate apartments. This means that if the femto penetration is equal to 20% or more, all traffic-heavy apartments include a femto eNodeB. Together with the fact that the coverage area of an OSG femto cell can extend beyond the walls of the femto apartment, the overall traffic offloading can become larger than 50%. Taking the scenario with $P_{femto}$ equal to 100 mW as an example, a deployment where all traffic-heavy apartments include a femto eNodeB results in an overall traffic offloading equal to 66%, which consists of 87% of the residential traffic, 38% of the non-residential ground floor traffic and 23% of the in-vehicle traffic. The difference between HVYR and HVYC is quite small, which means that most of the traffic offloading gains are achieved by focusing initially on the traffic-heavy apartments. However, the order in which the traffic-heavy apartments are selected is less important.

### 7.4.2 Impact on user performance

Impact of the targeted femto deployment on the overall user performance is evaluated for a scenario with femto eNodeB output power equal to 100 mW and offered area traffic equal to 100 GB/h/km². To start with, results for the observed downlink packet bit rates are collected in Figure 7.18. The figure on the left presents the results for the average (solid curves) and the cell-edge packet bit rate (dashed curves). Furthermore, the figure on the right presents the results for the average macro user (solid curves) and the

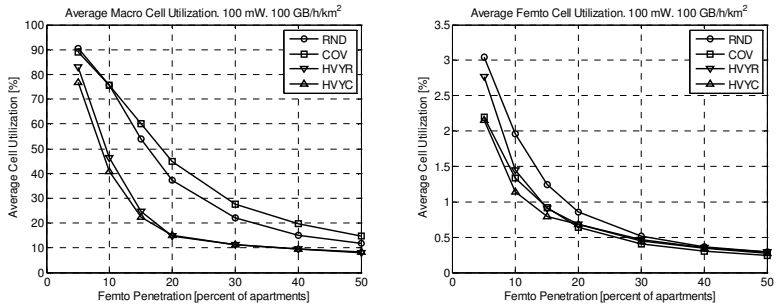


**Figure 7.19.** Average macro and femto cell utilization as a function of the femto penetration for the evaluated femto deployment alternatives.

average femto user packet bit rate (dashed curves). As can be seen, the traffic-based deployment alternatives result in a better user performance compared to the coverage-based or the random deployment. The coverage-based deployment performs the worst when it comes to the average and the cell-edge packet bit rate, and the average packet bit rate of the macro users. However, when it comes to the average packet bit rate of the femto users, the random deployment results in the worst performance.

The observed performance differences are a combination of both the differences in the traffic offloading (see Figure 7.16 and Figure 7.17) and the differences in the average cell utilizations, as shown in Figure 7.19. The traffic-based deployment alternatives result in a considerably higher level of traffic offloading and further in a considerably lower level of macro cell utilization compared to the coverage-based or the random deployment. As a result of the considerably lower level of inter-cell interference, the SINR, and further the throughput of the femto users is improved. Since the coverage-based deployment alternative results in a lower level of traffic offloading than the random deployment, both the overall system performance and the average macro user performance become worse. However, due to the fact that the offloaded users are located in apartments with a weak macro cell, they experience a lower level of inter-cell interference, which results in a better average femto user performance compared to the random deployment.

Average downlink user performance and the performance for the worst 5$^{th}$ percentile of users for the different locations is evaluated for a scenario with 30% femto penetration, $P_{femto}$ equal to 100 mW, and offered area traffic equal to 100 GB/h/km$^2$. Results for the observed user performance within the different locations are presented in Figure 7.20. Compared to the random deployment, the coverage-based deployment results in a reduced level of traffic offloading for all the evaluated user locations. At the same time, the coverage-based deployment leads to an improved average user

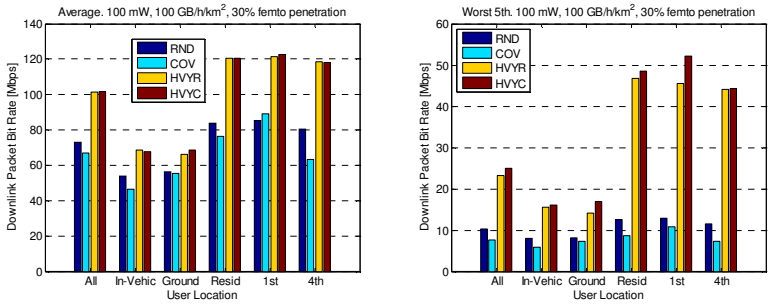


**Figure 7.20.** Observed user performance (average and the worst 5th percentile) for the different user locations.

performance for the 1st floor, while the average user performance is reduced for all the other user locations. The reason for this is the trade-off between the gain of offloading the users with the worst macro coverage, and the loss due to a reduced overall traffic offloading.

The traffic-based deployments result in a considerably increased offloading of the residential traffic. Since the traffic-heavy apartments are assumed to be uniformly distributed, offloading of the non-residential in-vehicle and ground floor users is not remarkably changed. However, even the non-residential users can enjoy the benefit of an increased overall traffic offloading, resulting in a reduced level of inter-cell interference and an increased amount of resources in the time domain, which both contribute to an improved user throughput.

### 7.4.3 Impact on system capacity

Results for the maximum downlink served area traffic as a function of the femto penetration are presented in Figure 7.21. The evaluations are performed for a low (1 mW) and a high (100 mW) femto eNodeB output power. Furthermore, a coverage requirement equal to 10 Mbps is assumed.

To start with, the system capacity is considerably increased as $P_{femto}$ becomes higher. As already discussed in Section 7.3 this is due to the increased offloading and the fact that a higher level of average cell utilization can be allowed before the desired minimum cell-edge performance is reached.

Secondly, the coverage-based femto deployment results in a clear capacity gain compared to the random deployment when $P_{femto}$ is low. However, in case of a higher $P_{femto}$, a capacity loss is observed instead, unless the level of femto penetration is less than 16%. The obtained results are a combination of two things: a) reduced overall traffic offloading, and b)

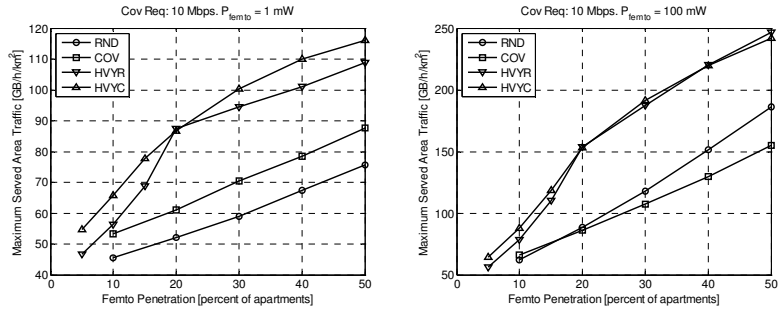


**Figure 7.21.** Maximum downlink served area traffic as a function of the femto penetration for the different femto deployment alternatives. Femto eNodeB output power equal to 1 mW or 100 mW, and coverage requirement equal to 10 Mbps are assumed.

increased offloading of the users with the largest coupling losses towards the serving macro eNodeBs. The reduced traffic offloading is expected to result in a worse system performance for the capacity-limited scenarios (low coverage requirement, high $P_{femto}$, high femto penetration), whereas the approach aiming to offload the users with the worst macro cell coverage is expected to benefit mostly the power-limited scenarios (high coverage requirement, low $P_{femto}$, low femto penetration).

The traffic-based deployments outperform both the coverage-based and the random deployment, which is a direct result of the greatly increased level of traffic offloading from the macro to the femto cell layer. Therefore, higher levels of both the average macro and the average femto cell utilization can be allowed. In addition, HVYC provides a higher system capacity than HVYR, even though the differences in the observed traffic offloading are quite small. This is due to the fact that by prioritizing the coverage-limited users, slightly higher levels of average cell utilization can be allowed. Similar to the difference between the coverage-based and the random deployment, the observed capacity gains are larger for the lower values of $P_{femto}$ or for the higher coverage requirements due to the fact that the system is more power-limited.

### 7.4.4 Impact on network dimensioning

The previous sections have demonstrated how the targeted deployment of OSG femto eNodeBs can improve both the user performance and the overall system capacity. This section will demonstrate how the observed capacity improvement will affect the number of femto sites required to fulfill the desired coverage and capacity requirements. The evaluation assumes a coverage requirement equal to 10 Mbps and two different capacity requirements, 50 GB/h/km² and 100 GB/h/km².

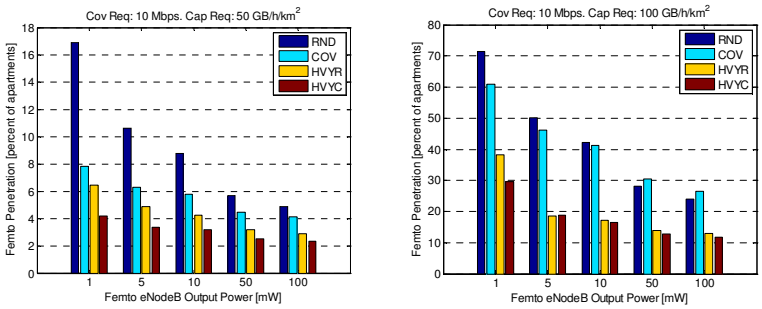


**Figure 7.22.** Required femto penetration to fulfill the desired coverage and capacity requirement, assuming different femto deployment alternatives and different femto eNodeB output powers.

The results presented in Figure 7.22 follow quite well the capacity gains shown in Figure 7.21. Hence, the coverage-based and the traffic-based deployment alternatives will in most of the cases result in a lower required number of femto eNodeBs compared to the random deployment. One can also see how the traffic-based deployments are beneficial for all the evaluated values of $P_{femto}$, while the coverage-based deployment reduces the required number of femto eNodeBs only if $P_{femto}$ is low, or if the capacity requirement is low. Finally, the approach combining both the traffic- and the coverage-based deployment is the most efficient one also from the required femto site density point of view.

If the capacity requirement is equal to 100 GB/h/km², the coverage-based deployment of femto eNodeBs requires 15% less femto sites to be deployed compared to the random deployment, when $P_{femto}$ is low (1 mW). However, when $P_{femto}$ is high (100 mW), the coverage-based deployment results in an 11% higher number of femto sites. When it comes to the traffic-based deployments, the required number of femto sites becomes 46% (HVYR) or 58% (HVYC) lower compared to the random deployment when $P_{femto}$ is low. In case of a high $P_{femto}$, the required number of femto sites becomes 46% or 50% smaller for the HVYR and HVYC, respectively, compared to the random deployment.

Table 7.9 presents a comparison between two femto deployments, RND and HVYC, and a number of network densification schemes based either on new macro or new micro sites. The comparison is performed for a coverage requirement of 10 Mbps and a capacity requirement of 100 GB/h/km². Furthermore, $P_{femto}$ equal to 100 mW has been assumed for both femto deployments. Keeping in mind that the traffic-heavy apartments are assumed to be uniformly distributed over all the residential floors, average performance of the deployments based on large or medium sized cells will remain approximately the same compared to the scenarios with uniform

**Table 7.9.** Ratio between the required number of new femto sites and the required number of new macro or micro sites to reach the same coverage and capacity requirement.

| Femto | Network Densification Alternative | | | | |
|---|---|---|---|---|---|
| | Macro | Micro 1 W | Micro 2 W | Micro 4 W | Micro 10 W |
| RND | 77 | 10.7 | 12.3 | 13.7 | 16.2 |
| HVYC | 38 | 5.3 | 6.1 | 6.8 | 8.1 |

subscriber traffic. However, the heterogeneous femto deployments can be made much more efficient by deploying femto eNodeBs initially within the traffic-heavy apartments. By doing so, the required number of femto sites can be approximately halved and as a result, the heterogeneous femto deployment becomes considerably more competitive compared to the other network densification alternatives.

Since the values in Table 7.9 are based on the technology potential of each of the network densification alternatives, they should be treated with care. Many of the simulation assumptions, in particular for the femto deployments, can be questioned and will most likely lead to overestimated network performance. For example, the values in Table 7.9 assume an unlimited backhaul capacity, and a fully exploited indoor-to-outdoor coverage. The first one is an unrealistic assumption for most of the residential femto deployments, while the latter one might in many cases be undesired for example from the mobility management point of view.

### 7.4.5 Impact on the uplink performance

The impact on uplink performance is visualized for a scenario with femto penetration equal to 30% and $P_{femto}$ equal to either 1 mW or 100 mW. Furthermore, it should be highlighted that for simplicity the applied $P_{0,macro}$ and $P_{0,femto}$ values are not assumed to depend on the selected femto deployment alternative. Due to the fact that the different femto deployment alternatives result in considerably different levels of traffic offloading, the $P_0$ values should be adjusted separately for each of the evaluated deployments. Based on the findings in Section 4.3.4, an educated guess would be that the adjusted $P_{0,macro}$ and $P_{0,femto}$ would be somewhat higher than the values assumed in the simulations, at least for the traffic-based deployment alternatives. Thus, the evaluation results presented in this section could potentially underestimate the uplink performance of the HVYR and HVYC deployments.

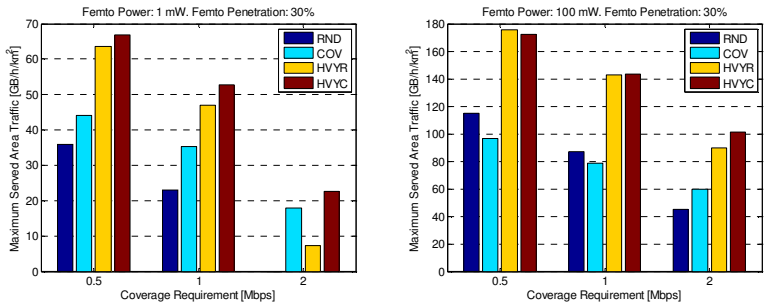


**Figure 7.23.** Maximum uplink served area traffic for the different femto deployment options and for three different coverage requirements. Femto eNodeB output power equal to 1 mW or 100 mW and femto penetration equal to 30% are assumed.

The uplink results in Figure 7.23 show partly similar trends as the corresponding downlink results, i.e. the largest gains can be obtained by focusing initially on the traffic-heavy apartments. Another thing that can be highlighted is the trade-off between the overall traffic offloading and the possibility to offload the most power-limited residential users. However, the fact that the femto deployments have difficulties in offloading the non-residential ground floor users is limiting the achievable offloading gains from the coverage point of view.

In case of a low $P_{femto}$, the coverage-based femto deployment results in a better system capacity than the random deployment. The difference between COV and RND, as well as the difference between HVYC and HVYR, is a direct result of the increased offloading of the most power-limited users on the ground floor and on the 1st floor.

When $P_{femto}$ is increased to 100 mW, the system capacity becomes considerably larger. As discussed in Section 7.3, the increased capacity is a result of a) increased level of traffic offloading, b) improved performance of the remaining macro users, and c) the fact that the network can be allowed to operate at a higher load level before the desired coverage limit is reached. When it comes to the observed system performance with the different femto deployment alternatives, reduced traffic offloading as a result of the coverage-based deployment is having a clear negative impact on the system capacity. However, in case of a lower network load target (low femto penetration and high coverage requirement), the system is more power-limited, and the gain of offloading users with poor macro cell coverage outweighs the loss of a reduced overall traffic offloading.

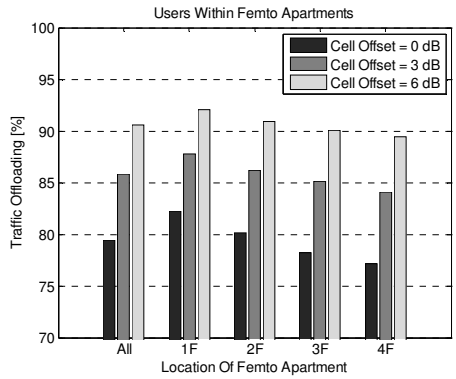


**Figure 7.24.** Observed CSG femto coverage probability with different values of the cell selection offset.

## 7.5 Performance of a heterogeneous CSG femto deployment

This section evaluates the performance of a heterogeneous CSG femto deployment. Three different aspects are considered: a) impact of access control, b) impact of network synchronization, and c) impact of spectrum allocation on the performance of the femto deployment.

### 7.5.1 Traffic offloading with CSG femto eNodeBs

One of the main assumptions during the CSG femto evaluations is that only the UEs, which are located within the same apartment as the CSG femto eNodeB, are allowed to connect to it. Furthermore, the normal cell selection criterion as defined in (3.3) has to be fulfilled as well. The first condition results in a certain maximum achievable level for the overall traffic offloading, which is equal to the total offered traffic within the CSG femto apartments. Furthermore, as a result of the second condition the observed traffic offloading will be less than the achievable maximum for scenarios where the femto eNodeBs are not able to offer sufficient coverage within the femto apartments.

Results for the observed traffic offloading within the CSG femto apartments (i.e. the CSG femto cell coverage probability) are presented in Figure 7.24. The traffic offloading has been evaluated for three different cell selection offsets ($O_{CSG}$): 0 dB, 3 dB and 6 dB. As can be seen, femto cell coverage probability with $O_{CSG} = 0$ dB is approximately equal to 80%. If the cell selection offset is increased to 6 dB, femto cell coverage probability increases to 90%. The results in Figure 7.24 demonstrate also how the traffic offloading is reduced as a function of the floor level, which is a result of both the increased $W_{macro}$, and the impact of $P_{min,CSG}$ and $P_{max,CSG}$.

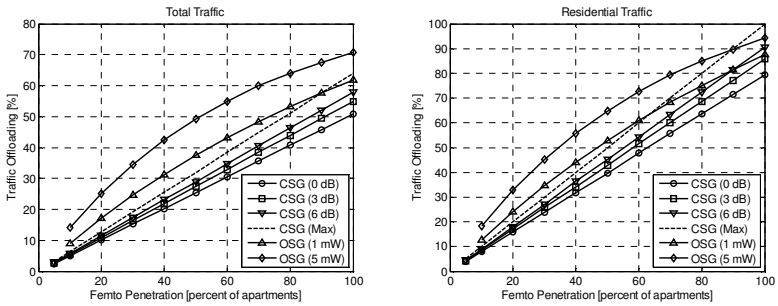


**Figure 7.25.** A comparison between a number of CSG and OSG femto deployments from the traffic offloading point of view.

Firstly, $W_{macro}$ is lower, and the probability that $P_{CSG}$ is equal to $P_{min,CSG}$ is higher on the lower floor levels compared to the upper floor levels. As a result, the average femto cell coverage area is reduced together with an increasing femto floor level. Secondly, together with an increasing $W_{macro}$ as a function of the floor level, the probability that $P_{CSG}$ is limited by the $P_{max,CSG}$ increases as well, which reduces the size of the femto cell even further.

Results for the overall traffic offloading as a function of the femto penetration are shown in Figure 7.25. Furthermore, the maximum achievable traffic offloading is indicated by the dashed line. The presented results are well in line with the results in Figure 7.24. For example, with $O_{CSG} = 0$ dB, the overall CSG femto coverage probability is equal to 80%, and hence, the overall traffic offloading becomes equal to 80% of the achievable maximum.

Figure 7.25 includes also curves for two different OSG femto deployments; with $P_{femto}$ equal to 1 mW and 5 mW. As can be noticed, the OSG deployments result in a better overall traffic offloading compared to the CSG deployments. This is a combination of both a higher femto eNodeB output power (for many of the femto eNodeBs), and the fact that the OSG cells can offload users also outside the femto apartment. However, when it comes to the ability to offload residential traffic, the differences between the OSG and the CSG deployments become smaller. In fact, if all the candidate apartments have a femto eNodeB (100% femto penetration), the OSG femto deployment with $P_{femto}$ equal to 1 mW provides a worse level of residential traffic offloading compared to the CSG femto deployment with $O_{CSG}$ equal to 6 dB. The reason for this is that the leakage between the floors and the apartments (OSG femto) is not able to compensate for the better coverage within the femto apartment (CSG femto) due to the applied $O_{CSG}$ and the fact that $P_{CSG} > P_{femto}$ when the level of $W_{macro}$ is sufficiently high.

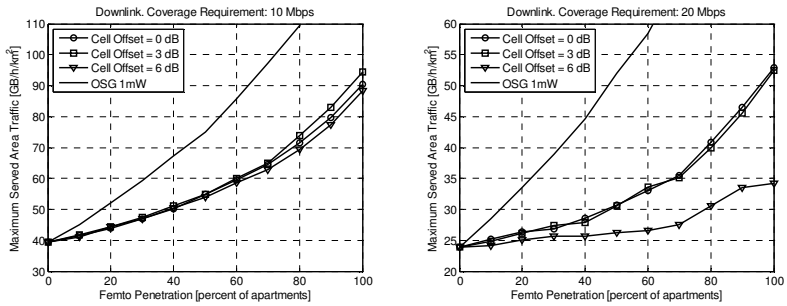


**Figure 7.26.** Maximum downlink served area traffic as a function of the femto penetration. The different curves correspond to CSG femto deployments with different cell selection offsets and an OSG femto deployment with cell selection offset equal to zero and femto eNodeB output power equal to 1 mW.

### 7.5.2 Synchronized deployment of CSG femto eNodeBs

In case of a synchronized deployment of CSG femto eNodeBs, the CSG cells are assumed to be synchronized with respect to both the macro cells and the neighboring CSG femto cells. The benefit of a synchronized deployment is that the inter-cell interference towards the data symbols will have an "on-off" behavior depending on the scheduling activity within the neighboring cells. The downside of a synchronized deployment is that the CRS, PBCH, and PSS/SSS are always interfered by the corresponding control signals in the neighboring cells. This means that they can suffer from a constantly high level of inter-cell interference, even when the neighboring cells are low-loaded.

Results for the maximum downlink served area traffic as a function of the femto penetration are shown in Figure 7.26, assuming three different values of $O_{CSG}$. As a comparison, the corresponding results for the OSG femto deployment with $P_{femto}$ equal to 1 mW and $O_{femto}$ equal to zero are also included.

A few things can be highlighted from the results. To start with, the biased cell selection offers only a very small capacity gain even though the traffic offloading is increased. Furthermore, only the lower coverage requirements benefit from the biased cell selection, since for them the gain due to the increased traffic offloading is able to compensate for the loss due to the increased downlink interference. However, if the applied $O_{CSG}$ is too large, the increased downlink interference for the femto users located within the range expansion area dominates over the gains related to the increased traffic offloading. Finally, even though the CSG femto deployment offers a clear capacity gain compared to the baseline deployment, it is not able to

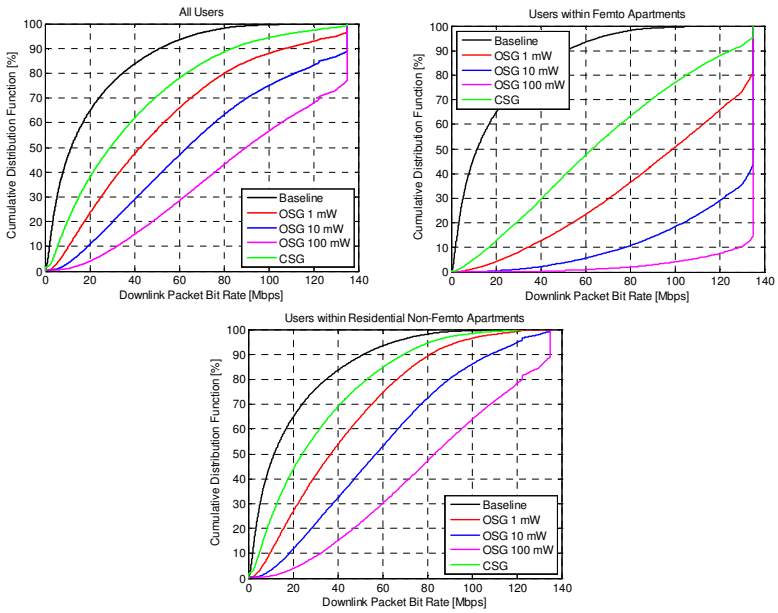


**Figure 7.27.** Distribution of the downlink packet bit rates for the baseline deployment, CSG femto deployment and three different OSG femto deployments with different femto eNodeB output powers, assuming an offered area traffic equal to 55 GB/h/km².

match the performance of the OSG femto deployment with $P_{femto}$ equal to 1 mW.

A more detailed evaluation of the performance of the CSG femto deployment is performed for a scenario with femto penetration equal to 30% and offered area traffic equal to 55 GB/h/km². The results are shown in Figure 7.27. In the presented graphs, the performance of the CSG femto deployment is compared against the performance of the baseline deployment as well as the performance of three different OSG deployments with $P_{femto}$ equal to 1 mW, 10 mW and 100 mW.

According to the results, the performance of the CSG femto deployment is clearly better than the performance of the baseline network. However, at the same time the performance of the OSG femto deployment is considerably better than the performance of the CSG femto deployment. There are three main reasons explaining the performance difference between the OSG and the CSG femto deployments:

- In many cases the assumed $P_{femto}$ is higher than the applied $P_{CSG}$, which results in higher downlink SINRs, achievable bit rates and throughputs for the OSG femto users.

- As a result of the higher femto eNodeB output power, and the fact that the OSG femto cells are able to offload users also from outside

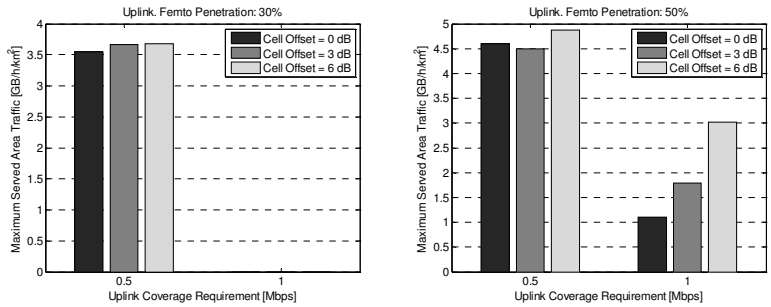


**Figure 7.28.** Maximum uplink served area traffic for CSG femto deployments with different cell selection offsets. Two different coverage requirements, 0.5 Mbps and 1 Mbps, and two different levels of femto penetration are evaluated.

the femto apartment, the observed traffic offloading is higher for the OSG deployments. For the evaluated scenarios, the observed traffic offloading is equal to 15% (CSG), 24% (OSG 1 mW), 40% (OSG 10 mW) and 56% (OSG 100 mW).

- Due to the higher level of overall traffic offloading, the average utilization of the macro cells becomes lower. As a result of that, the average level of inter-cell interference becomes lower, which improves the SINR, achievable bit rates and finally, the user throughputs. For the evaluated scenarios, the average macro cell utilization is equal to 49% (baseline deployment), 31% (CSG), 23% (OSG 1 mW), 14% (OSG 10 mW) and 9% (OSG 100 mW).

Uplink performance of the CSG femto deployment is evaluated in Figure 7.28 for two different levels of femto penetration: 30% and 50%. Similar to the downlink, the CSG femto deployment offers an improvement compared to the baseline network, but performs clearly worse than an OSG femto deployment with the same number of femto eNodeBs. As a comparison, the maximum uplink served area traffic is equal to 3.2 GB/h/km² (assuming a coverage requirement of 0.5 Mbps and taking the quality of the downlink control signaling into account) for the baseline deployment. Furthermore, the maximum uplink served area traffic with 30% OSG femto penetration ($P_{femto}$ equal to 1 mW and $O_{femto}$ equal to zero) is equal to 35.1 GB/h/km² (0.5 Mbps) or 23.8 GB/h/km² (1 Mbps). With 50% OSG femto penetration the maximum uplink served area traffic increases to 53.5 GB/h/km² (0.5 Mbps) or 39.1 GB/h/km² (1 Mbps). Finally, what is different compared to the downlink is that the uplink benefits more from the biased cell selection, in particular in case of the higher coverage requirements.

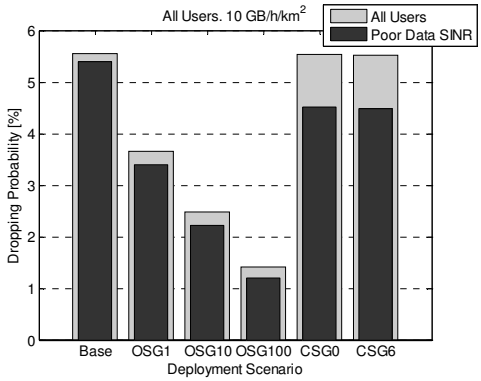


**Figure 7.29.** Observed user dropping probability for the evaluated network deployments.

Uplink capacity of the heterogeneous CSG femto deployment is affected by the quality of the downlink control signaling. This can be verified by evaluating the user performance within a scenario with offered traffic equal to 10 GB/h/km², and assuming that the femto penetration is equal to 30%. Results for the observed user dropping probability are shown in Figure 7.29. As can be seen, the overall dropping probability exceeds the limit of 5% for the baseline deployment, heterogeneous CSG femto deployment with $O_{CSG}$ equal to zero and heterogeneous CSG femto deployment with $O_{CSG}$ equal to 6 dB. In case of the evaluated heterogeneous OSG femto deployments (with $P_{femto}$ equal to 1 mW, 10 mW and 100 mW), the overall dropping probability is less than 5%, indicating that the maximum uplink capacity will be higher than the evaluated 10 GB/h/km². If the quality of the downlink control signaling is ignored, i.e. the users are dropped only if the uplink data SINR is too low, the dropping probability becomes lower. This indicates that the uplink capacity of the heterogeneous CSG femto deployments could be increased by improving the quality of the downlink control signaling. A closer look at the results reveals that the users dropped due to the poor uplink data SINR are to a large extent located on the ground floor, which means that they are suffering from a large coupling loss towards the serving macro eNodeB. What is also interesting is that in case of the CSG femto deployments, 90% of the users dropped due to a poor downlink quality are located indoors (30% on the ground floor, 60% on the residential floors). The main reason for this is the downlink interference from the CSG femto eNodeBs.

Results for the observed uplink packet bit rates are shown in Figure 7.30, and in Figure 7.31. Compared to the baseline deployment the introduction of CSG femto eNodeBs benefits mostly only the users that are located within the femto apartments, while the users outside the femto apartments

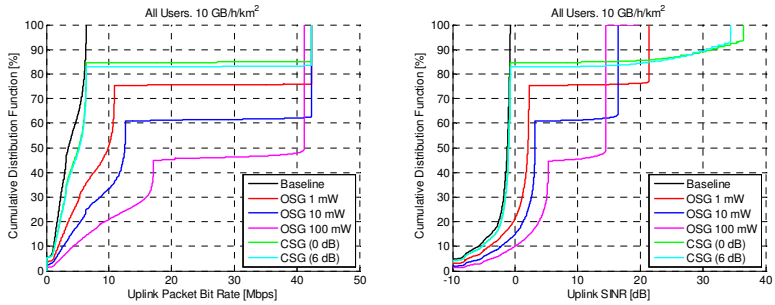


**Figure 7.30.** Distribution of the uplink packet bit rates and uplink SINRs for the baseline deployment and a few different heterogeneous OSG and CSG femto deployments.

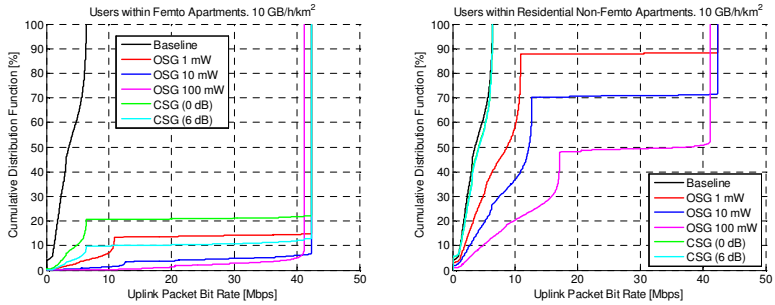


**Figure 7.31.** Distribution of the uplink packet bit rates for the residential users.

will experience only very marginal gains. If the CSG femto deployments are compared against the OSG femto deployments, the largest gains related to the open access are experienced by the users outside the femto apartments. These gains are caused both by the increased traffic offloading, and by the increased $P_{0,macro}$ (enabled by the increased traffic offloading). However, even the performance of the users within the femto apartments is slightly improved as a result of the increased femto cell coverage area. The performance is improved despite the fact that the $P_{0,femto}$ is lower than most of the applied $P_{0,CSG}$ values. The reason for this is that the uplink user performance within the femto cells is in many cases limited by the maximum allowed modulation and coding scheme, and hence, the differences in the achieved SINR have much less impact.

### 7.5.3 Unsynchronized deployment of CSG femto eNodeBs

As discussed in the previous section, performance of a synchronized CSG femto deployment can often be limited by the quality of the downlink control signaling. One possible way to improve the (average) quality of the downlink control signaling is to apply a time shift between the cells so that

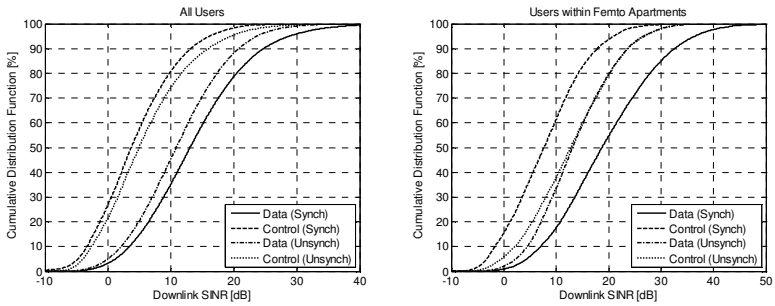


**Figure 7.32.** Distribution of the downlink SINR for a synchronized and an unsynchronized network deployment, assuming a scenario with femto penetration equal to 30% and offered area traffic equal to 55 GB/h/km².

the control symbols are interfered by the data symbols transmitted from the neighboring cells. In case the cell layers are tightly time-synchronized and time-shifted, the interfering cell can mute its data transmissions during the symbols that collide with the control signaling within the neighboring cells. The downside of the time shift is that the average inter-cell interference towards the data symbols will have a certain non-zero level, caused mainly by the CRS transmissions, even when the neighboring cells are idle. Hence, the time shift will improve the average quality of the downlink control signaling, but at the same time the average quality of the downlink data symbols will be reduced. It is also worth noting that the time shift does not affect the quality of the uplink data symbols.

Another reason why the performance of an unsynchronized CSG femto deployment is interesting is that in reality it could be quite challenging to achieve tight time synchronization between the macro and the CSG femto cells. This is related both to the type of the backhaul connection and to the difficulties in achieving a sufficient GPS coverage within indoor areas.

It is worth noting that a similar behavior can be obtained by properly assigning Physical Cell Identities (PCIs) for the neighboring cells, resulting in different CRS frequency shifts [100], see also the discussion in [151]. Assuming different frequency shifts for the CRS transmissions, the reference symbols of one cell would be at least partially interfered by the non-reference symbols of neighboring cells, improving the average quality of the CRS. However, this kind of *PCI planning* is not able to improve the quality of PBCH and PSS/SSS.

The performance difference between a synchronized and an unsynchronized network deployment is studied first within a scenario with 30% femto penetration and offered downlink area traffic equal to 55 GB/h/km². Distributions of the observed downlink data and control SINR are presented in Figure 7.32. Furthermore, distributions of the observed

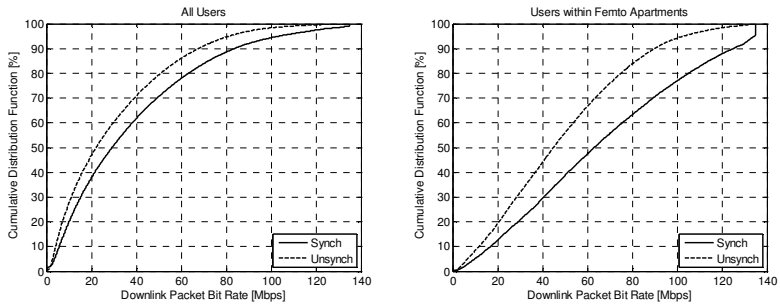


**Figure 7.33.** Distribution of the downlink packet bit rates for a synchronized and an unsynchronized network deployment, assuming a scenario with femto penetration equal to 30% and offered area traffic equal to 55 GB/h/km².

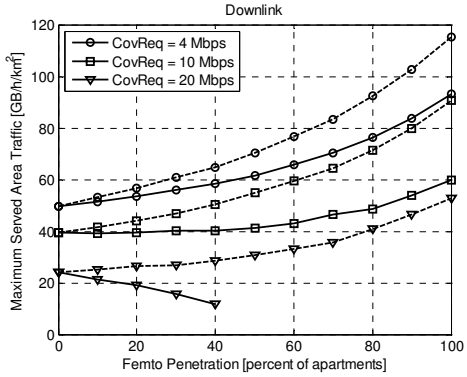


**Figure 7.34.** Maximum downlink served area traffic as a function of the femto penetration. The solid curves present the results for the unsynchronized deployment, while the dashed curves present the results for the synchronized deployment.

downlink packet bit rates are presented in Figure 7.33. The figures indicate that an unsynchronized deployment improves the quality of the downlink control signaling but reduces the quality of the downlink data transmission, as expected. Since the quality of the downlink control signaling is not limiting the performance in any larger extent in the assumed scenario, the overall downlink performance is reduced.

Results for the maximum downlink served area traffic as a function of the femto penetration are shown in Figure 7.34. Three different coverage requirements, 4 Mbps, 10 Mbps and 20 Mbps, are assumed. Furthermore, the solid curves present the results for the unsynchronized deployment, while the dashed curves present the results for the synchronized deployment. As indicated by the curves, the downlink performance of an unsynchronized network deployment is considerably worse than the performance of a synchronized network. This is in particular the case for the higher coverage requirements, which require a high cell-edge SINR and are therefore more sensitive to the inter-cell interference.

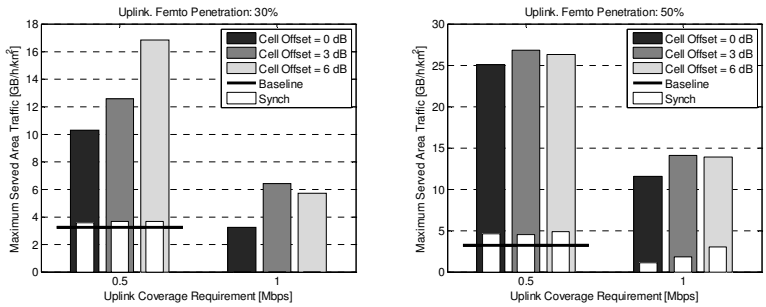


**Figure 7.35.** Maximum uplink served area traffic for two different coverage requirements and for two different values of the cell selection offset. Femto penetration equal to 30% or 50% is assumed.

A closer look at the results reveals that there is one fundamental difference between the CSG femto results in Figure 7.34 and the corresponding OSG results in Figure 7.5. While in case of OSG the increased traffic offloading allows also the use of higher average utilization of the cell resources, that is not the case for CSG, where the femto cells are not able to offload any ground floor or in-vehicle users. Thus, in case of CSG the system capacity is increased solely as a result of the traffic offloading. Since the average quality of the downlink data symbols is reduced as a result of the network unsynchronization, a lower level of average cell utilization will typically be allowed before the desired coverage requirement is reached. Therefore, also the maximum system capacity becomes lower.

Since the uplink performance of a synchronized network deployment can be limited by the quality of the downlink control signaling, an improved downlink control SINR can potentially have a large positive impact on the uplink capacity. This is demonstrated in Figure 7.35, which presents the results for the maximum uplink served area traffic for two different coverage requirements (0.5 Mbps and 1 Mbps) and for two different values of the femto penetration (30% and 50%). Furthermore, the impact of the biased cell selection is evaluated as well. The corresponding results for the synchronized network deployment are indicated by the white bars. As can be seen, the gains compared to both the baseline network and the synchronized CSG femto deployment are considerable.

### 7.5.4 Adjacent channel deployment of CSG femto eNodeBs

The quality of both the data and the control symbols can be improved also by deploying the CSG femto eNodeBs on a separate carrier frequency compared to the macro cells. The various CSG femto eNodeBs are still assumed to be sharing the same carrier frequency. The downside of this

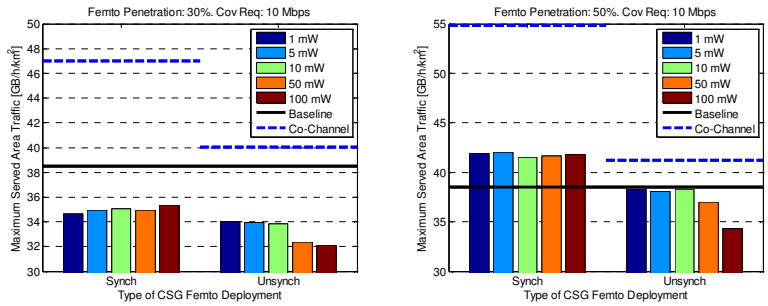


**Figure 7.36.** Maximum downlink served area traffic for a coverage requirement equal to 10 Mbps, assuming an adjacent channel deployment of femto eNodeBs. Femto penetration equal to 30% or 50% is assumed.

alternative is that the carrier bandwidths are reduced for both the macro cell layer and the CSG femto cell layer, which will in particular harm the performance of the users that are not suffering from the excessive inter-layer interference.

Downlink results are summarized in Figure 7.36. The carrier bandwidth is assumed to be equal to 15 MHz for the macro cell layer and 5 MHz for the femto cell layer. In addition to the femto penetration, also the type of the CSG femto deployment (synchronized/unsynchronized) and the value of $P_{CSG}$ are varied. It should be noted that in case of the adjacent channel deployment of CSG femto eNodeBs, the same $P_{CSG}$ is assumed for all femto cells. As a comparison, also the maximum capacities of both the baseline deployment and the co-channel CSG femto deployment are indicated in the figures.

As can be seen, downlink performance of the adjacent channel CSG femto deployment is clearly worse than the performance of the corresponding co-channel deployment. Even the facts that the adjacent channel deployment could allow the use of a higher femto eNodeB output power and a larger cell selection offset are not able to compensate for the loss caused by the reduced carrier bandwidth.

Uplink simulation results are shown in Figure 7.37. Similar to the downlink, the carrier bandwidth is assumed to be equal to 15 MHz for the macro cell layer and 5 MHz for the femto cell layer. If the results for the adjacent channel synchronized deployment are compared to the results for the co-channel synchronized deployment shown in Figure 7.28, it can be estimated that in case of a coverage requirement equal to 0.5 Mbps the maximum uplink served area traffic increases from approximately 3.5 to 17.5 GB/h/km², and from 4.5 to 24 GB/h/km² for femto penetration equal to 30% and 50%, respectively. Furthermore, in case of a coverage requirement equal to 1 Mbps, the served area traffic increases from 0 to 4

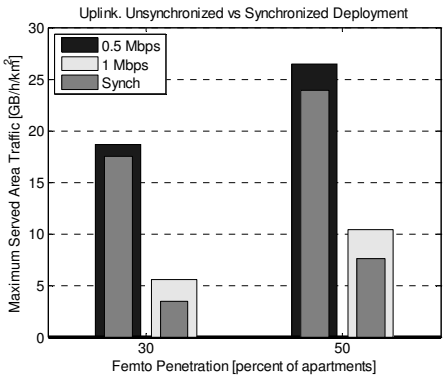


**Figure 7.37.** Maximum uplink served area traffic for an adjacent channel unsynchronized and a synchronized femto deployment. Two different coverage requirements, 0.5 Mbps and 1 Mbps, and two different values of the femto penetration, 30% and 50% are assumed.

GB/h/km² (femto penetration equal to 30%), and from 1-3 to 7.5 GB/h/km² (femto penetration equal to 50%). In all, the performance of the adjacent channel synchronized deployment is slightly worse than the performance of the co-channel unsynchronized deployment.

Uplink performance of the adjacent channel unsynchronized deployment is better than the uplink performance of the adjacent channel synchronized deployment. This is caused by the fact that even though the inter-layer interference has been considerably reduced, the interference between the neighboring femto cells is still affecting the quality of the downlink control signaling. Assuming an unsynchronized deployment between the femto cells, the inter-cell interference towards the downlink control signaling is reduced, and thus, the impact of the downlink quality on the uplink performance becomes smaller. Compared to the unsynchronized co-channel deployment, see Figure 7.35, the unsynchronized adjacent channel deployment results in a similar network performance.

## 7.6 Performance of a hybrid mode femto eNodeB

In addition to the OSG and the CSG mode, a femto eNodeB can operate also in a so-called hybrid access mode, where all users are allowed to connect to the eNodeB, but the users outside the CSG have access to only a limited amount of the cell resources [48][152]. This section provides a brief evaluation of the downlink performance of three different types of hybrid mode realizations:

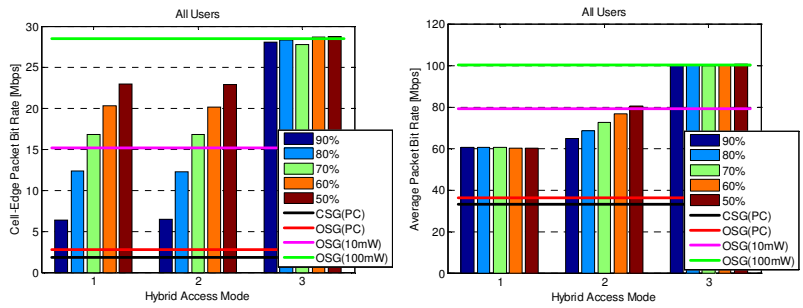


**Figure 7.38.** Downlink user performance for the different heterogeneous femto deployments.

1. A static resource split between the CSG and the non-CSG users. A total of Γ% of the resources are reserved for the CSG users and the remaining (100 – Γ)% of the resources are reserved for the non-CSG users.

2. A dynamic split of resources, where the resources are split only when the femto cell is serving non-CSG users. If the femto cell is serving only CSG users, they have access to all resources. However, if the femto cell is serving only non-CSG users, they have access to (100 – Γ)% of the resources.

3. A dynamic split of resources, where the resources are split only when the femto cell is serving both CSG and non-CSG users. If the femto cell is serving only CSG or non-CSG users, they have access to all resources.

The evaluations assume that all users located within a femto apartment are CSG users (of that particular femto cell), while all users located outside the femto apartment are non-CSG users. In addition to the hybrid mode deployment, results for a CSG femto deployment and three different types of OSG femto deployments are provided as well. The evaluations assume a femto penetration equal to 50% and offered area traffic equal to 75 GB/h/km$^2$. Furthermore, the femto eNodeB output power is assumed to be equal to 100 mW for the hybrid mode deployments.

Results for the cell-edge packet bit rate and the average packet bit rate are presented in Figure 7.38. The different bars correspond to different levels of the resources reserved for the CSG users, i.e. the value of parameter Γ. The horizontal lines present the results for the evaluated CSG and OSG femto deployments: CSG femto deployment with eNodeB power adjustment, OSG femto deployment with eNodeB power adjustment, OSG femto deployment

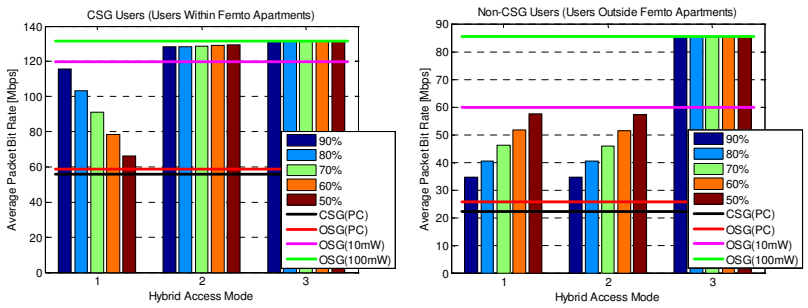


**Figure 7.39.** Average downlink packet bit rate for the CSG and for the non-CSG users, assuming a number of different heterogeneous femto deployments.

with $P_{femto}$ equal to 10 mW and OSG femto deployment with $P_{femto}$ equal to 100 mW. The obtained results demonstrate that the overall network performance can be improved by allowing also the non-CSG users to connect to the femto eNodeB. However, the gain of open access as such is small compared to the gain achieved by increasing the femto eNodeB output power. For example, when it comes to the overall traffic offloading, the assumed CSG deployment results in traffic offloading equal to 25%[11], while the three different OSG deployments (PC, 10 mW and 100 mW) result in an overall traffic offloading equal to 30%, 54% and 69%, respectively. With the hybrid mode operation, the overall traffic offloading becomes equal to 69%.

When it comes to the downlink user performance of the hybrid mode operation, the differences between the three realizations are clear. In case of the first realization, the performance of the CSG users is reduced together with the reduced amount of CSG resources, as demonstrated in Figure 7.39, but at the same time the performance of the non-CSG users will be improved. From the overall system performance point of view, the cell-edge user performance is improved, but the average user performance stays approximately the same.

In case of the second realization, the cost of the hybrid mode operation on the performance of the CSG users becomes considerably smaller compared to the first realization. In fact, the average performance of the CSG users is very close to the performance of the OSG femto deployment with the same femto eNodeB output power. The reason for this is that the probability of a femto cell simultaneously serving both CSG and non-CSG users is very small. However, since the maximum amount of resources available for the non-CSG users is following the same model as in the first realization, the performance of the non-CSG users is still approximately the same.

[11] It should be noted that the maximum achievable level of traffic offloading for the assumed CSG deployment is equal to 32%.

Finally, in case of the third realization of the hybrid mode operation, the overall system performance is almost identical with the performance of the OSG femto deployment with the same femto eNodeB output power. The reason for this is that now also the non-CSG users have an unlimited access to the resources when there are no active CSG users within the same femto cell. The performance of the hybrid mode operation would differ from the performance of the OSG during the periods when the same femto cell is serving both CSG and non-CSG users. However, since the probability of that kind of a scenario is very small, the overall system performance does not noticeably depend on the assumed value of parameter Γ.

## 7.7 Summary of the evaluation results

The presented downlink evaluation results indicate that the heterogeneous OSG femto deployment requires approximately 67-88 times as many new sites as the densified macro deployment to fulfill the same coverage and capacity requirements. Compared to the corresponding results for the heterogeneous micro deployment, approximately 8.3-11.9 times as many new femto sites are required. The reason for this is that while an outdoor micro eNodeB can potentially offer coverage inside multiple buildings and on multiple floors, the coverage area of an indoor femto cell is much more limited. That is why a much greater number of femto cells are required to offer the same level of coverage and traffic offloading. Looking at the uplink results, the corresponding ratios become equal to 40-88 and 10.9-15.5 with respect to the densified macro and the heterogeneous micro deployment, respectively.

The reason why the heterogeneous OSG femto deployment is more efficient compared to the densified macro deployment to improve the uplink performance than the downlink performance is that it is more efficient to improve the performance of the most coverage-limited indoor users. That is also the main reason why the heterogeneous femto deployment is less efficient than the heterogeneous micro deployment to improve the uplink performance: Since the non-residential ground floor is not assumed to contain any femto cells, the outdoor micro cells are able to provide a higher level of offloading for the ground floor users, which are often also the most expensive ones when it comes to the utilization of the macro cell resources.

Femto eNodeBs are designed to use a residential broadband connection as a backhaul. Therefore, the performance of a femto user will often be limited by the backhaul capacity instead of the air-interface throughput. However,

based on the presented evaluation results, the overall downlink system performance will not be affected unless the desired coverage requirement is close to the maximum achievable backhaul throughput of the femto cells. The impact of the backhaul limitation on the uplink performance has not been evaluated in this thesis, and should be studied before any firm conclusions on this topic can be made.

A targeted deployment of OSG femto eNodeBs is shown to benefit the overall system performance, which in practice means that the same system performance can be achieved with a lower density of femto cells compared to a random deployment of femto cells. By deploying femto eNodeBs initially in apartments with poor macro cell coverage, the most power-limited users can be offloaded from the macro cell. The coverage-based deployment is beneficial for scenarios which are mostly coverage-limited, that is for scenarios with a low femto eNodeB output power, low capacity requirement or high coverage requirement. However, due to the fact that the overall traffic offloading can become lower, performance of the more capacity-limited scenarios can become worse. If the femto eNodeBs are initially deployed within the most traffic-heavy apartments, the amount of offloaded traffic can be maximized with the minimum amount of femto eNodeBs. As a result of this kind of traffic-based femto deployment, the heterogeneous OSG femto deployment can be made more competitive compared to the other network densification alternatives.

Femto eNodeBs can operate either in OSG, CSG, or hybrid access mode. Due to the required interference mitigation mechanisms, the performance of a heterogeneous CSG femto deployment is much worse than the performance of a similar heterogeneous OSG or hybrid access mode femto deployment, which is well in line with the previously published results in [72] and [153]. The main reasons for the worse system performance are the considerably lower level of traffic offloading, worse performance of the femto users and the increased level of inter-layer interference towards the macro users.

# 8. Performance comparison of the different network densification alternatives

This chapter compares the different network densification alternatives, as introduced in the previous chapters, from the system performance point of view. First, the performance of the densification alternatives is compared within a scenario, where the various deployment alternatives have been dimensioned to fulfill the same coverage and capacity requirements. After that, the densification alternatives are compared from the maximum system capacity point of view, based on the results presented in Chapter 5, Chapter 6 and Chapter 7. Finally, the densification alternatives are compared within a simple dimensioning exercise, which takes both the downlink performance and the uplink performance into account.

## 8.1 Scenario comparison

In this section the performance of the different network densification alternatives is compared within a scenario, where the various deployment alternatives have been dimensioned to fulfill the same coverage and capacity requirements. The reference case for the comparison is assumed to be a densified macro deployment, where the number of macro sites has been doubled compared to the baseline network, i.e. the macro site density has been increased from 4.62 to 9.24 sites/km$^2$, resulting in an inter-site distance equal to 354 meters. The desired capacity requirement is derived by evaluating the maximum offered area traffic for the densified macro deployment so that the cell-edge packet bit rate is at least equal to 10 Mbps for downlink, or 1 Mbps for uplink. Based on the evaluations, offered downlink area traffic equal to 80 GB/h/km$^2$ and offered uplink area traffic equal to 40 GB/h/km$^2$ have been selected.

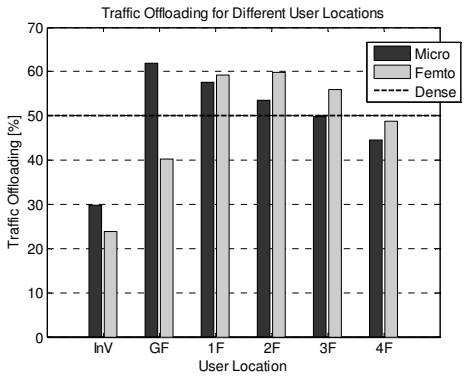


**Figure 8.1.** Observed traffic offloading for the different user locations.

### 8.1.1 Downlink performance

The first step is to evaluate the required low-power site densities for each of the heterogeneous network deployments so that both the downlink coverage requirement and the downlink capacity requirement are fulfilled at the same time. In case of the heterogeneous micro deployment, both requirements are fulfilled, when the average number of micro sites per traffic cluster is equal to 0.61 (27.1 micro sites/km$^2$). For the heterogeneous OSG femto deployment, femto penetration equal to 22% (298 femto sites/km$^2$) is required.

Assuming the given site densities, the corresponding levels of traffic offloading become equal to 50% (densified macro), 49% (heterogeneous micro) and 47% (heterogeneous OSG femto). Even though there are no major differences in the overall traffic offloading, the network densification alternatives differ considerably in the way they can offload users in different locations, as indicated by the results in Figure 8.1. To start with, the heterogeneous deployments have difficulties in offloading the in-vehicle users, in particular the ones located within the outdoor bins. Secondly, the heterogeneous deployments are more efficient in offloading the indoor users compared to the densified macro deployment. When it comes to the users located on the ground floor, the heterogeneous femto deployment suffers from the fact that the femto eNodeBs are assumed to be deployed only on the residential floors (1F-4F). However, since the femto eNodeBs have been deployed closer to the residential users compared to the outdoor micro eNodeBs, the heterogeneous femto deployment results in a higher level of traffic offloading on the residential floors. Finally, the level of traffic offloading is reduced for the heterogeneous deployments as a function of

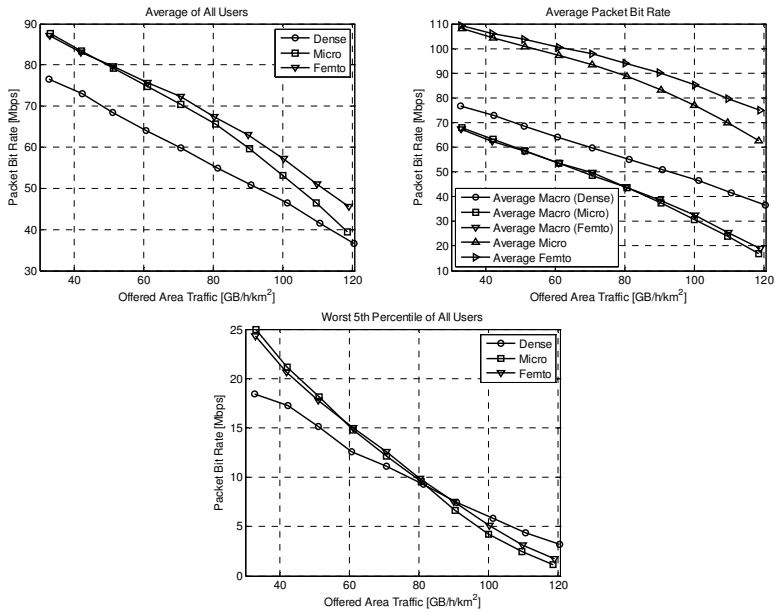


**Figure 8.2.** Average and cell-edge packet bit rate as a function of the offered area traffic for the evaluated network densification alternatives.

the floor level due to the fact that the macro cell signal strength is increasing.

The different network densification alternatives are compared in Figure 8.2 from the user performance point of view. As can be seen, the heterogeneous deployments result in a better average user performance compared to the densified macro deployment. Similarly, the average performance of the low-power cell users is clearly better than the average performance of the macro cell users.

There are two main reasons why the downlink performance of the heterogeneous deployments is better than the performance of the densified macro network. Firstly, as indicated by the curves in Figure 8.2, the users served by the low-power cells experience much better throughput compared to the users served by the macro cells. Even though the absolute level of downlink interference is higher within the heterogeneous deployments due to the higher average macro cell utilization, see Figure 8.3, the considerably higher serving cell signal strength is more than able to compensate for that. Therefore, the SINRs, and further, the achievable bit rates become higher compared to the macro cell users. The reason why the heterogeneous deployments result in a higher macro cell utilization is related to the fact that the dimensioning of the heterogeneous deployments aims to find the lowest density of low-power cells, which fulfills both the coverage and the capacity requirement. As a result of the enhanced offloading of the indoor

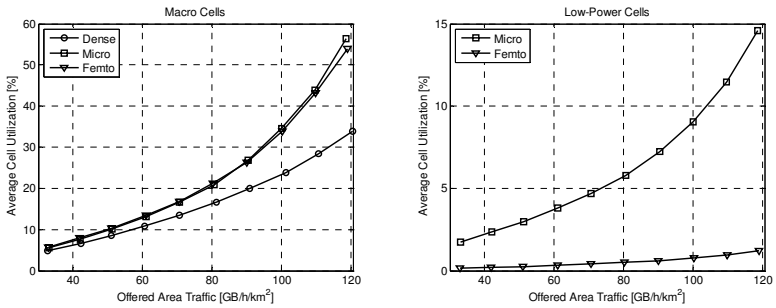


**Figure 8.3.** Average macro and low-power cell utilization as a function of the offered area traffic for the different network densification alternatives.

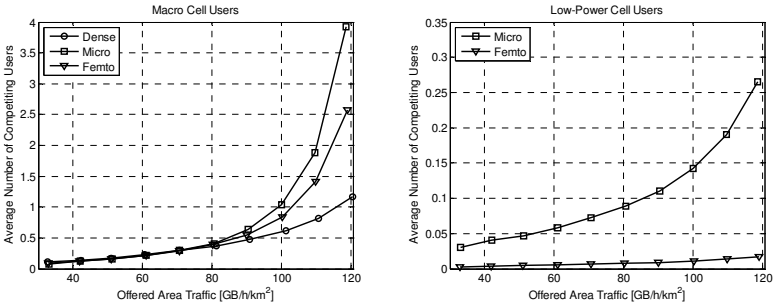


**Figure 8.4.** Average number of competing users for the macro and low-power cell users.

users, and in particular the performance advantage offered by the low-power cell users, the heterogeneous networks can be allowed to operate at a higher load level compared to the densified macro network, while still fulfilling the same coverage requirement. The differences in the observed average macro cell utilizations, together with the fact that the macro users within the heterogeneous network deployments have larger coupling losses towards the serving eNodeBs, explain why the average performance of the macro users is worse within the heterogeneous deployments compared to the densified macro deployment.

The second reason explaining the performance difference between the macro and the low-power cell users is the fact that the heterogeneous deployments result in a smaller number of simultaneously active users within the serving cell, as demonstrated by the results in Figure 8.4. In most of the cases, the users served by the low-power eNodeBs are alone in the cell. However, the macro users have a much higher probability of being forced to share the cell resources with other users.

In case of a low network load, the system is mostly power-limited, which means that the worst user throughputs are typically observed in locations with the largest coupling losses towards the serving eNodeBs. Another thing to note is that despite the reduced macro cell range, the highest

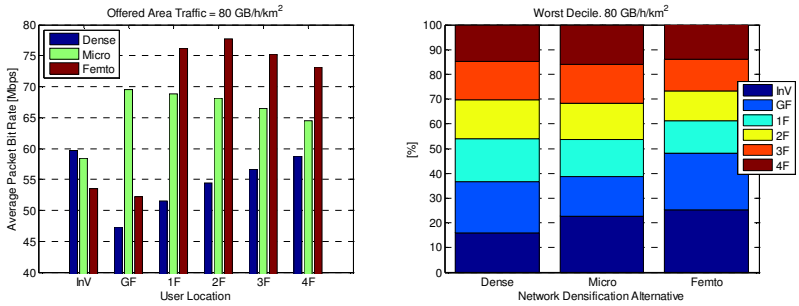


**Figure 8.5.** Observed average user performance for the different user locations and the locations of the worst performing users.

coupling losses towards the serving macro cell can be found within the densified macro deployment. This is due to the fact that in case of the heterogeneous deployments the indoor users experiencing the worst macro cell coverage are likely to be served by the low-power cells. As a result, the densified macro deployment results in a worse cell-edge performance compared to the heterogeneous deployments.

In case of a high network load, the macro eNodeBs are operating very close to their maximum capacity, which quite often leads to situations with very long scheduling queues within the macro cells, and low macro user throughputs. Now, the system is clearly capacity-limited, and the differences in coupling losses do not have any remarkable role. However, the fact that the average macro cell utilization is lower within the densified macro deployment compared to the heterogeneous deployments is an advantage. In case of the densified macro deployment, the worst users are fairly uniformly distributed over the different user locations. In case of the heterogeneous deployments, the worst performing users are concentrated in locations, which cannot fully enjoy the traffic offloading offered by the low-power cells.

The different network densification alternatives can be compared also by evaluating the average downlink performance for the different user locations, assuming offered area traffic equal to 80 GB/h/km². A few differences can be highlighted in the results presented in Figure 8.5. First of all, the impact of building penetration and floor height gain on the macro coverage is clearly visible: Performance of the in-vehicle users is better than the performance of the indoor users. Similarly, performance of the macro users improves as a function of the floor level. Secondly, the evaluated heterogeneous deployments result in a better indoor than in-vehicle user performance. The main reason for this is that while the low-power cells can offer many indoor users both better achievable bit rate and throughput, most of the in-vehicle users are still served by the macro eNodeBs and can

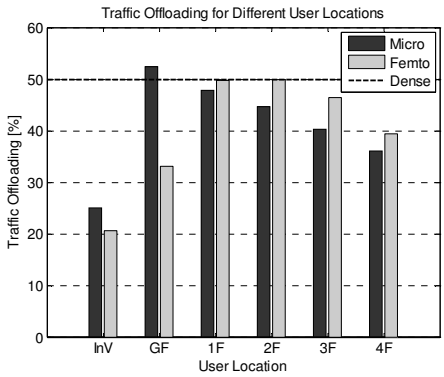


**Figure 8.6.** Observed levels of traffic offloading for the different user locations.

only enjoy the throughput gains offered by the traffic offloading. Thirdly, in case of the heterogeneous micro deployment, the average packet bit rate is better on the ground floor than on the upper floor levels. This is caused mainly by the fact that the macro cell signal strength increases, and the level of traffic offloading decreases as a function of the floor level. The situation is the opposite for the heterogeneous femto deployment. This is due to the assumption that the ground floor does not contain any femto eNodeBs.

### 8.1.2 Uplink performance

In case of the heterogeneous micro deployment, the desired uplink performance is reached when the average number of micro sites per traffic cluster is equal to 0.44 (corresponding to a density of 19.8 micro sites/km$^2$). For the heterogeneous OSG femto deployment, the evaluations assume a femto penetration equal to 16% (217 femto sites/km$^2$). Results for the observed levels of traffic offloading are shown in Figure 8.6. Due to a lower density of low-power sites, the traffic offloading becomes lower compared to the downlink evaluations: The micro cells offload approximately 40%, and the femto cells offload approximately 39% of the traffic. Since the heterogeneous deployments are more likely to offload (power-limited) indoor users than in-vehicle users, a lower level of the overall traffic offloading is sufficient to reach the same uplink performance compared to the densified macro deployment. Another reason why the heterogeneous deployments are so effective in improving the uplink performance is the big performance difference between the macro and the low-power cell users.

Results for the observed user performance as a function of the offered area traffic are shown in Figure 8.7. Similar to the downlink, the

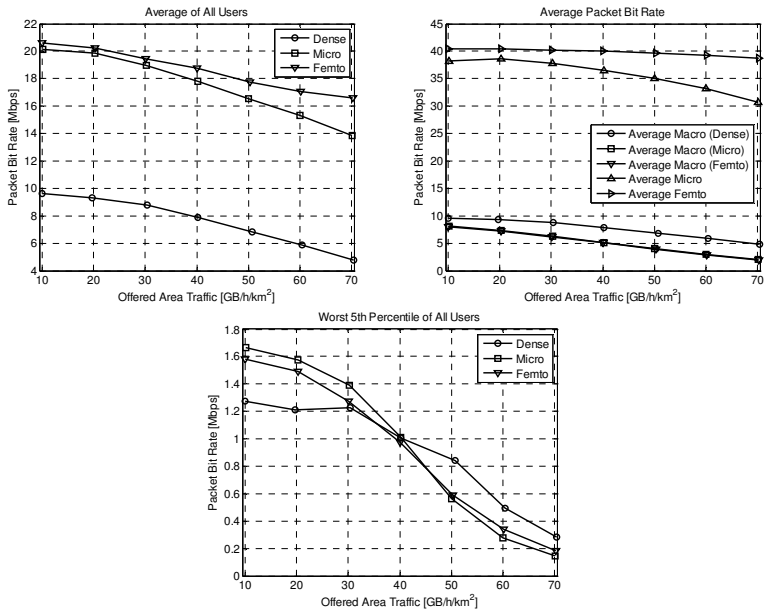


**Figure 8.7.** Average and cell-edge packet bit rate as a function of the offered area traffic for the evaluated network densification alternatives.

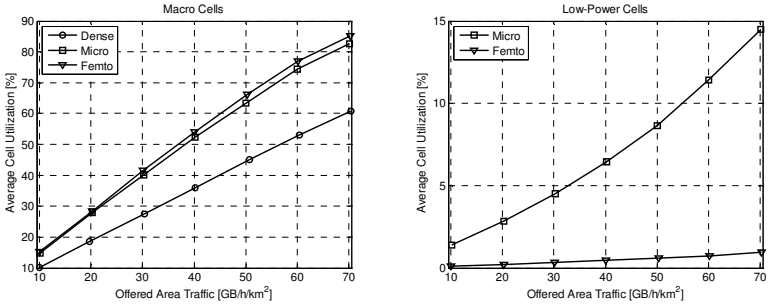


**Figure 8.8.** Average macro and low-power cell utilization as a function of the offered area traffic for the different network densification alternatives.

heterogeneous deployments result in a better average user performance compared to the densified macro deployment. Furthermore, the average performance of the low-power cell users is considerably better than the average performance of the macro cell users. Finally, as a result of the higher average macro cell utilization, see Figure 8.8, the average macro user performance becomes worse for the heterogeneous deployments compared to the densified macro deployment.

When it comes to the results for the uplink cell-edge packet bit rate, the main motivations for the poor user performance are the same as in the downlink: In case of a low network load, the worst performing users are suffering from large coupling losses towards the serving (macro) eNodeBs,

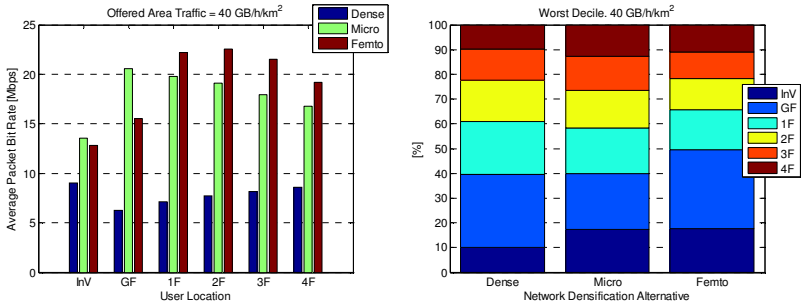


**Figure 8.9.** Observed average user performance for the different user locations and the locations of the worst performing users.

whereas in case of a high network load the main reason for the poor user performance is the fact that the users are forced to share the (macro) cell resources with other simultaneously active users.

In uplink, the assumed received power target, i.e. the value of parameter $P_0$, plays a major role. Here, $P_{0,macro}$ is assumed to be equal to -114, -115 and -115 dBm for the densified macro, heterogeneous micro and heterogeneous femto deployment, respectively. Furthermore, $P_{0,micro}$ is assumed to be equal to -102 dBm and $P_{0,femto}$ is assumed to be equal to -99 dBm. The reason why the value of $P_{0,macro}$ can be fairly similar for all the evaluated network densification alternatives, despite fairly large differences in the overall traffic offloading, is that the heterogeneous deployments are efficient in offloading the most power-limited indoor users.

Results for the average uplink user performance and the locations of the worst performing users are presented in Figure 8.9, assuming offered area traffic equal to 40 GB/h/km². The first thing to highlight is that the uplink performance of the densified macro deployment is affected by the differences in the coupling losses towards the serving eNodeBs: In-vehicle users experience better performance than indoor users, and the average performance of the indoor users is improved together with an increasing floor level. Secondly, the heterogeneous deployments result in considerably better average uplink performance than the densified macro deployment. This is caused by the fact that the low-power cell users experience much better performance than the macro cell users. Thirdly, the heterogeneous deployments result in a better indoor than in-vehicle coverage. Furthermore, the average user performance is reduced together with an increasing floor level. The main factor contributing to this is the observed traffic offloading from the macro to the low-power cell layer, as shown in Figure 8.6.

Since the worst performing uplink users are typically served by macro eNodeBs, the main factors affecting the results are the coupling loss, traffic

offloading and the number of simultaneously active users. Results for the densified macro network reflect clearly the impact of the coupling loss: The worst users are found within the locations with the largest coupling losses, i.e. on the ground and on the first floor, and the probability of a poor user performance is decreasing as a function of the floor level. In case of the heterogeneous deployments, the average macro cell utilization is higher, and the increased number of simultaneously active users has an impact on the results, making the distribution slightly less dependent on the coupling loss. Finally, in case of the heterogeneous femto deployment the fact that the ground floor areas do not have any femto eNodeBs is clearly affecting the results.

In all, when the uplink results are compared with the corresponding downlink results, it becomes quite obvious that the downlink is in general more capacity-limited than the uplink. In such scenarios it is more important to be able to offload as much of the traffic as possible, instead of focusing on the users that have the worst macro cell coverage. Therefore, the main question affecting the downlink results is: “How large part of the macro cell traffic can be offloaded?” In the more power-limited uplink, however, the main question is: “Which macro cell users can be offloaded?”

## 8.2 Capacity comparison

In this section the performance of the different network densification alternatives is compared from the system capacity point of view. The main thing to compare is the required number of new sites to be deployed in order to fulfill the desired coverage and capacity requirements. In addition, the impact of a number of design choices on the system performance is discussed.

### 8.2.1 Downlink performance

When the values in Table 6.1 and Table 7.1 are divided by the corresponding values in Table 5.3, ratios between the required density of new low-power sites and the required density of new macro sites can be obtained, see Table 8.1. As can be noticed, heterogeneous micro deployment requires approximately 7-9 times as many new sites as the densified macro deployment in order to fulfill the same downlink coverage and capacity requirements. In case of the heterogeneous OSG femto deployment, the corresponding ratio becomes roughly equal to 67-88.

**Table 8.1**. Ratio between the required number of new micro sites/OSG femto sites and the required number of new macro sites to satisfy the desired downlink coverage and capacity requirements.

| Coverage Req | Capacity Requirement | | | |
|---|---|---|---|---|
| | 50 GB/h/km² | 100 GB/h/km² | 150 GB/h/km² | 200 GB/h/km² |
| 4 Mbps | 7.5 / 88 | 7.7 / 80 | 6.7 / 77 | 8.4 / 74 |
| 10 Mbps | 7.6 / 86 | 7.1 / 78 | 6.7 / 77 | - / 71 |
| 20 Mbps | 7.0 / 78 | 6.7 / 79 | 8.8 / 73 | - / 68 |
| 30 Mbps | 7.1 / 84 | 8.5 / 79 | - / 72 | - / 67 |

Instead of looking at the density of new sites to be deployed, one can compare also the density of new cells, which gives a better indication on the densification of the radio resources within the system area. Keeping in mind that each new macro site introduces three new cells into the system, heterogeneous micro deployment requires roughly 2.3-3 times and heterogeneous OSG femto deployment roughly 22-29 times as many new cells as the densified macro deployment. Hence, the deployment of new macro sites seems to be the most efficient way to densify the baseline network.

Looking at the values for the heterogeneous micro deployment in Table 8.1, no clear trends with respect to either the coverage or the capacity requirement can be detected. However, in case of the heterogeneous OSG femto deployment the ratio between the required density of new femto sites and the required density of new macro sites becomes slightly smaller as the capacity requirement is increased. One possible explanation for this could be that the approach where the system coverage and the overall traffic offloading are improved by deploying indoor femto cells is expensive at first, but once a sufficient level of coverage has been reached, increasing the network capacity further is less expensive. In general, the obtained downlink results suggest that traffic offloading is playing a major role for many of the scenarios. The advantage of macro cells is that they can offer better signal strength within traffic hotspots that do not have dedicated low-power cells, within areas outside the traffic hotspots, on the upper floor levels, as well as within the indoor areas that are not directly illuminated by the micro eNodeBs. That is also why the densified macro deployment is more efficient in improving the performance of the system as a whole, when looking at the required number of new cells to be deployed within the system area. For the different heterogeneous deployments the traffic offloading is affected by the ability of the low-power cells to cover the whole

**Table 8.2**. Ratio between the required number of new micro sites/OSG femto sites and the required number of new macro sites to reach the desired average downlink packet bit rates and capacity requirements.

| Average Packet Bit Rate | Capacity Requirement | | | |
|---|---|---|---|---|
| | 50 GB/h/km² | 100 GB/h/km² | 150 GB/h/km² | 200 GB/h/km² |
| 50 Mbps | 5.9 / 66 | 5.8 / 60 | 5.5 / 58 | 6.8 / 54 |
| 60 Mbps | 5.7 / 62 | 5.4 / 58 | 5.0 / 55 | 6.7 / 53 |
| 70 Mbps | 5.2 / 58 | 5.0 / 53 | 5.3 / 52 | - / 49 |
| 80 Mbps | 4.8 / 53 | 4.6 / 50 | 5.9 / 48 | - / 42 |
| 90 Mbps | 4.0 / 45 | 4.9 / 49 | - / 43 | - / 37 |

hotspot area. While an outdoor micro eNodeB can potentially offer coverage inside multiple neighboring buildings and on multiple floors, the coverage area of an indoor femto eNodeB is much more limited. That is why a much greater number of indoor cells is required to offer the same level of coverage and traffic offloading.

It is also interesting to compare the traffic offloading values in Table 5.4, Table 6.2 and Table 7.2, and the average macro cell utilization values in Table 5.5, Table 6.3 and Table 7.3 with each other. As can be noticed, the heterogeneous network deployments result in both a higher level of traffic offloading and a higher level of average macro cell utilization compared to the densified macro deployment. The reason for this can be that since in downlink the main target is to offload as much traffic as possible from the baseline cells with as few new cells as possible, the situation becomes somewhat challenging for the low-power cells, which are deployed only within the traffic hotspots and have fairly small coverage areas compared to the macro cells. For all the evaluated network densification alternatives the most site-efficient way to improve the system coverage (under the same capacity requirement) is to deploy new sites and at the same time to reduce the average utilization of the cell resources. Similarly, the most site-efficient way to improve the system capacity is to deploy new sites and to increase the average utilization of the cell resources, when possible without sacrificing the desired coverage requirement.

The network densification alternatives can be compared also from the average packet bit rate point of view, see Table 8.2. If the values in Table 8.2 are compared with the values in Table 8.1 it becomes very clear that the heterogeneous deployments are more effective in providing a certain average user performance than a certain cell-edge user performance. This is caused by the fact that the users served by the low-power eNodeBs will

**Table 8.3**. Ratio between the required number of new micro sites/OSG femto sites and the required number of new macro sites to satisfy the desired uplink coverage and capacity requirements.

| Coverage Req | Capacity Requirement | | | |
|---|---|---|---|---|
| | 30 GB/h/km² | 60 GB/h/km² | 90 GB/h/km² | 120 GB/h/km² |
| 0.5 Mbps | 8.0 / 88 | 5.7 / 65 | 5.1 / 58 | 4.5 / 55 |
| 1 Mbps | 5.7 / 70 | 5.3 / 63 | 4.8 / 59 | 4.2 / 56 |
| 2 Mbps | 4.7 / 61 | 4.2 / 56 | 3.6 / 52 | 4.2 / 50 |
| 4 Mbps | 2.6 / 40 | 3.7 / 44 | - / 45 | - / 47 |

typically experience better throughput compared to the users served by the macro eNodeBs. While the cell-edge user performance is typically dominated by the performance of the macro cell users, the low-power cell users have a larger impact on the average user performance.

### 8.2.2 Uplink performance

Ratios between the required density of new low-power sites (Table 6.5 and Table 7.5) and the required density of new macro sites (Table 5.6) are listed in Table 8.3 for the desired uplink coverage and capacity requirements. As can be noticed, the ratios become smaller as the coverage requirement is increased, indicating an improved efficiency of the heterogeneous deployments. This is a clear difference compared to the downlink results. However, what is similar to the downlink is that the densified macro deployment is still the most efficient alternative to enhance the performance of the baseline network.

A closer comparison with the downlink results reveals that network densification with the help of heterogeneous deployments is more efficient for the uplink than it is for the downlink. One reason why the uplink benefits more from a heterogeneous network deployment is that the uplink in the baseline deployment is considerably more power-limited than the downlink. This means, that the worst uplink users can typically be found in locations having the highest coupling losses towards the serving eNodeBs. Furthermore, as a result of the EGoS scheduling, poor performance of the worst users will hurt the overall performance of the cell. When low-power sites are deployed within traffic clusters, indoor users experiencing large coupling losses towards the macro eNodeBs are likely to be served by the low-power eNodeBs instead. The macro cell can therefore experience a large offloading gain both as a result of a lower number of simultaneously

**Table 8.4**. Ratio between the required number of new micro sites/OSG femto sites and the required number of new macro sites to reach the desired average uplink packet bit rates and capacity requirements.

| Average Packet Bit Rate | Capacity Requirement | | | |
|---|---|---|---|---|
| | 30 GB/h/km² | 60 GB/h/km² | 90 GB/h/km² | 120 GB/h/km² |
| 10 Mbps | 2.1 / 21 | 2.5 / 24 | 2.6 / 26 | 2.7 / 27 |
| 15 Mbps | 1.7 / 18 | 1.7 / 18 | 1.9 / 19 | 2.1 / 22 |
| 20 Mbps | 1.4 / 14 | 1.6 / 17 | 1.8 / 18 | 1.9 / 20 |
| 25 Mbps | 1.8 / 20 | 1.8 / 20 | 1.8 / 20 | 1.8 / 20 |

served users, and also as a result of an improved achievable bit rate for the worst users. This is also the main reason for the increased efficiency of the heterogeneous deployments for the higher coverage requirements.

The above explains also the differences related to the required levels of traffic offloading and the average macro cell utilization for the desired network operating points. When the traffic offloading values in Table 5.7, Table 6.6 and Table 7.6, and the average macro cell utilization values in Table 5.8, Table 6.7 and Table 7.7 are compared with each other, it can be concluded that the heterogeneous deployments offer the desired network performance with a lower level of traffic offloading, but with a higher level of macro cell utilization compared to the densified macro deployment. The reason for this is that the heterogeneous deployments are efficient in offloading the most power-limited users, allowing the use of higher network load levels, while still fulfilling the desired coverage requirements.

Finally, in Table 8.4 the different network densification alternatives are compared from the average uplink packet bit rate point of view. Also in uplink, the heterogeneous deployments are efficient in providing average user performance. In fact, based on the results in Table 8.4, the heterogeneous micro deployment appears to be more resource-efficient than the densified macro deployment, i.e. it can provide the same average user performance and system capacity with a lower density of new cells to be deployed. One can also notice that the ratios are increasing together with an increasing capacity requirement, as well as when the coverage requirement becomes high. One reason for this can be that the heterogeneous deployments are less efficient in providing capacity, or very high average user performance, due to the fact that the ability to provide a sufficient level of traffic offloading is playing an important role for both targets.

### 8.2.3 Impact of various design choices

A number of different design choices affecting the performance of the heterogeneous network deployments have been evaluated in Chapter 6 and in Chapter 7. The findings can be summarized as follows:

- *Adjusting the output power of the low-power eNodeB*. The main outcome of the evaluation is that by increasing the output power of the low-power eNodeB, the coverage area of the low-power cell is increased. This will then result in an increased traffic offloading and an improved overall system performance.

- *Biased cell selection*. The service area of the low-power cell can be expanded also with the help of biased cell selection. The downside compared to the approach with an adjusted output power is that the downlink quality of the low-power cell users, in particular the ones located within the expanded cell area, will be worse.

- *Adjacent channel deployment of low-power cells*. Downlink, which is often capacity-limited, does not benefit from the spectrum splitting since the loss due to a reduced carrier bandwidth is greater than the gain due to an improved SINR. In case of uplink, the situation is different. Within the heterogeneous deployment scenarios assumed in this thesis, uplink performance is quite often limited either by the UE transmission power or by the quality of the downlink control channels. For both, the spectrum splitting can in fact be beneficial.

- *Introduction of the uplink interference margin*. By assigning a higher received power target for the uplink power control within the low-power cells compared to the neighboring macro cells, impacts of the uplink inter-layer interference can be reduced. The size of this interference margin is shown to depend on the transmission power difference between the eNodeBs, density of the low-power cells, applied cell selection offset and the spectrum allocation. In general, the size of the most appropriate interference margin will be a trade-off between the improved performance of the low-power cell users, and the increased uplink interference towards the macro cells.

- *Backhaul limitation*. Femto eNodeBs are typically designed to use a residential broadband connection as a backhaul. As a result, the femto user performance can often be limited by the backhaul

instead of the air-interface. However, the overall downlink system performance will not be affected unless the maximum achievable backhaul throughput is close to the desired coverage requirement. The impact of the backhaul limitation on the uplink performance has not been evaluated in this thesis.

- *Access control.* Due to the required interference mitigation mechanisms, the performance of a heterogeneous CSG femto deployment is much worse than the performance of a similar heterogeneous OSG or hybrid mode femto deployment. The main reasons for the worse system performance are the considerably lower level of traffic offloading, worse performance of the femto users and the increased level of inter-layer interference towards the macro users.

- *Coverage-based deployment of low-power eNodeBs.* By deploying low-power eNodeBs in locations with poor macro cell coverage, the most power-limited users can be offloaded from the macro cell. This kind of deployment is beneficial for scenarios with a low eNodeB output power, low capacity requirement or high coverage requirement. Hence, for scenarios which are mostly power-limited. However, due to the fact that the overall traffic offloading can become lower, performance of the more capacity-limited scenarios can become worse.

- *Traffic-based deployment of low-power eNodeBs.* By deploying low-power eNodeBs in locations close to (or within) the most traffic-heavy areas, the amount of offloaded traffic can be maximized with the minimum amount of low-power eNodeBs. This kind of approach is particularly efficient for the heterogeneous femto deployments, where the low-power cells can be more easily targeted towards the traffic-heavy apartments, or the traffic-heavy subscribers.

## 8.3 Dimensioning example

In the previous sections, the downlink and the uplink have been evaluated separately. However, in case of network dimensioning, both links should typically be evaluated at the same time. Therefore, this section presents a simple dimensioning exercise, where the performance of the different network densification alternatives is compared for a few different levels of

**Table 8.5**. Required system capacity for the dimensioning example.

| Monthly subscriber traffic [GB/subs/month] | Downlink served area traffic [GB/h/km²] | Uplink served area traffic [GB/h/km²] |
|---|---|---|
| 10 | 56.25 | 18.75 |
| 20 | 112.5 | 37.5 |
| 30 | 168.75 | 56.25 |
| 40 | 225 | 75 |

**Table 8.6.** Required density of new sites in order to fulfill the downlink/uplink coverage and capacity requirements. The numbers defining the required site densities for the desired network operating points have been highlighted.

| Monthly subscriber traffic [GB/subs/month] | Densified macro | Heterogeneous micro | Heterogeneous OSG femto |
|---|---|---|---|
| 10 | 1.35 / **1.57** | **10.31** / 8.43 | 108.6 / **111.7** |
| 20 | **4.99** / 3.11 | **34.91** / 17.53 | **384.1** / 210.4 |
| 30 | **8.38** / 4.60 | **67.30** / 24.71 | **629.8** / 293.8 |
| 40 | **12.28** / 6.09 | - / 30.85 | **848.3** / 369.0 |

monthly subscriber traffic. For simplicity, the downlink and the uplink coverage requirements are set to 10 Mbps and 1 Mbps, respectively.

Based on (4.16) and assuming further that 75% of the subscriber traffic is consumed on downlink, the desired downlink and uplink capacity requirements can be calculated, as shown in Table 8.5. Taking also the assumed downlink and uplink coverage requirements into account, the required site densities can be obtained, based on the performance evaluation results presented in Chapter 5, Chapter 6 and Chapter 7. The results are listed in Table 8.6 for both the downlink and the uplink. It should be noted that the values in Table 8.6 indicate the required densities of new sites to be deployed on top of the baseline deployment.

As can be noticed, a larger number of new sites is needed to fulfill the downlink performance requirements compared to the uplink for almost all of the densified network deployments and assumed system capacities. In practice this means that if the baseline deployment is densified to fulfill the downlink performance requirements, the resulting uplink performance will in most of the cases exceed the desired uplink requirements.

# 9. Energy efficiency of the different network densification alternatives

In this chapter the performance of the different network densification alternatives is compared from the total network power consumption point of view. Hence, the most power-efficient deployment alternative is the one that can provide the desired coverage and capacity with the lowest level of total network power consumption, measured as kilowatts per square kilometer.

First, the assumed eNodeB power consumption model is introduced. Then, some general examples are provided, demonstrating how the total network power consumption behaves as a function of both the network load and the density of low-power sites. After that, the impact of both an increased micro eNodeB power and a targeted femto deployment on the total network power consumption are evaluated. Finally, the performance of a few different network densification alternatives is compared from the daily energy consumption point of view.

It should be noted that only the downlink is considered in this chapter. Furthermore, the power consumed by the UEs or by the core network is not taken into account when calculating the total network power consumption.

Some of the results presented in this chapter have already been published as part of papers [154]-[156].

## 9.1 LTE eNodeB power consumption model

The eNodeB power consumption model assumed in this thesis is based on the EARTH model described in [98]. The only difference is related to the carrier bandwidth: the EARTH model is defined for 10 MHz, while the deployment scenarios in this thesis assume typically a 20 MHz carrier bandwidth. Based on the analysis in [98], the increased carrier bandwidth is assumed to affect the power consumption of the RF transceiver and the baseband interface. For simplicity, it is assumed in this thesis that by

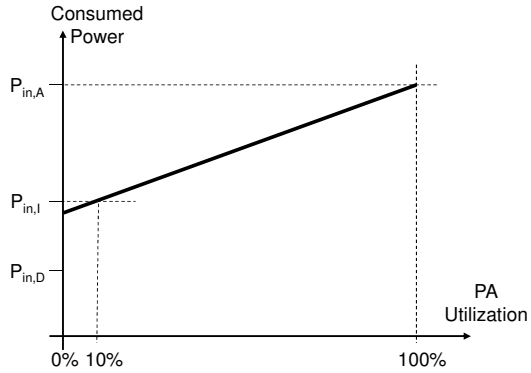


**Figure 9.1.** Assumed model for the eNodeB power consumption.

**Table 9.1.** Parameters for the eNodeB power consumption model.

| eNodeB type | $P_{eNB}$ [W] | $P_{in,A}$ [W] | $P_{in,I}$ [W] |
|---|---|---|---|
| Macro RRH | 40 | 336.3 | 238.4 |
| Micro | 1 | 152.4 | 129.3 |
| Femto | 0.1 | 16.6 | 14.4 |

doubling the carrier bandwidth, also the power consumption of those two components will be doubled.

The modeling in this thesis assumes further that an eNodeB is either in an active or an idle state. In case of an active state, eNodeB is scheduling a user with output power equal to the maximum eNodeB output power ($P_{eNB}$). In case of an idle state, only the minimum required downlink control signaling is transmitted, and the average output power is assumed to be equal to[12] 10% of $P_{eNB}$. From the power consumption point of view, this means that the average consumed power ($P_{in}$) is either equal to $P_{in,A}$ or $P_{in,I}$, as demonstrated in Figure 9.1. The assumed $P_{in,A}$ and $P_{in,I}$ values for the different eNodeB types are listed in Table 9.1. It should be noted that the values in Table 9.1 indicate the power consumption per cell. Hence, in case of a macro eNodeB with three sectors, the total eNodeB power consumption becomes equal to $3 \cdot P_{in,A}$ or $3 \cdot P_{in,I}$.

Looking at the values in Table 9.1, it becomes obvious that a cell is consuming a considerable amount of power even when no user data is being transmitted. In case of the low-power eNodeBs, the fixed power

[12] Two transmit antenna ports per cell are assumed. Furthermore, it is assumed that the CRSs are transmitted with 3 dB higher power than the other symbols. In addition to the CRS, also the PBCH and the PSS/SSS will be transmitted.

consumption ($P_{in,I}$) can be much larger than the variable power consumption ($P_{in,A} - P_{in,I}$). This suggests that there can be a high potential of reducing the total power consumption if sufficient ways to reduce the fixed power consumption can be found.

One simple way to reduce the fixed power consumption is to apply some form of *fast cell DTX* to the idle cells, as discussed in [92] and [99]. In [99] the following fast cell DTX modes have been defined:

- *Micro DTX*. Radio unit is turned off in time intervals less than 1 ms.
- *MBSFN-based DTX*. Radio unit is turned off in time intervals less than 10 ms. Radio frame consists of a combination of a micro DTX transmission configuration and MBSFN subframes.
- *Short DTX*. Radio unit is turned off in time intervals of 10 ms (but at least equal to 1 ms).
- *Long DTX*. Radio unit is turned off in time intervals of 10 ms or longer. However, the long DTX duration must not be so long that the UEs are not able to perform initial cell search and mobility measurements.

Micro DTX can be achieved by switching off the radio unit during the OFDM symbols in between CRS. Furthermore, with the help of MBSFN subframes even more time for micro DTX can be created. As estimated within [157], micro DTX without any MBSFN subframes would allow the radio to be in a low-power DTX mode up to 53% of the time, assuming that the cell is idle. Furthermore, if the maximum of six MBSFN subframes is configured, duration of the low-power DTX can be extended to 72% of the time. Unfortunately, an increased amount of micro DTX via an increased amount of MBSFN subframes can have also some negative consequences, both in terms of reduced cell capacity and degraded user throughput. Hence, it is of importance that fast switching between MBSFN configurations could be performed in an adaptive fashion. The adaptive mechanism would apply a larger density of MBSFN subframes at low-traffic scenarios, and react to changes in the traffic situation by reducing the number of MBSFN subframes when the traffic increases [92]. However, since the current LTE standard allows only a fairly infrequent adaptation of the MBSFN configuration, such fast schemes could be potential candidate features for future LTE releases.

An introduction of short DTX would require changes to the current version of the LTE standard, i.e. the standard should be changed to allow

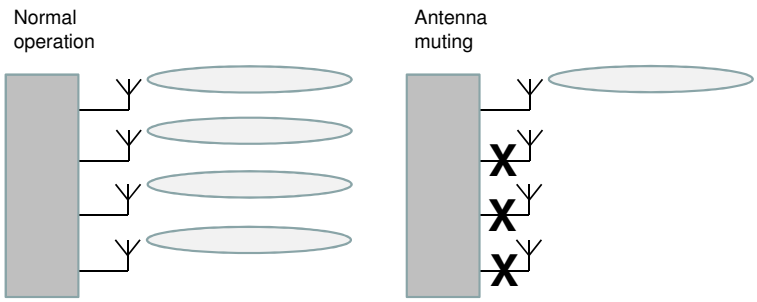


**Figure 9.2.** Description of the antenna muting scheme.

idle cells to avoid transmitting CRS, which are currently required for mobility measurements [99]. In case of long DTX, the basic idea is to avoid any downlink transmissions in a cell with no active terminals, except for intermittent periods of the signals necessary for close-by active terminals to find the cell. This can be especially useful in heterogeneous deployments, where macro cells overlay small low-power cells [99].

The cells can also be switched to a so-called *sleep mode*, when all the downlink transmissions are avoided for longer periods. In practice this means that the UEs will not be able to find cells that are in sleep mode. The sleeping cells can be re-activated for example periodically or based on the network load [158].

In addition to applying fast cell DTX or sleep mode, idle cells with multiple transmitter antennas can also decide to switch off transmitter chains to reduce the power consumption, see Figure 9.2. In case of this kind of *antenna muting* method one transmitter chain is kept active to ensure that the cell stays accessible for the close-by mobiles. All the other transmitter chains can then be activated and de-activated based on the actual traffic load, see for example the discussion and results in [99] and in [159].

The analysis presented in this chapter does not assume any specific type of fast cell DTX or antenna muting method. Instead, it is assumed that the average power consumption during the idle state is equal to $P_{in,D}$, see Figure 9.1, where

$$P_{in,D} = \delta P_{in,I} \quad , 0 \leq \delta \leq 1 \tag{9.1}$$

The cell DTX parameter $\delta$ takes into account both the fraction of time the idle cell can be in low-power DTX state, and the power consumed during the low-power DTX state. In general, the smaller the value of $\delta$, the more aggressive level of fast cell DTX will be assumed.

Taking the above into account, the total power consumption of a heterogeneous network deployment can be calculated as

$$\begin{aligned} P_{in}^{total} &= P_{in}^{macro} + P_{in}^{low-power} \\ &= \sum_{m=1}^{M} \left(u_m P_{in,A,m} + (1-u_m) P_{in,D,m}\right) + \\ &\quad \sum_{l=1}^{L} \left(u_l P_{in,A,l} + (1-u_l) P_{in,D,l}\right) \\ &= \sum_{m=1}^{M} \left(u_m P_{in,A,m} + (1-u_m) \delta_m P_{in,I,m}\right) + \\ &\quad \sum_{l=1}^{L} \left(u_l P_{in,A,l} + (1-u_l) \delta_l P_{in,I,l}\right) \end{aligned} \tag{9.2}$$

where $M$ and $L$ are the total number of macro and low-power cells, respectively. Furthermore, $u_m$ and $u_l$ indicate the average utilization of macro cell $m$ and low-power cell $l$. Assuming that

$$\begin{aligned} P_{in,A,m} &= P_{in,A}^{macro} \quad \forall m \\ P_{in,I,m} &= P_{in,I}^{macro} \quad \forall m \\ P_{in,A,l} &= P_{in,A}^{LPN} \quad \forall l \\ P_{in,I,l} &= P_{in,I}^{LPN} \quad \forall l \end{aligned} \tag{9.3}$$

and further that all idle cells within a cell layer apply the same amount of fast cell DTX, the expression for the total network power consumption can be written as

$$\begin{aligned} P_{in}^{total} = M \left( \left(P_{in,A}^{macro} - \delta_{macro} P_{in,I}^{macro}\right) \bar{u}_{macro} + \delta_{macro} P_{in,I}^{macro} \right) + \\ L \left( \left(P_{in,A}^{LPN} - \delta_{LPN} P_{in,I}^{LPN}\right) \bar{u}_{LPN} + \delta_{LPN} P_{in,I}^{LPN} \right) \end{aligned} \tag{9.4}$$

In (9.4) the average cell utilizations for the macro and the low-power cell layer are defined as

$$\bar{u}_{macro} = \frac{\sum_{m=1}^{M} u_m}{M} \tag{9.5}$$

$$\bar{u}_{LPN} = \frac{\sum_{l=1}^{L} u_l}{L} \tag{9.6}$$

The fact that an aggressive fast cell DTX can potentially have a negative impact on the observed user performance has been ignored in this thesis. Hence, the values of $\bar{u}_{macro}$ and $\bar{u}_{LPN}$ are not assumed to depend on the values of $\delta_{macro}$ and $\delta_{LPN}$, respectively.

In addition to the total network power consumption ($P_{in}^{total}$) another interesting performance indicator is the total network power consumption that is assumed to generate operational expenses for the operator ($P_{in}^{OPEX}$). Since macro and micro eNodeBs are assumed to be deployed, managed and owned by the operator, $P_{in}^{OPEX}$ can be assumed to be equal to $P_{in}^{total}$. Femto eNodeBs are assumed to be residential, which would also mean that the costs related to the energy consumed by the femto eNodeBs are paid by the subscribers. Therefore, $P_{in}^{OPEX}$ is in this thesis assumed to be equal to $P_{in}^{macro}$ for the heterogeneous femto deployments.

## 9.2 General examples

This section provides some examples on how the total network power consumption behaves as a function of a) network load, and b) density of low-power nodes. The impact of network load is demonstrated for the baseline deployment, whereas the impact of the density of low-power nodes is evaluated for the heterogeneous micro deployment. Furthermore, in case of the network densification, two different scenarios are evaluated. In the first one the micro site density is increased under the assumption of a fixed level of offered area traffic, while in the second one the micro layer is densified to fulfill the desired coverage requirement under the assumption of an increasing capacity requirement.

### 9.2.1 Impact of network load

The negative impact of the increasing network load on the user performance was discussed in Section 5.1.1. Here, the impact of network load on the total power consumption is demonstrated. Based on (9.4), the total power consumption of the baseline deployment can be calculated as

$$P_{in}^{total} = M\left(\left(P_{in,A}^{macro} - \delta_{macro}P_{in,I}^{macro}\right)\bar{u}_{macro} + \delta_{macro}P_{in,I}^{macro}\right) \qquad (9.7)$$

For the baseline deployment with ISD equal to 500 m, macro cell density $M$ becomes equal to 13.9 cells/km$^2$. The values for $P_{in,A}$ and $P_{in,I}$ are taken from Table 9.1, and the values for $\bar{u}_{macro}$ are obtained from Figure 5.1. Finally, the value of $\delta_{macro}$ is assumed to be equal to 1 (0% fast cell DTX), 0.8 (20% DTX), 0.6 (40% DTX), 0.4 (60% DTX) or 0.2 (80% DTX).

The curves in Figure 9.3 present the $P_{in}^{total}$ as a function of the served area traffic for different levels of fast cell DTX. As can be noticed, with an

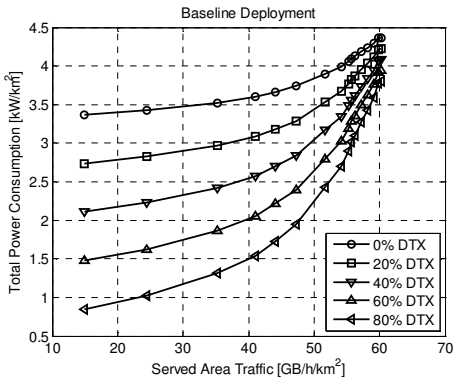


**Figure 9.3.** Total power consumption of the baseline deployment as a function of the served area traffic, assuming different levels of fast cell DTX.

increasing network load also the $P_{in}^{total}$ increases. However, with a low level of fast cell DTX the dependency of $P_{in}^{total}$ on the network load is quite modest. When the level of fast cell DTX is increased, the curves become much steeper. The largest gain of fast cell DTX can be observed at low network load, since there the probability of having empty subframes is higher. Together with an increasing network load also the average cell utilization increases, reducing the probability of having empty subframes. Therefore, also the achievable cell DTX gains are reduced. In all, the results in Figure 9.3 are very similar to the results published in [92] and [160].

### 9.2.2 Impact of network densification. Fixed level of offered area traffic

This section discusses the impact of network densification on $P_{in}^{total}$, when the offered area traffic is assumed to be fixed at 60 GB/h/km². The evaluation is performed for the heterogeneous micro deployment.

Total network power consumption is calculated as a sum of the power consumed by the macro cell layer and the power consumed by the low-power (micro) cell layer, see (9.4). The analysis assumes that the same amount of fast cell DTX is applied to all cells, i.e. $\delta_{macro} = \delta_{LPN} = \delta$. Furthermore, $M$ is equal to 13.9 cells/km², while the value of $L$ is increased from 0 to 89.7 cells/km² (see Table 4.6). The values of $P_{in,A}$ and $P_{in,I}$ are read from Table 9.1, and the values of $\bar{u}_{macro}$ and $\bar{u}_{LPN}$ are obtained from Figure 6.2. Similar to the previous example, cell DTX parameter $\delta$ is assumed to be equal to {0.2, 0.4, 0.6, 0.8, 1}.

Results for $P_{in}^{macro}$ and $P_{in}^{low-power}$ are shown in Figure 9.4, and the results for $P_{in}^{total}$ are shown in Figure 9.5. The results in Figure 9.4 demonstrate

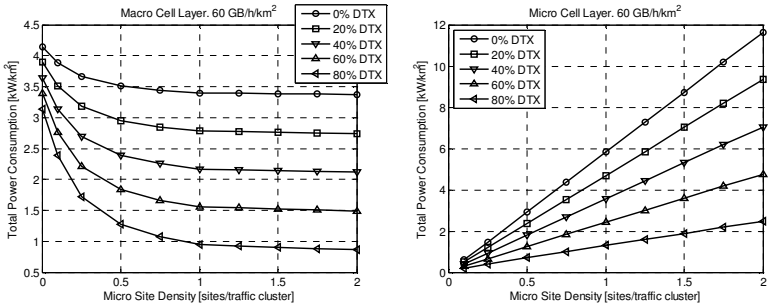


**Figure 9.4.** Total power consumption within the macro cell layer and within the micro cell layer as a function of the micro site density.

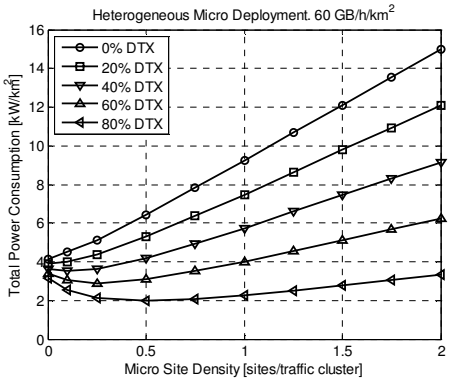


**Figure 9.5.** Total network power consumption as a function of the micro site density.

how the increased traffic offloading and the reduced cell utilization lead to a reduced $P_{in}^{macro}$. It is also very evident that the power savings can be further enhanced with the help of fast cell DTX. As a result of the reduced average macro cell utilization, the cell DTX gain increases together with the increasing micro site density. In case of the micro cell layer, the price of an increased micro site density is an increased $P_{in}^{low-power}$, even though the average micro cell utilization is reduced. Since the fixed power consumption of a micro eNodeB is much larger than the variable power consumption, $P_{in}^{low-power}$ increases almost linearly as a function of the micro site density. Fast cell DTX can reduce the steepness of the slope, but it is not able to change the overall behavior.

When it comes to $P_{in}^{total}$ as a function of the micro site density (Figure 9.5), a clear dependency on the assumed level of fast cell DTX can be seen. When the level of fast cell DTX is low, the reduced $P_{in}^{macro}$ is not able to compensate for the increased $P_{in}^{low-power}$, and hence, the total network power consumption increases as a function of the micro site density. Basically, this means that if the desire is to fulfill a certain coverage

requirement, the most power-efficient deployment is the one that minimizes the amount of micro sites. The situation becomes slightly different with a high level of fast cell DTX. Taking the scenario with 60% fast cell DTX as an example, the most power-efficient deployment to serve area traffic equal to 60 GB/h/km² seems to be the one with an average of 0.25 micro sites per traffic cluster. Based on the evaluation results in Section 6.1, that kind of deployment is able to satisfy a coverage requirement up to 5 Mbps. So, for higher coverage requirements it is still valid to aim for deployments that minimize the required density of micro sites.

The results shown above assume a level of offered area traffic, which is close to the maximum capacity of the baseline deployment. However, evaluations for a few other levels of network load indicate a similar behavior. Hence, it seems that at least for the heterogeneous micro deployment the most power-efficient way to provide the desired coverage and capacity is to aim for a deployment that satisfies the coverage and capacity requirements with the minimum amount of micro sites, unless a very high level of fast cell DTX is assumed. For such extreme scenarios, it could be slightly more power-efficient to overdimension the network deployment. This topic will be discussed further in Section 9.3.

### 9.2.3 Impact of network densification. Increasing level of offered area traffic

This section evaluates how the $P_{in}^{total}$ (during a peak hour) will increase as the baseline network is densified to be able to serve the increased area traffic, while still fulfilling the desired coverage requirement. In this example the coverage requirement is set to 10 Mbps, and the capacity requirement is assumed to increase from 10 GB/h/km² to 147 GB/h/km². The required density of micro sites (parameter $L$), as well as the average cell utilizations for both the baseline macro cells ($\bar{u}_{macro}$) and the low-power micro cells ($\bar{u}_{LPN}$) are shown in Figure 9.6. As can be seen, the baseline network, with macro cell density $M$ equal to 13.9 cells/km², is able to serve the area traffic up to a level of 39 GB/h/km², after which the network has to be densified by deploying micro sites within the traffic clusters. Finally, at the level of 147 GB/h/km², all traffic clusters have received a micro site.

Results for $P_{in}^{total}$ as a function of the capacity requirement are shown in Figure 9.7, assuming a few different levels of fast cell DTX. For simplicity, it has been assumed that the same amount of fast cell DTX has been applied to all cells, i.e. $\delta_{macro} = \delta_{LPN} = \delta$. Furthermore, the values of $\delta$, $P_{in,A}$ and $P_{in,I}$ are assumed to be fixed for all levels of the network densification, i.e.

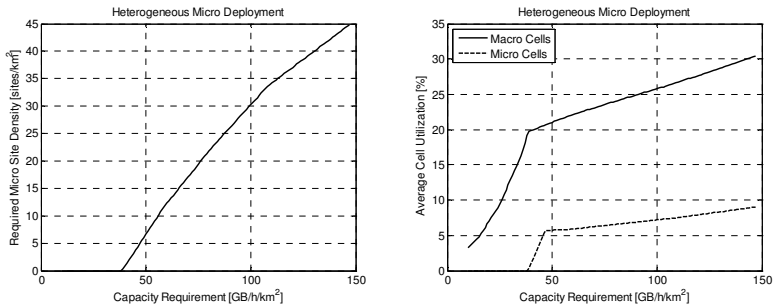


**Figure 9.6.** Required micro site density and the corresponding average cell utilizations to fulfill both the coverage requirement of 10 Mbps, and the desired capacity requirement as indicated by the x-axis.

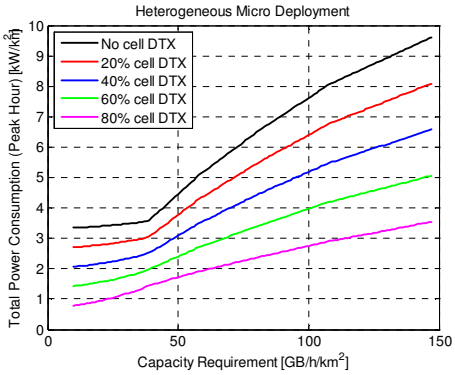


**Figure 9.7.** Total network power consumption as a function of the capacity requirement.

the impact of gradual network modernization, as discussed for example in [96], has not been taken into account. As can be seen, the total network power consumption increases considerably together with an increasing capacity requirement, i.e. when new micro sites are added into the system. By introducing fast cell DTX, the total network power consumption can be reduced. However, in order to compensate for the loss due to an increased number of sites, introduction of advanced energy saving methods resulting in high levels of fast cell DTX are required.

Results for the total network power consumption of the different network densification alternatives (*Dense*/*Micro*/*Femto*) are summarized in Table 9.2, assuming the desired downlink coverage and capacity requirements. The values have been calculated based on the input from Chapter 5-Chapter 7, and assuming the eNodeB power consumption values listed in Table 9.1. Furthermore, no fast cell DTX has been assumed. As can be seen, the densified macro deployment is clearly the most power-efficient densification alternative, while the heterogeneous femto deployment is the least power-efficient densification alternative.

**Table 9.2**. Total network power consumption (kW/km²) for the different network deployment alternatives (Dense/Micro/Femto).

| Coverage Req | Capacity Requirement | | | |
|---|---|---|---|---|
| | 50 GB/h/km² | 100 GB/h/km² | 150 GB/h/km² | 200 GB/h/km² |
| 4 Mbps | 3.9/3.9/3.9 | 6.4/7.1/7.6 | 8.7/9.2/10.6 | 11.1/13.7/13.3 |
| 10 Mbps | 4.3/4.5/4.7 | 6.9/7.6/8.4 | 9.3/10.1/11.7 | 11.9/ - /14.6 |
| 20 Mbps | 5.3/5.7/6.3 | 8.1/8.8/10.5 | 11.0/14.9/14.0 | 14.1/ - /17.1 |
| 30 Mbps | 6.5/7.3/8.5 | 9.8/13.0/13.3 | 13.2/ - /17.1 | 16.9/ - /20.9 |

## 9.3 Increased micro eNodeB output power vs. targeted femto eNodeB deployment

This section compares the different network densification alternatives from the total network power consumption point of view, taking into account both the impact of the micro eNodeB output power (discussed in Section 6.3) and the impact of a targeted OSG femto eNodeB deployment (discussed in Section 7.4).

The assumed $P_{in,A}$ and $P_{in,I}$ values are listed in Table 9.3. The values have been derived from the EARTH power consumption model [98] in a similar way as for the previous sections. Furthermore, it has been assumed that the increased micro eNodeB output power does not have any impact on the efficiency of the power amplifier or on the power consumption of the RF transceiver and the baseband interface. Finally, it has been assumed that the same level of fast cell DTX is applied to all cells, i.e. $\delta_{macro} = \delta_{LPN} = \delta$.

The different network densification alternatives have been dimensioned to fulfill both a coverage requirement equal to 10 Mbps and a capacity requirement equal to 100 GB/h/km². Based on the system-level evaluations in Chapter 5, Chapter 6 and Chapter 7, the required cell densities to fulfill both requirements, together with the corresponding average cell utilizations, are listed in Table 9.4. The values indicate clearly that an increased $P_{micro}$ reduces the required micro cell density to reach the desired coverage and capacity requirements. Similarly, targeting the femto eNodeB deployment towards the traffic-heavy subscribers (*Femto HVYC*) is much more efficient compared to the random selection of femto apartments (*Femto RND*). When it comes to the results for the average cell utilization, an increased $P_{micro}$ increases the size of the micro cell, and hence, the average micro cell utilization. At the same time the average macro cell

**Table 9.3.** Parameters for the eNodeB power consumption model.

| eNodeB type | $P_{eNB}$ [W] | $P_{in,A}$ [W] | $P_{in,I}$ [W] |
|---|---|---|---|
| Macro RRH | 40 | 336.3 | 238.4 |
| Micro 1 W | 1 | 152.4 | 129.3 |
| Micro 2 W | 2 | 157.5 | 132.6 |
| Micro 4 W | 4 | 167.8 | 139.0 |
| Micro 10 W | 10 | 198.9 | 158.7 |
| Femto | 0.1 | 16.6 | 14.4 |

**Table 9.4.** Required cell densities and average cell utilizations to fulfill the desired coverage and capacity requirement.

| Network Densification Alternative | Cell Density [cells/km²] | | Average Cell Utilization [%] | |
|---|---|---|---|---|
| | $M$ | $L$ | $\bar{u}_{macro}$ | $\bar{u}_{LPN}$ |
| Dense | 26.9 | - | 22.5 | - |
| Micro 1 W | 13.9 | 30.3 | 25.8 | 7.2 |
| Micro 2 W | 13.9 | 26.4 | 25.6 | 8.1 |
| Micro 4 W | 13.9 | 23.7 | 24.8 | 9.0 |
| Micro 10 W | 13.9 | 20.0 | 24.6 | 10.8 |
| Femto RND | 13.9 | 329.6 | 27.1 | 0.63 |
| Femto HVYC | 13.9 | 162.9 | 28.0 | 0.89 |

utilization is reduced as a result of the increased traffic offloading. Furthermore, when the femto eNodeB deployment is targeted towards the traffic-heavy subscribers, the femto cells have a higher probability of being in an active state compared to the random deployment of femto eNodeBs.

Results for the densified macro deployment (*Dense Macro*), heterogeneous micro deployment with 1 W eNodeB output power (*Micro 1W*), heterogeneous femto deployment with a random selection of femto apartments (*Femto RND*), and heterogeneous femto deployment with a traffic-based selection of femto apartments (*Femto HVYC*) are visualized in Figure 9.8. Furthermore, results for all the evaluated deployments are summarized in Table 9.5, where the values are expressed as differences compared to the densified macro deployment.

The results indicate that with a low level of fast cell DTX, densified macro deployment is more power-efficient than the heterogeneous micro

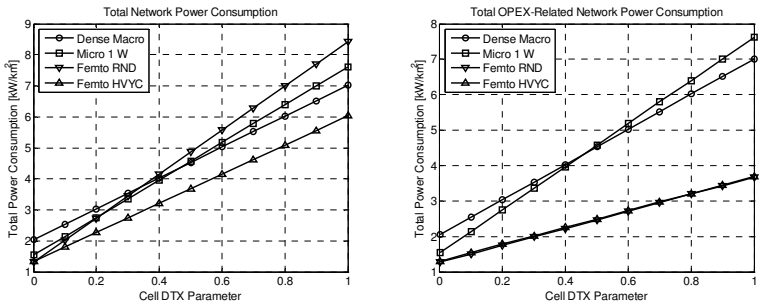


**Figure 9.8.** Total power consumption and the total OPEX-related power consumption as a function of the cell DTX parameter for a few different network densification alternatives.

**Table 9.5.** Total power consumption of the evaluated heterogeneous deployments relative to the total power consumption of the densified macro deployment.

| Network Densification Alternative | Cell DTX Parameter | | | | |
|---|---|---|---|---|---|
| | 0.2 | 0.4 | 0.6 | 0.8 | 1 |
| Micro 1 W | -9% | -2% | +3% | +6% | +9% |
| Micro 2 W | -12% | -6% | -2% | +0.8% | +3% |
| Micro 4 W | -14% | -8% | -4% | -2% | -0.3% |
| Micro 10 W | -13% | -8% | -5% | -3% | -2% |
| Femto RND<br>OPEX | -10%<br>-42% | +3%<br>-45% | +11%<br>-46% | +16%<br>-47% | +20%<br>-48% |
| Femto HVYC<br>OPEX | -25%<br>-41% | -20%<br>-44% | -17%<br>-46% | -15%<br>-47% | -14%<br>-47% |

deployments with a low $P_{micro}$. At the same time, the heterogeneous femto deployment with a random selection of femto apartments is the most power-inefficient alternative. Power-efficiency of the heterogeneous deployments can be improved either by reducing the required density of low-power cells, or by reducing the power consumption of idle eNodeBs. The first can be obtained by increasing the micro eNodeB output power or by targeting the femto deployment towards the most traffic-heavy subscribers. The latter can be achieved by increasing the level of fast cell DTX.

Furthermore, the results demonstrate that when the level of fast cell DTX is increased, all the evaluated heterogeneous network deployments become more power-efficient than the densified macro deployment. There are two main reasons why the heterogeneous deployments benefit more from fast cell DTX than the densified macro deployment: a) average utilization of the low-power cells is much lower, and b) in case of low-power eNodeBs, the

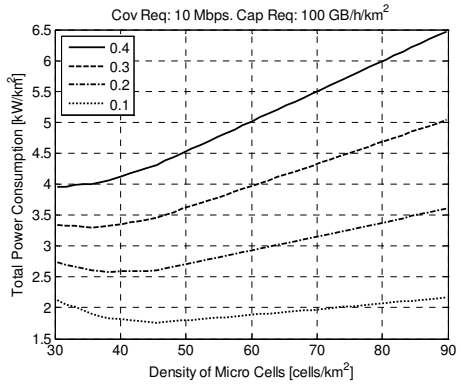


**Figure 9.9.** Total power consumption as a function of the micro cell density, assuming different values of the cell DTX parameter.

fixed power consumption is much larger than the variable power consumption.

Finally, the results indicate that the heterogeneous femto deployments require by far the lowest $P_{in}^{OPEX}$ to fulfill the desired coverage and capacity requirements. This is due to the assumption that the costs related to the total network power consumption are shared between the operator and the subscribers. For example, compared to the densified macro deployment, the OPEX-related power consumption of the heterogeneous femto deployment is 41-48% smaller, depending on the assumed value of the cell DTX parameter.

All the evaluations presented above have assumed that the most power-efficient deployment is the one that aims at minimizing the required cell density in order to achieve the desired network performance. However, as discussed in Section 9.2.2, and demonstrated by the results in Figure 9.9, this is not necessarily the case for high levels of fast cell DTX. The curves in Figure 9.9 present the $P_{in}^{total}$ as a function of the density of micro cells with 1 W eNodeB output power, assuming four different values of the cell DTX parameter $\delta$. Furthermore, it is assumed that the cell-edge packet bit rate is equal to 10 Mbps or more, and that the served area traffic is equal to 100 GB/h/km². The lowest density of micro cells that is able to fulfill both requirements is approximately equal to 30 micro cells/km². As can be seen, for $\delta = 0.4$ that deployment is also the one that results in the lowest total network power consumption. For $\delta = 0.3$, $\delta = 0.2$ and $\delta = 0.1$, however, it would be more power-efficient to overdimension the network deployment. The reason for this is that with the aggressive level of fast cell DTX, the cost of the fixed power consumption becomes sufficiently low compared to the cost of the variable power consumption. By overdimensioning the network, the average macro and micro cell utilization become lower, reducing the

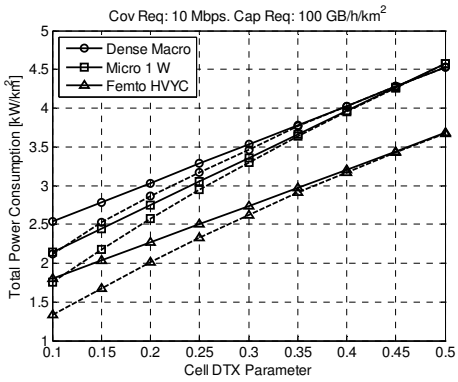


**Figure 9.10.** Total network power consumption as a function of the cell DTX parameter for the most site-efficient (solid curves) and the most power-efficient approach (dashed curves).

**Table 9.6.** Comparison between the most site-efficient and the most power-efficient deployment, assuming that the cell DTX parameter is equal to 0.1.

| Network Densification Alternative | Site [cells/km²] | Power [cells/km²] | $\Delta cell$ [%] | $\Delta P_{in}^{total}$ [%] |
|---|---|---|---|---|
| Dense Macro | $M$ = 26.9 | $M$ = 41.2 | +53 | -16 |
| Micro 1 W | $L$ = 30.3 | $L$ = 44.9 | +48 | -18 |
| Femto HVYC | $L$ = 162.9 | $L$ = 271.2 | +66 | -26 |

level of the variable power consumption. As long as the gains achieved by reducing the average cell utilization are larger than the losses related to the increased density of cells, $P_{in}^{total}$ becomes lower.

Figure 9.10 presents a comparison between the most site-efficient and the most power-efficient deployments for three different network densification alternatives. Solid curves represent the results for the approach aiming to minimize the number of sites, while the dashed curves represent the results for the approach aiming to minimize the total network power consumption. As can be noticed, both the densified macro deployment and the evaluated heterogeneous network deployments will benefit from overdimensioning, if the cell DTX parameter is smaller than 0.4-0.5. Taking the case with $\delta = 0.1$ as an example, the results listed in Table 9.6 can be obtained. The results indicate that network overdimensioning can lead to 16-26% lower $P_{in}^{total}$, but with the cost of a much larger number of sites to be deployed. Thus, in the end the required overdimensioning might not be feasible from the total network cost point of view. However, the situation becomes different for scenarios, where idle cells are switched off to save energy. There, the question is whether it is more beneficial to switch off all cells that

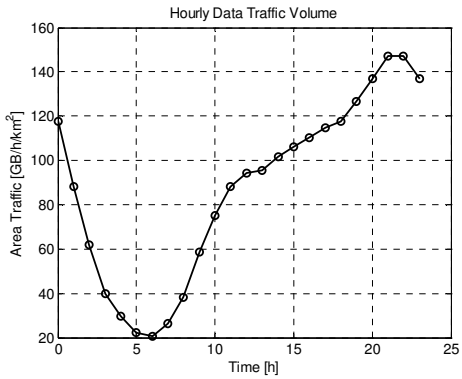


**Figure 9.11.** Assumed daily variation of the hourly area traffic volume.

are not needed to satisfy the coverage and capacity needs, or would it be better to keep some of the cells operational. This question will be discussed more in the next section.

## 9.4 Comparison based on the daily energy consumption

Previous sections have compared the total power consumption of different network densification alternatives for a few different network operating points. This section compares the performance of the different network densification alternatives from the daily energy consumption point of view.

Similar to the traditional voice traffic, also the hourly data volumes will vary during the day. The evaluation presented in this section is based on the typical daily variation in Europe, as given in [98]. In the assumed model, see Figure 9.11, the daily maximum is approximately 7 times as high as the daily minimum. The absolute hourly data volumes are selected so that the peak traffic, 147 GB/h/km$^2$, can be served with a heterogeneous micro deployment with one micro site per traffic cluster, while at the same time fulfilling the coverage requirement equal to 10 Mbps.

The performance of three different network adaptation methods is evaluated in the following sub-sections:

- *Fixed deployment*. In case of a fixed network deployment, the density of sites is dimensioned so that the network is able to serve the peak hour traffic with acceptable user quality. During the periods of lower traffic volumes, none of the cells are switched off, which means that the available network capacity is overdimensioned, and the observed user performance exceeds the

minimum requirements. Energy-efficiency can be enhanced by applying fast cell DTX to the idle cells.

- *Variable deployment*. In case of a variable network deployment, the density of operational cells is adjusted to satisfy the hourly traffic volume [152]. In practice this means that when the required network capacity is reduced, a number of cells are switched off to avoid network overdimensioning, while still fulfilling the desired coverage requirement. In addition to off-switching, fast cell DTX can be applied to operational, but idle, cells.

- *Sleep mode deployment*. Sleep mode deployment is a mixture of the fixed and the variable deployment. The difference compared to the variable deployment is that the cells are not switched off entirely, but certain parts of the eNodeBs are left active to enable the possibility to wake up the cells when needed. For example, the eNodeBs in *sleep mode* could still be monitoring the levels of the received uplink power to estimate the average uplink load level and/or whether there are any active mobiles close-by.

The evaluations in this section are based on the assumption that the baseline network is able to provide basic coverage throughout the system area, and that the network densification is required to enhance the network capacity. Therefore, the cells that have been deployed on top of the baseline deployment are labeled as *capacity cells*.

A few simplifications are made: In order to secure a certain level of basic coverage, only the capacity cells are seen as candidates for the off-switching and the sleep mode schemes. Furthermore, when a cell has been switched off, the power consumption of that cell is assumed to be equal to zero. Finally, in case of the sleep mode deployment, an ideal activation and deactivation of capacity cells based on the existence of close-by UEs is assumed. In all, since the evaluations do not consider any dynamic algorithms to utilize the different energy saving mechanisms, the results presented in this section should be interpreted as the technology potential of the variable and the sleep mode deployments.

Taking the above into account, the total network power consumption as a function of time can be calculated as

$$P_{in}^{total}(t) = P_{in}^{bln}(t) + P_{in}^{cap}(t) \tag{9.8}$$

The total power consumption for the baseline deployment (*bln*), with cell density equal to 13.9 cells/km$^2$, is calculated as

**Table 9.7.** Assumed density of the capacity cells and the observed level of traffic offloading for the fixed deployment.

| Network Densification Alternative | Density of capacity cells [cells/km²] | Traffic Offloading [%] |
|---|---|---|
| Dense Macro | 21.3 | 61 |
| Micro 1 W | 44.9 | 64 |
| Femto RND | 543.7 | 63 |
| Femto HVYC | 259.3 | 64 |

$$P_{in}^{bln}(t) = 13.9 \cdot \left( \left( P_{in,A}^{macro} - \delta_{bln} P_{in,I}^{macro} \right) \bar{u}_{bln}(t) + \delta_{bln} P_{in,I}^{macro} \right) \tag{9.9}$$

Furthermore, the total power consumption of the capacity cells, with cell density equal to $C(t)$, is calculated as

$$P_{in}^{cap}(t) = C(t) \left( \left( P_{in,A}^{cap} - \delta_{cap} P_{in,I}^{cap} \right) \bar{u}_{cap}(t) + \delta_{cap} P_{in,I}^{cap} \right) \tag{9.10}$$

The values of $P_{in,A}$ and $P_{in,I}$ can be read from Table 9.1. The values for the other parameters will depend on the assumed network adaptation method.

### 9.4.1 Performance of the fixed deployment

In case of fixed deployment, the number of operational cells is kept intact even though the required network capacity is varying. The evaluated network deployments have been dimensioned so that during the peak hour the observed cell-edge packet bit rate fulfills the coverage requirement of 10 Mbps. The corresponding cell densities are listed in Table 9.7.

Since all the cells are operational also during the low-traffic hours, the available network capacity is overdimensioned, and the user performance will exceed the minimum requirement with a clear margin. This is demonstrated in Figure 9.12, where the observed cell-edge and average packet bit rates are presented as a function of time. Furthermore, the results for the average macro and low-power cell utilization are shown in Figure 9.13. As can be seen, the different deployments offer very similar cell-edge user performances for all the other time periods except the hours with the lowest level of traffic volume. During the low-traffic hours, the level of inter-cell interference is very low and hence, the system is power-limited. As a result, the worst users can typically be found in locations with

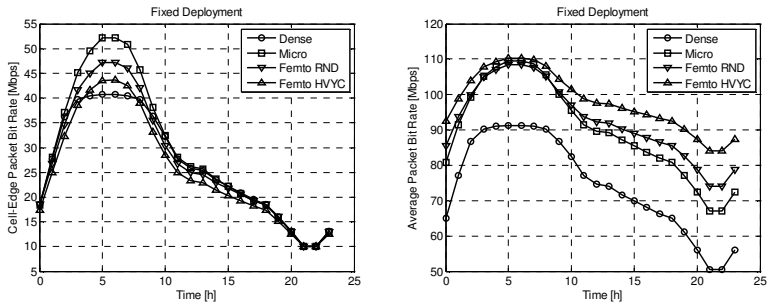


**Figure 9.12.** Cell-edge and average packet bit rate as a function of time.

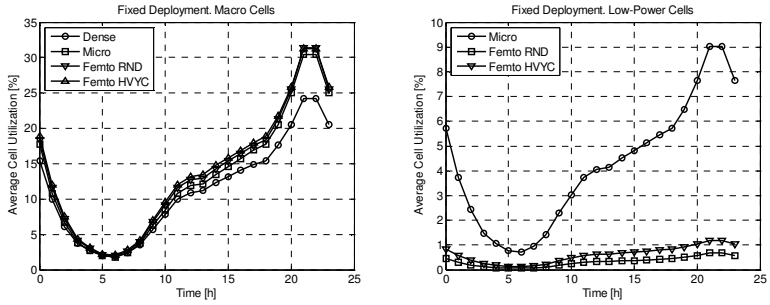


**Figure 9.13.** Average macro and low-power cell utilization as a function of time.

the highest coupling loss towards the serving eNodeB. Since the heterogeneous deployments are efficient in offloading the indoor users, the cell-edge performance becomes better than in case of the densified macro deployment. Furthermore, as discussed in Section 8.1.1, the differences in the average user performance can be explained by the fact that the low-power eNodeBs are able to provide the users considerably better average performance compared to the macro eNodeBs.

As indicated by the curves in Figure 9.13, the average cell utilizations will vary a lot during the day, in particular in case of the macro cells. During the hours with the lowest traffic volume the average macro cell utilization is around 2%, while it is equal to 24-31% during the peak traffic hours. Furthermore, the average macro cell utilization becomes somewhat higher for the heterogeneous deployments compared to the densified macro deployment. Based on the discussion in Chapter 8, the increased macro cell utilization is caused by both the more focused offloading of the indoor users, and the aim to offload as much traffic as possible with as few low-power sites as possible.

Next step is to compare the network densification alternatives from the total network power consumption point of view. The required input values can be found in Table 9.7 (parameter $C(t)$) and in Figure 9.13 ($\bar{u}_{bln}(t)$ and

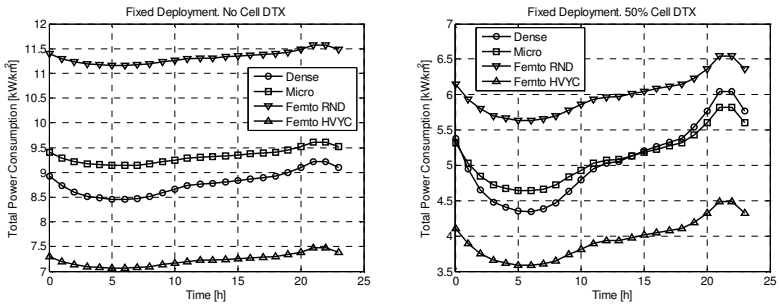


**Figure 9.14.** Total power consumption as a function of time without cell DTX and with 50% cell DTX.

$\bar{u}_{cap}(t)$). Finally, the evaluations are performed for two different values of the cell DTX parameter: $\delta = 1$ (*No Cell DTX*) and $\delta = 0.5$ (*50% Cell DTX*). It should be noted that the same level of fast cell DTX is assumed for all cells, i.e. $\delta_{bln} = \delta_{cap} = \delta$.

Results for $P_{in}^{total}(t)$ are presented in Figure 9.14. Looking at the curves, a few observations can be made. Firstly, the total network power consumption shows only a minor dependency on the network load when no fast cell DTX is applied. When fast cell DTX is introduced, the overall power consumption becomes lower, and it becomes also load-dependent. If $\delta = 0.5$, the total network power consumption is almost halved for the low-traffic hours. This is related to the fact that in 98-99% of the time the cells are in idle state. The gain is reduced for the hours with a higher network load, but even for the peak traffic hour the total network power consumption becomes 34-43% lower than without fast cell DTX. The second observation is that the heterogeneous deployments result in a higher total network power consumption compared to the densified macro deployment, which is in line with the findings in Section 9.3. The difference is reduced when the level of fast cell DTX is increased, and/or with the help of a targeted deployment of femto cells to increase the traffic offloading. Furthermore, the difference decreases together with an increasing network load.

Results for the daily energy consumption are presented in Figure 9.15. The daily energy consumption is obtained by calculating a sum over the hourly power consumption values shown in Figure 9.14. As demonstrated by the results, introduction of fast cell DTX can lead to considerable savings in the daily energy consumption. For example, with 50% fast cell DTX the daily energy consumption becomes 42-47% lower than without fast cell DTX. Furthermore, the results indicate that *Femto HVYC* is the most energy-efficient, and *Femto RND* is the most energy-inefficient deployment.

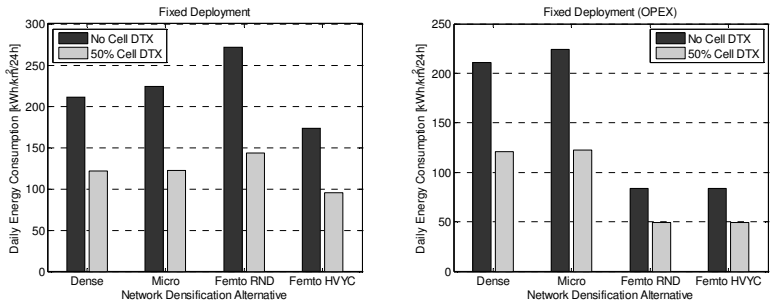


**Figure 9.15.** Daily energy consumption with the fixed deployment.

From the OPEX-related energy consumption point of view, the evaluated heterogeneous femto deployments consume approximately 60% less energy than the densified macro, and 62% less energy than the heterogeneous micro deployment. With 50% fast cell DTX the differences become marginally smaller.

### 9.4.2 Performance of the variable deployment

As discussed in the previous section, capacity of the fixed network deployment is overdimensioned during the low-traffic hours, which offers the possibility to switch off cells without sacrificing the desired user performance. However, since the process of switching cells on and off cannot in practice be done instantaneously, the decisions should be based on a more long-term estimate of the network performance, see for example the discussion in [161] and [162].

Variable deployment is evaluated by searching for the lowest density of capacity cells, which can serve the required hourly traffic volume while still fulfilling the coverage requirement of 10 Mbps. The output of the system level evaluations consists of $C(t)$, $\bar{u}_{bln}(t)$ and $\bar{u}_{cap}(t)$. Similar to the fixed deployment, it is assumed that $\delta_{bln} = \delta_{cap} = 1$ (*No Cell DTX*) or $\delta_{bln} = \delta_{cap} = 0.5$ (*50% Cell DTX*).

The variable density of operational capacity cells (i.e. the value of parameter $C(t)$) is illustrated in Figure 9.16. During the peak hour, the density of operational cells is the same as for the fixed deployment, see Table 9.7. However, as soon as the required network capacity becomes lower, the density of operational cells is adjusted by switching off capacity cells. Finally, during the hours with the lowest network load, all the capacity cells have been switched off, and the required network coverage and capacity is provided by the baseline deployment.

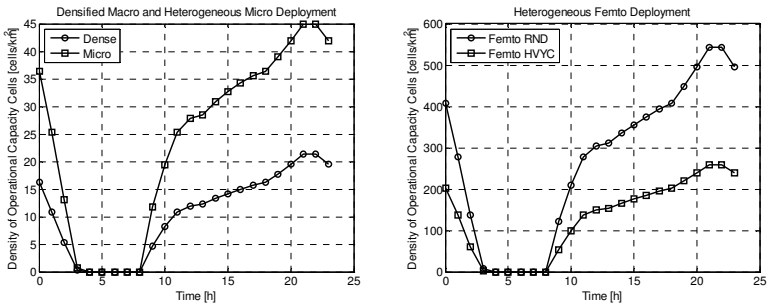


**Figure 9.16.** Density of the operational capacity cells as a function of time for the different network densification alternatives.

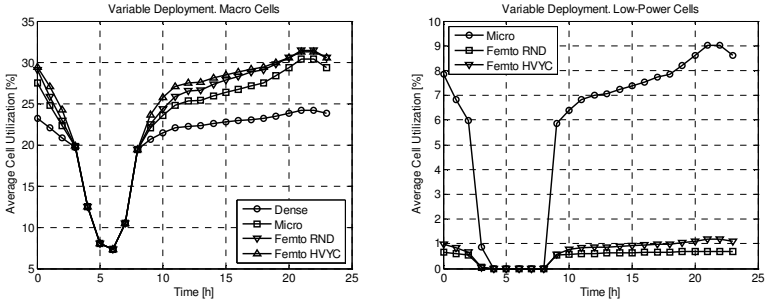


**Figure 9.17.** Average macro and low-power cell utilization as a function of time.

Results for the average macro and low-power cell utilization are presented in Figure 9.17. If the curves are compared to the corresponding results for the fixed deployment in Figure 9.13, it becomes clear that as a result of the reduced density of operational cells the average cell utilizations are increased. This is due to the fact that the same amount of area traffic has to be served by a lower number of operational cells.

Results for $P_{in}^{total}(t)$ are presented in Figure 9.18. Compared to the fixed deployment, the total power consumption is considerably reduced for all the non-busy hours. This is due to the fact that by switching off underutilized capacity cells, the cost of idle state power consumption can be reduced. For example, looking at the results for $P_{in}^{total}(t = 6)$, variable deployment results in 52-70% lower power consumption compared to the fixed deployment when no fast cell DTX is applied. With 50% fast cell DTX, the difference becomes equal to 48-67%. The achievable gains are reduced together with an increasing network load. In case of $P_{in}^{total}(t = 12)$, variable deployment results in 19-29% (*No Cell DTX*) or 9-22% (*50% Cell DTX*) lower power consumption compared to the fixed deployment. For all cases, *Femto RND* benefits the most and *Femto HVYC* benefits the least from the variable deployment.

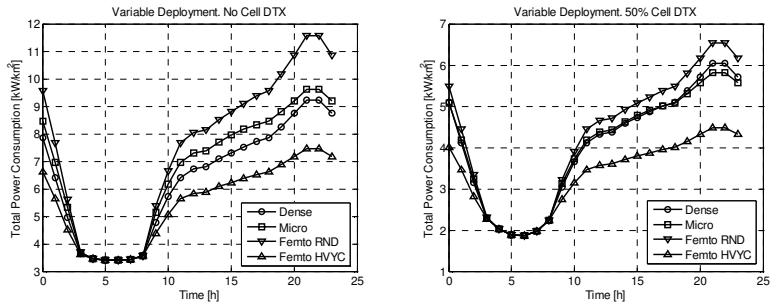


**Figure 9.18.** Total power consumption as a function of time without fast cell DTX and with 50% fast cell DTX.

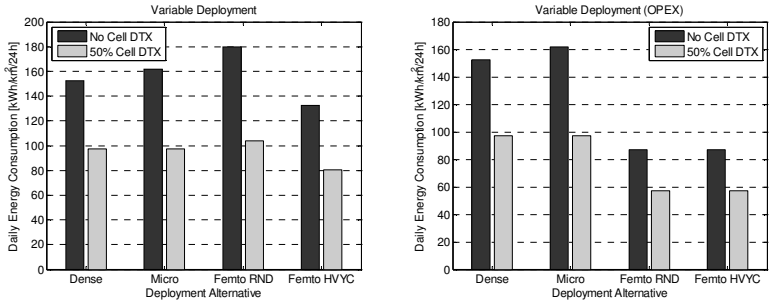


**Figure 9.19.** Daily energy consumption with the variable deployment.

Results for the daily energy consumption are provided in Figure 9.19. Compared to the approach with a fixed network deployment, daily energy consumption with a variable network deployment becomes 24-34% lower. Furthermore, if the scenario with 50% fast cell DTX is assumed, variable deployment consumes 15-28% less energy than the fixed deployment. Similar to the fixed deployment, *Femto HVYC* is the most energy-efficient and *Femto RND* the most energy-inefficient alternative. However, the differences between the network densification alternatives are smaller. Finally, from the OPEX point of view, heterogeneous femto deployments consume approximately 43% less energy than the densified macro, and 46% less energy than the heterogeneous micro deployment. Again, the introduction of fast cell DTX reduces slightly the difference between the network densification alternatives. An interesting detail is that in case of the heterogeneous femto deployments, the OPEX-related energy consumption increases slightly compared to the fixed deployment. This is due to the increased average utilization of the macro cells, as demonstrated in Figure 9.17.

### 9.4.3 Performance of the sleep mode deployment

The difference between the *sleep mode deployment* and the variable deployment is that the underutilized capacity cells are not switched off entirely. Instead, certain parts of the eNodeBs are left active to enable the possibility to wake up the cells fairly quickly when needed. For example, sleeping capacity cells can be re-activated by the network or the macro cells when the observed macro cell load exceeds a certain predefined threshold [158]. Alternatively, the sleeping eNodeBs could be monitoring the levels of the received uplink power to estimate the average uplink load level and/or whether there are any active UEs close-by.

The model assumed in this thesis is quite simple and at the same time somewhat ideal: Density of the deployed capacity cells is based on the fixed deployment, see Table 9.7, but during the network operation all idle capacity cells are assumed to be in sleep mode, with power consumption equal to 10% of the idle mode power consumption ($\delta_{cap} = 0.1$). What is ideal with this approach is that as soon as the system contains a UE, for which the RSRP from a (currently) sleeping capacity cell would be better than the RSRP from the strongest active cell, the sleeping capacity cell is reactivated. Hence, the model ignores the impacts of measurement uncertainties, delays and the ability to detect close-by UEs. An example of the sleep mode deployment is shown in Figure 9.20. In case of scenario 1, both capacity cell A and capacity cell B are idle, and hence, are assumed to be in sleep mode. In case of scenario 2, a user has entered the coverage area of capacity cell A. As a result, capacity cell A has been switched back to an active state, and is serving the close-by user. However, capacity cell B is still in sleep mode.

In case of a more practical (algorithm-based) sleep mode deployment with delays and uncertainties, the system would most likely contain a fair amount of idle capacity cells, which are not in sleep mode. Hence, $\delta_{cap}$ would in practice become larger than 0.1. Furthermore, depending on how aggressive sleep mode algorithm is assumed, it would also be possible that during the high-traffic hours the observed cell-edge user performance could become worse than the desired 10 Mbps.

In order to guarantee a certain level of basic coverage, the cells belonging to the baseline deployment are not switched to sleep mode. However, a moderate level of fast cell DTX can still be applied to the idle baseline cells. In the following evaluation, the cell DTX parameter $\delta_{bln}$ is assumed to be equal to 1 (*No Cell DTX*) or 0.5 (*50% Cell DTX*). Furthermore, since the cell density is the same as in the fixed deployment, also the average cell

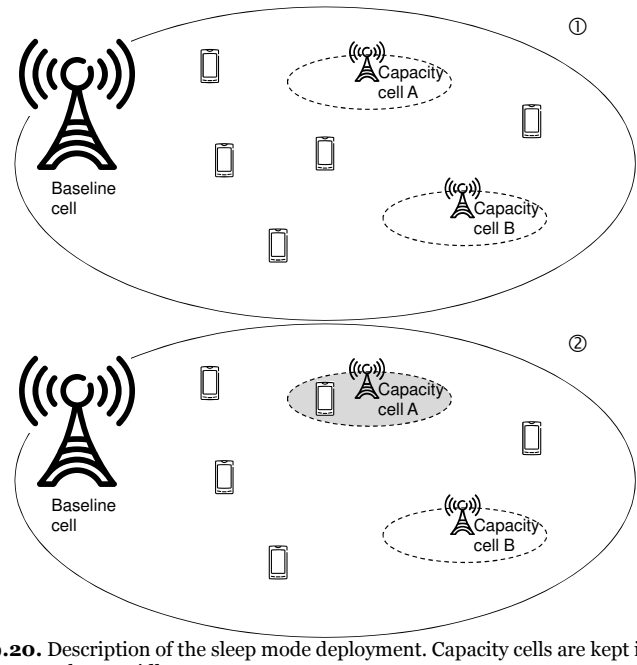


**Figure 9.20.** Description of the sleep mode deployment. Capacity cells are kept in sleep mode whenever they are idle.

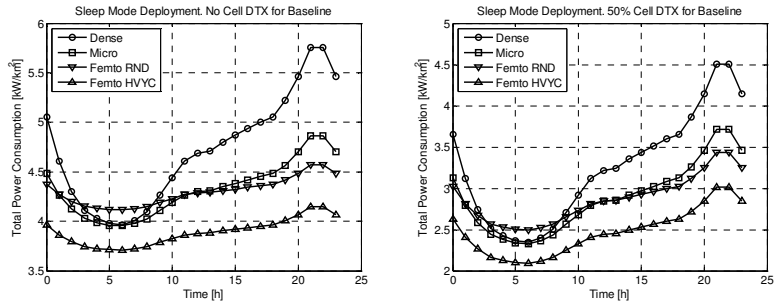


**Figure 9.21.** Total network power consumption as a function of time without fast cell DTX and with 50% cell DTX for the baseline cells.

utilizations are the same. Hence, the values for $\bar{u}_{bln}(t)$ and $\bar{u}_{cap}(t)$ can be read from Figure 9.13.

Compared to both the fixed and the variable deployment, the results for $P_{in}^{total}(t)$ without fast cell DTX look quite different, see Figure 9.21. Now, the heterogeneous deployments result in a lower total network power consumption compared to the densified macro deployment. Only during the hours with the lowest network load, the total power consumption of the densified macro network is similar to the total power consumption of the heterogeneous micro deployment, and slightly lower than the power consumption of the heterogeneous femto deployment with a random selection of femto apartments. Furthermore, the heterogeneous micro

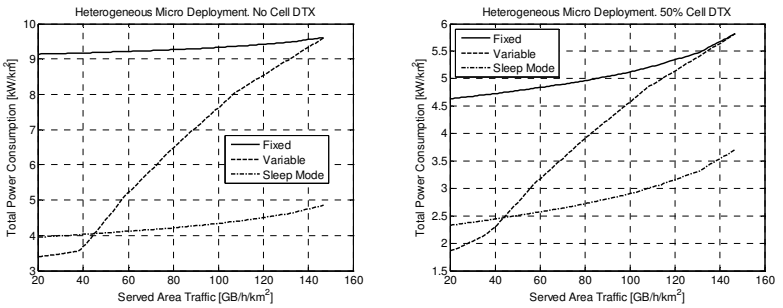


**Figure 9.22.** Total network power consumption as a function of the served area traffic for the different network adaptation methods. Heterogeneous micro deployment is assumed.

deployment is more power-efficient than *Femto RND* when the network load is high, but the situation becomes the opposite during the low-traffic hours. Finally, the heterogeneous femto deployment with the traffic-based selection of femto apartments is shown to be the most power-efficient network densification alternative for all the time instants.

When fast cell DTX is introduced for the baseline macro cells, total power consumption of the baseline network is reduced. The highest reduction (49%) is observed during the hours with the lowest traffic, since then the baseline cells are idle in 98% of the time. The gain is reduced for the hours with a higher network load, but even during the peak traffic hour the baseline network consumes 31% less power than without fast cell DTX. Since the introduction of fast cell DTX does not affect the total power consumption of the capacity cells, the cell DTX gains on the overall network power consumption become smaller, ranging from 22-27% (peak traffic hour) to 39-44% (low-traffic hour).

Compared to the fixed deployment, the sleep mode deployment results in 47-63% (*No Cell DTX*) or 42-56% (*50% Cell DTX*) lower total power consumption, depending on the network densification alternative (as an example Figure 9.22 presents the results of the performance comparison for the heterogeneous micro deployment). The gain is reduced together with an increased traffic load, but even during the peak traffic hour the sleep mode deployment results in 38-60% (*No Cell DTX*) or 26-48% (*50% Cell DTX*) lower total power consumption compared to the fixed deployment. *Femto RND* benefits the most, while *Femto HVYC* (low-traffic) or the densified macro deployment benefits the least from the sleep mode deployment.

When it comes to the difference compared to the variable deployment, sleep mode scheme consumes 9-21% (*No Cell DTX*) or 12-34% (*50% Cell DTX*) more power during the hours with the lowest network load, i.e. when all the capacity cells have been switched off in case of the variable

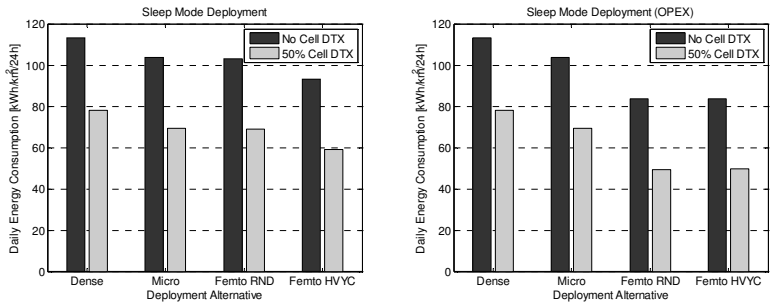


**Figure 9.23.** Daily energy consumption with the sleep mode deployment.

deployment. However, if the hourly area traffic is higher than 43-48 GB/h/km² (35-47 GB/h/km² with fast cell DTX) sleep mode deployment is more power-efficient than the variable deployment. The gain increases together with the network load, and becomes equal to 38-60% (*No Cell DTX*) or 26-48% (*50% Cell DTX*) during the peak traffic hour, i.e. when none of the capacity cells are switched off.

When the daily energy consumption is evaluated, see Figure 9.23, the findings listed above become even more obvious. Densified macro deployment is indeed the most energy-inefficient alternative, and the heterogeneous micro and *Femto RND* deployments result in very similar daily energy consumption. Furthermore, similar to the fixed and variable deployment, *Femto HVYC* is the most energy-efficient alternative. Looking at the OPEX-related daily energy consumption, heterogeneous femto deployments result in 26% lower daily energy consumption than the densified macro and 19% lower daily energy consumption than the heterogeneous micro deployment. With fast cell DTX, the corresponding differences increase to 37% and 29%.

In order to summarize the differences between the different energy saving methods, the normalized daily energy consumption values have been collected in Figure 9.24. Compared to the fixed deployment, the sleep mode deployment results in 46% - 62% (*No Cell DTX*) or 36-52% (*50% Cell DTX*) lower daily energy consumption. Furthermore, the gain compared to the variable deployment becomes equal to 26-43% (*No Cell DTX*) or 20-34% (*50% Cell DTX*). *Femto RND* benefits the most, and the densified macro deployment benefits the least from the sleep mode deployment. In all, the combination of fast cell DTX and sleep mode deployment results in 63-75% lower daily energy consumption compared to scenarios without any special energy saving mechanisms. Even though the results are not fully comparable, the findings presented above are similar to the conclusions in [158] and in [163], i.e. the utilization of fast power saving mechanisms, such

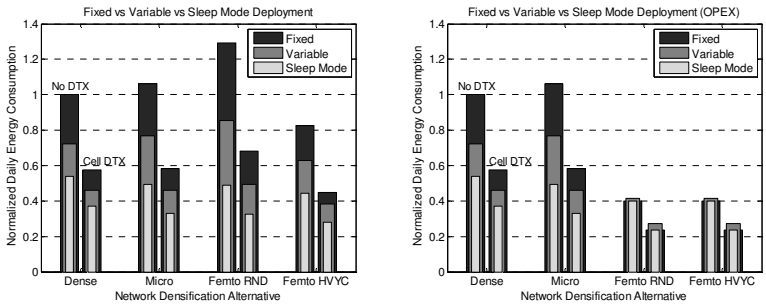


**Figure 9.24.** Normalized daily energy consumption for the different network densification alternatives and the different energy saving methods.

as micro DTX and sleep mode, within the underutilized low-power cells can result in a considerably lower total network energy consumption.

Finally, when it comes to the normalized OPEX-related daily energy consumption, the sleep mode deployment results in 46% (*Dense*) and 54% (*Micro*) lower daily energy consumption compared to the fixed deployment. Assuming fast cell DTX, the corresponding gains are reduced to 36% and 44%. In case of the heterogeneous femto deployments, sleep model deployment results in the same daily energy consumption as the fixed network deployment. Compared to the variable network deployment without fast cell DTX, daily energy consumption becomes 26% (*Dense*), 36% (*Micro*) or 4% (*Femto RND*, *Femto HVYC*) lower with the sleep mode deployment. With the fast cell DTX the corresponding differences become equal to 20% (*Dense*), 29% (*Micro*) and 13% (*Femto RND*, *Femto HVYC*).

# 10. Conclusions and further research

## 10.1 Summary and conclusions

The main contribution of this thesis is two-fold: Firstly, to introduce both a system simulator platform and a deployment scenario enabling fair performance comparisons between different types of network densification alternatives. Secondly, to evaluate the performance and energy-efficiency of a few different network densification alternatives within an urban environment.

The thesis has evaluated also the impact of a few design choices, for example with respect to the eNodeB transmission power, spectrum allocation, biased cell selection and access control, on the system performance. Furthermore, a few different ways to enhance the energy-efficiency of dense network deployments have been discussed and evaluated.

The main difference between the existing heterogeneous network models and the deployment scenario introduced in this thesis is related to the modeling of the traffic hotspot, both when it comes to the user and the eNodeB locations within the traffic hotspot, and the wave propagation between the nodes. Furthermore, a three-dimensional model of both the user locations and the wave propagation is introduced, which has been ignored in most of the existing deployment scenarios. The purpose of the changes is to enable more reliable performance comparisons for deployment scenarios, where the environment and traffic distribution is assumed to be fixed, but the types and the locations of the eNodeBs are varied.

When it comes to the performance comparison the obtained results indicate that the most efficient way to enhance the overall coverage and capacity of the existing baseline macro network is to deploy new macro sites, i.e. to densify the existing macro cell layer. If the existing baseline network is densified by deploying outdoor micro eNodeBs into the traffic hotspots, the required number of new sites becomes approximately 4-8 times as large as the required number of new macro sites to reach the same

system performance. Furthermore, if the baseline network is densified by deploying open access femto eNodeBs inside the residential apartments, the required number of new sites becomes roughly 50-90 times as large as the required number of new macro sites.

The results indicate also that network densification with the help of low-power eNodeBs is more efficient for the uplink than it is for the downlink. This is due to the fact that uplink is in general more power-limited than downlink. Therefore, the ability of the new cells to offload the most power-limited users is playing an important role. What is important for the capacity-limited downlink, is the ability of the new cells to offload as much of the traffic as possible from the macro cells.

The presented results demonstrate that the coverage area of a low-power cell can be extended, and the level of overall traffic offloading increased either by increasing the transmission power of the micro or femto eNodeB, or with the help of a biased cell selection. What is different between these two approaches is that in case of the biased cell selection, the downlink quality of the users within the extended cell area can become very poor. This problem can be mitigated with the help of the enhanced inter-cell interference control mechanism, which is introduced as part of 3GPP LTE Release-10.

Another typical problem with the different kinds of heterogeneous network deployments is the uplink interference from macro mobiles towards the co-channel low-power eNodeBs. In this thesis a solution is proposed to resolve this problem, where a special interference margin is introduced to the uplink power control within the low-power cell. The most appropriate size of this interference margin is found to depend on the assumed scenario. Furthermore, it will be a trade-off between the improved uplink performance of the low-power cell users and the increased uplink interference towards the macro cell.

When it comes to heterogeneous femto deployments, it has been demonstrated that the applied access control mode has a large impact on the achieved system performance. If the femto cells are operating on the closed subscriber group (CSG) mode, a full frequency reuse between the macro and the femto cell layer becomes difficult. In practice, it would require quite stringent interference management actions in power domain; both for the CSG femto eNodeB transmission power and for the femto UE transmission power. As a result of the reduced femto cell performance (due to these interference mitigation actions) the achievable system-level gains become quite limited. One particular problem area is the potentially poor quality of the downlink control signaling, for example the Cell-Specific Reference Symbols (CRS), which will have a negative impact on the

achievable user performance. An effective way to reduce the potential near-far problems, and to considerably increase the system-level performance, is to allow the femto cells to operate either on an open access mode, or a hybrid access mode. In both cases, all users can access the femto cell, but in case of hybrid access, the users outside the CSG have only a limited access to the radio resources within the femto cell.

Another possible way to efficiently reduce the inter-cell interference in case of heterogeneous CSG femto deployments is to allocate separate carriers for the macro and the femto cell layer. The spectrum allocation method considered in this thesis has been to split the original 20 MHz carrier, which as a default is used by both the macro and the femto cell layer, into a macro carrier (e.g. 10 MHz) and an adjacent channel femto carrier (e.g. 10 MHz). The downside of this kind of approach is that as a result of the reduced carrier bandwidths, the achievable peak bit rates are reduced also for the users that are not suffering from an excessive inter-layer interference. Based on the obtained results, the downlink performance will become worse as a result of this kind of spectrum splitting due to the fact that the improved signal quality is not able to compensate for the losses related to the reduced carrier bandwidth. However, the situation is slightly different for the uplink, where the users are considerably more power-limited compared to the downlink. As indicated by the results, in some uplink scenarios the overall system performance can in fact be improved by splitting the spectrum into separate macro and femto carriers.

The obtained results demonstrate also that the heterogeneous femto deployments can be made more efficient if the femto cells are initially targeted to the residential areas with poor macro coverage, or in particular towards the most traffic-heavy users, because then the amount of offloaded traffic can be maximized with the minimum amount of femto cells to be deployed. Compared to a deployment with random selection of femto apartments, the traffic-based approach requires an approximately 50% lower density of femto cells to fulfill the same coverage and capacity requirements.

This thesis has compared the different network densification alternatives also from the total network power consumption, or the total network energy consumption, point of view. The most energy-efficient deployment alternative is defined to be the one that can provide the desired network performance (coverage and capacity) with the lowest amount of power or energy consumed, measured as $W/km^2$ or $kWh/km^2$. The results demonstrate that the densified macro network is not only the most radio-resource-efficient, but in many cases it is also the most power- or energy-

efficient deployment alternative. If some form of fast cell DTX, for example micro sleep and antenna muting, is applied to the idle cells, heterogeneous deployments become much more competitive. This is due to the fact that the size of the fixed power consumption with respect to the variable power consumption is reduced. The energy-efficiency of dense network deployments can be further enhanced by switching off unnecessary capacity cells during low-traffic hours, or the introduction of the shared cell identity scheme, where the capacity cells are active only when they are needed to transmit data to the close-by users. Instead of completely switching off cells, underutilized capacity cells can also be switched to a sleep mode, and re-activated whenever needed to serve close-by users. The fundamental assumption for all of these network adaptation schemes is that the baseline network is able to provide the basic coverage and that the network densification is required to enhance the capacity. The observed results demonstrate that by applying both a decent level of fast cell DTX for idle macro cells and an ideal sleep mode scheme for idle low-power capacity cells, the daily energy consumption can be reduced by 60-70%, while still fulfilling the same coverage and capacity requirements. If a targeted deployment of femto cells is assumed, the daily energy consumption can be reduced even further.

## 10.2 Further research

In general, evaluation results are typically tightly coupled with the corresponding evaluation assumptions and models. This means that the results and conclusions presented in this thesis are valid only for the assumed deployment scenario. Therefore, in order to get a more complete picture of the applicability of the different heterogeneous network deployments with respect to the traditional way of densifying macro cellular networks, performance evaluations should be performed for other types of deployment scenarios as well. One such scenario could be a suburban or rural environment consisting mainly of detached houses. In such scenarios, the baseline deployment could be more power-limited than in the urban deployment scenario assumed in this thesis. Hence, network densification would in many cases be needed to improve the coverage (i.e. to enable the use of higher data rates) instead of improving only the area capacity.

In addition to evaluating new types of deployment scenarios, also the models for the urban deployment scenario can be improved in many different ways, enhancing the accuracy and the reliability of the results. These enhancements include for example the following:

- Enhanced modeling of the three-dimensional macro cellular propagation, in particular in case of the densified macro deployment. Features to be improved include for example the line-of-sight and street canyon propagation and the floor height gain.

- Dynamic modeling of various (3GPP LTE Release-8) RRM algorithms, such as scheduler, CSI measurement and reporting, handover and inter-cell interference coordination.

- Impact of user mobility on the performance of heterogeneous indoor deployments, for example when it comes to the leakage of indoor cell coverage towards outdoor users. From the static traffic offloading point of view, as assumed in this thesis, achieving as high level of traffic offloading as possible can be favorable. However, this might no longer be the case if dynamic system behavior with user mobility and realistic handover modeling is assumed instead.

- Modeling of the impact of CRS interference, including realistic models for CRS interference suppression.

- More accurate modeling of the impact of the quality of the downlink control signaling on the user performance.

- Modeling the impact of femto backhaul limitation in a more realistic way, including also the uplink.

- Performance of the escape carrier deployment compared to full frequency reuse or adjacent channel deployment.

- Performance of other types of public or private in-building solutions, such as DAS, indoor pico cells and enterprise femto cells.

Another interesting topic for future research is the applicability and performance of the various enhancements introduced in 3GPP LTE Release-10 and beyond, such as eICIC (together with biased cell selection), carrier aggregation, CoMP, shared cell identity and dual-connectivity. For example it could be worth investigating how eICIC and biased cell selection could be integrated into the overall SON framework in the most efficient way to enhance the system performance. After all, one could expect that the applied cell selection offset should be cell-specific, and that it would depend for example on the location of the low-power cell, traffic distribution, network load and other network parameters. Furthermore, the impact of different types of backhaul solutions on the performance of CoMP and

shared cell identity should be evaluated. Finally, since in practice a 3GPP LTE Release-10+ system has to support both Release-10-capable terminals and legacy terminals, one possible topic of future research could be to investigate how to operate such a network with different portions of new and legacy mobiles in the most efficient way.

One of the fundamental assumptions in this thesis is that the cell layers are operating on the same radio access technology, namely LTE. However, there has been an increasing interest to enhance the possibilities for WLAN offloading, for example by enhancing the mobility mechanisms between the 3GPP-based radio access technologies and WLAN. Related to this, suitable topics for future release would be to investigate the overall applicability and expected system performance, as well as the required radio resource management algorithms for WLAN offloading.

When it comes to the energy-efficiency comparison, one obvious area of future research is to enhance the power consumption models, including also models for fast cell DTX and sleep mode, for the different base station types. Furthermore, the possibilities to dynamically adjust the network cell layout, based on the actual traffic needs, should be more carefully evaluated. These investigations should take into account the possible challenges related to sleep mode and switching cells off and on. Yet another thing worth evaluating would be to combine the predicted traffic growth, evolution of terminals and the expected upgrade of network equipment, and map that into an evaluation of the total network power consumption as a function of time, in a similar fashion as has been done for example in [96].

Last but not least, one of the most important open questions is the total cost of the different network deployment alternatives. This thesis has investigated the required site densities, and the total energy consumption, but in order to obtain the full picture of the overall cost, both CAPEX and OPEX, a lot more work is required.

# Bibliography


[1] Cisco, “Cisco Visual Networking Index: Global Mobile Data Traffic Forecast Update, 2010-2015”, White Paper, February 2011.

[2] Terry Norman, Analysys Mason, “Wireless Network Traffic Worldwide: Forecasts and Analysis 2011-2016”, Analysys Mason Ltd, May 2011.

[3] Ericsson, “Ericsson Mobility Report – On The Pulse Of The Networked Society”, White Paper, November 2012.

[4] Moray Rumney, “IMT-Advanced: 4G Wireless Takes Shape in an Olympic Year”, Agilent Measurement Journal, Agilent Technologies Inc., September 2008.

[5] Nokia Siemens Networks, “2020: Beyond 4G – Radio Evolution for the Gigabit Experience”, White Paper, 2011.

[6] Sara Landström, Anders Furuskär, Klas Johansson, Laetetia Falconetti, Fredric Kronestedt, ”Heterogeneous Networks – increasing cellular capacity”, Ericsson Review, Volume 89, 2011.

[7] Albrecht Fehske, Gerhard Fettweis, Jens Malmodin, Gergely Biczók, “The Global Footprint of Mobile Communications: The Ecological and Economic Perspective”, IEEE Communications Magazine, vol. 49, no. 8, August 2011, pp. 55-62.

[8] R. Steele, “Towards a high-capacity digital cellular mobile radio system”, IEE Proceedings, vol. 132, Pt. F, no. 5, pp. 405-415, August 1985.

[9] R. Steele, V.K. Prabhu, “High-user-density digital cellular mobile radio systems”, IEE Proceedings, vol. 132, Pt. F, no. 5, pp. 396-404, August 1985.

[10] K.H.H. Wong, “Transmission of digital speech in highway microcells”, Journal of the Institution of Electronic and Radio Engineers, vol. 57, no. 6 (Supplement), pp. S246-S254, November/December 1987.

[11] Sami A. El-Dolil, Wai-Choong Wong, Raymond Steele, “Teletraffic Performance of Highway Microcells with Overlay Macrocell”, IEEE Journal on Selected Areas in Communications, vol. 7, no. 1, pp. 71-78, January 1989.

[12] Ta-Shing Chu, Michael J. Gans, “Fiber Optic Microcellular Radio”, IEEE Transactions on Vehicular Technology, vol. 40, no. 3, pp. 599-606, August 1991.

[13] W.C.Y. Lee, “Efficiency of a New Microcell System”, in Proc. 42nd IEEE VTS Conference, Denver, CO, USA, May 1992, pp. 37-42.

[14] Larry J. Greenstein et al., ”Microcells in Personal Communications System”, IEEE Communications Magazine, vol. 30, no. 12, pp. 76-88, December 1992.

[15] Xavier Lagrange, “Multitier Cell Design”, IEEE Communications Magazine, vol. 35, no. 8, pp. 60-64, August 1997.

[16] Joseph Sarnecki, C. Vinodrai, Alauddin Javed, Patrick O'Kelly, Kevin Dick, "Microcell Design Principles", IEEE Communications Magazine, vol. 31, no. 4, pp. 76-82, April 1993.

[17] Chih-Lin I, Larry J. Greenstein, Richard D. Gitlin, "A Microcell/Macrocell Cellular Architecture for Low- and High-Mobility Wireless Users", IEEE Journal on Selected Areas in Communications, vol. 11, no. 6, pp. 885-891, August 1993.

[18] Mitsuru Murata, Etsuhiro Nakano, "Enhancing the Performance of Mobile Communications Systems", in Proc. IEEE International Conference on Universal Personal Communications (ICUPC) 1993, vol. 2, pp. 732-736, Ottawa, Canada, October 1993.

[19] Akira Yamaguchi, Hideo Kobayashi, Toshio Mizuno, "Integration of Micro and Macro Cellular Networks for Future Land Mobile Communications", in Proc. IEEE International Conference on Universal Personal Communications (ICUPC) 1993, vol. 2, pp. 737-742, Ottawa, Canada, October 1993.

[20] Joseph Shapira, "Microcell Engineering in CDMA Cellular Networks", IEEE Transactions on Vehicular Technology", vol. 43, no. 4, pp. 817-825, November 1994.

[21] Donald M. Grieco, "The Capacity Achievable with a Broadband CDMA Microcell Underlay to an Existing Cellular Macrosystem", IEEE Journal on Selected Areas in Communications, vol. 12, no. 4, pp. 744-750, May 1994.

[22] Qualcomm Inc., "The CDMA Network Engineering Handbook", March 1993.

[23] Ermanno Berruto, Mikael Gudmundson, Raffaele Menolascino, Werner Mohr, Marta Pizarroso, "Research Activities on UMTS Radio Interface, Network Architectures, and Planning", IEEE Communications Magazine, vol. 36, no. 2, pp. 82-95, February 1998.

[24] S. Marano, C. Mastroianni, "A Hierachical Network Scheme for Multilayered Cellular Systems", in Proc. IEEE Vehicular Technology Conference (VTC) 1997, vol. 3, pp. 1792-1796, Phoenix, AZ, USA, May 1997.

[25] Seppo Hämäläinen, Harri Lilja, Jouko Lokio, Marko Leinonen, "Performance of a CDMA Based Hierarchical Cell Structure Network", in Proc. IEEE International Symposium on Personal, Indoor and Mobile Radio Communications (PIMRC) 1997, vol. 3, pp. 863-866, Helsinki, Finland, September 1997.

[26] Nicolas Guérin, "Adjacent Channel Interface in a WCDMA HCS Network", in Proc. FRAMES Workshop, Delft, The Netherlands, 18-19 January 1999, pp. 158-164.

[27] Robert S. Karlsson, Jens Zander, "On Hierarchical Cell Structures for Future Wideband Wireless Access", in Proc. Nordic Radio Seminarium 1997, May 1997.

[28] Robert Karlsson, Jens Zander, "Hierarchical Cell Structures for FRAMES Wideband Wireless Access", in Proc ACTS Mobile Telecommunications Summit, 27-29 November, 1996, pp. 785-791.

[29] Mahboubeh Lohi, Dilshan Weerakoon, A.H. Aghvami, "Trends in Multi-Layer Cellular System Design and Handover Design", in Proc. IEEE Wireless Communications and Networking Conference (WCNC) 1999, vol. 2, pp. 898-902, New Orleans, USA, September 1999.

[30] Kari Heiska, Achim Wacker, Kari Sipilä, Jaana Laiho-Steffens, "WCDMA Network Planning Case with Hierarchical Cell Structures", in Proc. IEEE International Symposium on Personal, Indoor and Mobile Radio Communications (PIMRC) 1999, Osaka, Japan, 1999.

[31] Chris Johnson, Jamal Khalab, Albert Hoglund, "Inter and Intra Operator Coexistence of WCDMA HCS Layers", in Proc. IEEE Vehicular Technology

Conference (VTC) 2002 Spring, vol. 1, Birmingham, AL, USA, May 2002, pp. 115-119.

[32] Terhi Rautiainen, "Breaking the Hierarchical Cell Structure in WCDMA Networks", in Proc. IEEE Vehicular Technology Conference (VTC) 2002 Spring, vol. 1, Birmingham, AL, USA, May 2002, pp.110-114.

[33] Jaana Laiho, Achim Wacker, Tomáš Novosad (ed.), "Radio Network Planning and Optimisation for UMTS", John Wiley & Sons, 2002.

[34] Chang-Young Kim, "The Evaluation of HCS Scenarios included in HSDPA", in Proc. IEEE Vehicular Technology Conference (VTC) 2004 Fall, Los Angeles, CA, USA, September 2004, pp. 4772-4776.

[35] Henrik Andersson, Robert S. Karlsson, Per Larsson, Patrik Wikström, "Improving System Performance in a WCDMA FDD Network using Indoor Pico Base Stations", in Proc. IEEE Vehicular Technology Conference (VTC) 2002 Fall, Vancouver, Canada, September 2002, pp. 467-471.

[36] Kimmo Hiltunen, Birgitta Olin, Magnus Lundevall, "Using Dedicated In-Building Systems to Improve HSDPA Indoor Coverage and Capacity", in Proc. IEEE Vehicular Technology Conference (VTC) 2005 Spring, Stockholm, Sweden, May 2005.

[37] 3GPP TS 25.104, "Base Station (BS) radio transmission and reception (FDD) (Release 6)", V6.18.0, May 2009.

[38] 3GPP TR 25.951, "FDD Base Station (BS) classification (Release 6)", V6.3.0, October 2006.

[39] Hamid R. Karimi, Lester T.W. Ho, Holger Claussen, Louis G. Samuel, "Evolution Towards Dynamic Spectrum Sharing in Mobile Communications", in Proc IEEE International Symposium on Personal, Indoor and Mobile Radio Communications (PIMRC) 2006, Helsinki, Finland, September 2006.

[40] Holger Claussen, Lester T.W. Ho, Louis G. Samuel, "Financial Analysis of a Pico-Cellular Home Network Deployment", in Proc. International Conference on Communications (ICC) 2007, Glasgow, Scotland, UK, 24-28 June 2007, pp. 5604-5609.

[41] Holger Claussen, "Performance of Macro- and Co-Channel Femtocells in a Hierarchical Cell Structure", in Proc. IEEE International Symposium on Personal, Indoor and Mobile Radio Communications (PIMRC) 2007, Athens, Greece, September 2007.

[42] Lester T.W. Ho, Holger Claussen, "Effects of User-Deployed, Co-Channel Femtocells on the Call Drop Probability in a Residential Scenario", in Proc. IEEE International Symposium on Personal, Indoor and Mobile Radio Communications (PIMRC) 2007, Athens, Greece, September 2007.

[43] Holger Claussen, Lester T.W. Ho, Louis G. Samuel, "Self-optimization of Coverage for Femtocell Deployments", in Proc. IEEE Wireless Telecommunications Symposium (WTS) 2008, Pomona, CA, USA, pp. 278-285.

[44] Small Cell Forum home page, http://www.smallcellforum.org.

[45] 3GPP TR 25.820, "3G Home NodeB Study Item Technical Report (Release 8)", V8.2.0, September 2008.

[46] 3GPP TR 25.967, "Home Node B Radio Frequency (RF) Requirements (FDD) (Release 8)", V8.0.1, March 2009.

[47] 3GPP TR 36.921, "Evolved Universal Terrestial Radio Access (E-UTRA); FDD Home eNodeB (HeNB) Radio Frequency (RF) requirements analysis (Release 9)", V9.0.0, March 2010.

[48] 3GPP TR 36.922, "Evolved Universal Terrestial Radio Access (E-UTRA); TDD Home eNodeB (HeNB) Radio Frequency (RF) requirements analysis (Release 9)", V9.1.0, June 2010.

[49] 4G Americas, “4G Mobile Broadband Evolution: Release 10, Release 11 and Beyond – HSPA+, SAE/LTE and LTE-Advanced”, October 2012.

[50] Femto Forum, “Interference Management in UMTS Femtocells”, White Paper, February 2010.

[51] Femto Forum, “Interference Management in OFDMA Femtocells”, White Paper, March 2010.

[52] Small Cell Forum, “W-CDMA Open Access Small Cells”, White Paper, May 2012.

[53] Small Cell Forum, “Enterprise femtocell deployment guidelines”, White Paper, February 2012.

[54] Small Cell Forum, “Integrated Femto-WiFi networks”, White Paper, February 2012.

[55] Small Cell Forum, “Femto Forum Becomes Small Cell Forum as Femtocell Technology Extends Beyond the Home”, Press Release, 15th February 2012.

[56] 3GPP TR 36.814, “Evolved Terrestial Radio Access (E-UTRA); Further advancements for E-UTRA physical layer aspects (Release 9)”, V9.0.0, March 2010.

[57] 3GPP TR 36.931, “Evolved Universal Terrestial Radio Access (E-UTRA); Radio Frequency (RF) requirements for LTE Pico Node B”, V10.0.0, March 2011.

[58] Femto Forum, “Interference Management in UMTS Femtocells”, White Paper, December 2008.

[59] ITU-R Report M.2135, “Guidelines for evaluation of radio interface technologies for IMT-Advanced”, 2008.

[60] 3GPP TR 25.814, “Physical layer aspects for evolved Universal Terrestial Radio Access (UTRA) (Release 7)”, V7.1.0, September 2006.

[61] 3GPP TSG RAN WG4, R4-092042, “Simulation assumptions and parameters for FDD HeNB RF requirements”, San Francisco, CA, USA, May 2009.

[62] Anders Furuskär, Magnus Almgren, Klas Johansson, “An Infrastructure Cost Evaluation of Single- and Multi-Access Networks with Heterogeneous Traffic Density”, in Proc. IEEE Vehicular Technology Conference (VTC) 2005 Spring, Stockholm, Sweden, May 2005, pp. 3166-3170.

[63] Klas Johansson, Jens Zander, Anders Furuskär, “Modelling the cost of heterogeneous wireless access networks”, Int. J. Mobile Network Design and Innovation, vol. 2, no. 1, 2007.

[64] Klas Johansson, Jens Zander, Anders Furuskär, “Cost Efficient Deployment of Heterogeneous Wireless Access Networks”, in Proc. IEEE Vehicular Technology Conference (VTC) 2007 Spring, Dublin, Ireland, April 2007, pp. 3200-3204.

[65] Jan Markendahl, Östen Mäkitalo, “A comparative study of deployment options, capacity and cost structure for macrocellular and femtocell networks”, in Proc. IEEE International Symposium on Personal, Indoor and Mobile Radio Communications (PIMRC) 2010, Istanbul, Turkey, September 2010.

[66] Aydin Karaer, Ömer Bulakci, Simone Redana, Bernhard Raaf, Jyri Hämäläinen, “Uplink Performance Optimization in Relay Enhanced LTE-Advanced Networks”, in Proc. IEEE International Symposium on Personal, Indoor and Mobile Radio Communications (PIMRC) 2009, Tokyo, Japan, September 2009.

[67] 3GPP TSG RAN WG4, R4-093644, “HeNB Interference management for LTE Rel-9 via power control”, Miyazaki, Japan, October 2009.

[68] 3GPP TSG RAN WG1, R1-101926, “Performance and interference aspects of macro with outdoor pico hotspot”, Beijing, China, April 2010.

[69] 3GPP TSG RAN WG1, R1-102619, “UL power control in hotzone deployments”, Montreal, Canada, May 2010.

[70] Jacek Góra, Klaus I. Pedersen, Agnieszka Szufarska, Stanisław Strzyż, “Cell-Specific Uplink Power Control for Heterogeneous Networks in LTE”, in Proc. IEEE Vehicular Technology Conference (VTC) 2010 Fall, Ottawa, Canada, September 2010.

[71] Luis G. U. Garcia, Klaus I. Pedersen, Preben E. Mogensen, “Uplink Performance of Dynamic Interference Coordination under Fractional Power Control for LTE-Advanced Femtocells”, in Proc. IEEE Vehicular Technology Conference (VTC) 2010 Fall, Ottawa, Canada, September 2010.

[72] Agnieszka Szufarska, Krystian Safjan, Stanisław Strzyż, Klaus I. Pedersen, Frank Frederiksen, “Interference Mitigation Methods for LTE-Advanced Networks with Macro and HeNB Deployments”, in Proc. IEEE Vehicular Technology Conference (VTC) 2011 Fall, San Francisco, CA, USA, September 2011.

[73] 3GPP TSG RAN WG1, R1-083813, “Range expansion for efficient support of heterogeneous networks”, Prague, Czech Republic, September 2008.

[74] 3GPP TSG RAN WG1, R1-083814, “Serving cell association in heterogeneous networks”, Prague Czech Republic, September 2008.

[75] 3GPP TSG RAN WG1, R1-102150, “On Range Extension in Open-access Heterogeneous Networks”, Beijing, China, April 2010.

[76] Hisham A. Mahmoud, İsmail Güvenç, Fujio Watanabe, “Performance of Open Access Femtocell Networks with Different Cell-Selection Methods”, in Proc. IEEE Vehicular Technology Conference (VTC) 2010 Spring, Taipei, Taiwan, May 2010.

[77] Abdallah Bou Saleh, Ömer Bulakci, Simone Redana, Bernhard Raaf, Jyri Hämäläinen, “Enhancing LTE-Advanced Relay Deployments via Biasing in Cell Selection and Handover Decision”, in Proc. IEEE International Symposium on Personal, Indoor and Mobile Radio Communications (PIMRC) 2010, Istanbul, Turkey, September 2010, pp. 2277-2281.

[78] David Choi, Pooya Monajemi, Shinjae Kang, John Villasenor, “Dealing with Loud Neighbors: The Benefits and Tradeoffs of Adaptive Femtocell Access”, in Proc. IEEE Global Telecommunications Conference (GLOBECOM) 2008, New Orleans, LA, USA, November 2008.

[79] Luis G. U. Garcia, Klaus I. Pedersen, Preben E. Mogensen, “On Open versus Closed LTE-Advanced Femtocells and Dynamic Interference Coordination”, in Proc. IEEE Wireless Communications and Networking Conference (WCNC) 2010, Sydney, Australia, April 2010.

[80] Juan Espino, Jan Markendahl, Aurelian Bria, “On spectrum allocation and interference management for WCDMA and OFDMA femtocells”, in Proc. IEEE International Symposium on Personal, Indoor and Mobile Radio Communications (PIMRC) 2010, Istanbul, Turkey, September 2010, pp.1561-1566.

[81] Home page of the BeFemto (Broadband evolved FEMTO Networks) project: http://www.ict-befemto.eu/

[82] Holger Claussen, Lester T. W. Ho, Florian Pivit, ”Effects of Joint Macrocell and Residential Picocell Deployment on the Network Energy Efficiency”, in Proc. IEEE International Symposium on Personal, Indoor and Mobile Radio Communications (PIMRC) 2008, Cannes, France, September 2008.

[83] Holger Claussen, Lester T. W. Ho, Florian Pivit, ”Leveraging Advances in Mobile Broadband Technology to Improve Environmental Sustainability”, Telecommunications Journal of Australia, vol. 59, no. 1, pp. 04.1-04.18, 2009.

[84] Oliver Arnold, Fred Richter, Gerhard Fettweis, Oliver Blume, “Power Consumption Modeling of Different Base Station Types in Heterogeneous Cellular Networks”, in Proc. Future Network and Mobile Summit 2010, Florence, Italy, June 2010.

[85] Imran Ashraf, Lester T. W. Ho, Holger Claussen, “Improving Energy Efficiency of Femtocell Base Stations via User Activity Detection”, in Proc. IEEE Wireless Communications and Networking Conference (WCNC) 2010, Sydney, Australia, April 2010.

[86] M. Jada, J. Hämäläinen, R. Jäntti, ”Energy Savings in Mobile Networks: Case Study on Femtocells”, in Proc. URSI Finnish Convention on Radio Science 2010, Oulu, Finland, August 2010.

[87] M. Jada, M. M. A. Hossain, J. Hämäläinen, R. Jäntti, “Impact of Femtocells to the WCDMA Network Energy Efficiency”, in Proc. IEEE International Conference on Broadband Network and Multimedia Technology (IC-BNMT) 2010, Beijing, China, October 2010.

[88] Fred Richter, Gerhard Fettweis, “Cellular Mobile Network Densification Utilizing Micro Base Stations”, in Proc. IEEE International Communications Conference (ICC) 2010, Cape Town, South Africa, May 2010.

[89] Wei Wang, Gang Shen, “Energy Efficiency of Heterogeneous Cellular Network”, in Proc. IEEE Vehicular Technology Conference (VTC) 2010 Fall, Ottawa, Canada, September 2010.

[90] Fred Richter, Gerhard Fettweis, Markus Gruber, Oliver Blume, “Micro Base Stations in Load Constrained Cellular Mobile Radio Networks”, in Proc. IEEE International Symposium on Personal, Indoor and Mobile Radio Communications (PIMRC) 2010, Istanbul, Turkey, September 2010.

[91] Remco Litjens, Ljupco Jorguseski, “Potential of Energy-Oriented Network Optimisation: Switching Off Over-Capacity in Off-Peak Hours”, in Proc. IEEE International Symposium on Personal, Indoor and Mobile Radio Communications (PIMRC) 2010, Istanbul, Turkey, September 2010.

[92] Pål Frenger, Peter Moberg, Jens Malmodin, Ylva Jading, István Gódor, ”Reducing Energy Consumption in LTE with Cell DTX”, in Proc. IEEE Vehicular Technology Conference (VTC) 2011 Spring, Budapest, Hungary, May 2011.

[93] Mårten Ericson, “Total Network Base Station Energy Cost vs. Deployment”, in Proc. IEEE Vehicular Technology Conference (VTC) 2011 Spring, Budapest, Hungary, May 2011.

[94] Gilbert Micallef, Preben Mogensen, Hans-Otto Scheck, Ekkehard Lang, “Energy Efficient Evolution of Mobile Networks – Macro-Only Upgrades vs. a Joint-Pico Deployment Strategy”, in Proc. IEEE Vehicular Technology Conference (VTC) 2011 Spring, Budapest, Hungary, May 2011.

[95] L. Saker, S.E. Elayoubi, Letian Rong, Tijani Chahed, “Capacity and energy efficiency of picocell deployment in LTE-A networks”, in Proc. IEEE Vehicular Technology Conference (VTC) 2011 Spring, Budapest, Hungary, May 2011.

[96] Gilbert Micallef, Preben Mogensen, Hans-Otto Scheck, Jyrki Louhi, “Reversing the Energy Trend in Mobile Networks – Equipment Replacement for Increased Capacity at a Fraction of the Energy”, in Proc. IEEE Vehicular Technology Conference (VTC) 2011 Fall, San Francisco, CA, USA, September 2011.

[97] Energy Aware Radio and Network Technologies (EARTH) Home Page: http://www.ict-earth.eu.

[98] INFSO-ICT-247733 EARTH, Deliverable D2.3, “Energy efficiency analysis of the reference systems, areas of improvements and target breakdown”, 2010.

[99] INFSO-ICT-247733 EARTH, Deliverable D4.3, “Final Report on Green Radio Technologies”, 2012.

[100] Erik Dahlman, Stefan Parkvall, Johan Sköld, ”4G – LTE/LTE-Advanced for Mobile Broadband”, Academic Press, 2011.

[101] Harri Holma, Antti Toskala (ed.), ”LTE for UMTS – Evolution to LTE-Advanced”, Second Edition, John Wiley & Sons Ltd, 2011.

[102] Stefania Sesia, Issam Toufik, Matthew Baker (ed.), “LTE – The UMTS Long Term Evolution, From Theory to Practice”, Second Edition, John Wiley & Sons Ltd, 2011.

[103] 3GPP Technical Specifications for Evolved Universal Terrestial Radio Access (E-UTRA), 36-series. http://www.3gpp.org/ftp/Specs/html-info/36-series.htm.

[104] Erik Dahlman, Anders Furuskär, Ylva Jading, Magnus Lindström, Stefan Parkvall, ”Key features of the LTE radio interface”, Ericsson Review, No. 2, 2008.

[105] 3GPP TS 36.213, “Evolved Universal Terrestial Radio Access (E-UTRA); Physical layer procedures (Release 9)”, V9.3.0, September 2010.

[106] Arne Simonsson, Anders Furuskär, “Uplink Power Control in LTE – Overview and Performance”, in Proc. IEEE Vehicular Technology Conference (VTC) 2008 Fall, Calgary, Canada, September 2008.

[107] Carlos Úbeda Castellanos, Dimas López Villa, Claudio Rosa, Klaus I. Pedersen, Francesco D. Calabrese, Per-Henrik Michaelsen, Jürgen Michel, “Performance of Uplink Fractional Power Control in UTRAN LTE”, in Proc. IEEE Vehicular Technology Conference (VTC) 2008 Spring, Marina Bay, Singapore, May 2008.

[108] Volker Pauli, Juan Diego Naranjo, Elko Seidel, “Heterogeneous LTE Networks and Inter-Cell Interference Coordination”, White Paper, Nomor Research GmbH, Munich, Germany, December 2010.

[109] 3GPP TS 36.211, “Evolved Universal Terrestial Radio Access (E-UTRA); Physical Channels and Modulation (Release 9)”, V9.1.0, March 2010.

[110] 3GPP TS 36.101, “Evolved Universal Terrestial Radio Access (E-UTRA); User Equipment (UE) radio transmission and reception (Release 9)”, V9.11.0, March 2012.

[111] 3GPP TS 36.104, “Evolved Universal Terrestial Radio Access (E-UTRA); Base Station (BS) radio transmission and reception (Release 9)”, V9.11.9, March 2012.

[112] Vikram Chandrasekhar, Jeffrey G. Andrews, Alan Gatherer, “Femtocell Networks: A Survey”, IEEE Communications Magazine, vol.46, no. 9, pp. 59-67, September 2008.

[113] Christian Hoymann, Wanshi Chen, Juan Montojo, Alexander Golitschek, Chrysostomos Koutsimanis, Xiaodong Shen, “Relaying Operation in 3GPP LTE: Challenges and Solutions”, IEEE Communications Magazine, vol. 50, no. 2, pp. 156-162, February 2012.

[114] Afif Osseiran, Klaus Doppler, Cassio Ribeiro, Ming Xiao, Mikael Skoglund, Jawad Manssour, “Advances in Device-to-Device Communications and Network Coding for IMT-Advanced”, in Proc. ICT-Mobile Summit 2009, Santander, Spain, June 2009.

[115] Pekka Jänis, Visa Koivunen, Cássio Ribeiro, Juha Korhonen, Klaus Doppler, Klaus Hugl, “Interference-aware resource allocation for device-to-device radio underlaying cellular networks”, in Proc. IEEE Vehicular Technology Conference (VTC) 2009 Spring, Barcelona, Spain, April 2009.

[116] Chia-Hao Yu, Olav Tirkkonen, Klaus Doppler, Cássio Ribeiro, “On the performance of Device-to-Device underlay communication with simple

power control", in Proc. IEEE Vehicular Technology Conference (VTC) 2009 Spring, Barcelona, Spain, April 2009.

[117] Gábor Fodor, Norbert Reider, "A Distributed Power Control Scheme for Cellular Network Assisted D2D Communications", in Proc. IEEE Global Communications Conference (GLOBECOM) 2011, Houston, TX, USA, December 2011.

[118] Gábor Fodor, Erik Dahlman, Gunnar Mildh, Stefan Parkvall, Norbert Reider, György Miklós, Zoltán Turányi, "Design Aspects of Network Assisted Device-to-Device Communications", IEEE Communications Magazine, vol. 50, no. 3, pp. 170-177, March 2012.

[119] Small Cell Forum, "Small cells – what's the big idea?", White Paper, 15 February 2012.

[120] Sara Landström, Hideshi Murai, Arne Simonsson, "Deployment Aspects of LTE Pico Nodes", in Proc. IEEE International Conference on Communications (ICC) 2011, Kyoto, Japan, June 2011.

[121] Stefan Parkvall, Erik Dahlman, George Jöngren, Sara Landström, Lars Lindbom, "Heterogeneous network deployments in LTE", Ericsson Review, no. 2, 2011.

[122] 3GPP TR 36.839, "Evolved Universal Terrestial Radio Access (E-UTRA); Mobility enhancements in heterogeneous networks (Release 11)", V11.0.0, September 2012.

[123] Riikka Susitaival, Henning Wiemann, Jessica Östergaard, Anna Larmo, "Internet access performance in LTE TDD", in Proc. IEEE Vehicular Technology Conference (VTC) 2010 Spring, Taipei, Taiwan, May 2010.

[124] Nokia Siemens Networks, "Coexistence of asynchronous TDD networks", White Paper, 2011.

[125] 3GPP TR 36.828, "Evolved Universal Terrestial Radio Access (E-UTRA); Further enhancements to LTE Time Division Duplex (TDD) for Downlink-Uplink (DL-UL) interference management and traffic adaptation (Release 11)", V11.0.0, June 2012.

[126] Volker Pauli, Eiko Seidel, "Inter-Cell Interference Coordination for LTE-A", White Paper, Nomor Research GmbH, Munich, Germany, September 2011.

[127] 3GPP TS 36.104, "Evolved Universal Terrestial Radio Access (E-UTRA); Base Station (BS) radio transmission and reception (Release 10)", V10.6.0, March 2012.

[128] 3GPP TSG RAN WG1, R1-104968, "Summary of the description of candidate eICIC solutions", Madrid, Spain, August 2010.

[129] David López-Pérez, İsmail Güvenç, Guillaume de la Roche, Marios Kountouris, Tony Q. S. Quek, Jie Zhang, "Enhanced Intercell Interference Coordination Challenges in Heterogeneous Networks", IEEE Wireless Communications, vol. 18, no. 3, pp. 22-30, June 2011.

[130] Jianguo Liu, Dongyao Wang, Jun Wang, Jing Li, Jiyong Pang, Gang Shen, Qi Jiang, Huan Sun, Yan Meng, "Uplink Power Control and Interference Coordination for Heterogeneous Network", in Proc. IEEE International Symposium on Personal, Indoor and Mobile Radio Communications (PIMRC) 2012, Sydney, Australia, September 2012.

[131] Motoki Morita, Takahiro Nobukiyo, Kojiro Hamabe, "Uplink Power Control Method for LTE Femtocells Based on Resource Usage Aggregation", in Proc. IEEE International Symposium on Personal, Indoor and Mobile Radio Communications (PIMRC) 2012, Sydney, Australia, September 2012.

[132] 3GPP TR 36.819, "Coordinated multi-point operation for LTE physical layer aspects (Release 11)", V11.1.0, December 2011.

[133] Daewon Lee, Hanbyul Seo, Bruno Clerckx, Eric Hardouin, David Mazzarese, Satoshi Nagata, Krishna Sayana, "Coordinated Multipoint

Transmission and Reception in LTE-Advanced: Deployment Scenarios and Operational Challenges", IEEE Communications Magazine, vol. 50, no. 2, pp. 148-155, February 2012.

[134] Preben Mogensen, Wei Na, István Z. Kovács, Frank Frederiksen, Akhilesh Pokhariyal, Klaus I. Pedersen, Troels Kolding, Klaus Hugl, Markku Kuusela, "LTE Capacity compared to the Shannon Bound", in Proc. IEEE Vehicular Technology Conference (VTC) 2007 Spring, Dublin, Ireland, April 2007.

[135] Karsten Brueninghaus, David Astély, Thomas Sälzer, Samuli Visuri, Angeliki Alexiou, Stephan Karger, Gholam-Ali Seraji, "Link Performance Models for System Level Simulations of Broadband Radio Access Systems", in Proc. IEEE International Symposium on Personal, Indoor and Mobile Radio Communications (PIMRC) 2005, Berlin, Germany, September 2005, pp. 2306-2311.

[136] Population density within Stockholm City Centre http://en.wikipedia.org/wiki/Stockholm_City_Centre http://www.usk.stockholm.se/arsbok/b039.htm

[137] Population density within London http://data.london.gov.uk/datastore/package/land-area-and-population-density-borough

[138] Jens Zander, Seong-Lyun Kim, Magnus Almgren, Olav Queseth, "Radio Resource Management for Wireless Networks", Artech House, 2001.

[139] ITU-R Recommendation P.1411-4, "Propagation data and prediction methods for the planning of short-range outdoor radiocommunication systems and radio local area networks in the frequency range 300 MHz to 100 GHz".

[140] Fredrik Gunnarsson, Martin N. Johansson, Anders Furuskär, Magnus Lundevall, Arne Simonsson, Claes Tidestav, Mats Blomgren, "Downtilted Base Station Antennas – A Simulation Model Proposal and Impact on HSPA and LTE Performance", in Proc. IEEE Vehicular Technology Conference (VTC) 2008 Fall, Calgary, Canada, September 2008.

[141] Eraldo Damosso, Luis M. Correia (ed.), "Digital Mobile Radio Towards Future Generation Systems", COST 231 Final Report.

[142] Jan-Erik Berg, "A Recursive Method For Street Microcell Path Loss Calculations", in Proc. IEEE International Symposium on Personal, Indoor and Mobile Radio Communications (PIMRC) 1995, Toronto, Canada, September 1995, pp. 140-143.

[143] Jan-Erik Berg, "Building Penetration Loss Along Urban Street Microcells", in Proc. IEEE International Symposium on Personal, Indoor and Mobile Radio Communications (PIMRC) 1996, Taipei, Taiwan, October 1996, pp. 795-797.

[144] 3GPP TSG RAN WG1, R1-113482, "System performance evaluations on FeICIC", Zhuhai, China, October 2011.

[145] Janne Peisa, Eva Englund, "TCP Performance over HS-DSCH", in Proc. IEEE Vehicular Technology Conference (VTC) 2002 Spring, Birmingham, AL, USA, May 2002.

[146] Kimmo Hiltunen, "Comparison of Different Network Densification Alternatives from the LTE Downlink Performance Point of View", in Proc. IEEE Vehicular Technology Conference (VTC) 2011 Fall, San Francisco, CA, USA, September 2011.

[147] Kimmo Hiltunen, "Comparison of Different Network Densification Alternatives from the LTE Uplink Point of View", in Proc. IEEE International Symposium on Personal, Indoor and Mobile Radio Communications (PIMRC) 2011, Toronto, Canada, September 2011.

[148] S. F. Yunas, T. Isotalo, J. Niemelä, M. Valkama, ”Impact of Macrocellular Network Densification on the Capacity, Energy and Cost Efficiency in Dense Urban Environment”, International Journal of Wireless & Mobile Networks (IJWMN), vol. 5, no. 5, October 2013.

[149] Yuanye Wang, Klaus I. Pedersen, “Performance Analysis of Enhanced Inter-cell Interference Coordination in LTE-Advanced Heterogeneous Networks”, in Proc. IEEE Vehicular Technology Conference (VTC) 2012 Spring, Yokohama, Japan, May 2012.

[150] Kimmo Hiltunen, “The Gain of a Targeted Introduction of OSG Femtocells into a LTE Macro Network”, in Proc. IEEE Vehicular Technology Conference (VTC) 2012 Spring, Yokohama, Japan, May 2012.

[151] Zubin Bharucha, Gunther Auer, Tetsushi Abe, Nobuhiko Miki, “Femto-to-Macro Control Channel Interference Mitigation via Cell ID Manipulation in LTE”, in Proc. IEEE Vehicular Technology Conference (VTC) 2011 Fall, San Francisco, CA, USA, September 2011.

[152] 3GPP TS 36.300, “Evolved Universal Terrestial Radio Access (E-UTRA) and Evolved Universal Terrestial Radio Access Network (E-UTRAN); Overall description; Stage 2 (Release 9)”, V9.9.0, December 2011.

[153] Jacek Góra, Troels E. Kolding, “Deployment Aspects of 3G Femtocells”, in Proc. IEEE International Symposium on Personal, Indoor and Mobile Radio Communications (PIMRC) 2009, Tokyo, Japan, September 2009.

[154] Kimmo Hiltunen, “Total Power Consumption of Different Network Densification Alternatives”, in Proc. IEEE International Symposium on Personal, Indoor and Mobile Radio Communications (PIMRC) 2012, Sydney, Australia, September 2012.

[155] Kimmo Hiltunen, “Improving the Energy-Efficiency of Dense LTE Networks by Adaptive Activation of Cells”, in Proc. IEEE International Conference on Communications (ICC) 2013, 2nd International Workshop on Small Cell Wireless Networks (SmallNets), Budapest, Hungary, June 2013.

[156] Kimmo Hiltunen, “Utilizing eNodeB Sleep Mode to Improve the Energy-Efficiency of Dense LTE Networks” in Proc. IEEE International Symposium on Personal, Indoor and Mobile Radio Communications (PIMRC) 2013, London, The United Kingdom, September 2013.

[157] INFSO-ICT-247733 EARTH, Deliverable D4.1, “Most Promising Tracks of Green Radio Technologies”, 2010.

[158] Laetitia Falconetti, Pål Frenger, Harald Kallin, Thomas Rimhagen, “Energy Efficiency in Heterogeneous Networks”, in Proc. IEEE Online Conference on Green Communications (GreenCom) 2012.

[159] Per Skillermark, Pål Frenger, “Enhancing Energy Efficiency in LTE with Antenna Muting”, in Proc. IEEE Vehicular Technology Conference (VTC) 2012 Spring, Yokohama, Japan, May 2012.

[160] Gunther Auer, Vito Giannini, Claude Desset, István Gódor, Per Skillermark, Magnus Olsson, Muhammad Ali Imran, Dario Sabella, Manuel J. Gonzalez, Oliver Blume, Albrecht Fehske, “How Much Energy is Needed to Run a Wireless Network?”, IEEE Wireless Communications Magazine, vol. 18, no. 5, pp. 40-49, October 2011.

[161] Saulius Samulevičius, Torben Bach Pedersen, Troels Bundgaard Sørensen, Gilbert Micallef, ”Energy savings in mobile broadband network based on load predictions: opportunities and potentials”, in Proc. IEEE Vehicular Technology Conference (VTC) 2012 Spring, Yokohama, Japan, May 2012.

[162] Zhisheng Niu, “TANGO: Traffic-Aware Network Planning and Green Operation”, IEEE Wireless Communications, vol. 18, no. 5, pp. 25-29, October 2011.

[163] INFSO-ICT-247733 EARTH, Deliverable D6.4, “Final Integrated Concept”, 2012.

[164] Mikael Gudmundson, “Correlation model for shadow fading in mobile radio systems”, Electronics Letters, vol. 27, no. 23, November 1991, pp. 2145-2146.

[165] Kathrein Inc., Scala Division, “800 10438 – 65° Panel Antenna”, Data Sheet.

[166] ETSI Technical Report 101 112, “Selection Procedures for the Choice of Radio Transmission Technologies of UMTS (UMTS 30.03)”, version 3.2.0, April 1998.

[167] IST-4-027756 WINNER II D1.1.2 V1.2, “WINNER II Channel Models – Part I Channel Models”, February 2008.

[168] Fredrik Harrysson, Tommy Hult, Fredrik Tufvesson, “Evaluation of an Oudoor-to-In-Car Radio Channel with a Four-Antenna Handset and a User Phantom”, in Proc. IEEE Vehicular Technology Conference (VTC) 2011 Fall, San Francisco, CA, USA, September 2011.

[169] Jukka Lempiäinen, Matti Manninen, “Radio Interface System Planning for GSM/GPRS/UMTS”, Kluwer Academic Publishers, 2001.

[170] Arne Simonsson, Martin Johansson, Magnus Lundevall, “Antenna and Propagation Parameters Modeling Live Networks”, in Proc. IEEE Vehicular Technology Conference (VTC) 2011 Fall, San Francisco, CA, USA, September 2011.

[171] Ari Asp, Yaroslav Sydorov, Mikko Valkama, Jarno Niemelä, “Radio Signal Propagation and Attenuation Measurements for Modern Residential Buildings”, in Proc. 4th International Workshop on Heterogeneous and Small Cell Networks (HetSNets), in connection with IEEE Global Communications Conference (GLOBECOM) 2012, Anaheim, CA, USA, December 2012.

[172] Jie Zhang, Guillaume de la Roche, “Femtocells: Technologies and Deployment”, John Wiley & Sons Ltd, 2010.

[173] Hideaki Okamoto, Koshiro Kitao, Shinichi Ichitsubo, “Outdoor-to-Indoor Propagation Loss Prediction in 800-MHz to 8-GHz Band for an Urban Area”, IEEE Transactions on Vehicular Technology, vol. 58, no. 3, March 2009, pp. 1059-1067.

[174] E. F. T. Martijn, M. H. A. J. Herben, “Characterization of Radio Wave Propagation Into Buildings at 1800 MHz”, IEEE Antennas and Wireless Propagation Letters, vol. 2, no. 1, 2003, pp. 122-125.

[175] Peter Nysten, “Radio Wave Propagation from LOS to Street-Level in Urban Area”, Master of Science Thesis, Royal Institute of Technology, 2002.

[176] Hal Schrank, “Directivity of Omnidirectional Antennas”, IEEE Antennas and Propagation Magazine, vol. 35, no. 5, October 1993, pp. 50-51.

[177] Jan-Erik Berg, Email discussion, 25.5.2010.

# Annex A. Statistical Uncertainty

Both the number of snapshots and the duration of a snapshot are trade-offs between the simulation speed and the accuracy of the results. If a larger number of independent snapshots is assumed, the accuracy of the end-results is improved, but at the same time the required simulation time will increase. Similarly, if the system is evaluated for a longer time during a snapshot, the number of users contributing to the final results becomes larger. Here, the impact of both parameters on the accuracy of the end-results is evaluated a bit further.

The evaluations are performed for the downlink of the baseline deployment. The basic principle is that the statistics for the evaluated output values are collected from 100 independent simulation runs with identical simulation parameters, but with random seeds. When the impact of the number of snapshots is evaluated, each simulation run is assumed to consist of $X$ snapshots, and the duration ($D$) of each snapshot is assumed to be equal to 30 seconds. The value of $X$ is assumed to be equal to 10, 25, 50, 100, 150 or 200. During the second phase of the evaluation, the impact of the duration of the snapshot is evaluated. There, it is assumed that $X$ is equal to 100, while the value of $D$ is equal to 5, 10, 15, 30 or 60 seconds.

The evaluations assume a packet transmission traffic model with an average of one simultaneously active user per cell, i.e. a total of 21 simultaneously active users within the system area. Furthermore, the evaluated simulation output consists of the served area traffic, average packet bit rate and the cell-edge packet bit rate.

Results for the impact of the number of snapshots are presented in Figure A.1 and in Figure A.2. The circles indicate the average value over all the 100 simulation runs, and the error bars indicate the values of the $5^{th}$ and the $95^{th}$ percentile. As can be seen, by increasing the number of snapshots, the variance of the key simulation output values becomes smaller. For all the evaluations presented in this thesis, $X$ is assumed to be equal to 100, which seems to provide a fairly good accuracy.

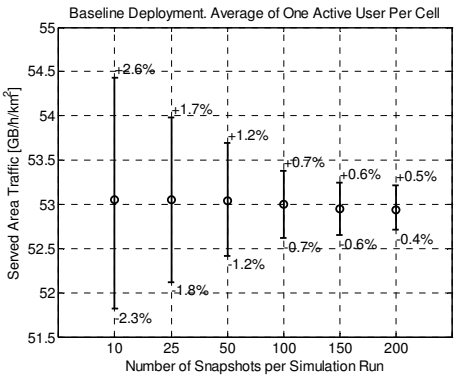


**Figure A.1.** Results for the served area traffic, assuming different values for the number of snapshots per simulation run.

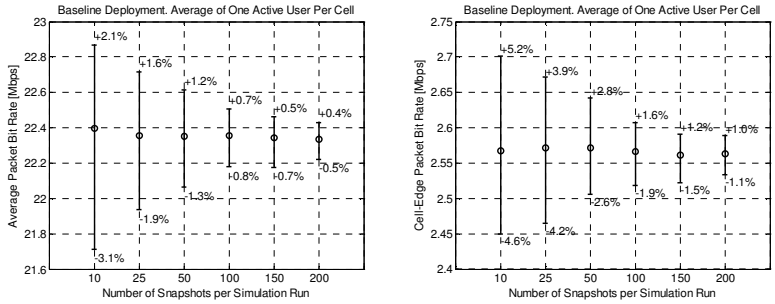


**Figure A.2.** Results for the average and the cell-edge packet bit rate, assuming different values for the number of snapshots per simulation run.

Maximum system capacity is in this thesis defined as a combination of both the served area traffic and the cell-edge user performance. Taking that into account, Figure A.3 presents an alternative way to evaluate the impact of the number of snapshots on the accuracy of the end-results. In the figure, circles are drawn so that they cover the results for 95% of the simulation runs. As can be noticed, the radius of the circle becomes the smaller, the larger the value of $X$ is.

The impact of the assumed duration of a snapshot ($D$) is evaluated in Figure A.4 – Figure A.6. Looking at the results, the impact of $D$ on the served area traffic and the average packet bit rate is clearly noticeable. However, at the same time, the impact on the (average) cell-edge performance is only minor. For all the evaluated outputs, an increased value of $D$ results in an improved accuracy of the results. The fact that an increased value of $D$ results both in an reduced area traffic, and in an improved average packet bit rate suggests that the average cell utilization is reduced. The reason for the reduced cell utilization is that when the system is evaluated for a longer time, the impact of the finite user buffers on the

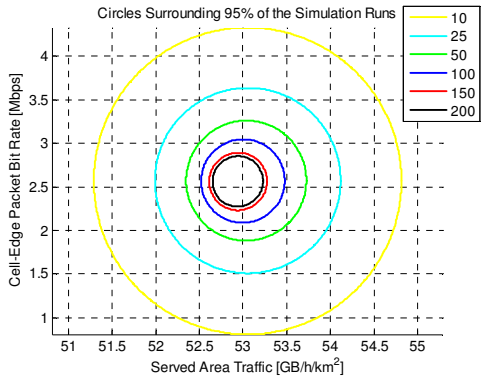


**Figure A.3.** Circles surrounding the results for 95% of the simulation runs, assuming different values for the number of snapshots per simulation run.

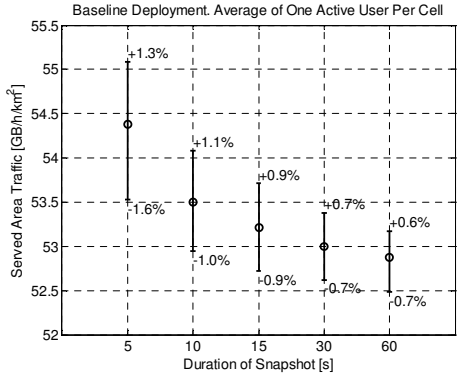


**Figure A.4.** Results for the served area traffic, assuming different values for the duration of a snapshot.

cell utilization and further on the level of inter-cell interference becomes more visible. Since the main reason for a poor downlink user performance is the fact that users have to share the cell resources with other simultaneously active users, the reduced inter-cell interference does not have any major impact on the cell-edge performance.

For all the downlink simulations assumed in this thesis, the value of $D$ is assumed to be equal to 30 seconds, which seems to provide a fairly good accuracy. If the simulations would be made twice as long ($D$ = 60 seconds), the results for the served area traffic and average packet bit rate would become only marginally better. Even though the impact on the cell-edge packet bit rate is slightly bigger, it is still small enough so that the selected value of $D$ can be justified.

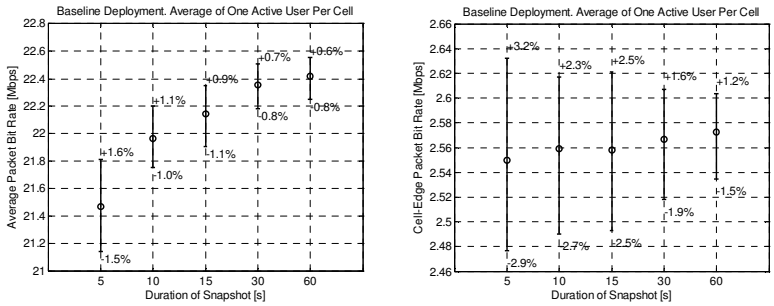


**Figure A.5.** Results for the average and the cell-edge packet bit rate, assuming different values for the duration of a snapshot.

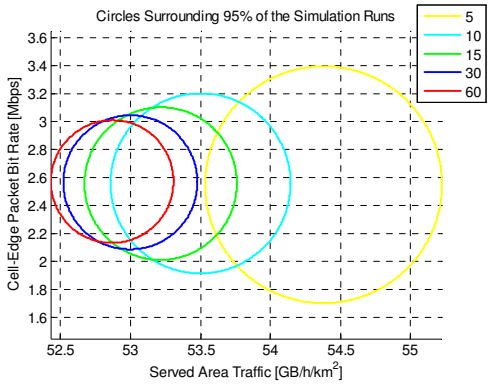


**Figure A.6.** Circles surrounding 95% of the snapshot runs, assuming different values for the duration of a snapshot.

# Annex B. Description of the applied propagation models

## B.1 General

In a general form, coupling loss between a UE $m$ and an eNodeB $b$ can be expressed as

$$L_{m,b} = \max\left(L_{fsp,m,b},\ L_{scen,m,b} + \chi_{m,b}\right) - G_{eNB,m,b} - G_{UE,m,b} \quad \text{[dB]} \qquad \text{(B.1)}$$

where $L_{fsp}$ is the free-space loss and $L_{scen}$ is the corresponding scenario-specific path loss, including the distance-dependent path loss and the penetration losses. Furthermore, $G_{eNB}$ is the eNodeB antenna gain, including feeder losses, towards the direction of the UE. Finally, $G_{UE}$ is the UE antenna gain, including body losses, and $\chi$ is the log-normally distributed shadow fading variable.

The assumed shadow fading model consists of two independent log-normally distributed components, $\chi_{pos}$ and $\chi_{path}$. For a certain UE, $\chi_{pos}$ is fully defined by the position of the UE. Consequently, the fading between the UE and any of the eNodeBs is the same. The value of $\chi_{path}$ is a function of the location of the eNodeB as well as the location of the UE. Thus, for a certain UE the $\chi_{path}$ value will be different for all different eNodeBs.

Intuitively, $\chi_{pos}$ corresponds to changes in the radio environment of the UE pertaining to all eNodeBs, for instance being up on a hill, or down in a basement. Furthermore, $\chi_{path}$ can be thought to correspond to a situation, where the radio signals are blocked in just one direction, creating a direction-dependent fading profile. These two components are then summed up to form a value for the total shadow fading between a UE $m$ and an eNodeB $b$ [138]:

$$\chi_{m,b} = \sigma\left(\sqrt{\rho} \cdot \chi_{pos,m} + \sqrt{1-\rho} \cdot \chi_{path,m,b}\right) \qquad \text{(B.2)}$$

where $\sigma$ is the standard deviation of the shadow fading and $\rho$ defines the correlation of fading values between a UE and the different eNodeBs. On the one hand, if $\rho = 1$, $\chi_{m,b}$ will be equal to $\chi_{pos,m}$, and a complete correlation is obtained between fading values for the different eNodeBs. On the other hand, setting $\rho$ equal to zero results in uncorrelated fading to different eNodeBs.

To fully specify the shadow fading it is necessary to also define its spatial correlation, i.e. how fast the fading changes as a UE moves around [138][164]. Due to the shadow fading process versus distance $\Delta x$, adjacent fading values are correlated. Its normalized autocorrelation function $R(\Delta x)$ is exponential and has the property of being symmetric in all directions. Thus,

$$R(\Delta x) = e^{-\frac{|\Delta x|}{d_{cor}}} \tag{B.3}$$

where $d_{cor}$ is the decorrelation distance.

In this thesis, the same type of UEs are assumed for all deployments. Hence, $G_{UE}$ is always assumed to be omnidirectional, and to have a value equal to -1 dBi. However, the other parameters in (B.1) will depend on the assumed deployment scenario.

## B.2 Macro propagation

A three-dimensional antenna model is assumed for the macro eNodeB [140], with the antenna parameters listed in Table B.1. The parameter values have been selected so that the resulting antenna pattern corresponds to the one achievable with the Kathrein 800 10438 antenna [165]. In addition, the macro eNodeB antennas are assumed to be downtilted to improve the system performance. The assumed values of antenna downtilt, as listed in Table B.1, have been selected to maximize the uplink cell-edge user performance, and they depend also on the assumed inter-site distance (ISD).

Both the standard deviation of the shadow fading and the decorrelation distance are scenario-dependent, and multiple different values applied for macro-cellular deployments can be found in the literature. For example, in [56] the standard deviation is equal to 10 dB for both outdoor and indoor users, in [59] it is equal to 4-7 dB depending on whether the user is located outdoor or indoor, and whether the user is in LOS or NLOS. Furthermore, in [60], the standard deviation is equal to 8 dB for all connections towards

**Table B.1.** Assumed parameter values for the macro eNodeB antenna model.

| Parameter | Value |
|---|---|
| Maximum antenna gain | 18 dBi |
| Horizontal half-power beamwidth | 65 degrees |
| Vertical half-power beamwidth | 5 degrees |
| Front-back ratio | 25 dB |
| Side lobe level | -18 dB |
| Downtilt angle | 6 degrees (ISD = 500 m)<br>8 degrees (ISD = 400 m)<br>12 degrees (ISD = 300 m)<br>14 degrees (ISD = 250 m)<br>17 degrees (ISD = 200 m) |

a macro site, and in [166] it is equal to 10 dB for vehicular users and 12 dB for indoor users. Finally, in [167] the standard deviation is defined to be equal to 4-6 dB for LOS connections, 8 dB for NLOS and 10 dB for indoor users. When it comes to the decorrelation distance, in [59] and [60] it is defined to be equal to 50 meters, while in [166] it is defined to be equal to 20 meters.

In this thesis, the standard deviation of the shadow fading is assumed to be equal to 8 dB, and the decorrelation distance is assumed to be equal to 50 m for the macro-cellular propagation. Furthermore, similar to [60] the shadow fading is assumed to be fully correlated, i.e. $\rho = 1$, towards the sectors belonging to the same macro site, while it is assumed that $\rho = 0.5$ between the different macro sites.

### B.2.1 Macro eNodeB ⇔ In-vehicle UE

The scenario-dependent path loss between a macro eNodeB and an in-vehicle UE is expressed as

$$L_{scen} = L_{outdoor} + L_{penet} \quad [\text{dB}] \qquad \text{(B.4)}$$

where $L_{outdoor}$ is the distance-dependent path loss for a corresponding outdoor user, and $L_{penet}$ is the car penetration loss, which models the loss due to the bodywork of a car (or other vehicle). The value of the car penetration loss depends on the materials used, as well as on the scenario and orientation of the car with respect to the eNodeB [168]. According to [169], the car penetration losses typically vary between 5 and 15 dB. For

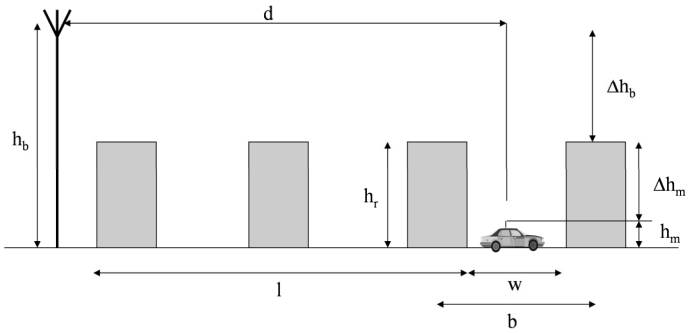


**Figure B.1.** Definition of the parameters for the ITU-R P.1411 non-line-of-sight propagation model.

example, in [59] the car penetration loss is modeled as a log-normally distributed variable, with median equal to 9 dB and the standard deviation equal to 5 dB. In this thesis, the value of the car penetration loss is assumed to be equal to 6 dB for all in-vehicle UEs.

In the simulator, the distance dependent path loss $L_{outdoor}$ is based on the non-line-of-sight model defined in ITU-R P.1411 [139]. In the model, the loss between isotropic antennas is expressed as the sum of free-space loss ($L_{fsp}$), the diffraction loss from roof-top to street ($L_{rts}$), and the reduction due to multiple screen diffraction past rows of buildings ($L_{msd}$):

$$L_{outdoor,dB} = \begin{cases} L_{fsp,dB} + L_{rts,dB} + L_{msd,dB} & , L_{rts,dB} + L_{msd,dB} > 0 \\ L_{fsp,dB} & , L_{rts,dB} + L_{msd,dB} \leq 0 \end{cases} \quad \text{(B.5)}$$

The free-space loss is given by

$$L_{fsp,dB} = 32.4 + 20\log_{10}\left(\frac{d}{1000}\right) + 20\log_{10}(f) \quad \text{(B.6)}$$

where $d$ is the path length in meters and $f$ is the carrier frequency in MHz.

The term $L_{rts}$ describes the coupling of the wave propagating along the multiple-screen path into the street where the UE is located. It takes into account the width of the street and its orientation.

$$L_{rts,dB} = -8.2 - 10\log_{10}(w) + 10\log_{10}(f) + 20\log_{10}(\Delta h_m) + L_{ori} \quad \text{(B.7)}$$

$$L_{ori} = \begin{cases} -10 + 0.354\varphi & , 0° \leq \varphi < 35° \\ 2.5 + 0.075(\varphi - 35) & , 35° \leq \varphi < 55° \\ 4.0 - 0.114(\varphi - 55) & , 55° \leq \varphi < 90° \end{cases} \quad \text{(B.8)}$$

$$\Delta h_m = h_{roof} - h_m \quad \text{(B.9)}$$

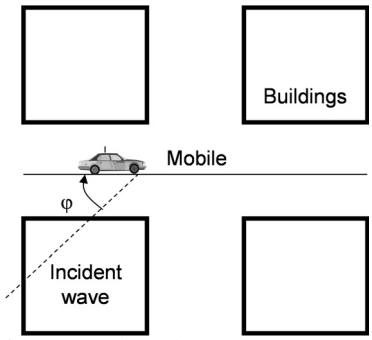


**Figure B.2.** Definition of the street orientation angle $\varphi$.

The term $L_{ori}$ is the street orientation factor, which takes into account the effect of rooftop-to-street diffraction into streets that are not perpendicular to the direction of the propagation, see Figure B.2.

The multiple screen diffraction loss from the eNodeB due to propagation past rows of buildings depends on the eNodeB antenna height relative to the building heights and the incidence angle. A criterion for grazing incidence is the *settled field distance*, $d_s$:

$$d_s = \frac{\lambda d^2}{(\Delta h_b)^2} \tag{B.10}$$

where

$$\Delta h_b = h_b - h_{roof} \tag{B.11}$$

For the calculation of $L_{msd}$, $d_s$ is compared to the distance $l$ over which the buildings extend. The calculation for $L_{msd}$ uses the following procedure to remove any discontinuity between the different models used when the length of buildings is greater or less than the $d_s$.

The overall multiple screen diffraction model is given by:

$$L_{msd} = \begin{cases} -\tanh\left(\frac{d_r}{0.1}\right)(L1_{msd}(d) - L_{mid}) + L_{mid} & , l > d_s\,, dh_{bp} > 0 \\ \tanh\left(\frac{d_r}{0.1}\right)(L2_{msd}(d) - L_{mid}) + L_{mid} & , l \le d_s\,, dh_{bp} > 0 \\ L2_{msd}(d) & , dh_{bp} = 0 \\ L1_{msd}(d) - \tanh\left(\frac{d_r}{\zeta}\right)(L_{upp} - L_{mid}) - L_{upp} + L_{mid} & , l > d_s\,, dh_{bp} < 0 \\ L2_{msd}(d) + \tanh\left(\frac{d_r}{\zeta}\right)(L_{mid} - L_{low}) + L_{mid} - L_{low} & , l \le d_s\,, dh_{bp} < 0 \end{cases} \tag{B.12}$$

where

$$d_r = \log\left(\frac{d}{d_{bp}}\right) \tag{B.13}$$

$$dh_{bp} = L_{upp} - L_{low} \tag{B.14}$$

$$\zeta = 0.0417\left(L_{upp} - L_{low}\right) \tag{B.15}$$

$$L_{mid} = 0.5\left(L_{upp} + L_{low}\right) \tag{B.16}$$

$$L_{upp} = L1_{msd}\left(d_{bp}\right) \tag{B.17}$$

$$L_{low} = L2_{msd}\left(d_{bp}\right) \tag{B.18}$$

$$d_{bp} = |\Delta h_b|\sqrt{\frac{l}{\lambda}} \tag{B.19}$$

The individual losses, $L1_{msd}(d)$ and $L2_{msd}(d)$ are defined as follows:

$$L1_{msd}(d) = L_{bsh} + k_a + k_d \log_{10}\left(\frac{d}{1000}\right) + k_f \log_{10}(f) - 9\log_{10}(b) \tag{B.20}$$

$$L2_{msd}(d) = -10\log_{10}(Q_M^2) \tag{B.21}$$

In (B.20), assuming also that the carrier frequency $f$ is larger than 2000 MHz:

$$L_{bsh} = \begin{cases} -18\log_{10}(1 + \Delta h_b) & , h_b > h_r \\ 0 & , h_b \le h_r \end{cases} \tag{B.22}$$

$$k_a = \begin{cases} 71.4 & , h_b > h_r \\ 73 - 0.8\Delta h_b & , h_b \le h_r \, , d \ge 500\ m \\ 73 - 1.6\Delta h_b \, d/1000 & , h_b \le h_r \, , d < 500\ m \end{cases} \tag{B.23}$$

$$k_d = \begin{cases} 18 & , h_b > h_r \\ 18 - 15\dfrac{\Delta h_b}{h_r} & , h_b \le h_r \end{cases} \tag{B.24}$$

$$k_f = -8 \tag{B.25}$$

The term $k_a$ represents the increase of path loss for eNodeB antennas below the rooftops of the adjacent buildings. The terms $k_d$ and $k_f$ control

**Table B.2.** Assumed parameter values for the macro-cellular propagation model.

| Parameter | Value |
|---|---|
| $f$ | 2600 MHz |
| $w$ | 25 m |
| $b$ | 100 m |
| $h_r$ | 19 m |
| $h_b$ | 24 m |
| $h_m$ | 1.5 m |
| $\varphi$ | 45° |

the dependency of the multi-screen diffraction loss versus the distance and carrier frequency, respectively.

Furthermore, in (B.21)

$$Q_M = \begin{cases} 2.35\left(\frac{\Delta h_b}{d}\sqrt{\frac{b}{\lambda}}\right)^{0.9} & , h_b > h_r + \delta h_u \\ \frac{b}{d} & , h_b \le h_r + \delta h_u \, , h_b \ge h_r + \delta h_l \\ \frac{b}{2\pi d}\sqrt{\frac{\lambda}{\rho}}\left(\frac{1}{\theta} - \frac{1}{2\pi + \theta}\right) & , h_b < h_r + \delta h_l \end{cases} \tag{B.26}$$

and

$$\theta = \arctan\left(\frac{\Delta h_b}{b}\right) \tag{B.27}$$

$$\rho = \sqrt{\Delta h_b^2 + b^2} \tag{B.28}$$

$$\delta h_u = 10^{-\log\left(\sqrt{\frac{b}{\lambda}}\right) - \frac{\log(d)}{9} + \frac{10}{9}\log\left(\frac{b}{2.35}\right)} \tag{B.29}$$

$$\delta h_l = \frac{0.00023b^2 - 0.1827b - 9.4978}{(\log(f))^{2.938}} + 0.000781b + 0.06923 \tag{B.30}$$

For simplicity, it has been assumed in this thesis that parameter $l$ is always equal to $d/2$, i.e. the buildings extend over half of the path length. In addition to that, the parameter values listed in Table B.2 have been assumed. Parameters $w$, $b$ and $h_r$ are related to the assumed scenario with

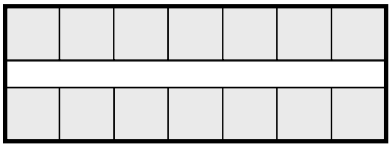

**Figure B.3.** Layout of a building floor.

traffic clusters. Furthermore, the other parameters are selected so that the resulting coupling losses do not become unreasonably small compared to the real-life networks, which is the case for example for the commonly assumed 3GPP Case 1 network deployment model [60], as demonstrated for example in [170]. In practice this means that the macro cells assumed in this thesis are considerably more coverage-limited compared to the cells in 3GPP Case 1.

### B.2.2 Macro eNodeB ⇔ Indoor UE

In order to calculate the path loss between macro eNodeBs and indoor users, a simple building penetration model is assumed, based on the non-line-of-sight building penetration model in [141]. In the model, the total path loss $L_p$ is related to the outside loss $L_{outdoor}$ at 1.5 m height above the ground. The total loss between isotropic antennas is defined with the following equation:

$$L_p = L_{outdoor} + W_{ext} + \alpha d_i + pW_i - G_{FH} \quad \text{[dB]} \qquad \text{(B.31)}$$

The outside loss $L_{outdoor}$ is calculated using the same model as for the in-vehicle users. Parameter $W_{ext}$ models the penetration loss of the outer building wall. The losses caused by the inner walls and furniture are modeled as a combination of both a log-linear term depending on the distance between the outer wall and the indoor UE, and a term that depends on the number of traversed thick walls between apartments, as drawn in Figure B.3.

The wall losses will typically depend strongly on the assumed material and the thickness of the walls. Furthermore, the penetration loss depends on whether the wall has windows or not. In [141], $W_{ext}$ is modeled as a sum $W_e + W_{ge}$, where the value of $W_e$ is defined to be in between 4 and 10 dB and the value of $W_{ge}$ is defined to be in between 5 and 7 dB. Furthermore, in [56] the penetration loss of an outer wall is assumed to be equal to 20 dB. As discussed for example in [171], the increasing popularity of energy-efficient housing will result in considerably increased penetration losses for

the outer building walls. In general, when the building penetration losses are increased, obtaining outdoor-to-indoor coverage becomes more difficult, and hence, a denser deployment of outdoor sites is required to fulfill the desired coverage and capacity requirements. However, the situation is improved from the in-building solutions' point of view. The reason for this is that the increased wall penetration loss will attenuate the inter-cell interference coming from the outdoor cells, which will improve the coverage and capacity of the in-building cells.

When it comes to the penetration losses for the inner walls, values in between 3 dB and 15 dB can be found in the literature. For example, in [141], the value of parameter $W_i$ is assumed to be in between 4 and 10 dB (4 dB for a plasterboard wall, 7 dB for a concrete wall). Furthermore, in [172] the loss per a concrete wall is defined to be equal to 15 dB, while the loss per a plasterboard wall is defined to be equal to 5 dB. In [167], the loss per a light wall is assumed to be equal to 5 dB, and the loss per a heavy wall is assumed to be equal to 12 dB. In [56] the loss between walls between apartments is assumed to be equal to 5 dB. Finally, in [166], the loss per a light internal wall (e.g. plasterboard) is assumed to be equal to 3.4 dB and the loss per a heavy internal wall (e.g. concrete or brick) is assumed to be equal to 6.9 dB.

The value of $\alpha$ will depend on the material and thickness of the inner walls, as well as the sizes of the rooms, i.e. the average distance between the inner walls. All of this means that the value of $\alpha$ will typically be different for different types of buildings (for example residential buildings, office buildings, hotels, shopping malls and so on).

In this thesis, $W_{ext}$ is assumed to be equal to 12 dB, $\alpha$ equal to 0.8 dB/m and $W_i$ equal to 10 dB.

In case of a non-line-of-sight macro cellular propagation, where the dominant part of the received power in the street originates from rays that due to reflections and diffraction have propagated from the surrounding roof level, the penetration loss decreases with an increasing floor level [141][173-175], see Figure B.4. Similar to the wall penetration losses discussed above, also the value of the *floor height gain* will be highly scenario-dependent. For example, in [141] the floor height gain is found to be varying from 1.5-2 dB per floor to 4-7 dB per floor (or 1.1-1.6 dB/m). In [173], a value equal to 0.6 dB/m is proposed. In [174], it is observed that the floor height gain is equal to 1.4-2.2 dB/floor. What is interesting in [174] is that it demonstrates also how the floor height gain becomes negative for the upper floor levels, which are above the (downtilted) main antenna beam of the macro base station antenna. Finally, in [175] it is concluded that the floor height gain is not linear, but will in many cases increase as a function

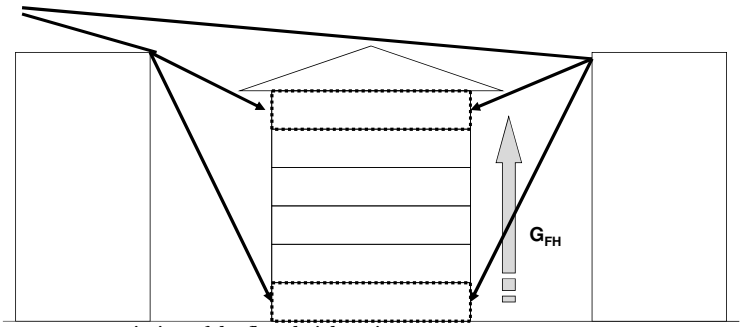


**Figure B.4.** Description of the floor height gain.

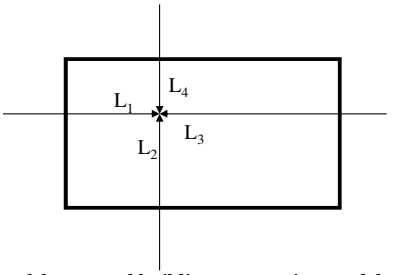


**Figure B.5.** Description of the general building penetration model.

of the floor level, that is when the propagation becomes closer to a line-of-sight towards the macro site.

In (B.31), the floor height gain is modeled by $G_{FH}$, assuming that the UE antenna height is equal to $h_m$

$$G_{FH} = 0.7(h_m - 1.5) \qquad \text{[dB]} \qquad \text{(B.32)}$$

Within [141] it has been suggested that the best way to estimate the received power at a fixed location within a building is to consider all the paths through the external walls as shown in Figure B.5. For each path, the received power $P_{Rx}$ is determined according to the methods described above and the linear sum of these separate powers will then be the total received power. Thus, the scenario-dependent path loss $L_{scen}$ can be calculated in the following way, with all entities expressed in linear terms:

$$P_{Rx} = \frac{P_{Tx}}{L_{scen}} = P_{Tx} \cdot \sum_{p=1}^{4} \frac{1}{L_p} \qquad \text{(B.33)}$$

which results in

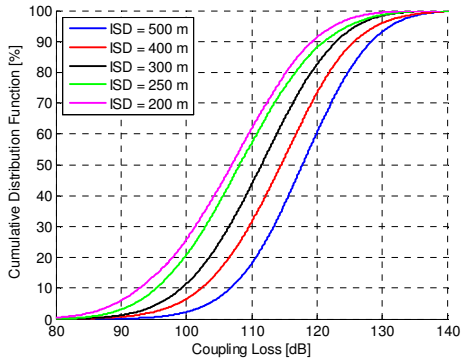


**Figure B.6.** Distribution of the coupling loss between a UE and the serving macro eNodeB with different values of the inter-site distance (ISD).

$$L_{scen} = \frac{1}{\sum_{p=1}^{4} \left(\frac{1}{L_p}\right)} \tag{B.34}$$

or in

$$L_{scen} = -10 \log_{10} \left( \sum_{p=1}^{4} 10^{-0.1 L_{p,dB}} \right) \quad \text{[dB]} \tag{B.35}$$

### B.2.3 Examples of coupling loss distributions

Distributions of the observed coupling loss values between a UE and the serving macro eNodeB are shown in Figure B.6 for different values of the inter-site distance (ISD). The curves assume that 80% of the users are located inside buildings, and 20% of the users are located inside vehicles.

## B.3 Micro propagation

In the simulator, the micro eNodeB antenna is assumed to be omnidirectional, and have a maximum antenna gain of 5 dBi [56]. One major simplification compared to the macro eNodeB antenna model is that the micro eNodeB antenna model is two-dimensional, ignoring the vertical antenna pattern. In reality, the omnidirectional antennas will typically have a "doughnut-like" radiation pattern with minimum radiation levels both upwards and downwards, as described for example in [176]. The decision to ignore the vertical pattern is expected to overestimate the radiation both

towards areas close the micro eNodeB, and towards areas high up inside the buildings. However, the overall impact of this simplification is expected to be minor.

A number of different values for both the standard deviation and the decorrelation distance of the shadow fading can be found in the literature. For the standard deviation, values like 10 dB [56][60], 10-12 dB [166], and 3-7 dB [59][167] can be found, depending on the propagation conditions (LOS/NLOS/outdoor-to-indoor). For the decorrelation distance, a value equal to 5 meters is assumed in [166] and values equal to 10/13/7 meters (LOS/NLOS/outdoor-to-indoor) are assumed in [59].

In this thesis, the standard deviation of the shadow fading is assumed to be equal to 10 dB, and the decorrelation distance is assumed to be equal to 10 m. Furthermore, the shadow fading correlation factor $\rho$ is assumed to be equal to 0.5.

### B.3.1 Micro eNodeB ⇔ In-vehicle UE

The scenario-dependent path loss ($L_{scen}$) for in-vehicle mobiles is calculated as a combination of the path loss measured outside the vehicle ($L_{outdoor}$) and the penetration loss equal to 6 dB, as described in (B.4). In order to calculate the value of $L_{outdoor}$ for a certain link between a micro eNodeB and a UE, the applied propagation model depends on whether the UE is located within the same or different bin as the micro eNodeB in question, see Figure B.7. In the figure, UE1, UE2 and UE3 illustrate mobiles that are located within the same bin as the micro eNodeB, whereas UE4 and UE5 are located in neighboring bins. The difference between UE4 and UE5 is that UE5 is located within the same *street canyon* as the micro eNodeB.

The propagation within a bin follows the recursive micro-cellular model presented in [139]. According to the model the path loss between isotropic antennas is determined by the *illusory distance* $d_n$ and is calculated as

$$L = 20\log_{10}\left(\frac{4\pi d_n}{\lambda}\right) \quad \text{[dB]} \qquad \text{(B.36)}$$

In (B.36) $\lambda$ is the wavelength and $n$ is the number of straight street segments between the eNodeB and the UE. The illusory distance $d_n$ is a sum of these street segments and is defined by the recursive expression

$$\begin{cases} k_j = k_{j-1} + d_{j-1}q_{j-1} \\ d_j = k_j s_{j-1} + d_{j-1} \end{cases} \qquad \text{(B.37)}$$

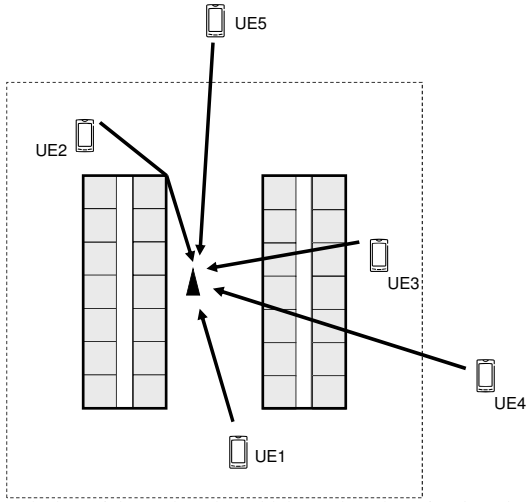


**Figure B.7.** Description of the various in-vehicle UE locations for the micro-cellular propagation.

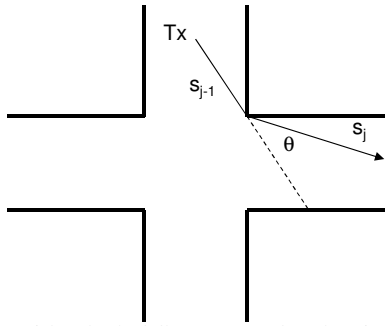


**Figure B.8.** Description of the physical distance $s_j$ and angle $\theta$ for the recursive micro-cellular propagation model.

with the initial values $k_0 = 1$ and $d_0 = 0$. The parameter $s_{j-1}$ is the physical distance of the street segment in meters and $d_j$ is the corresponding illusory distance. The parameter $q_j$ defines the angle dependency of the path loss, and is based on (B.38).

$$q_j(\theta_j) = \left(\theta_j \cdot \frac{q_{90}}{90}\right)^{\nu} \tag{B.38}$$

Parameter $\theta_j$ is the change of direction (in degrees) between street segments $j$-1 and $j$, see Figure B.8. Furthermore, it is assumed that $q_{90}$ is equal to 0.5 and $\nu$ is equal to 1.5 for all street crossings [142].

Looking at Figure B.7, UE1 has a line-of-sight towards the micro eNodeB, and hence, $n = 1$. UE2 is located behind a corner, resulting in $n = 2$. Finally, UE3 is located on the other side of the building with $n = 3$. For

UE3, the total path loss is calculated as a combination of three paths: two paths covering the street-level propagation around both ends of the shadowing building, and the third path propagating over the rooftop. The over-the-rooftop propagation is assumed to be based on the same non-line-of-sight model defined in ITU-R P.1411 [139], which is used also for the macro-cellular propagation. The only difference is that the eNodeB antennas are located below the rooftop level ($h_b < h_r$).

The same over-the-rooftop model is applied to calculate the path losses towards mobiles in neighboring bins that are not within the same street canyon with the micro eNodeB (UE4 in Figure B.7). For the mobiles located within the same street canyon (UE5 in Figure B.7) the propagation model defined in [141] is applied. Hence,

$$L_{outdoor} = 42.6 + 26\log_{10}\left(\frac{d}{1000}\right) + 20\log_{10}(f) \qquad \text{[dB]} \qquad \text{(B.39)}$$

where the distance $d$ is given in meters and the carrier frequency $f$ is given in MHz.

### B.3.2 Micro eNodeN ⇔ Indoor UE

The applied micro-cellular building penetration model is based on both the non-line-of-sight (NLOS) building penetration model described in Section B.2.2, and the line-of-sight (LOS) building penetration model described in [141] and [143]. If the indoor UE is located within the same bin, or along the same street canyon as the micro eNodeB in question, the total penetration loss is a combination of both the NLOS and the LOS building penetration. Otherwise, the total penetration loss is based on the NLOS building penetration.

An example is shown in Figure B.9, where both the micro eNodeB and the indoor UE are within the same bin, and the micro eNodeB is located on the “east” side of the building. As already explained in Section B.2.2, the total path loss is calculated as a combination of the penetration from four directions, illustrated by paths 1-4 in the figure. In the simulator, however, it is assumed that the signal coming from the opposite side of the building (paths 4a and 4b) is so much weaker compared to the other three signal components that it can be ignored when calculating the total path loss. Hence, only paths 1, 2 and 3 are modeled. Path 1 is modeled as LOS building penetration, while paths 2 and 3 are modeled as NLOS building penetration.

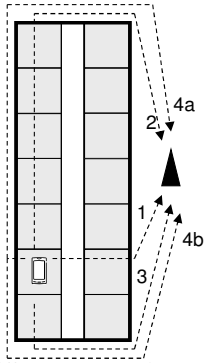


**Figure B.9.** Description of the different propagation paths contributing to building penetration.

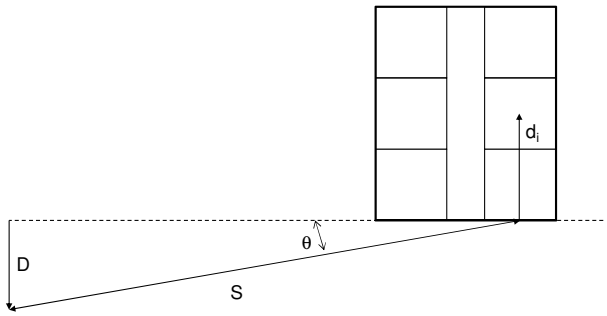


**Figure B.10.** Description of the grazing angle $\theta$, and the distances $D$, $S$ and $d_i$.

The applied LOS building penetration model is based on the model proposed in [141] and [143]. The model parameters are described in Figure B.10. Parameter $S$ is the physical distance from the external antenna to the external wall of the building, while parameter $d_i$ is the distance between the indoor UE and the external wall. The grazing angle $\theta$ is related to distances $D$ and $S$ through the expression:

$$\sin\theta = \frac{D}{S} \tag{B.40}$$

The only case when $\theta$ is equal to 90 degrees is when the external antenna is located at the same height as the actual floor and at perpendicular distance from the external wall, i.e. when $D$ is equal to $S$. Hence, $\theta$ changes considerably with floor height at short distances $D$.

The total path loss $L_p$ is described by the following expression, where all the distances are given in meters:

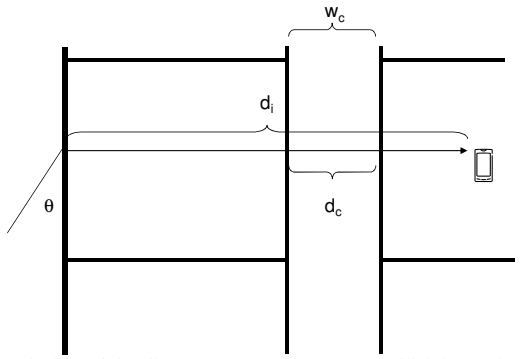


**Figure B.11.** Description of the distance $d_a$ ($d_a = d_i - d_c$), which is used to calculate the indoor wall and furniture losses.

$$L_p = 32.4 + 20\log_{10}(f_{GHz}) + 20\log_{10}(S + d_i) + W_e + W_{Ge}\left(1 - \frac{D}{S}\right)^2 + \max(\Gamma_1, \Gamma_2) \quad \text{[dB]} \qquad \text{(B.41)}$$

$$\Gamma_1 = 0.8d_a + pW_i \qquad \text{(B.42)}$$

$$\Gamma_2 = 0.6(d_i - 2)\left(1 - \frac{D}{S}\right)^2 \qquad \text{(B.43)}$$

In (B.41), $W_e$ is the penetration loss in decibels through the outer building wall at perpendicular penetration ($\theta = 90$ degrees) while $W_{Ge}$ considers the increased wall loss in decibels at small grazing angle ($\theta = 0$ degrees). Parameter $W_i$ is the internal wall loss in decibels and $p$ is the number of penetrated internal walls between the apartments. The loss due to light internal walls and furniture within apartments is modeled as a log-linear value, ignoring the width of the corridor, $w_c$, when applicable. In the case of no internal walls, the indoor loss is mainly determined through $\Gamma_2$. Distance $d_a$ in (B.42) is the 2-dimensional distance within the apartments, as shown in Figure B.11. Hence, assuming that $d_c$ is the travelled distance within the corridor, then $d_a = d_i - d_c$. It should be noted that in case of the assumed micro-cellular propagation, distance $d_c$ will be equal to the width of the corridor ($w_c$).

In this thesis, $W_e$ is assumed to be equal to 7 dB, and $W_{Ge}$ is assumed to be equal to 20 dB, which both are aligned with the recommended parameter values in [141].

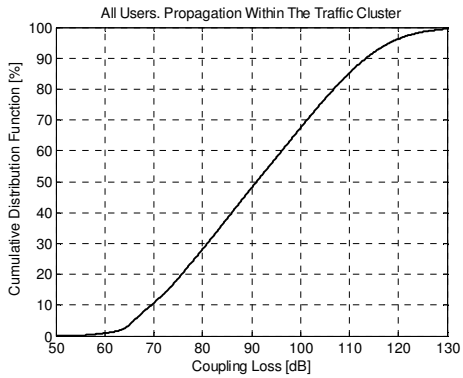


**Figure B.12.** Distribution of the coupling loss between a UE and a micro eNodeB, assuming that both of them are located within the same traffic cluster.

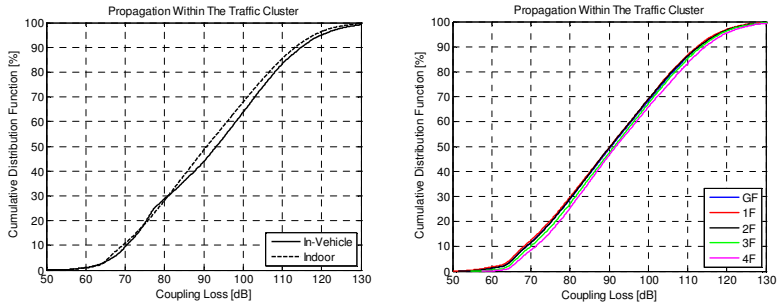


**Figure B.13.** Distribution of the coupling loss between a UE and a micro eNodeB, assuming that both of them are located within the same traffic cluster.

### B.3.3 Examples of coupling loss distributions

Distribution of the observed coupling loss values between a UE and a micro eNodeB are shown in Figure B.12, assuming that both nodes are located within the same traffic cluster.

The curves in Figure B.13 evaluate the impact of the location of the UE on the experienced coupling loss. The figure on the left compares the in-vehicle users against the indoor users, while the figure on the right compares the indoor users on different floor levels against each other. As can be seen, there are no major differences between the different user locations. However, two observations can be made: a) in-vehicle users experience marginally larger coupling losses than the indoor users and b) coupling losses towards the indoor users increase slightly as a function of the floor level. The first one can be explained by both the car penetration loss (6 dB) and the fact that only a fraction of the in-vehicle users are in a line-of-sight with the micro site. The reason why the indoor loss increases together with

the increasing floor level is two-fold: Distance $S$ increases and at the same time the grazing angle $\theta$ decreases, which both contribute to larger coupling losses for the indoor users.

## B.4 Indoor propagation

The femto eNodeB antenna is assumed to be omnidirectional, and the antenna gain is assumed to be equal to 2 dBi [166], i.e. roughly equal to the gain of a half dipole antenna. Furthermore, the vertical antenna gain is not modeled.

When it comes to the standard deviation of the shadow fading, in [166] a value equal to 12 dB is assumed for an indoor office environment, while in [56] a values in between 4-10 dB are assumed for a residential environment. Finally, in [59] the standard deviation is defined to be equal to 3-4 dB. Depending on the reference, the decorrelation distance is assumed to be equal to 5-10 meters.

In this thesis the standard deviation of the shadow fading is assumed to be equal to 10 dB, and the decorrelation distance is assumed to be equal to 10 m for the indoor propagation. The shadow fading is assumed to be uncorrelated between the different indoor eNodeBs, i.e. $\rho = 0$, indicating that the shadow fading is mostly used to model the prediction errors caused by variations in internal wall structures and furniture, instead of variations caused by large-scale objects.

### B.4.1 In-building eNodeB ⇔ In-vehicle UE

Path loss $L_{scen}$ between an in-building eNodeB and an in-vehicle UE is calculated using the same principles and models as the path loss between a micro eNodeB and an indoor UE, see section B.3.2. Furthermore, an additional penetration loss of 6 dB is added for each connection.

In order to simplify the calculations, $L_{scen}$ values are calculated only for the in-vehicle UEs that are located within the same traffic cluster as the in-building eNodeB in question. Hence, the interference to/from in-vehicle UEs that are located in neighboring bins is ignored during the simulations.

### B.4.2 In-building eNodeB ⇔ Indoor UE within the same building

Path loss $L_{scen}$ between an in-building eNodeB and an indoor UE located within the same building is based on both the multi-wall model in [141] and

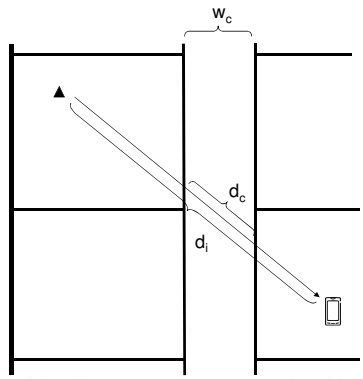


**Figure B.14.** Description of the distance $d_a$ ($d_a = d_i - d_c$), which is used to calculate the indoor wall and furniture losses.

the indoor propagation model given in [166]. The logarithmic path loss between isotropical antennas is calculated as

$$L_{scen} = 20\log_{10}\left(\frac{4\pi d_{3D}}{\lambda}\right) + 18.3k^{(k+2)/(k+1)-0.46} + \alpha d_a + pW_i \qquad \text{(B.44)}$$

where $d_{3D}$ is the (three-dimensional) distance from the transmitter to the receiver, $\lambda$ is the wavelength, and $k$ is the number of floors traversed by the direct wave. The wall loss is calculated as a sum of a log-linear term taking into account the losses caused by the walls inside apartments and furniture, and a term that adds an additional loss per each penetrated heavy wall separating the apartments. As already discussed, distance $d_a$ is equal to the two-dimensional indoor distance between the transmitter and the receiver, ignoring the distance travelled within the corridor, see Figure B.14.

Similar to the building penetration models described above, $\alpha$ is assumed to be equal to 0.8 dB/m, and $W_i$ is assumed to be equal to 10 dB.

### B.4.3 In-building eNodeB ⇔ Indoor UE within the neighboring building

If the in-building eNodeB and the indoor UE are located within neighboring buildings, but still within the same traffic cluster, as described in Figure B.15, path loss $L_{scen}$ is calculated using an extended version of the LOS building penetration model [177].

In the extended model, the logarithmic path loss $L_{scen}$ is calculated as

$$\begin{aligned} L_{scen} = {} & 32.4 + 20\log_{10}(f_{GHz}) + 20\log_{10}(S + d_1 + d_2) + 2W_e + \\ & 2W_{Ge}\left(1 - \frac{D}{S}\right)^2 + \max(\Gamma_{11}, \Gamma_{12}) + \max(\Gamma_{21}, \Gamma_{22}) \end{aligned} \qquad \text{(B.45)}$$

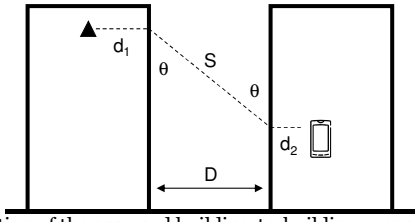


**Figure B.15.** Description of the assumed building-to-building propagation model.

$$\Gamma_{11} = 0.8d_{a1} + 10p_1 \tag{B.46}$$

$$\Gamma_{12} = 0.6(d_1 - 2)\left(1 - \frac{D}{S}\right)^2 \tag{B.47}$$

$$\Gamma_{21} = 0.8d_{a2} + 10p_2 \tag{B.48}$$

$$\Gamma_{22} = 0.6(d_2 - 2)\left(1 - \frac{D}{S}\right)^2 \tag{B.49}$$

It is worth noting that $L_{scen}$ includes only the LOS penetration between the two buildings, and ignores the NLOS penetration through the other building walls. Furthermore, the simulator ignores the interference to/from indoor UEs that are located within neighboring traffic clusters.

### B.4.4 Examples of coupling loss distributions

Examples of the indoor coupling loss distributions are obtained for the femto deployment described in Figure B.16. The coupling loss calculations assume a femto eNodeB, which has been deployed at a random position inside apartment A on the 2nd floor (2F).

To start with, the curves in Figure B.17 indicate the coupling losses between the femto eNodeB and random UE positions within selected apartments on the same floor as the femto eNodeB. The curve for *apartment A* presents the distribution of coupling losses within the femto apartment, while the other curves indicate the coupling losses towards the selected neighboring apartments.

Distributions of the coupling losses within the femto floor (2F) and towards two other floors (3F and 4F) are shown in Figure B.18. The impact of the floor penetration loss is clearly visible on the curves.

Distribution of the coupling loss between the femto eNodeB and an UE located either in the same or the neighboring building is shown in Figure B.19. An interesting thing to note is that in most of the cases the coupling

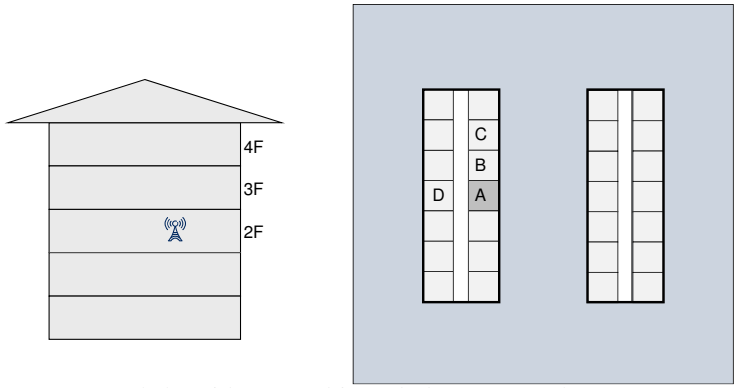


**Figure B.16.** Description of the assumed femto deployment scenario.

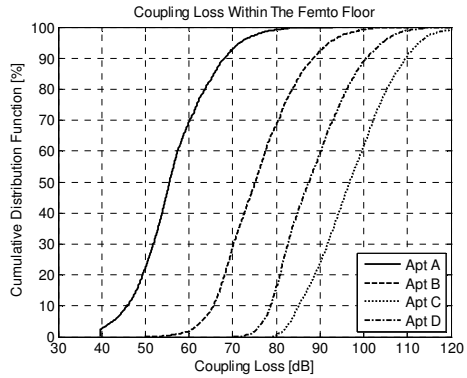


**Figure B.17.** Distribution of the coupling loss between a UE and a femto eNodeB, assuming that both are located on the same floor.

losses towards the neighboring building are smaller than the coupling losses within the femto building. This is due to the fact that the femto eNodeB is located within an apartment that is in direct line-of-sight with the neighboring building. Compared to the floor penetration losses within the femto building, the losses caused by the LOS building penetration are typically smaller.

Finally, the distribution of the coupling losses between the femto eNodeB and in-vehicle UEs is presented in Figure B.20. As a result of the LOS penetration and no penetrated heavier indoor walls, the coupling loss is quite modest towards the users located within the street area in between the buildings. However, the coupling loss is found to be quite high towards the other outdoor areas.

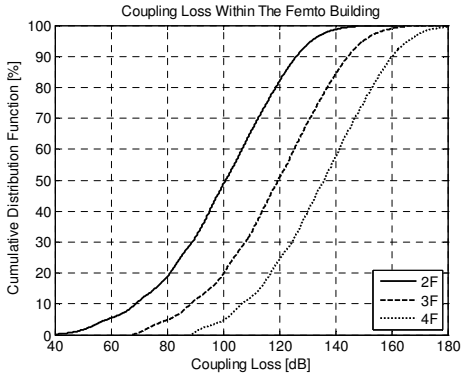


**Figure B.18.** Distribution of the coupling loss between a UE, located either on the 2nd, 3rd, or 4th floor and a femto eNodeB (located on the 2nd floor).

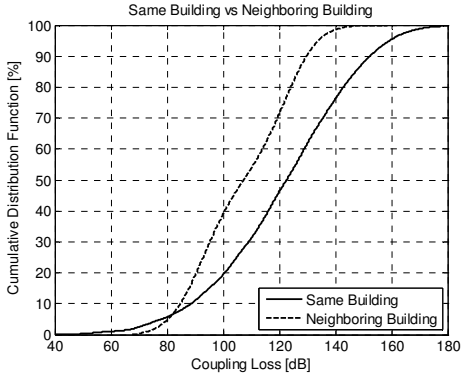


**Figure B.19.** Distribution of the coupling loss between a UE and a femto eNodeB, assuming that they are located either in the same or in the neighboring building.

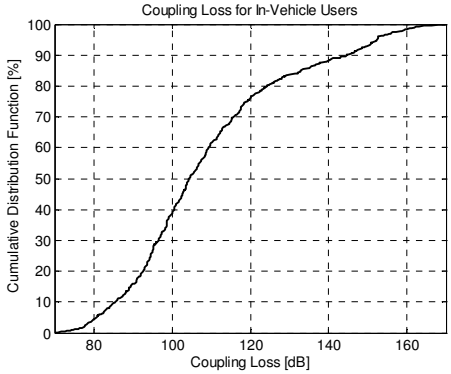


**Figure B.20.** Distribution of the coupling loss between a femto eNodeB and an in-vehicle UE located within the same traffic cluster.

# Annex C. $P_0$ values for uplink power control

This annex lists the applied uplink $P_0$ values for the different heterogeneous network deployments. For the deployments with a full frequency reuse between the macro and the low-power cell layer, parameter $\phi$ is also provided. The $\phi$ values are derived from (3.25):

$$\phi = P_{0,LPN} + P_{0,macro} + P_{LPN} - P_{macro} + O_{LPN} \qquad \text{[dB]} \qquad \text{(C.1)}$$

where $P_{macro}$ is assumed to be equal to 46 dBm. Furthermore, unless stated otherwise, $P_{LPN}$ is assumed to be equal to 30 dBm for micro eNodeBs and equal to 20 dBm for femto eNodeBs.

**Table C.1.** Uplink power control parameters for heterogeneous micro deployment with full frequency reuse. One micro site per traffic cluster.

| $O_{LPN}$ [dB] | $P_{LPN}$ [W] | $P_{0,macro}$ [dBm] | $P_{0,LPN}$ [dBm] | $\phi$ [dB] |
|---|---|---|---|---|
| 0 | 1 | -111 | -100 | -5 |
| 0 | 2 | -111 | -101 | -3 |
| 0 | 4 | -109 | -104 | -5 |
| 0 | 10 | -109 | -104 | -1 |
| 1 | 1 | -111 | -100 | -4 |
| 2 | 1 | -111 | -100 | -3 |
| 3 | 1 | -111 | -101 | -3 |
| 4 | 1 | -111 | -101 | -2 |
| 5 | 1 | -110 | -103 | -4 |
| 6 | 1 | -109 | -104 | -5 |
| 7 | 1 | -109 | -104 | -4 |
| 8 | 1 | -109 | -104 | -3 |
| 9 | 1 | -109 | -104 | -2 |
| 10 | 1 | -109 | -104 | -1 |
| 11 | 1 | -109 | -104 | 0 |
| 12 | 1 | -109 | -104 | 1 |

**Table C.2.** Uplink power control parameters for heterogeneous micro deployment with full frequency reuse. In average one micro site per macro cell.

| $O_{LPN}$ [dB] | $P_{LPN}$ [W] | $P_{0,macro}$ [dBm] | $P_{0,LPN}$ [dBm] | $\phi$ [dB] |
|---|---|---|---|---|
| 0 | 1 | -116 | -103 | -3 |
| 0 | 2 | -115 | -104 | -2 |
| 0 | 4 | -115 | -107 | -2 |
| 0 | 10 | -115 | -108 | 1 |
| 1 | 1 | -116 | -103 | -2 |
| 2 | 1 | -115 | -104 | -3 |
| 3 | 1 | -115 | -104 | -2 |
| 4 | 1 | -115 | -104 | -1 |
| 5 | 1 | -115 | -106 | -2 |
| 6 | 1 | -115 | -107 | -2 |
| 7 | 1 | -115 | -107 | -1 |
| 8 | 1 | -115 | -108 | -1 |

**Table C.3.** Uplink power control parameters for heterogeneous adjacent channel micro deployments. One micro site per traffic cluster.

| Macro BW [MHz] | Micro BW [MHz] | $O_{LPN}$ [dB] | $P_{0,macro}$ [dBm] | $P_{0,LPN}$ [dBm] |
|---|---|---|---|---|
| 15 | 5 | 0 | -110 | -94 |
| 15 | 5 | 3 | -109 | -94 |
| 15 | 5 | 6 | -108 | -96 |
| 10 | 10 | 0 | -108 | -97 |
| 10 | 10 | 6 | -107 | -99 |
| 10 | 10 | 12 | -105 | -101 |
| 10 | 10 | 18 | -105 | -101 |
| 5 | 15 | 0 | -105 | -98 |
| 5 | 15 | 6 | -101 | -100 |
| 5 | 15 | 12 | -101 | -102 |
| 5 | 15 | 18 | -100 | -102 |
| 5 | 15 | 24 | -100 | -103 |

**Table C.4.** Uplink power control parameters for heterogeneous adjacent channel micro deployments. In average one micro site per macro cell.

| Macro BW [MHz] | Micro BW [MHz] | $O_{LPN}$ [dB] | $P_{0,macro}$ [dBm] | $P_{0,macro}$ [dBm] |
|---|---|---|---|---|
| 15 | 5 | 0 | -114 | -95 |
| 15 | 5 | 3 | -114 | -95 |
| 15 | 5 | 6 | -113 | -96 |
| 15 | 5 | 9 | -113 | -98 |
| 10 | 10 | 0 | -113 | -98 |
| 10 | 10 | 6 | -113 | -100 |
| 10 | 10 | 12 | -113 | -100 |
| 10 | 10 | 15 | -113 | -101 |
| 10 | 10 | 17 | -113 | -102 |
| 5 | 15 | 0 | -110 | -98 |
| 5 | 15 | 6 | -110 | -98 |
| 5 | 15 | 12 | -109 | -100 |
| 5 | 15 | 18 | -109 | -104 |
| 5 | 15 | 24 | -109 | -109 |

**Table C.5.** Uplink power control parameters for heterogeneous OSG femto deployment.

| Femto Penetration [%] | Femto Site Density [sites/km²] | Femto Users [%] | $P_{0,macro}$ [dBm] | $P_{0,LPN}$ [dBm] | $\phi$ [dB] |
|---|---|---|---|---|---|
| 0 | 0 | 0 | -119 | - | - |
| 5 | 68.0 | 15.8 | -118 | -99 | -7 |
| 10 | 135.9 | 27.9 | -118 | -99 | -7 |
| 20 | 271.2 | 44.5 | -115 | -99 | -10 |
| 30 | 407.1 | 55.7 | -113 | -99 | -12 |
| 40 | 542.4 | 63.4 | -112 | -99 | -13 |
| 50 | 678.3 | 69.0 | -111 | -98 | -13 |
| 60 | 814.2 | 73.4 | -110 | -98 | -14 |
| 70 | 949.5 | 76.7 | -109 | -98 | -15 |
| 80 | 1085.4 | 79.2 | -108 | -97 | -15 |
| 90 | 1220.7 | 81.3 | -108 | -96 | -14 |
| 100 | 1356.6 | 83.0 | -107 | -96 | -15 |

**Table C.6.** Uplink power control parameters for heterogeneous OSG femto deployments with different femto eNodeB output powers.

| Femto Penetration [%] | $P_{LPN}$ [mW] | $P_{0,macro}$ [dBm] | $P_{0,LPN}$ [dBm] | $\phi$ [dB] |
|---|---|---|---|---|
| 30 | 1 | -116 | -92 | -22 |
| 30 | 5 | -115 | -95 | -19 |
| 30 | 10 | -115 | -97 | -18 |
| 30 | 50 | -114 | -98 | -13 |
| 30 | 100 | -113 | -99 | -12 |
| 50 | 1 | -115 | -90 | -21 |
| 50 | 5 | -114 | -92 | -17 |
| 50 | 10 | -113 | -95 | -18 |
| 50 | 50 | -113 | -97 | -13 |
| 50 | 100 | -111 | -98 | -13 |

Traffic in the mobile networks is expected to grow very rapidly in the coming years. This traffic growth is caused both by the evolution of mobile terminals and by the increased use of more traffic-heavy services. In order to be able to meet the increased capacity needs, the existing mobile networks have to be densified, either by deploying new macro sites or by deploying new low-power sites within traffic hotspots. This thesis provides an overview of a few different network densification alternatives and compares their performance and energy-efficiency with the help of advanced radio network simulations. In addition, the impact of different network design choices is evaluated.

Aalto-DD 51/2014

ISBN 978-952-60-5650-0
ISBN 978-952-60-5651-7 (pdf)
ISSN-L 1799-4934
ISSN 1799-4934
ISSN 1799-4942 (pdf)

**Aalto University**
**School of Electrical Engineering**
**Department of Communications and Networking**
**www.aalto.fi**

BUSINESS + ECONOMY

ART + DESIGN + ARCHITECTURE

SCIENCE + TECHNOLOGY

CROSSOVER

**DOCTORAL DISSERTATIONS**